Co-nanoprecipitation:

Preparation of Sterically Stabilised Polymer Nanoparticles for Drug Delivery Applications

Thesis submitted in accordance with the requirements of the

University of Liverpool for the degree of Doctor in Philosophy by:

Jane Ford

September 2015

UNIVERSITY OF LIVERPOOL

Acknowledgments

First and foremost, my appreciation and greatest thanks goes to Professor Steve Rannard for giving me the opportunity to carry out this Ph.D. research. During the past 4 years Steve has provided me with constant guidance, support, positivity and endless cups of tea! I will really miss working with Steve, attending conferences and the being part of the Rannard research group.

I would like to give a special thanks to Dr. Pierre Chambon for all his help, ideas, inspiration, and excellent guidance throughout this research, and I will definitely miss Friday drinks at the AJ with him and the group! I would also like to thank past and present members of the Rannard group including; Fiona Hatton and Sam Auty for help with experiments, support and creating a friendly environment when I joined the group. I am also very grateful to all the current members of the research group, in particular; Marco, Jay, Maude, Andy and especially Hannah for all the laughs, Starbucks sessions, proof reading and keeping me sane during writing up. I would also like to thank my friends in the department that I have made throughout my time studying, especially Samantha Chadwick for all the fun, laughs, endless phone calls and for being my daily stress release! Professor Peter Myers deserves a special thank you for all his support and advice throughout this Ph.D. and keeping me calm. I would also like to thank Jocelyn North, Joshua Turner and Kate Roffey who have contributed to this Ph.D. during their undergraduate research projects.

With regards to the pharmacology work presented throughout this thesis, I would like to thank Dr. Lee Tatham and Louise Tidbury who conducted the pharmacological studies in the Department of Molecular and Clinical Pharmacology under the supervision of Professor Andrew Owen. I would like to thank Jonathan Evans who also conducted pharmacological studies in the Department of Molecular and Clinical Pharmacology under the supervision of Dr. Neil Kitteringham.

Lastly, I would like to thank my family and friends for their continuous support and putting up with me throughout this Ph.D., especially my sister who can relate to the Ph.D. journey! A special thanks to my brother in law David and my nephews Jack and Harry for always putting a smile on my face. My warmest thanks are extended to my mum for her love and support both emotionally and financially throughout my many years of studying. Finally, I would like to dedicate this thesis to my dad who always believed in me and encouraged me to reach my goals.

Abstract

Co-nanoprecipitation: Preparation of Sterically Stabilised Nanoparticles for Drug Delivery Applications

The co-nanoprecipitation of linear amphiphilic A-B block copolymers and branched hydrophobic co/terpolymers has been used for the first time to generate uniform, salt stable dispersions of aqueous polymer nanoparticles. The nanoprecipitation of the branched polymers was studied in the absence of A-B block copolymers and the conditions chosen for further co-nanoprecipitation studies were chosen on the ability to ensure the mixed solvent system immediately after good solvent addition would guarantee nanoparticle formation. Variation of the ratio of the two polymer architectures using this simple technique has led to varying z-average diameters, narrow polydispersity particle distributions and tuneable stability to salt addition and storage within aqueous salt conditions. Polarity studies provided further evidence that during addition of increasing amounts of A-B block copolymer, the hydrophobicity of the internal core was maintained and only slight deviations were observed suggesting the PEG chains were located on the nanoparticle surface. Multiple nanoprecipitations were also shown to be possible through direct addition of polymer solutions to aqueous nanoparticle dispersions after solvent removal, leading to particle concentration increase without modification of the initial nanoprecipitate size.

The dye molecule fluoresceinamine was selected as a model guest molecule for encapsulation during co-nanoprecipitation (10 wt %). Nanoparticles which were stable under physiologically relevant conditions were generated and studied for their cytotoxicity and transcellular permeability using Caco-2 cells. These materials showed low toxicity at the concentrations studied and enhanced permeation though the Caco-2 cell monolayer, which is a model of the intestinal epithelial cells. A nanomaterial was taken forward for accumulation studies and transcellular permeability in the presence of endocytic inhibitors, suggesting uptake proceeded *via* an active mechanism. Excellent drug loading potentials were observed during co-nanoprecipitation experiments with HIV anti-retrovirals, and up to 25 wt % of efavirenz and ritonavir and 20 wt % lopinavir were encapsulated. As well as anti-retrovirals, encapsulation of an anti-cancer drug molecule SN-38 was studied and colloidally stable nanoparticles with narrow polydispersity particle distributions were obtained. I*n vitro* cytotoxicity testing of the materials showed a comparable toxicity to that of SN-38. Multiple nanoprecipitations including SN-38 were successful and an increased concentration of SN-38 was achieved, whilst maintaining the same volume of anti-solvent.

Overall, the co-nanoprecipitation approach has provided a fast and efficient route to sterically stabilised nanoparticles without the need for additional surfactants or filtration. Particles can be loaded with various drug molecules and pharmacological benefits were observed for some materials, suggesting future use for drug delivery applications.

Contents

Chapter 1 – General Introduction

List of General Abbreviations

ANOVA	Analysis of variance
ATHP-1	Activated Tamm Horsfall Protein (Monocyte derived macrophages)
ATP	Adenosine triphosphate
ATRP	Atom transfer radical polymerisation
BBB	Blood brain barrier
Caco-2	Human epithelial colorectal adenocarcinoma cell line
CAR	Cellular accumulation ratio
CMC	Critical micelle concentration
CRP	Controlled radical polymerisation
CT26	Mouse colon carcinoma cell line
$Đ$	Dispersity (GPC)
DDS	Drug delivery system
DLS	Dynamic light scattering
DLVO	Derjaguin, Landau, Verwey and Overbeek
D_n	Number average diameter
DP_n	Degree of polymerisation
D_z	Z-average diameter
EPR	Enhanced permeation retention
ES	Electrospray
FRP	Free radical polymerisation
GI	Gastrointestinal
GPC	Gel permeation chromatography
HAART	Highly active antiretroviral therapy
HCT116	Human colon carcinoma cell line
HIV	Human immunodeficiency virus
IV	Intravenous
logP	Partition coefficient
MALDI-TOF	Matrix assisted laser desorption ionisation time of flight
M_n	Number average molecular weight
MPS	Mononuclear phagocytic system
M_w	Weight average molecular weight
MWCO	Molecular weight cut off
NMP	Nitroxide mediated polymerisation
NMR	Nuclear magnetic resonance
o/w	Oil in water
P_{app}	Apparent permeability
PdI	Polydispersity index (DLS)
PNO	Polymer nano-objects
PRINT	Particle replication in non-wetting templates
RALS	Right angle light scattering (GPC)
RAFT	Reversible addition-fragmentation transfer
RI	Refractive index (GPC)

SEM	Scanning electron microscopy
TBS	Transport buffer solution
w/o	Water in oil
w/o/w	Water in oil in water
ζ	Zeta potential (mV)

List of Chemical Abbreviations

ACN	Acetonitrile
Bpy	2,2'-bipyridine
DCC	*N*,*N'*-dicyclohexylcarbodiimide
DCM	Dichloromethane
DMAP	4-dimethyl-aminopyridine
DMF	Dimethylformamide
DMSO	Dimethyl sulfoxide
EBiB	Ethyl α-bromoisobutyrate
EFV	Efavirenz
EGDMA	Ethylene glycol dimethacrylate
FA	Fluoresceinamine
HEMA	2-hydroxyethyl methacrylate
HPMA	2-hydroxypropyl methacrylate
IBU	Ibuprofen
IbuPMA	2-((2-(4-isobutylphenyl)propanoyl(oxy)propyl methacrylate
IPA	Isopropyl alcohol
IR	Irinotecan
LPV	Lopinavir
MeO-PEG$_y$-Br	Poly(ethylene glycol) macroinitiator (2000 & 5000 g/mol)
MTT	3-(4,5-dimethylthiazol-2-yl)-2,5-diphenyltetrazolium bromide
MTS	3-(4,5-dimethylthiazol-2-yl)-5-(3-carboxymethoxyphenyl)-2-(4-sulfophenyl)-2H-tetrazolium
PCL	Poly(caprolactone)
PEG	Poly(ethylene glycol)
PLA	Poly(lactic acid)
PLGA	Poly(lactic-*co*-glycolic acid)
PMMA	Poly(methyl methacrylate)
PS	Polystyrene
PVA	Poly(vinyl alcohol)
RTV	Ritonavir
SN-38	7-ethyl-10-hydroxyl camptothecin
t-BMA	*t*-butyl methacrylate
TEA	Triethylamine
THF	Tetrahydrofuran

Chapter 1

General Introduction

1.1 Introduction to Nanomedicine

Nanotechnology is an area of scientific research devoted to the development and design of functional materials existing within the nanometre range (1–1000 nm).[1] Nanomedicine is one of the fastest growing sub-disciplines of nanotechnology and is defined by the National Institute of Health as the advancement of treatment, diagnosis, monitoring and control of biological systems *via* nanomaterials. Materials within the nanometre size range have physicochemical properties that are distinct from those of bulk materials or single molecules or atoms. The development of a new nanomedicine is a slow process (Figure 1.1) and usually requires three different stages. The initial development ranges from 7 – 20 years, followed by a further 1 – 7 years of clinical studies through to the production of a commercial product.

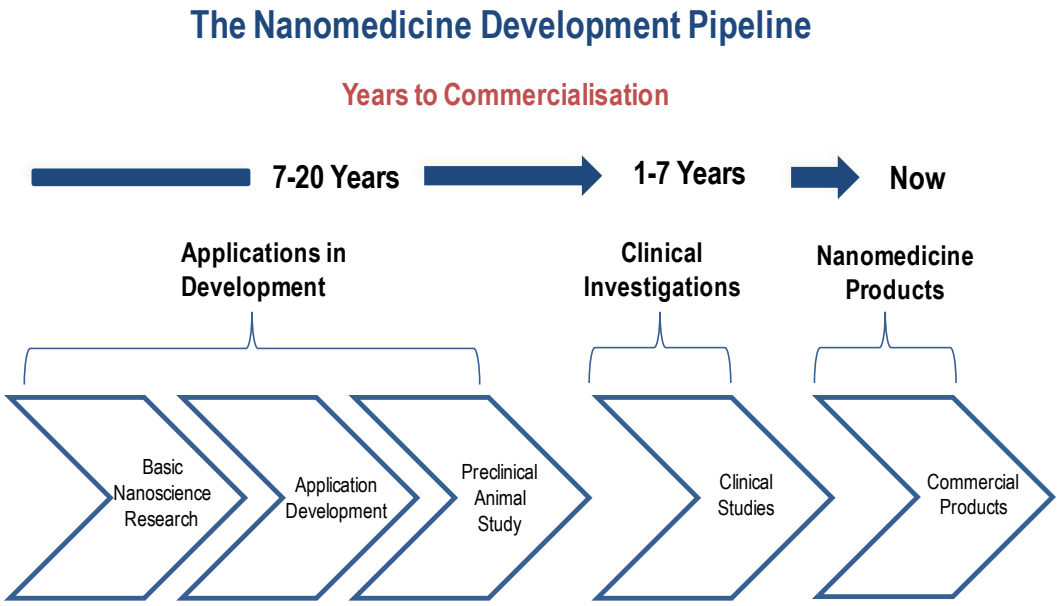

Figure 1.1 The three general stages of nanomedicine development.**Adapted from ref* [2]

During the past two decades, nanomedicine has played a major role towards the development of new treatments for a range of diseases and conditions such as cancer, diabetes, asthma, allergies and kidney disease. To date there are 77 approved nanomedicine products and ~70 in various stages of preclinical and clinical development.[3] Nanomedicines are beneficial as they can provide alternative routes of drug administration, lower therapeutic toxicity and provide a reduction in healthcare costs.[4] For many reasons, the majority of research within the nanomedicine field has focused upon cancer and several new formulations have successfully entered routine clinical use.[5, 6] Current drug delivery systems (DDS) are effective at releasing drug molecules at

relatively high concentrations *in vivo*, yet the scope is limited to targeting tissues rather than individual cells.[7] Over the coming years, nanomedicine will continue to provide benefits for an increasing number of patients, therefore having a positive impact on global health.

1.2 Nanocarriers for drug delivery

A nanocarrier can be defined as a material within the nanometre size range, which transports therapeutic molecules to target sites for improved drug delivery. The potential advantages of therapeutic nanocarriers include; (1) ability to improve the pharmaceutical and pharmacological properties of drugs (e.g. solubility) whilst not altering the drug molecules themselves; (2) preparation of targeted DDSs to enhance therapeutic effects; (3) delivery of drugs across biological barriers (e.g. gut, skin); (4) delivery of drugs to intracellular sites; and (5) ability to deliver drug molecules *via* combination therapies.[8] Selected nanocarriers include micelles, vesicles, polymer-drug conjugates, dendrimers and polymer nanoparticles (Figure 1.2). Current drug molecules which are cytotoxic or unstable active compounds (e.g. anti-tumour medication) can be encapsulated, dispersed, adsorbed or conjugated[9] to improve their pharmacokinetic properties and reduce adverse effects.[10] The particle shape and morphology strongly influence carrier performance and the various types of carrier will be discussed below.

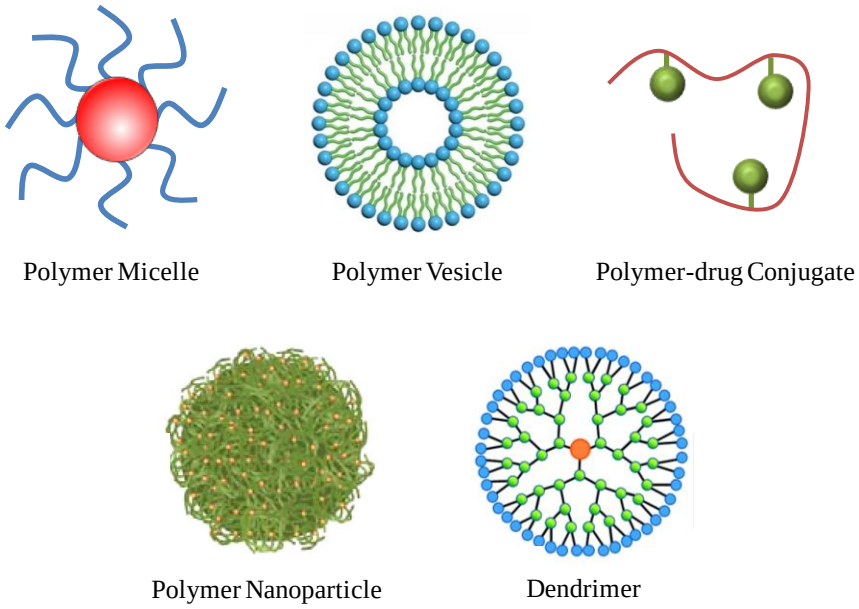

Figure 1.2 Schematic representation of types of polymer nanocarriers commonly used in drug delivery research.

1.2.1 Brief introduction to block copolymers

The first report of block copolymers was during the 1950s using anionic polymerisation,[11] however, their renaissance didn't occur until the 1990s when controlled polymerisation developed rapidly. Controlled polymerisation techniques such as atom transfer radical polymerisation (ATRP),[12] reversible addition-fragmentation chain transfer (RAFT)[13] and nitroxide mediated polymerisation (NMP)[14] can yield block copolymers with both hydrophilic and hydrophobic moieties present within the same molecule. The advantage of these methods is the excellent control that can be achieved over composition and molecular weight distribution of the synthesised polymers.[15] For these reasons, the amphiphilic nature of these polymers has led to many actual and potential applications within many fields including nanomedicine,[16] biomedicine,[17] emulsion polymerisations[18] and cosmetics.[19] The hydrophobic block is often composed of styrene, acrylates, olefins and polyethers. Hydrophilic blocks are typically made up of positively or negatively charged monomers, such as acrylic or vinylic bearing amino group, carboxylic, sulfonated, or neutral blocks such as poly(ethylene) glycol (PEG) or water soluble methacrylates such as hydroxyl ethyl methacrylate (HEMA).[15] Combinations of these monomers in the formation of various amphiphilic block copolymers have been studied for their self-assembling properties. In aqueous solutions, A-B amphiphilic copolymers form a range of various morphologies and are virtually all stabilised by hydrophobic forces. Particulate structures formed *via* self assembly, such as micelles, are prepared in solvents which selectively dissolve one of the block segments. A-B copolymers form well defined micelles with the core consisting of the insoluble block and will be discussed in detail below.[20]

1.2.2 Polymeric micelles

Polymeric micelles are colloidal particles generally formed *via* the self-assembly of amphiphilic block copolymers in an aqueous environment.[21-23] The micelle adopts a core-shell structure; the inner core is composed of the hydrophobic block and the outer hydrophilic shell provides sufficient hydrophilicity to stabilise the core and maintain the micelle dispersion. The formation of micelles is an entropy-driven process and their formation depends on the critical micelle concentration (CMC). The CMC is the minimum concentration of amphiphilic block copolymer required to form micelles in aqueous solution; below the CMC the co-polymer will solubilise and exist as unimers (Figure 1.3). The average size of reported micelles ranges from ~5-100 nm,[24-26] which is dependent on

the materials' properties such as block segment chemistry, segment chain length and experimental preparation conditions, including concentration and temperature.[15]

Block copolymer micelles have become particularly interesting for the formation of DDSs for many reasons. Firstly, the solubility of hydrophobic drugs can be enhanced by encapsulation inside the hydrophobic core; therefore, they can be transported at much higher concentrations than would ever be possible if administered alone. Secondly, the chemical composition, block lengths, and molecular weights can all be varied to control the size and architecture of the micelles.[27, 28] Examples of such DDSs utilising polymer micelles for clinical applications will be discussed in section 2.1.

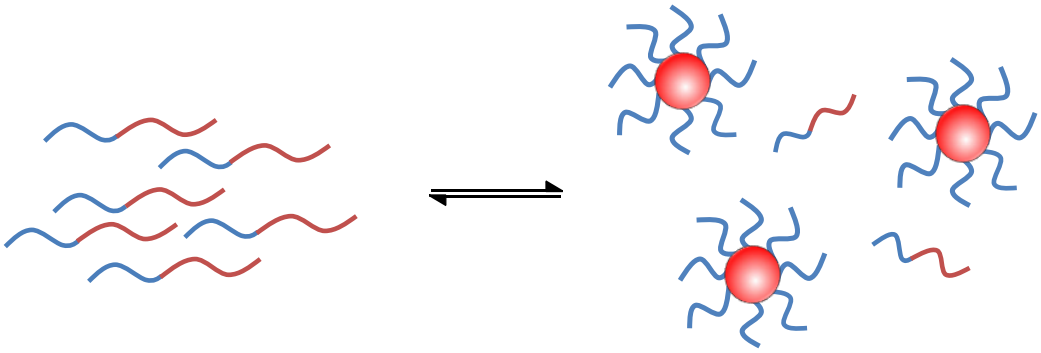

Figure 1.3 Schematic representation of the equilibrium between unimers (left) and polymeric micelles (right).

1.2.3 Polymer vesicles (a.k.a. polymersomes, liposomes)

Vesicles can be prepared from many different compounds including surfactants,[29] phospholipids[30] and block copolymers.[31-34] The preparation of vesicles from block copolymers has been a growing area of interest due to the potential versatility of engineered polymers to match desired design criteria i.e. varying block length and block composition to optimise towards various applications. A major difference between vesicles and other nanocarriers is their hollow and lamellar bilayer structure which has the potential to solubilise both hydrophobic and hydrophilic drug molecules and dimensions can vary within the range of nanometres to micrometres depending on the chemical composition and application required. The main research and development focus has been for vesicles within the nanometre range.[35] Vesicle formation can be thought of as a two step self-assembly process in which the amphiphilic polymer forms a bilayer which then closes to form the vesicle structure.[36] Vesicles allow encapsulation of both hydrophilic and hydrophobic drug molecules, due to their unique bilayer structure, and have been used in the clinical drug delivery of anti-cancer drugs for tumour treatment in humans.[37]

1.2.4 Polymer-drug conjugates

A polymer-drug conjugate, also known as a prodrug, can be defined as an inactive precursor of a drug molecule that usually requires an enzymatic or chemical transformation to release the active drug. The development of polymer-drug conjugates was first reported during the 1950s when Jatzkewitz prepared a polyvinylpyrrolidone–mescaline conjugate that contained a short peptide spacer between the drug and the polymer.[38] However, the main research focus was a study of the chemical interactions between different polymers and drug molecules without the consideration of the biological applications.[39, 40] The first model which explored both chemical and biological aspects necessary for the design of prodrugs was during 1975.[41] Ringsdorf recognised the full potential of prodrugs and all that was needed was polymer chemists, biologists and pharmacologists to collaborate within this field. The Ringsdorf prodrug model includes a polymeric backbone, spacer molecule, solubilising group (if required), targeting group and the drug molecule (Figure 1.4 A). Polymer-drug conjugates are not limited to a linear architecture and include monofunctional linear, polyfunctional linear, branched, micellar and dendritic architectures (Figure 1.4 B).

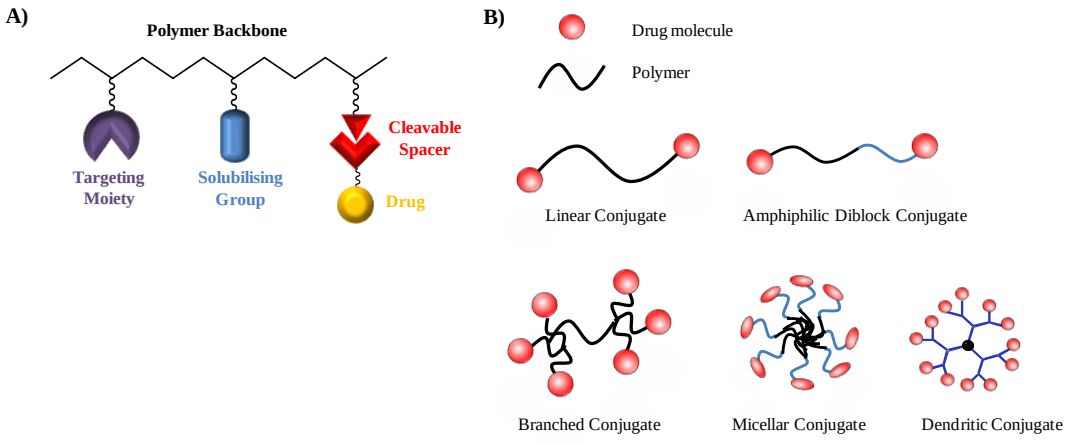

Figure 1.4 A) The Ringsdorf Model (*Adapted from ref* [40]) B) Various polymer-drug conjugate architectures.[42]

The attachment of a pharmaceutical agent to a polymer including; synthetic polymers, polysaccharides & proteins, can significantly increase water solubility, protect the active drug molecule during transportation, improve the pharmacokinetics and, depending on size, can avoid first pass metabolism.[43] First pass metabolism occurs when an administered drug enters the body and is transported to the liver *via* the hepatic portal vein. This process greatly reduces the drug molecule concentration, due to breakdown in

the liver before entry into the systemic circulation, therefore a higher circulating dose may be achieved if small drug molecules are conjugated to polymers.[44]

1.2.5 Dendrimers

From a polymer chemistry point of view, dendrimers are nearly perfect monodisperse macromolecules with a regular and highly branched three-dimensional architecture consisting of a core, branching points and surface groups. This class of polymeric material were first synthesised during the late 1970s into early 1980s by Vögtle and co-workers,[45] Tomalia *et al*[46] and Newkome *et al*.[47] The technique used during the first reports of dendrimer synthesis was referred to as divergent growth. The divergent method is often a repetitive two-step process, whereby the reaction starts at a multifunctional core to which layers of repeat units are attached consecutively. The unreactive terminal groups are activated to create bonding sites for the next generation of growth. The divergent approach is very effective for the preparation of large dendrimers but, unfortunately, incomplete reaction steps and unwanted side reactions may lead to a low yield and polydisperse products. As a response to the weaknesses of the divergent approach, Hawker and Fréchet[48] first reported a convergent growth approach, during which, the dendrimer growth begins at the periphery and proceeds to the core. This method provided a greater control over the preparation of dendrimers and reduced the need for excess reagents; however, product yields were still a problem. During recent years, click reactions have been developed providing simplified and faster routes to dendritic materials, employing diels alder reactions,[49] thiol-ene reactions[50] and azide-alkyne reactions.[51]

Since their discovery, dendrimers have been studied for many different applications, in particular towards biomedical applications.[52] The first successful encapsulation experiments utilising dendrimers was reported by Meijer *et al*.[53] A water soluble poly(propylene imine) dendrimer (64 functional groups at the periphery) with a diameter of ~5 nm was used to encapsulate a host molecule named Bengal rose dye and prolonged heating was required to promote release of the dye. To date, there are numerous examples of dendrimers being evaluated as potential drug delivery vehicles in the literature[54] and an example of a current tumour targeting dendrimer is the generation 3 PEG_x-poly(amidoamine) which is conjugated to folic acid, PEG, and doxorubicin as an anti-cancer therapy.[55]

Despite continued efforts to improve dendritic materials, the synthesis remains very challenging, time consuming and expensive. As an alternative to dendrimers, 'hyperbranched polydendrons' have been developed by Hatton *et al*, describing the synthesis of new dendritic branched polymer hybrids for drug delivery applications (Figure 1.5). The preparation of hyperbranched polydendrons combines controlled radical polymerisation, hyperbranched vinyl polymerisation and linear dendritic hybrids to form this new polymer architecture. These materials present a new approach to maintain surface functionality within a relatively rapid time scale, yet bypass the extensive dendrimer synthesis.[56]

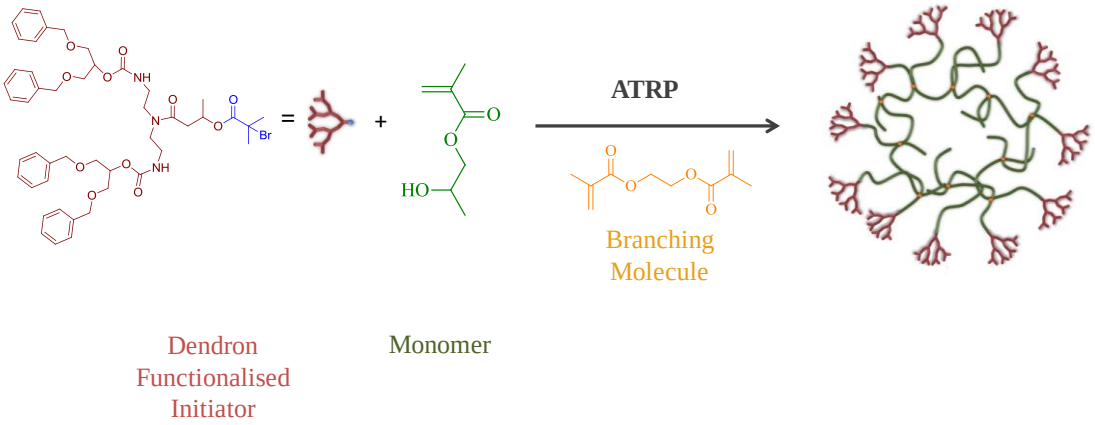

Figure 1.5 Schematic representation of the formation of a hyperbranched polydendron. *Adapted from ref*[56]

1.3 Polymer nanoparticles

The research interest in polymer nanoparticles has increased dramatically, as can be seen by the number of publications each year when searching for "polymer nanoparticle" using the scientific database, SciFinder (April 2015) (Figure 1.6).

Nanoparticles are generally defined as solid, colloidal particles within the range 10 –1000 nm.[27] The term nanoparticle encompasses both nanospheres and nanocapsules to which the drug of interest can be dissolved, entrapped, absorbed, attached, and encapsulated into the nanoparticle. Nanospheres have a 'matrix like' structure whereby active compounds can be firmly adsorbed at their surface or dissolved/entrapped in the core, whilst nanocapsules have a core-shell morphology with the drug molecule dissolved within the core by a unique polymer membrane or, in some cases, adsorbed at the surface.[57]

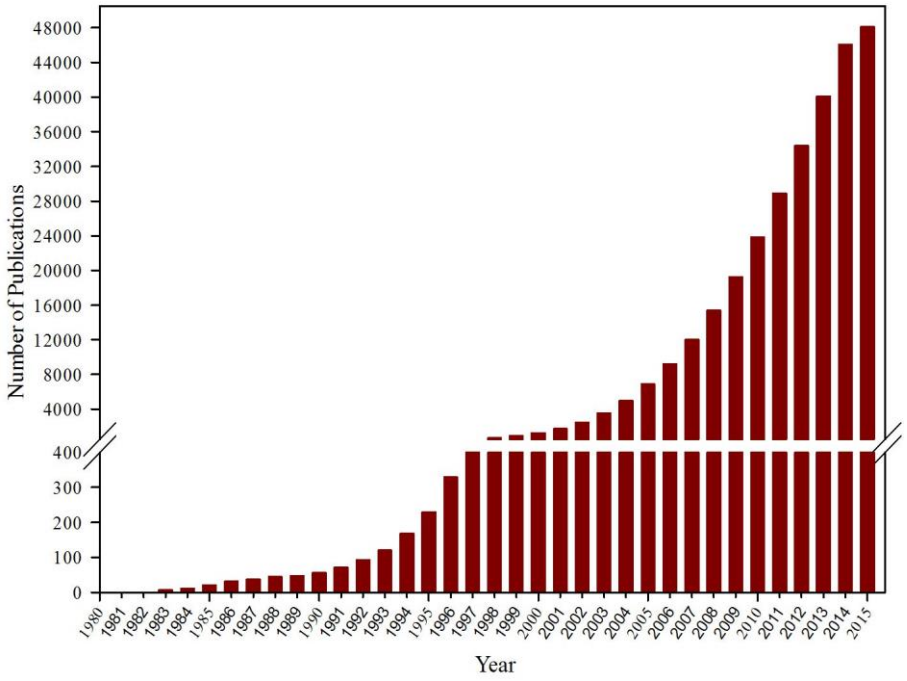

Figure 1.6 Graphical representation of the number of publications cited in SciFinder® based on the search term 'Polymer nanoparticle' (1980 - April 2015).

1.3.1 Preparation of polymer nanoparticles

Polymer nanoparticles can be prepared by both polymerisation of monomers and by use of preformed polymers during the following processes; emulsion diffusion, emulsion evaporation, double emulsification, emulsion-coacervation, layer by layer, polymer coating and nanoprecipitation.[57] The general fabrication processes for the formation of nanoparticles are outlined below (Figure 1.7). Collectively, these methods offer control over key parameters such as particle diameter, polydispersity, encapsulation efficiency, porosity and drug compartmentalisation for preparation of spherical nanoparticles.[58]

The emulsion–evaporation method (Figure 1.8) has also been employed for the preparation of nanoparticles and in terms of experimental technique, is closely related to the nanoprecipitation process.[59] Emulsion-evaporation is often preferable over other emulsification methods as the experimental conditions are often milder than for the other techniques. During a typical emulsion-evaporation experiment, the organic solvent, organic compound, water and stabiliser are emulsified in an aqueous solution, which is then exposed to a high-energy source, such as a homogeniser.

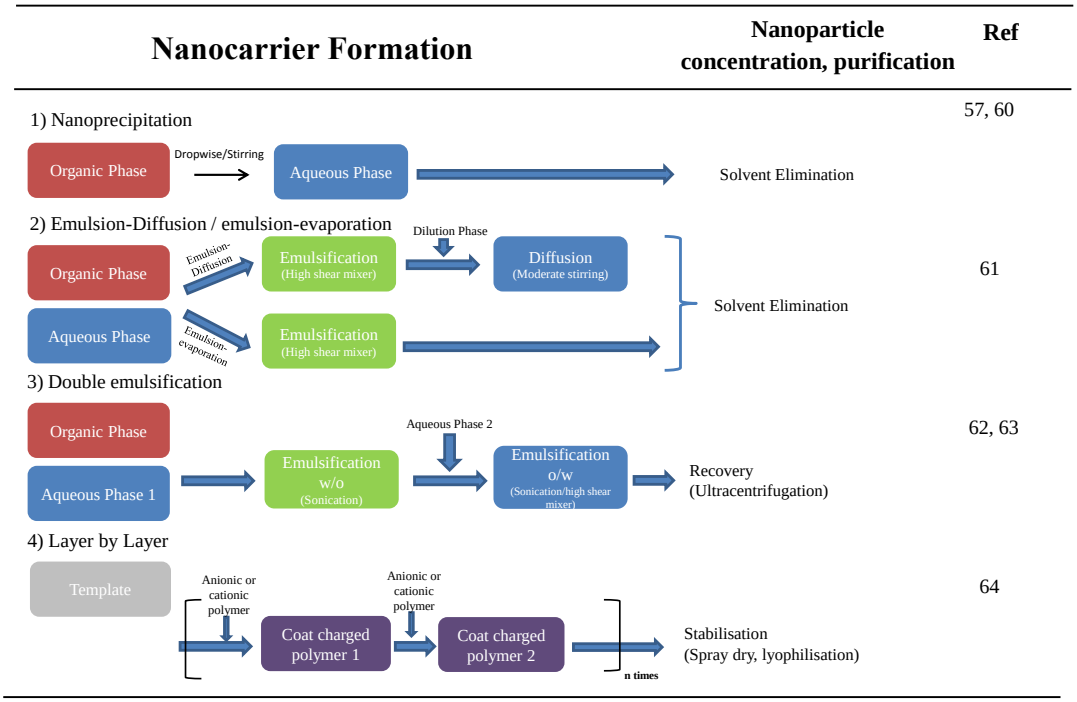

Figure 1.7 Most frequently used processes for formation of nanoparticles. *Adapted from ref*[57]

The subsequent removal of the organic solvent by vacuum, heat, or both results in the formation of an aqueous dispersion of particles. Although there have been many reports of this technique being used for nano-encapsulation,[65] the majority of research has been focused upon micro-encapsulation and, unlike nanoprecipitation,[57] this still requires a high energy source. Due to this, no further discussion will be presented.

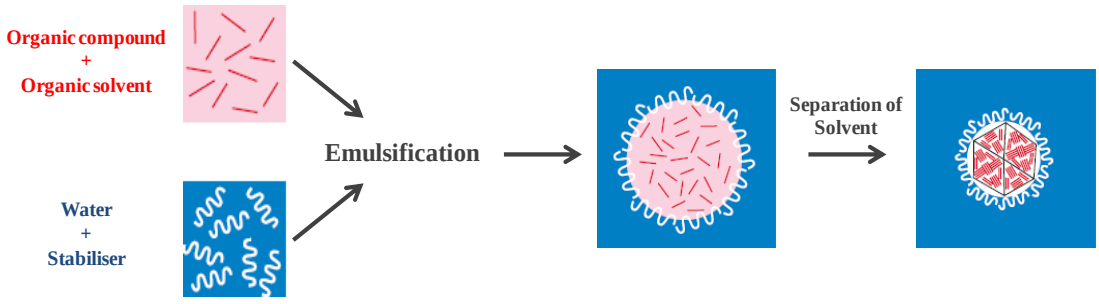

Figure 1.8 Schematic representation of the emulsion-evaporation technique**.** *Adapted from ref*[59]

1.3.2 Preparation of non-spherical polymeric nanoparticles

The majority of research into the properties and applications of polymer nanoparticles has been focused upon the formation of spherical morphologies as discussed above, and there is limited knowledge of shape effects. Non-spherical nanoparticles of varying shape and architectures have been prepared, named polymer nano-objects (PNOs) which are not

limited to but include, worms, branched worms, disks and ribbons.[66, 67] Preparation strategies often include grafting chemistry and block copolymer self-assembly which both result in a narrow size distributions. An example includes the preparation of hairy spherical PNO's which are composed of a cross-linked block copolymer which has been modified with fluorescent dye molecules[68] and super-paramagnetic Fe_2O_3[69] for early biomedicine applications. The lack of research into this area is due to the extensive difficulties in preparation and synthesis of these polymer structures. However, scientists have demonstrated that the shape of nanoparticles does have a large effect *in vivo* and *in vitro* so there is clearly a need for investigation into this area further.[70]

In contrast to the bottom-up approaches, previously discussed for formation of spherical nanoparticles, is the particle replication in non-wetting templates (PRINT) strategy; a top-down fabrication method which has been more recently developed (Figure 1.9). PRINT enables independent control over nanoparticle size, shape, surface chemistry and composition. There are a wide range of biocompatible and biodegradable polymers which are compatible with the PRINT technology.[71] Although the PRINT process has been successful, due to the top-down fabrication process of the nanomaterials they are not within the scope of this work and polymeric nanoparticles *via* nanoprecipitation will be the focus of later discussion.

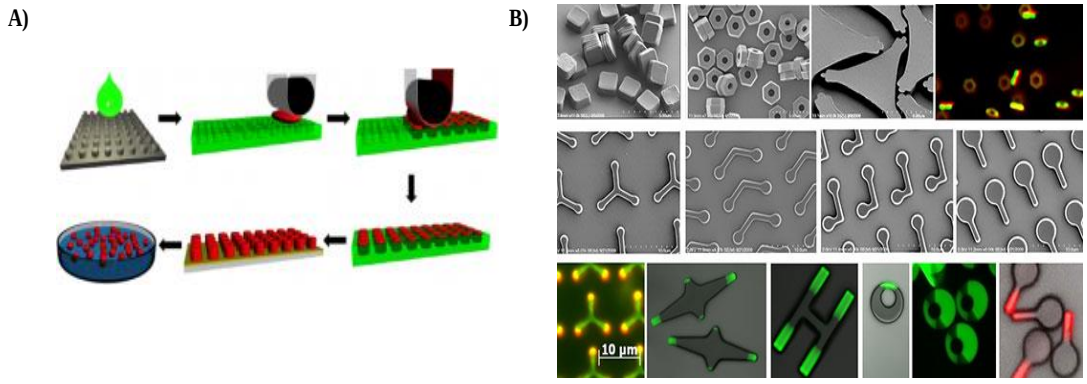

Figure 1.9 Particle Replication in Non-wetting Templates (PRINT) technologies A) Schematic representation of the PRINT process B) Examples of various PRINT particles. **Taken from ref*[72]

1.3.3 Nanoprecipitation

The formation of spherical nanoparticles *via* nanoprecipitation has most relevance to the research presented within this thesis, and will be discussed in detail below. Nanoprecipitation is the most commonly used of the nanoparticle preparation methods and accounts for ~50% of the nanoparticles reported (Figure 1.10). This technique, also known as solvent displacement or solvent shifting, was first developed by Fessi *et al* in 1989.[60] The technique employs a solution of hydrophobic polymer within a good, water-miscible organic solvent, followed by addition to water as a miscible anti-solvent; the order of addition can also be reversed so that the anti-solvent can be added to the polymer dissolved in the good solvent. The organic solvent is usually water miscible and volatile (e.g. acetone) and can be quickly removed to leave the nanoparticles as an aqueous dispersion.

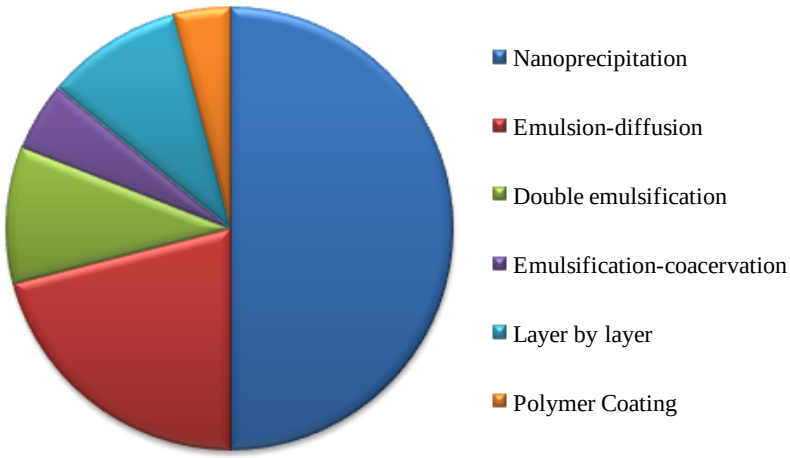

Figure 1.10 Method selection for nanoparticle preparation.******Adapted from ref*[57]

There are two main preparation techniques which can be applied to the manufacturing of polymeric nanoparticles *via* nanoprecipitation, namely dialysis and the dropping technique[73] (Figure 1.11 A). The dropping technique is often preferred because any miscible solvents can be used, which reduces the cost of consumables such as dialysis tubing, and is overall less time consuming. However, dialysis is a milder process and enables the complete removal of any monomers or initiator molecules, which may still be present from previous polymerisation steps. Both methods differ from each other in the rate of nanoparticle formation; the dropping technique instantly shocks the system whereas dialysis takes a long time to equilibrate and polymers are slowly introduced to the poor solution environment. Generally, both methods enable a controlled and complete

exchange of solvents, including solvents with high boiling points (i.e. DMF, DMSO) and depend highly upon the choice of solvent/non-solvent, temperature, agitation speed (if necessary) and the polymer concentration.[73] In addition to dialysis and the dropping technique, nanoparticles can also be prepared by microfluidics, a technique that is still in the early stages of development but has shown a great potential for the preparation of nanoparticles on a large scale (Figure 1.11 B).[74-76]

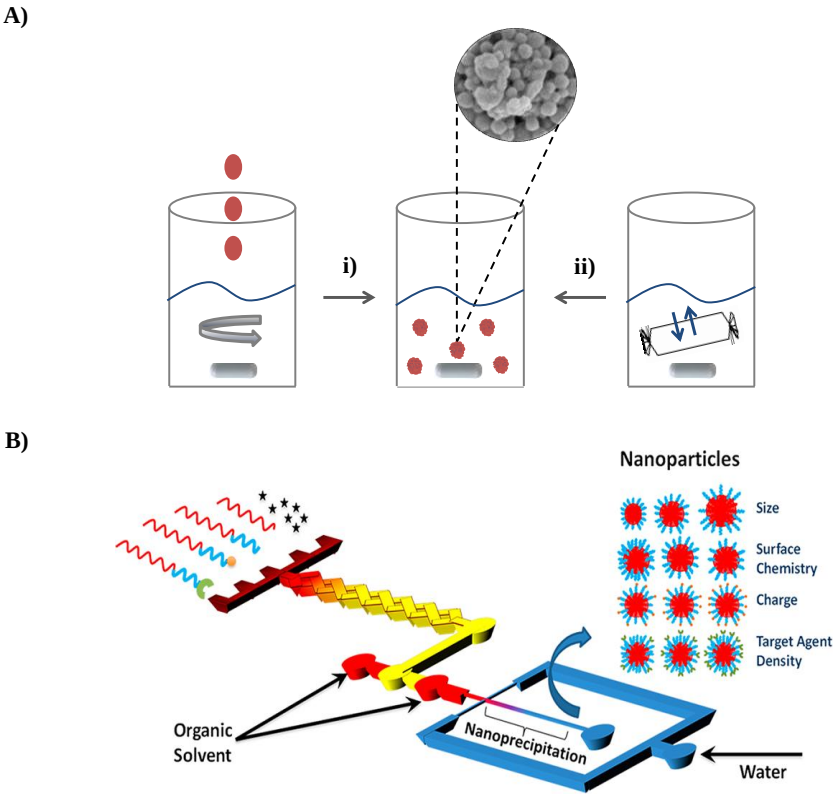

Figure 1.11 Schematic representation of nanoprecipitation techniques, A) i) Drop nanoprecipitation, ii) dialysis. *Adapted from ref*[77] B) Microfluidics. *Taken from ref*[75]

The nanoprecipitation technique does not require an external energy source (e.g. high-energy mixing or sonication) and can be regarded as a low input procedure with low cost in comparison to the previously discussed emulsion techniques. In contrast to the preparation of nanoparticles *via* emulsion methods, surfactants are not necessarily required for nanoprecipitation, which can have an effect on the surface characteristics and increase toxicity of the nanoparticles. Additionally, a broad variety of solvents, such as acetone or DMSO, can be utilised. The size and shape of nanoparticles can be influenced by changing concentration, solvent/non-solvent selection, and preparation technique.[73]

1.3.4 Theoretical background to nanoprecipitation

The proposed mechanism for nanoprecipitation can be divided into three stages; nucleation, growth and aggregation. Firstly, polymeric materials are dissolved in a 'good' solvent (Figure 1.12 i), followed by addition to the anti-solvent. At this stage, the polymer progressively collapses to form nuclei and the solvent and anti-solvent exchange (Figure 1.12 ii&iii). The small nuclei increase in size, aggregate to form swollen assemblies and grow until they reach a colloidally stable size (Figure 1.12 iv-vi). Finally, the assemblies desolvate and decrease slightly in hydrodynamic diameter (Figure 1.12 vii).

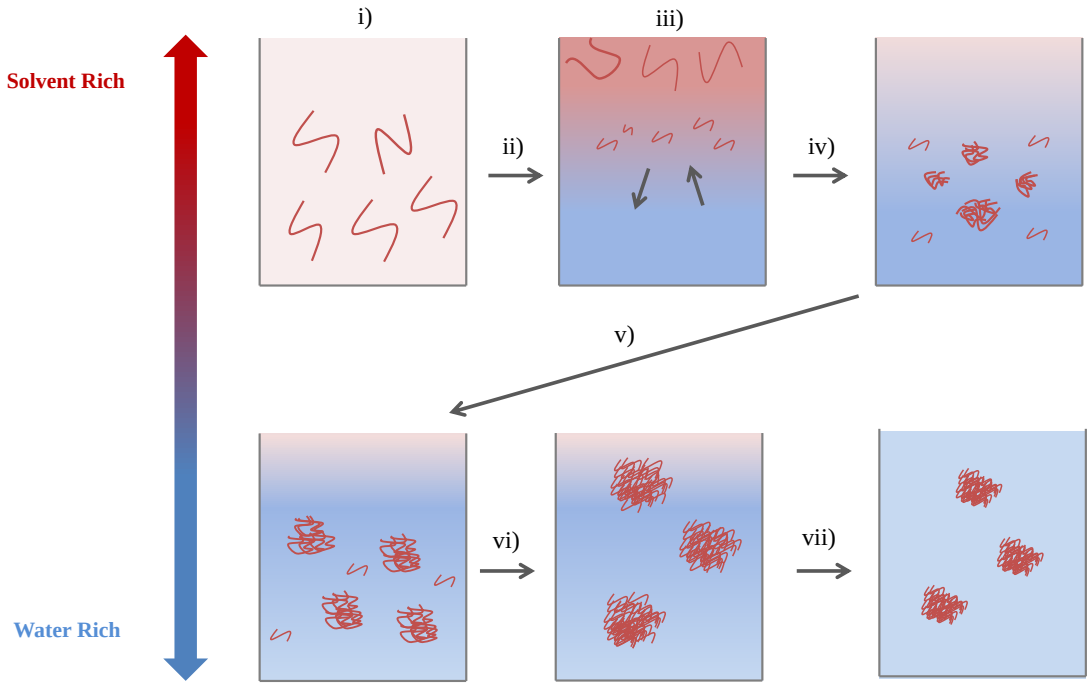

Figure 1.12 Schematic representation of the nanoprecipitation approach, i) solubilisation of polymer molecules in a 'good' solvent, ii) addition of polymer in good solvent to anti-solvent, iii) exchange of 'good' and anti-solvent, iv) association of polymer molecules in an increasing concentration of anti-solvent, v) progressive collapse of solvated polymers to form nuclei, vi) association of nuclei to form swollen assemblies vii) desolvation of assemblies, resulting in a slight decrease in hydrodynamic diameter.

The rate of these stages, especially aggregation, strongly correlates with the polymer concentration and consequently the viscosity of the solution.[56, 78] A low viscosity is favoured due to the reduced possibility of entanglements between polymer chains, which can reduce the potential of nanoparticle formation or, in some cases, result in polymer precipitation. The amount of polymer added to the anti-solvent is also an important factor in order to obtain colloidally stable nanoparticles.

1.3.5 Examples of nanoprecipitation

Examples of the most often used polymers for nanoprecipitation include; poly(lactic acid) (PLA), poly(lactic-*co*-glycolic acid) PLGA and poly(caprolactone) (PCL) (Figure 1.13 A, B, C respectively) due to their evident biocompatibility and bioavailability, which are necessary when considering a new candidate for drug delivery (Figure 1.13). Other alternative polymeric materials such as poly(styrene), poly(methacrylates) (Figure 1.13 D), poly(cyanoacrylates), poly(methyl vinyl ether-*co*-maleic anhydride) and cellulose derivatives have also been investigated. Recent research has reported nanoprecipitation of block copolymers, which form core-shell structures due to their amphiphilic nature. This approach has been very successful for the large-scale generation of polymer nanoparticles under clinically relevant conditions as highlighted in different reports of positive Phase II human clinical trial results from nanoprecipitates. The formulations were derived from linear A-B block copolymers from poly(ethylene glycol) and PLGA or Accurin technology (will be discussed in Section 1.4.1).[79-81] The small range of polymers which have been investigated using the nanoprecipitation technique are shown in Table 1.1, and to date the influence of polymer architecture and further mechanistic studies of nanoprecipitation have not been widely studied.[82]

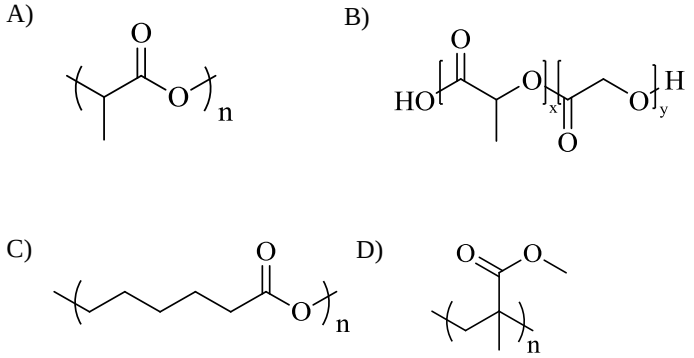

Figure 1.13 Examples of polymers used for nanoprecipitation A) Poly(lactic acid) (PLA); B) Poly(lactic-*co*-glycolic acid) (PLGA) C) Poly(caprolactone) (PCL) D) Poly(methyl methacrylate) (PMMA).

Closely related to the research within this thesis, Slater *et al* reported the first controlled nanoprecipitation of branched poly(2-hydroxyl propyl methacrylate) in the absence of stabilisers.[82] The branched polymer nanoparticles were within a controllable size range of 60-800 nm, which was governed by the primary chain length and nanoparticle conditions. They were also stable to other external conditions such as temperature. When compared with linear *p*(HPMA), the formation of nanoparticles using branched *p*(HPMA) demonstrated

enhanced stability for extended periods of time, suggesting the formation of nanoparticles can be architecture dependant and the use of branched polymers for the preparation of nanoparticles *via* nanoprecipitation is yet to be further investigated.

1.4 Clinical application and design of polymer nanocarriers

During the last two decades, there has been significant progress in the field of nanomedicine, including the control of physical, chemical and biological properties of nanocarriers, their stability in physiological environments (i.e. blood) and distribution to target sites. Polymeric nanoparticles offer a versatile approach for a range of both therapeutic and biomedical applications and continue to enter clinical trials (Table 1.2). To date, many clinically administered drug molecules have a short half-life in the blood stream and a high clearance rate due to their relatively low molecular weight (> 500 g/mol) and when administrated, diffuse rapidly into healthy tissue and are distributed evenly throughout the body. Consequently, minimal amounts of the drug reach the target site and unwanted side effects are experienced. These disadvantages are mainly associated with drugs which have a narrow therapeutic index, such as anti-cancer agents, which limit the higher doses due to toxic side effects and therefore less effective treatments.[42] Polymeric based nanocarriers have demonstrated great potential towards the enhancement of transport of drug molecules for a wide range of diseases, mainly cancer but also conditions including but not limited to diabetes,[83] renal failure,[84] asthma.[85]

1.4.1 Approved and preclinical drug delivery nanocarriers

Early examples of nanocarrier drug delivery systems were based on liposomes and polymer-drug conjugates. One of the first non-targeted, liposome-encapsulated nanotherapy, containing doxorubicin (Doxil®), was approved for use in 1995 (Table 1.2) by the US Food and Drug Administration (FDA). Doxil® is an intravenously (IV) administered therapy which was originally developed for HIV-related Kaposi's sarcoma and later approved for ovarian and metastatic breast cancer (Table 1.2).

Table 1.1 Examples of polymer nanoparticles prepared *via* nanoprecipitation.

Polymer	Good Solvent	Anti-solvent	Encapsulated molecule	Surfactant	Size (d. nm)	Ref
PMMA	DMF	H_2O	-	Poly(*N*,*N*-dimethylacrylamide) Poly(poly(ethylene glycol)methacrylate) Poly(2-methoxyacrylate-*co*-poly(ethylene glycol)acrylate)	130-225	[86]
PMMA	Acetone	H_2O	-	-	95-150	[78]
PLGA	ACN	H_2O	Procaine HCl	-	160-210	[87]
PLGA	Acetone	H_2O	Curcumin	Poly(vinyl alcohol)	95-560	[88]
PLGA	Acetone/Ethanol	H_2O	DiI	Tween 20	65-90	[89]
PCL	Acetone	H_2O	Griseofulvin	Polysorbate 80	250-400	[90]
PCL	Acetone	H_2O	Primidone	PE/F68	310-350	[91]
PCL	Acetone	H_2O	Spironolactone	Span 20	740-925	[92]
PLA	THF	H_20	-	-	100-300	[93]
PLA	Acetone	H_2O	MTP-Chol	Synperonic PE/F68	200-300	[94]
PHPMA	Acetone	H_2O	-	-	60-800	[82]
PLGA	Acetone, ACN	H_2O	Ubiquinone	-	165-170	[95]
PS	THF	H_2O or H_2O/NaCl	-	-	50-300	[96]

The Doxil® liposomal formulation is composed of hydrogenated soya phosphatidylcholine, cholesterol and PEG modified phosphatidylcholine.[97] This formulation has been proven to significantly reduce cardiotoxicity, enhance its deposition in tumours and increase drug circulation half-life when compared with freely administered doxorubicin.[98, 99] Further examples of liposome encapsulated doxorubicin therapies that have been approved include; Myocet® and Daunoxome® (Table 1.2).

Another nanocarrier system which has been extensively investigated and approved for clinical applications are polymer-drug conjugates.[4,1] PEG, has been one of the most widely studied polymers for polymer-drug conjugate systems due to its biocompatibility and versatility. Polymer-drug conjugates have a prolonged circulation *in vivo* and have demonstrated the ability to reduce cellular uptake *via* the endocytic route which in turn enhances the delivery of drugs to target sites with leaky blood vessels e.g. tumours.[100] During 1994, Oncaspar® (PEG-$_L$-asparaginase) became one of the first polymer-drug conjugates to receive approval by the FDA for the treatment of acute lymphocytic leukaemia *via* IV administration. Other approved PEGylated therapeutics include Adagen® (PEG–adenosine deaminase), for treatment of severe combined immunodeficiency disease, and Genoxal-PM® for breast cancer therapy. Many other examples have been approved and others are in phase I-III clinical trials, as shown in Table 1.2. In addition to PEG, another hydrophilic polymer used for polymer-drug conjugates is *N*-2-hydroxypropyl methacrylamide. This polymer provides functional side chains for drug attachment or addition of targeting ligands. It is also non-toxic, biodegradable and can improve aqueous drug solubility. Examples include ProLindac currently in Phase II clinical trials for the transport of the active form of the approved drug oxaliplatin to tumors.[101]

Besides liposomes and polymer-drug conjugates, other common nanocarrier systems that have also demonstrated therapeutic potential include polymeric micelles and polymer nanoparticles. Polymeric micelles within the 10-200 nm size range provide an ideal structure for a drug delivery nanocarrier, due to their core-shell micellar structure and loading capability. The hydrophilic shell often includes PEG which can provide a steric 'stealth' outer surface, which enhances the stability in a physiological environment, and functional groups can be incorporated for targeting.[4] The addition of stealth qualities increases the ability of a nanocarrier to avoid immune recognition, therefore, their time *in vivo* is enhanced and the chance of reaching the target is increased. PLA, PLGA, PCL and

their copolymers are all biodegradable and often synthesised to incorporate PEG, for the preparation of polymeric micelle formulations.[102, 103]

In terms of nanoparticle systems, Transdrug® is a novel formulation of poly(isohexylcyanoacrylate) loaded with doxorubicin *via* the emulsion evaporation technique and has been approved for the treatment of multidrug-resistant protein-over-expressing hepatocellular carcinoma.[104] Additionally, BIND Therapeutics, Inc. have utilised the nanoprecipitation and emulsification evaporation processes to prepare polymer nanoparticles on a large-scale under clinically relevant conditions. The polymer nanoparticles are commercially known as Accurins™ and are currently undergoing Phase II clinical trials. They are designed to have a stealth outer layer for prolonged circulation within the bloodstream, target specific sites within the body and have a controlled and timely release of encapsulated therapeutic molecules.[79, 80] (Table 1.2).

1.4.2 Design of polymeric nanocarriers towards nanomedicine

Significant research efforts continue towards the design and development of polymeric nanocarriers for drug delivery applications.[4, 39, 105] A safe and effective drug delivery system could potentially improve the performance of medicines currently on the market and assist development of new therapeutic strategies.[106] One of the current obstacles of drug delivery is poor aqueous drug solubility and there are approximately 30-40% of new drug candidates which have not been further investigated, due to problems encountered during formulation.[107] Nanocarriers show great potential for improved delivery of hydrophobic drugs and through careful design can be further modified to enhance the biodistribution of the encapsulated drug.[7] Drug encapsulation within polymer micelles and polymer vesicles is typically less than 10%.[108-110] Formulations which have demonstrated potential increased drug loading are those prepared *via* the nanoprecipitation technique.[107] An increase in drug loading levels offers the potential for an increased amount of drug at desired sites and therefore a lower dosage to achieve the same therapeutic effect of both hydrophilic and hydrophobic drug molecules. Nanomaterials continue to enter clinical trials and achieve approval, however, there are still barriers to overcome and further research is required, which forms the basis of this research project, to design polymeric nanoparticles for biomedical applications.

Table 1.2 Nanocarriers currently used for clinical practice and applications.[4, 104, 111]

Nanocarrier	Name	Compound	Administration	Disease/Condition	Status	Ref
Liposome	Doxil	Doxorubicin	Intravenous	Ovarian, metastatic breast cancer, Kaposi sarcoma	Approved	-
	Myocet	Doxorubicin	Intravenous	Breast cancer	Approved	-
	Daunoxome	Daunorubicin	Intravenous	Kaposi Sarcoma	Approved	[112]
	Markibo	Vincristine	Intravenous	Various leukemia, melanoma	II	-
	Amphotec	Colloidal suspension of lipid based amphotericin B	Subcutaneous	Invasive aspergillosis patients who are refractory to or intolerant of conventional amphotericin B	Approved	-
Polymer Drug Conjugate	Cyclosert	Camptothecin	Intravenous	Various cancers, Metastatic colon or rectal cancer	II	[113, 114]
	Oncaspar	L-asparaginase	Intravenous	Acute lymphocytic leukaemia	Approved	
	Xyotax	Paclitaxel	Intravenous	Breast, ovarian	II	[115]
	PK1	Doxorubicin	Intravenous	Breast, lung, colon	II	[116]
	PK2	Doxorubicin	Intravenous	Various cancers, particularly lung and breast	II	[117]
	DE-310	Camptothecin	Intravenous	Various cancers	I	[118]
	CT-2106	Camptothecin	Intravenous	Various cancers	I	[119]
	EZN-2208	SN38	Intravenous	Breast, colorectal, pancreatic	I	[120]
	NKTR-102	Irinotecan	Intravenous	Various cancer Breast cancer	II III	[121]
	Adagen	Adenosine deaminase ADA	Intramuscular	Severe combined immunodeficiency disease (SCID)	Approved	-
	Cimzia	TNF-a inhibitor	Subcutaneous	Crohn's disease, rheumatoid arthritis	Approved	-
	Macugen	Pegaptanib	Intravitreal	Age-related macular degeneration	Approved	-

Table 1.2 continued Nanocarriers currently used for clinical practice and applications.

Nanocarrier	Name	Compound	Administration	Disease/Condition	Status	Ref
Polymeric Micelle	Genoxel-PM	Paclitaxel	Intravenous	Breast cancer	Approved	122, 123
	ProLindac	Oxaliplatin	Intravenous	Ovarian cancer	II	101
	FCE28068	Doxorubicin	Intravenous	Liver	I/II	124
	NK911	Doxorubicin	Intravenous	Various cancers, particularly lung and breast	I	125
	NK105	Paclitaxel	Intravenous	Ovarian, breast and non-small cell lung cancer	II	126
	Estrasorb	Estradiol hemihydrate	Transdermal	Reduction in vasomotor symptoms in menopausal women	Approved	-
	Nanoxel	Paclitaxel	Intravenous	Advanced breast cancer	I	127
	SP1049C	Doxorubicin	Intravenous	Oesophageal carcinoma	II	128
	Taxotere	Docetal	Intravenous	Breast, prostate, non-small cell lung cancer,stomach and head and neck cancer	Approved	-
	Abraxane	Paclitaxel	Intravenous	Breast cancer, non-small cell lung cancer, pancreatic	Approved	129
Nanoparticle	Transdrug	Doxorubicin	Intravenous	Hepatocarcinoma	Approved	130
	Accurin	Docetaxel	Intravenous	Non-small cell lung cancer metastatic castrate-resistant prostate cancer, various cancers	II	-
	Rondel	CALAA-01	Intravenous	Tumour reduction, various cancers	I	131

1.4.3 Factors affecting the biodistribution of nanoparticles

There are many factors to consider when designing a new drug delivery nanocarrier, including size, charge, stealth and various routes of administration (Figure 1.15), which will be discussed in detail below. The surface functionalisation and addition of targeting moieties will be discussed in Section 2.2.2 under active targeting.

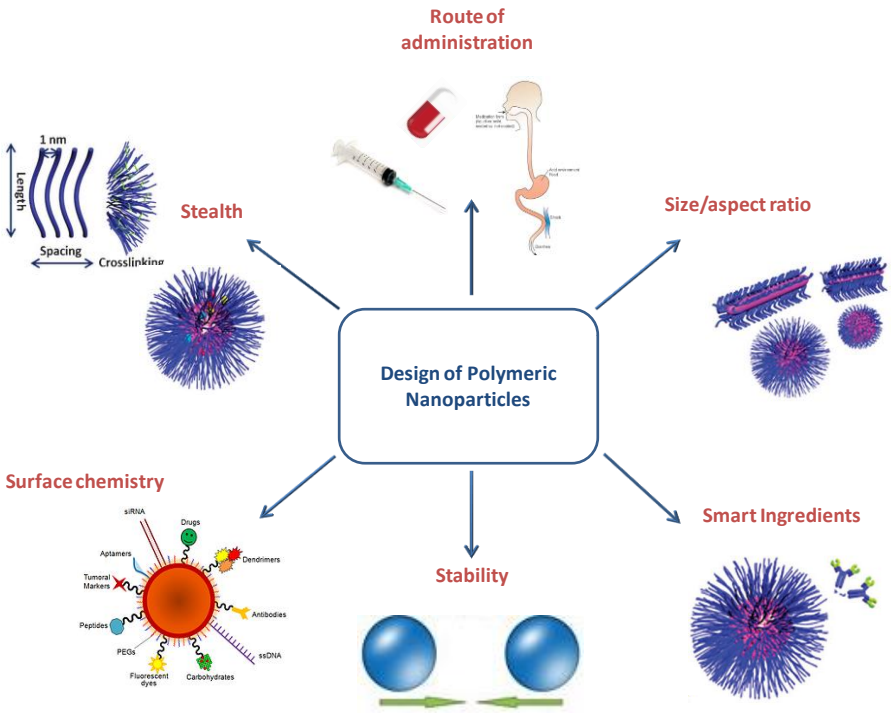

Figure 1.15 Design properties for polymeric nanoparticles. *Information from ref*[132]

1.4.3.1 Size and surface charge

The size, surface characteristics and shape of nanocarriers all play a key role within *in vivo* biodistribution. There are many reports within the literature which state that nanocarriers for therapeutics are often within the size range of 10-100 nm,[98] but further research shows this is not essential and larger particles can be just as effective *in vivo*. After IV administration, small particles < 20-30 nm are rapidly eliminated by renal clearance,[133] whereas larger particles are usually taken up by the mononuclear phagocytic system (MPS). The MPS is a vital part of the immune system, consisting of phagocytic cells, which engulf foreign particles if they have been tagged by a specific marker known as a opsonin.[134] Opsonins are blood serum proteins, which are responsible for selectivity and enable phagocytes to recognise and attack only foreign substances and not their own macromolecules. Nanoparticles between 150–300 nm are often found in the liver and

spleen and the slightly smaller range (30–150 nm) are generally located in bone marrow, the heart, the kidney and the stomach.[135] It has been reported that nanoparticles should be less than 150 nm to cross endothelial barriers, but cancerous tumour growth results in a discontinuous endothelium, therefore larger particles can penetrate due to fenestrations, which allow the passage of nanoparticles up to 780 nm.[136] The optimum size of nanoparticles for cancer treatment has been reported within the 70 – 200 nm range.[132]

The surface chemistry of nanocarriers can be modified to modulate hydrophilicity, *in vivo* circulation, bioavailability and biodistribution.[132] The interaction of nanocarriers with their local environment e.g. shape, surface charge, determines the fate of nanoparticles within the body. For example, the introduction of steric stabilisation using PEG, which has a minimal positive or negative charge, is likely to have minimal interactions. Additionally, the negative charges which dominate the surface of cells and inside blood vessels would repel any negative charge, hence a neutral polymer would have a negligible effect on uptake by the MPS. An increase in surface charge (either positive or negative) can lead to a greater clearance rate by the MPS system. Therefore, controlling the surface charge of nanoparticles is important to minimise particle loss to undesired locations.[98] The addition of targeting ligands onto nanocarriers has been extensively researched to enhance cellular uptake and maintain a high concentration of drug at desired sites for a prolonged period of time in order for their therapeutic action to take effect.[137]

1.4.3.2 Stealth nanocarriers

As briefly discussed in Section 1.4.1, nanocarriers are often coated with a hydrophilic polymer to prevent adsorption of proteins and to avoid recognition by the MPS, which can cause clearance of materials from circulation.[138] PEG is a linear or branched polyether diol, synthesised by linking repeated units of ethylene oxide to obtain a wide range of molecular weights. PEG can be modified to form a monomethoxy PEG (MeO-PEG), which can be useful in PEGylation and preparation of amphiphilic A-B and A-B-A block copolymers.[139, 140] MeO-PEG is also chemically inert and the terminal hydroxyl group enables selective reactions with many different functional groups.[141] PEG is most commonly used to coat particles, and it has been shown that the length and number of chains can have an effect on blood circulation times *vs.* elimination in clearance organs.[142-144] Additionally, PEG chains can provide steric stabilisation of particles and prevent aggregation, which is observed experimentally for charge stabilised nanocarriers.[82] There have been reports that low molecular weight PEG chains (shorter than 400 g/mol) are

transformed to toxic metabolites *in vivo* and longer PEG chains (<20 kg/mol) are likely to be excreted in urine. Although research has suggested very high molecular weight PEG (>20 kg/mol) is also excreted through kidney filtration, other pathways such as liver uptake *via* the immune system may dominate.[145] Webster and co-workers have suggested PEG chains of varying molecular weights are excreted unchanged in the urine and higher molecular weight PEG molecules generally give rise to an increase in the residence time in the body rather than a fundamental change in excretory route.[146, 147] Although the research of stealth nanocarriers has been focused upon PEG, other examples of hydrophilic polymers which have been used to coat nanoparticles include poly(acrylic acid),[148] poly(acrylamides), poly(vinyl alcohol) (PVA) and polysaccharides.[134, 149]

1.4.4 Permeation through biological barriers

In order to successfully deliver therapeutic molecules there are various biological barriers to overcome and they can be classified as external (skin and mucosa), *en route* (blood and extracellular matrix) and cellular (cellular uptake, endosomal, translocation to subcellular organelles) (Figure 1.12).[132]

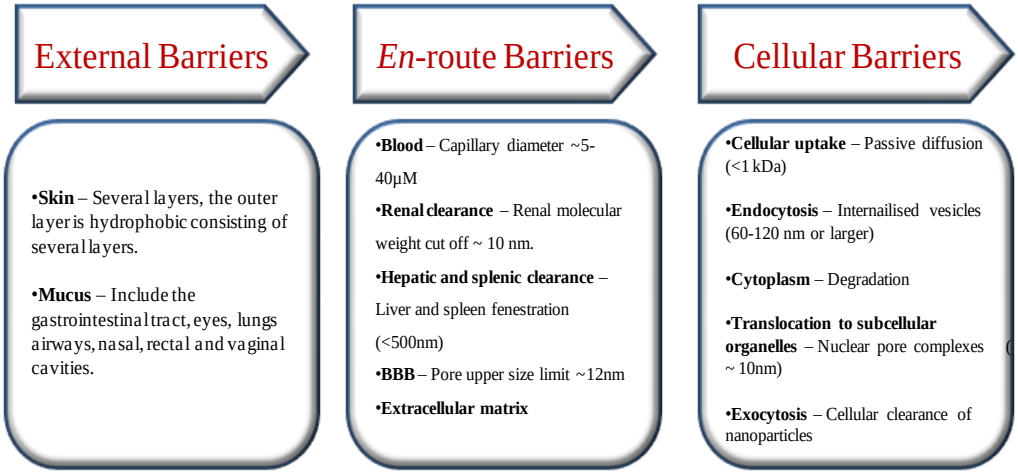

Figure 1.12 Barriers towards the delivery of nanocarriers; external, *en* route and cellular. *Adapted from ref*[132]

External Barriers. The initial external barrier will vary depending on the route of administration. The skin is made up of thick tissues; stratum corneum (10 – 20 µm), epidermis (50 – 100 µm), dermis and subcutaneous tissues (1 -2 mm).[150] The dermis and subcutaneous tissues have a rich blood supply, which can be used for trandermal delivery; however, the lipid bilayers of the stratum corneum must be penetrated for permeation through the skin.

Mucus is a viscoelastic gel, which is secreted by mucosal glands to protect the lung airways, gastrointestinal (GI) tract, eye and other mucosal surfaces. Mucus is a viscous and sticky layer which lines tissues to trap and remove foreign particles and other hydrophobic molecules.[151] Oral drug delivery *via* the GI tract can be challenging due to the presence of digestive enzymes and an extreme pH switch from 1 to 3.5 in the stomach to and pH 5 to 7 in the small intestine.

En-route Barriers. The injection of polymer nanocarriers into the systemic circulation bypasses the skin and mucosal barriers. Although IV is the most common method of nanocarrier administration, the procedure often lowers patient adherence as it is considered invasive and unfavourable. Adherence is defined as the extent to which patients take medication as prescribed by their healthcare providers, however, the full benefits are not often realised because approximately 50% of patients do not take their medications as advised.[152] Nanocarriers in the blood become subject to many barriers such as renal and hepatic clearance, aggregation, opsonisation and clearance by the MPS. In order to reach their intended destination, nanocarriers must avoid multiple organ clearance mechanisms such as those operating in the spleen and liver. The spleen has fenestrations which are within the range of 200–500 nm,[133] therefore particles exceeding ~200 nm must be modified in order to remain within circulation. Opsonisation, the process of elimination by phagocytes, is a major challenge *in vivo*. There are many opsonins, which adsorb onto the surface of nanocarriers and make them more susceptible for attack by the MPS.

The BBB is a highly selective, semi-permeable membrane that regulates movement of molecules from the circulatory system into the central nervous system. There are a range of methods of molecular transport for entry of compounds into the brain including paracellular diffusion, passive diffusion, active transport (*via* membrane transporters) and endocytosis. The passage across the BBB is more feasible for smaller molecules than for larger ones,[153] and there are still many transport problems since 98% of drug molecules are not able to pass from the blood to the brain.[154] Passive anti-cancer targeting of micelles, liposomes, polymer nanoparticles and dendrimers are still lacking the selectivity needed to target the brain, thus, preventing drug delivery to the central nervous system.[155]

Cellular Barriers. Cellular uptake is highly challenging and there are several biological barriers at the cellular level which nanocarriers must overcome, starting with penetration of the phospholipid cell membrane which has a cut off of ~1 kDa. Endocytosis is an energy dependent process by which materials move into a cell by engulfing extracellular fluid

(including any materials dissolved or suspended in it) without passing through the cell membrane.[132] The endocytic pathway depends on various properties of the nanoparticles including size, morphology, surface chemistry and varies from one cell line to another.[156] To date, there are three main mechanisms for the cellular uptake of nanoparticles; phagocytosis, pinocytosis and receptor-mediated endocytosis and the preferred process depends on the assisting proteins during the process.[157] Phagocytosis plays a crucial role in the defence against organisms such as bacteria, viruses and drug delivery vehicles.[158] The phagocytic process occurs in macrophages, monocytes, neutrophils and dendtritic cells.[159] Other cells which express a lower phagocytic activity include epithelial and endothelial cells.[160] Opsonisation, as mentioned briefly above, is one of the most important biological barriers to control drug delivery. Opsonin proteins are present in the blood, and bind to non-stealth nanoparticles, allowing macrophages of the MPS to easily recognise and remove them before achieving their therapeutic effect. A macrophage is a large specialised white blood cell which can remove 'unprotected' particles from the blood within seconds after IV administration.[161] As discussed previously, the introduction of PEG onto the surface of nanoparticles minimises opsonisation, which allows them to bypass recognition by the MPS and increase their circulation half-life.

Following endocytosis, entry of the nanocarrier into the endosome can trigger degradation due to the decrease in pH and the presence of enzymes. The nanoparticles or drug molecules if intact, can exit the endosomes into the cytoplasm, which is essential for them to reach the targeted subcellular organelles, if these are the target. The movement to subcellular organelles i.e. nucleus, mitochondria also can be challenging due to their membrane bound nature. Nanocarriers can also be excreted from cells *via* a process known as exocytosis.

1.5 Passive and active drug delivery

Drug targeting strategies for the preparation of nanomaterials may be classified as either 'passive' or 'active'. The properties of passively targeted nanocarriers depend upon the nanocarrier size and surface properties (no affinity ligands) which directs them towards particular organs and across biological barriers. To date, most clinically validated therapeutic and imaging nanoparticles are considered passively targeted.[162] This is due to their straightforward methods of preparation, prolonged circulation times *in vivo* and their accumulation at particular sites due to diffusive mechanisms. The PEGylated micelle formulations SP1049C and NK911 (Table 1.2) are examples of passive nanocarriers,

which are now in early phase clinical trials for treating a variety of cancers. Passive targeting was widely researched for oncology applications since tumours facilitate the accumulation of nanocarriers *via* enhanced permeation retention (EPR), which will be discussed below.

1.5.1 Passive targeting of tumours *via* the enhanced permeation retention (EPR) effect

When designing a new drug delivery vehicle, passive targeting to solid tumour sites can be achieved through the EPR, which was first reported during the 1980s by Matsumura and Maeda.[163] Since then, there have been many *in vivo* studies which have demonstrated the EPR effect using polymer-drug conjugates,[164] liposomes,[165] micelles[166] and nanoparticles.[167] Solid tumour tissue is highly heterogenous and blood vessels in tumours possess different characteristics to normal blood vessels. These characteristics include defective vascular architecture, large gaps in endothelial cell-cell junctions (varying from one tumour type to another), lack of smooth muscle layer cells and impaired lymphatic clearance of macromolecules and lipids from interstitial tissue.[168] After IV administration, the therapeutic drug molecules encapsulated within nanocarriers can passively target tumours and accumulate at much higher concentrations in tumour tissues as opposed to normal tissues/organs. When they reach normal tissue, the endothelial cells are tightly compacted and only very small molecules can penetrate them, contrasting to tumour tissue which have an unorganised arrangement of endothelial cells (Figure 1.14). Smaller molecules accumulate faster within tumour tissues, whilst larger molecules remain for a prolonged time periods. EPR is most effective with macromolecules of >40 kDa or a hydrodynamic radius from 1 - 1000 nm, and can occur in the absence of targeting ligands on nanoparticles.[169] There are a number of PEGylated polymeric nanoparticles in early phase clinical trials for treating a range of cancers *via* the EPR effect.[8, 170]

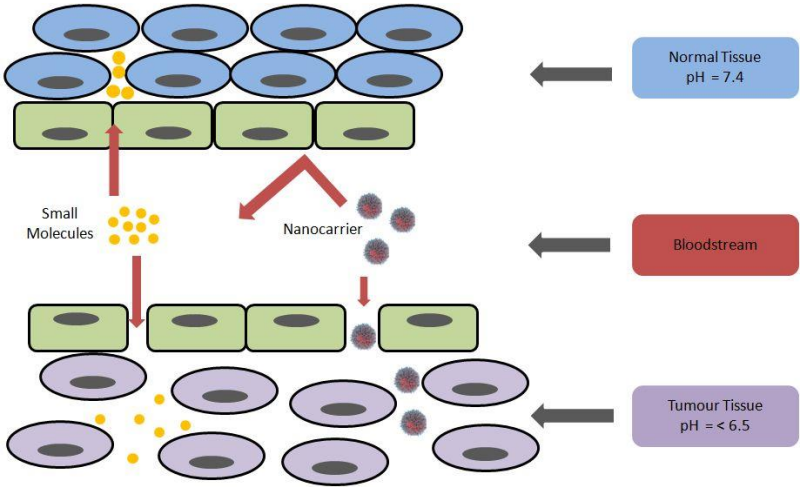

Figure 1.14 Schematic representation for passive or active targeting of drug delivery nanocarriers using the EPR effect. *Redrawn from ref*[42]

1.5.2 Active targeting

Active targeting is used to describe specific interactions between the nanocarrier and the target cells, usually ligand-receptor interactions. Targeted nanocarriers have attached ligands, which can vary from antibodies to nucleic acid aptamers, peptides or small molecules (e.g. folic acid and sugar molecules). To ensure a maximum therapeutic effect, the actively targeted nanocarriers include 'stealth' properties for prolonged circulation. Stealth nanocarriers, both actively and passively targeted, usually arrive at the tumour *via* EPR. However, there is an improvement in therapeutic effect when a drug molecule is encapsulated into targeted particles due to ligand-receptor interactions.[171, 172] The development of active therapies has been mainly focused upon cancer, as tumour cells express different molecules on their surface in comparison to normal cells. During the last 30 years, there have been no actively targeted particle formulations approved by regulatory authorities but there are a number being explored in clinical trials. Some of the targeted polymeric nanoparticle formulations undergoing clinical trials are BIND-014,[81] CALAA-01[131] and SEL-068.[8] As previously discussed, there are a number of ways to prepare polymeric nanocarriers. Most techniques make use of the self-assembly of block copolymers, with varying block solubilities. The choice of preparation technique can be dependent upon the properties of the encapsulated drug molecule and particle size requirement.

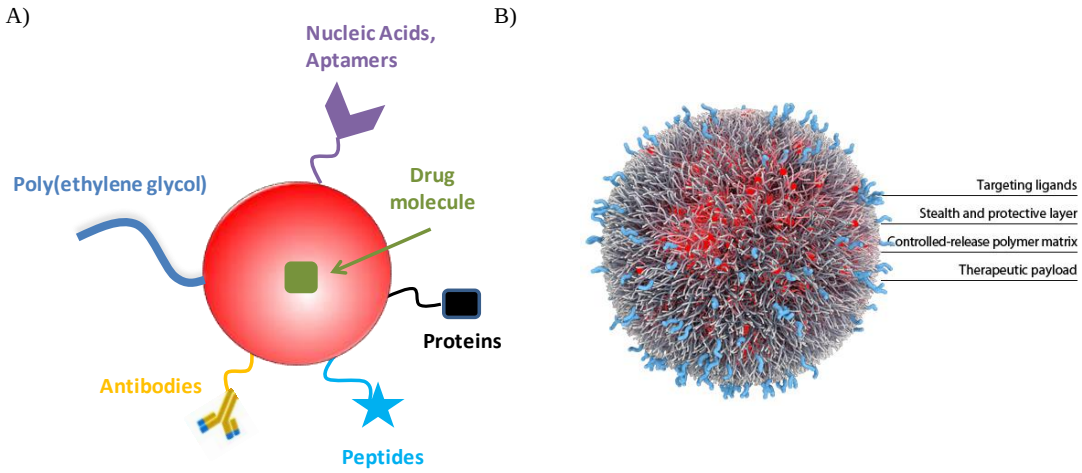

Figure 1.14 A) Schematic representation of an actively targeted nanocarrier, **B)** BIND therapeutic nanoparticles and properties to achieve selective targeting of diseased cells and tissues.[173]

The use of hydrophobic-hydrophilic PEG based A-B block copolymers during nanoparticle preparation, results in a hydrophobic core, entrapped hydrophobic drugs and a PEG shell providing steric stabilisation. BIND-014 is a prostate membrane specific antigen targeted docetaxel encapsulated polymeric nanoparticle formulation and is prepared *via* nanoprecipitation on a large-scale. This formulation has demonstrated promising preliminary results in an open label Phase II clinical study in 40 patients.[173] It is evident that actively targeted particles require a much more complex formulation process, expensive ligands, complex scale up and difficulty to make large quantities for *in vivo* studies.

1.6 Aims of the project

1.6.1 Previous research

Previous literature has compared the architectural effect of linear and branched hydrophobic polymers and their formation of aqueous nanoparticles *via* nanoprecipitation, however, only the branched polymer derived nanoparticles were stable for extended periods of time. Unfortunately, their stability was compromised during small additions of an electrolyte such as NaCl, as they are charge stabilised, as shown by their highly negative zeta potential (ζ).[82] This limited the application of the nanoparticles as potential drug delivery vehicles, because after introduction of buffers/salts to the system to mimic the electrolyte concentration in the blood, the nanoparticles became unstable and aggregated.

More recently, Hatton *et al* introduced the concept of hyperbranched polydendrons and the preparation of aqueous nanoparticles from these materials. The synthesis of hyperbranched polydendrons, and subsequent polymerisation of dendron functionalised initiators, presents a fast and efficient one step synthesis to combine dendrons and maintain surface functionality, without the need for complex dendrimer synthesis. Polymer nanoparticles were then prepared *via* nanoprecipitation and due to the hydrophobic nature of dendron and monomer, a highly negative ζ was obtained, which is representative of charge stabilisation.[56] Similar to the branched nanoparticles discussed above, pharmacology testing was limited, as the addition of an electrolyte to the hyperbranched polydendron nanoparticles resulted in aggregation.

As a continuation of the hyperbranched polydendron research, Hatton *et al* described the preparation of hydrophilic PEG modified polydendron nanoparticles and their permeation through a model gut epithelium. As previously discussed, many successful drug delivery systems include a PEG coating on the outer surface to improve their bioavailabilty and biocompatabilty. In order to achieve this, PEG functional groups were incorporated by the use of a mixed initiator system of PEG:dendron at various ratios during the synthesis of the branched polymers. Again, the nanoparticles were prepared *via* nanoprecipitation (Figure 1.15). The nanoparticles demonstrated potential in a gut epithelium model, but the drug loading capability is yet to be fully investigated.[174]

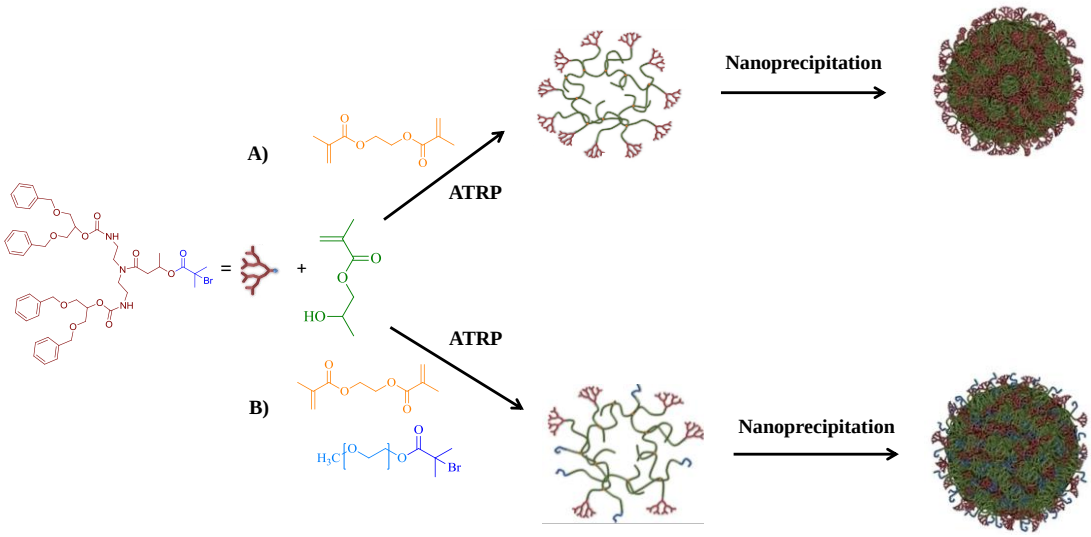

Figure 1.15 Schematic representation of idealised *hyp*-polydendron synthesis. Atom transfer radical copolymerization (ATRP) of 2-hydroxypropyl methacrylate and ethylene glycol dimethacrylate initiated by the functional G2 dendron to form, A) hyp-polydendrons; and B) inclusion of a PEG_x-initiator to form hyp-polydendrons with controlled and mixed surface functionality.

1.6.2 Project aims

The research presented here aims to investigate the potential for forming biologically-relevant polymer nanoparticles using highly branched, high molecular weight copolymers which builds upon previous reports. The lack of colloidal stability during electrolyte addition has hampered the use of these systems and direct synthetic strategies have sought to overcome this problem. Within this project, the potential to utilise combinations of amphiphilic block copolymers with branched hydrophobic copolymers will be studied, as this would provide a highly flexible platform for nanoparticle production under controlled conditions. The chemical compositions of both branched and A-B block copolymers will be varied to investigate the encapsulation of hydrophobic drug molecules and assessment of their suitability towards drug delivery applications.

1.6.2.1 Synthetic aims

The project aims to generate a series of branched high molecular weight statistical copolymers and a complementary series of linear block copolymers to investigate the effects of copolymer composition and molecular weight, within a mixed polymer nanoprecipitation process. The target synthetic aims of this project are summarised in Figure 1.16 and polymers will be prepared *via* ATRP.

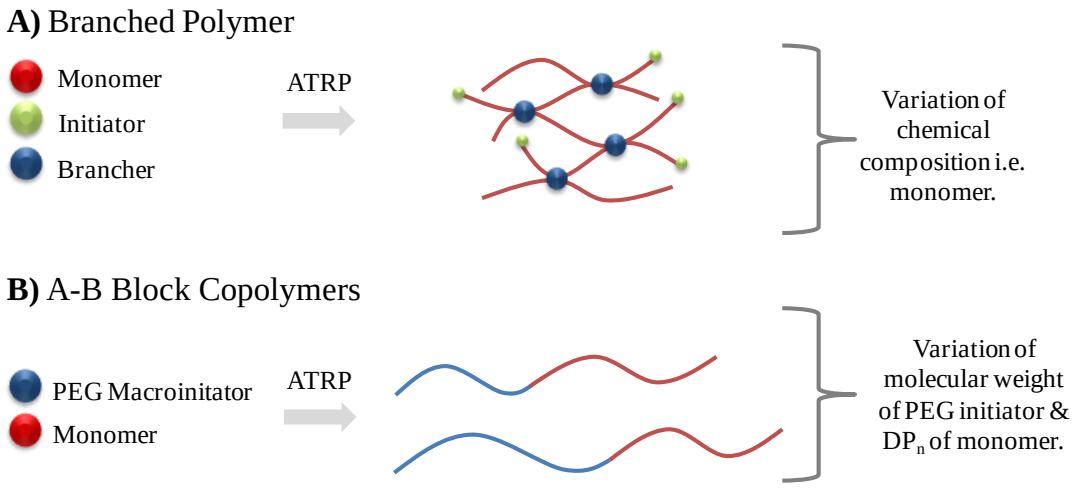

Figure 1.16 Schematic representation of the target synthetic aims of this project.

The copolymerisation of mono- and bi-functional monomers to produce high molecular weight branched polymers will not be limited to 2-hydroxypropyl methacrylate (HPMA), and will include the synthesis of polymers utilising other hydrophobic monomers such as, *n*-butyl methacrylate (*n*-BMA) and *t*-butyl methacrylate (*t*-BMA) (Figure 1.16 A). The

amphiphilic A-B block copolymers (Figure 1.16 B) will be synthesised from a PEG macroinitator and HPMA with a varying degree of polymerisation (DP_n). The ATRP polymerisation experiments appear feasible and, if successful, will provide a range of polymeric materials for subsequent nano and co-nanoprecipitation studies.

1.6.2.2 Nanoparticle formulations

After synthesis of the component materials, the formation of nanoparticles *via* the nanoprecipitation approach will be studied (Figure 1.17).

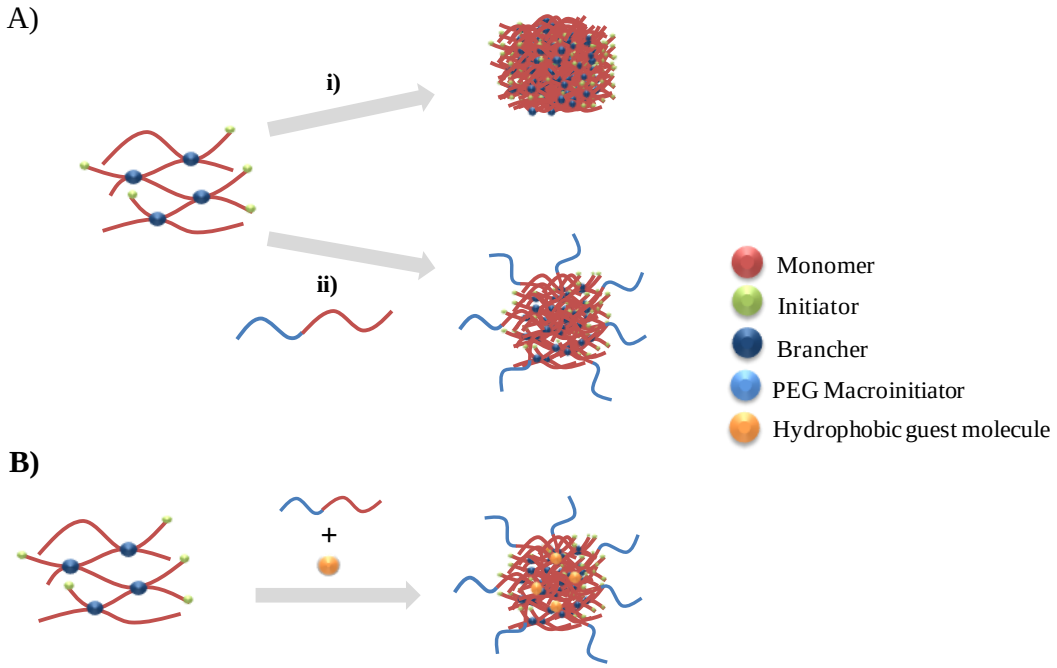

Figure 1.17 Schematic representation of the nanoparticle aims of the project for both nanoprecipitated and co-nanoprecipitated aqueous nanoparticles, **A) i)** Previously reported collapse of the branched polymer core to form charge stabilised nanoparticles; **ii)** Addition of an A-B block copolymer to potentially form sterically stabilised nanoparticles; **B)** Nanoprecipitation of a branched polymer core, A-B block copolymer and potential encapsulation of a guest molecule i.e. dye or drug.

The inclusion of an A-B block copolymer during the nanoprecipitation of a branched hydrophobic copolymer will be investigated to assess if the formation of sterically stabilised nanoparticles would be possible. It is of interest to study if non-covalently bound A-B block copolymers could become involved in the nanoprecipitation of a branched copolymer and sufficiently improve the stabilisation during the nanoprecipitation procedure. The nanoparticle compositions of branched polymer:A-B block copolymer will be varied to determine the optimum ratio in order to achieve steric stabilisation. The stability of the polymeric nanoparticles is a crucial factor if the materials are to be

considered for *in vitro* experiments; therefore, stable nanodispersions will be tested using electrolyte and buffer solutions to mimic physiological conditions. The proposed nanoparticles (Figure 1.17 B) would be expected to be composed of a hydrophobic core with PEG from the A-B block copolymer remaining on the surface providing steric stabilisation. Such nanoparticles could potentially increase loading capabilities within the high molecular weight branched core. If successful, the ultimate aim of the nanoparticles would be to encapsulate drug molecules and evaluate loading capacities.

1.6.2.3 Pharmacology studies

Polymer nanoparticles have been widely reported widely for cancer therapies but other diseases such as HIV, may receive considerable benefits if tailored materials were available. In order to determine the suitability of nanomaterials as potential drug delivery vehicles, their *in vitro* behaviour must firstly be ascertained. Cytotoxicity assays were deemed appropriate to ensure the nanomaterials were non-toxic to cells and act only as nanocarriers of the drug molecules. The route of administration of a drug delivery vehicle will determine which type of pharmacological assay is to be carried out. For example, for orally administered therapeutics, a well-known transwell plate assay using the Caco-2 cell line is typically used to predict the permeability of molecules across a model intestinal tract into the systemic circulation. This assay will be considered if nanoprecipitated nanodispersions are stable to electrolyte/buffer solutions used during these assays and if so, the dispersion will be taken forward for further studies such as apparent permeability ratios and the cellular accumulation ratio (CAR).

Alternatively, for IV administered anti-cancer therapies, it would be desirable to carry out cell viability studies and dose response experiments using a human cancer cell line, to determine if the encapsulated drug molecules are toxic to cancerous cells when encapsulated within nanoparticles and assess how this compares with the toxicity of the free drug molecules.

Overall, the research presented within this thesis aims to provide a detailed study into a modified nanoprecipitation approach, which could provide a facile route to a variety of sterically stabilised nanoparticles. Varying polymers will be studied to evaluate the versatility of the process and the nanoparticle behaviour will be thoroughly investigated with respect to ratio, chemical composition and mechanism. If stable nanoparticles are formed, the encapsulation of a range of hydrophobic guest molecules will be carried out to determine their potential within a pharmacological setting.

1.7 References

1. R. Duncan, *Nature Reviews Cancer*, 2006, **6**, 688-701.
2. M. L. Etheridge, S. A. Campbell, A. G. Erdman, C. L. Haynes, S. M. Wolf and J. McCullough, *Nanomedicine: Nanotechnology, Biology and Medicine*, 2013, **9**, 1-14.
3. www.etp-nanomedicine.eu/public/about-nanomedicine/what-is-nanomedicine, accessed June 2015.
4. L. Zhang, F. X. Gu, J. M. Chan, A. Z. Wang, R. S. Langer and O. C. Farokhzad, *Clinical Pharmacology & Therapeutics*, 2008, **83**, 761-769.
5. F. Ehmann, K. Sakai-Kato, R. Duncan, D. H. Pérez de la Ossa, R. Pita, J.-M. Vidal, A. Kohli, L. Tothfalusi, A. Sanh, S. Tinton, J.-L. Robert, B. Silva Lima and M. P. Amati, *Nanomedicine*, 2013, **8**, 849-856.
6. L. Y. Rizzo, B. Theek, G. Storm, F. Kiessling and T. Lammers, *Current Opinion in Biotechnology*, 2013, **24**, 1159-1166.
7. M. Goldberg, R. Langer and X. Jia, *Journal of Biomaterials Science, Polymer Edition*, 2007, **18**, 241-268.
8. N. Kamaly, Z. Xiao, P. M. Valencia, A. F. Radovic-Moreno and O. C. Farokhzad, *Chemical Society Reviews*, 2012, **41**, 2971-3010.
9. K. Werengowska-Ciećwierz, M. Wiśniewski, A. P. Terzyk and S. Furmaniak, *Advances in Condensed Matter Physics*, 2015.
10. S. Youqing, R. Maciej and S. Qihang, *Rational Design of Translational Nanocarriers*, Royal Society of Chemistry, 2013.
11. M. Szwarc, M. Levy and R. Milkovich, *Journal of the American Chemical Society*, 1956, **78**, 2656-2657.
12. K. Matyjaszewski and J. Xia, *Chemical Reviews*, 2001, **101**, 2921-2990.
13. G. Moad, E. Rizzardo and S. H. Thang, *Australian Journal of Chemistry*, 2006, **59**, 669-692.
14. C. J. Hawker, A. W. Bosman and E. Harth, *Chemical Reviews*, 2001, **101**, 3661-3688.
15. P. Raffa, D. A. Z. Wever, F. Picchioni and A. A. Broekhuis, *Chemical Reviews*, 2015, **115**, 8504-8563.
16. M. L. Adams, A. Lavasanifar and G. S. Kwon, *Journal of Pharmaceutical Sciences*, 2003, **92**, 1343-1355.
17. A. Blanazs, S. P. Armes and A. J. Ryan, *Macromolecular Rapid Communications*, 2009, **30**, 267-277.
18. J. Zhou, L. Wang and J. Ma, *Designed Monomers & Polymers*, 2009, **12**, 19-41.
19. P. Alexandridis, *Current Opinion in Colloid & Interface Science*, 1996, **1**, 490-501.

20. K. A. Davis and K. Matyjaszewski, *Statistical, Gradient and Segmented Copolymers by Controlled/Living Radical Polymerizations* Springer, 2002.
21. M. C. Jones and J. C. Leroux, *European Journal of Pharmaceutics and Biopharmaceutics*, 1999, **48**, 101-111.
22. J. Rodríguez-Hernández, F. Chécot, Y. Gnanou and S. Lecommandoux, *Progress in Polymer Science*, 2005, **30**, 691-724.
23. A. Rösler, G. W. M. Vandermeulen and H.-A. Klok, *Advanced Drug Delivery Reviews*, 2012, **64**, 270-279.
24. P. Alexandridis, J. F. Holzwarth and T. A. Hatton, *Macromolecules*, 1994, **27**, 2414-2425.
25. J. Nicolas, S. Mura, D. Brambilla, N. Mackiewicz and P. Couvreur, *Chemical Society Reviews*, 2013, **42**, 1147-1235.
26. D. Peer, J. M. Karp, S. Hong, O. C. Farokhzad, R. Margalit and R. Langer, *Nature Nanotechnolgy*, 2007, **2**, 751-760.
27. L. Yang and P. Alexandridis, *Current Opinion in Colloid & Interface Science*, 2000, **5**, 132-143.
28. C. Allen, D. Maysinger and A. Eisenberg, *Colloids and Surfaces B: Biointerfaces*, 1999, **16**, 3-27.
29. M. J. Lawrence, *Chemical Society Reviews*, 1994, **23**, 417-424.
30. Y. Barenholz, D. Gibbes, B. J. Litman, J. Goll, T. E. Thompson and F. D. Carlson, *Biochemistry*, 1977, **16**, 2806-2810.
31. J. Prakash Jain, W. Yenet Ayen and N. Kumar, *Current Pharmaceutical Design*, 2011, **17**, 65-79.
32. L. Zhang and A. Eisenberg, *Science*, 1995, **268**, 1728-1731.
33. S. Holder, N. J. Sommerdijk, S. Williams, R. M. Nolte, R. Hiorns and R. Jones, *Chemical Communications*, 1998, 1445-1446.
34. B. M. Discher, Y. Y. Won, D. S. Ege, J. C. M. Lee, F. S. Bates, D. E. Discher and D. A. Hammer, *Science*, 1999, **284**, 1143-1146.
35. K. Kita-Tokarczyk, J. Grumelard, T. Haefele and W. Meier, *Polymer*, 2005, **46**, 3540-3563.
36. M. Antonietti and S. Förster, *Advanced Materials*, 2003, **15**, 1323-1333.
37. P. P. Deshpande, S. Biswas and V. P. Torchilin, *Nanomedicine*, 2013, **8**, 1509-1528.
38. H. Jatzkewitz, *Hoppe-Seyler's Zeitschrift Fur Physiologische Chemie*, 1953, **297**, 149-156.
39. R. Duncan and M. J. Vicent, *Advanced Drug Delivery Reviews*, 2013, **65**, 60-70.
40. K. Hoste, K. De Winne and E. Schacht, *International Journal of Pharmaceutics*, 2004, **277**, 119-131.

41. H. Ringsdorf, *Journal of Polymer Science: Polymer Symposia*, 1975, **51**, 135-153.
42. R. Haag and F. Kratz, *Angewandte Chemie International Edition*, 2006, **45**, 1198-1215.
43. J. Khandare and T. Minko, *Progress in Polymer Science*, 2006, **31**, 359-397.
44. E. Markovsky, H. Baabur-Cohen, A. Eldar-Boock, L. Omer, G. Tiram, S. Ferber, P. Ofek, D. Polyak, A. Scomparin and R. Satchi-Fainaro, *Journal of Controlled Release*, 2012, **161**, 446-460.
45. E. Buhleier, W. Wehner and F. Vögtle, *Synthesis-stuttgart*, 1978, 155-158.
46. D. A. Tomalia, H. Baker, J. Dewald, M. Hall, G. Kallos, S. Martin, J. Roeck, J. Ryder and P. Smith, *Polymer Journal*, 1985, **17**, 117-132.
47. G. R. Newkome, Z. Yao, G. R. Baker and V. K. Gupta, *The Journal of Organic Chemistry*, 1985, **50**, 2003-2004.
48. C. J. Hawker and J. M. J. Frechet, *Journal of the American Chemical Society*, 1990, **112**, 7638-7647.
49. G. Franc and A. K. Kakkar, *Chemistry – A European Journal*, 2009, **15**, 5630-5639.
50. K. L. Killops, L. M. Campos and C. J. Hawker, *Journal of the American Chemical Society*, 2008, **130**, 5062-5064.
51. G. Franc and A. Kakkar, *Chemical Communications*, 2008, **42**, 5267-5276.
52. E. R. Gillies and J. M. J. Fréchet, *Drug Discovery Today*, 2005, **10**, 35-43.
53. E. Meijer, J. Jansen and E. De Brabander-van den Berg, *Science*, 1994, **266**, 1226-1229.
54. U. Boas and P. M. H. Heegaard, *Chemical Society Reviews*, 2004, **33**, 43-63.
55. Y. Chang, N. Liu, L. Chen, X. Meng, Y. Liu, Y. Li and J. Wang, *Journal of Materials Chemistry*, 2012, **22**, 9594-9601.
56. F. L. Hatton, P. Chambon, T. O. McDonald, A. Owen and S. P. Rannard, *Chemical Science*, 2014, **5**, 1844-1853.
57. C. Mora-Huertas, H. Fessi and A. Elaissari, *International Journal of Pharmaceutics* 2010, **385**, 113-142.
58. J. A. Champion, Y. K. Katare and S. Mitragotri, *Journal of Controlled Release*, 2007, **121**, 3-9.
59. D. Horn and J. Rieger, *Angewandte Chemie International Edition*, 2001, **40**, 4330-4361.
60. H. Fessi, F. Puisieux, J. P. Devissaguet, N. Ammoury and S. Benita, *International Journal of Pharmaceutics*, 1989, **55**, R1-R4.
61. D. Quintanar-Guerrero, E. Allémann, E. Doelker and H. Fessi, *Pharmaceutical Research*, 1998, **15**, 1056-1062.
62. W. Seifriz, *The Journal of Physical Chemistry*, 1924, **29**, 738-749.

63. N. Garti, *Colloids and Surfaces A: Physicochemical and Engineering Aspects*, 1997, **123–124**, 233-246.
64. G. B. Sukhorukov, E. Donath, H. Lichtenfeld, E. Knippel, M. Knippel, A. Budde and H. Möhwald, *Colloids and Surfaces A: Physicochemical and Engineering Aspects*, 1998, **137**, 253-266.
65. C. E. Astete, C. S. S. R. Kumar and C. M. Sabliov, *Colloids and Surfaces A: Physicochemical and Engineering Aspects*, 2007, **299**, 209-216.
66. A. Blanazs, J. Madsen, G. Battaglia, A. J. Ryan and S. P. Armes, *Journal of the American Chemical Society*, 2011, **133**, 16581-16587.
67. G. Arunagirinathan and J. R. Bellare, *Indian Journal of Experimental Biology*, 2007, **45**, 133-159.
68. Z. Li, G. Liu, S. J. Law and T. Sells, *Biomacromolecules*, 2002, **3**, 984-990.
69. G. Liu, H. Yang, J. Zhou, S.-J. Law, Q. Jiang and G. Yang, *Biomacromolecules*, 2005, **6**, 1280-1288.
70. Y. Chen, *Macromolecules*, 2012, **45**, 2619-2631.
71. J. Wang, J. D. Byrne, M. E. Napier and J. M. DeSimone, *Small*, 2011, **7**, 1919-1931.
72. http://desimone-group.chem.unc.edu/, accessed 2015.
73. S. Schubert, J. J. T. Delaney and U. S. Schubert, *Soft Matter*, 2011, **7**, 1581-1588.
74. C. Lorenzo, C. Wei, C. Dario, L. K. Orestis, H. Martyn and Z. Xunli, *Nanotechnology*, 2012, **23**, 375-602.
75. P. M. Valencia, O. C. Farokhzad, R. Karnik and R. Langer, *Nature Nanotechnology*, 2012, **7**, 623-629.
76. P. M. Valencia, E. M. Pridgen, M. Rhee, R. Langer, O. C. Farokhzad and R. Karnik, *ACS Nano*, 2013, **7**, 10671-10680.
77. C. RemziáBecer, *Journal of Materials Chemistry*, 2009, **19**, 3838-3840.
78. J. Aubry, F. Ganachaud, J. P. Cohen Addad and B. Cabane, *Langmuir*, 2009, **25**, 1970-1979.
79. J. Cheng, B. A. Teply, I. Sherifi, J. Sung, G. Luther, F. X. Gu, E. Levy-Nissenbaum, A. F. Radovic-Moreno, R. Langer and O. C. Farokhzad, *Biomaterials*, 2007, **28**, 869-876.
80. N. Kamaly, G. Fredman, M. Subramanian, S. Gadde, A. Pesic, L. Cheung, Z. A. Fayad, R. Langer, I. Tabas and O. Cameron Farokhzad, *Proceedings of the National Academy of Sciences of the United States of America*, 2013, **110**, 6506-6511.
81. J. Wright, *Nature*, 2014, **509**, S58-S59.
82. R. A. Slater, T. O. McDonald, D. J. Adams, E. R. Draper, J. V. M. Weaver and S. P. Rannard, *Soft Matter*, 2012, **8**, 9816-9827.

83. P. Fonte, F. Araújo, C. Silva, C. Pereira, S. Reis, H. A. Santos and B. Sarmento, *Biotechnology Advances*, 2015.
84. C. H. J. Choi, J. E. Zuckerman, P. Webster and M. E. Davis, *Proceedings of the National Academy of Sciences of the United States of America*, 2011, **108**, 6656-6661.
85. J. C. Sung, B. L. Pulliam and D. A. Edwards, *Trends in Biotechnology*, 2007, **25**, 563-570.
86. M. Miao, Q. Chen, C. Zhang, X. Cao, W. Zhou, Q. Qiu and Z. An, *Macromolecular Chemistry and Physics*, 2013, **214**, 1158-1164.
87. T. Govender, S. Stolnik, M. C. Garnett, L. Illum and S. S. Davis, *Journal of Controlled Release*, 1999, **57**, 171-185.
88. M. M. Yallapu, B. K. Gupta, M. Jaggi and S. C. Chauhan, *Journal of Colloid and Interface Science*, 2010, **351**, 19-29.
89. J. Chang, Y. Jallouli, M. Kroubi, X. Yuan, W. Feng, C. Kang, P. Pu and D. Betbeder, *International Journal of Pharmaceutics*, 2009, **379**, 285-292.
90. Z. Zili, S. Sfar and H. Fessi, *International Journal of Pharmaceutics*, 2005, **294**, 261-267.
91. V. Ferranti, H. Marchais, C. Chabenat, A. M. Orecchioni and O. Lafont, *International Journal of Pharmaceutics*, 1999, **193**, 107-111.
92. I. L. Blouza, C. Charcosset, S. Sfar and H. Fessi, *International Journal of Pharmaceutics*, 2006, **325**, 124-131.
93. P. Legrand, S. Lesieur, A. Bochot, R. Gref, W. Raatjes, G. Barratt and C. Vauthier, *International Journal of Pharmaceutics*, 2007, **344**, 33-43.
94. I. Seyler, M. Appel, J.-P. Devissaguet, P. Legrand and G. Barratt, *Journal of Nanoparticle Research*, 1999, **1**, 91-97.
95. B. J. Nehilla, M. Bergkvist, K. C. Popat and T. A. Desai, *International Journal of Pharmaceutics*, 2008, **348**, 107-114.
96. C. Zhang, V. J. Pansare, R. K. Prud'homme and R. D. Priestley, *Soft Matter*, 2012, **8**, 86-93.
97. S. A. Abraham, D. N. Waterhouse, L. D. Mayer, P. R. Cullis, T. D. Madden and M. B. Bally, *Methods in Enzymology*, 2005, **391**, 71-97.
98. M. E. Davis and D. M. Shin, *Nature Reviews Drug discovery*, 2008, **7**, 771-782.
99. G. Berry, M. Billingham, E. Alderman, P. Richardson, F. Torti, B. Lum, A. Patek and F. J. Martin, *Annals of Oncology*, 1998, **9**, 711-716.
100. T. Tanaka, S. Shiramoto, M. Miyashita, Y. Fujishima and Y. Kaneo, *International Journal of Pharmaceutics*, 2004, **277**, 39-61.

101. D. P. Nowotnik and E. Cvitkovic, *Advanced Drug Delivery Reviews*, 2009, **61**, 1214-1219.
102. A. V. Kabanov, E. V. Batrakova and V. Y. Alakhov, *Journal of Controlled Release*, 2002, **82**, 189-212.
103. V. P. Torchilin, *Pharmaceutical Research*, 2007, **24**, 1-16.
104. S. Sultana, M. R. Khan, M. Kumar, S. Kumar and M. Ali, *Journal of Drug Targeting*, 2013, **21**, 107-125.
105. K. Riehemann, S. W. Schneider, T. A. Luger, B. Godin, M. Ferrari and H. Fuchs, *Angewandte Chemie International Edition*, 2009, **48**, 872-897.
106. G. Orive, R. M. Hernandez, A. R. g. Gascón, A. Domínguez-Gil and J. L. Pedraz, *Current Opinion in Biotechnology*, 2003, **14**, 659-664.
107. K. M. Pustulka, A. R. Wohl, H. S. Lee, A. R. Michel, J. Han, T. R. Hoye, A. V. McCormick, J. Panyam and C. W. Macosko, *Molecular pharmaceutics*, 2013, **10**, 4367-4377.
108. F. Ahmed, R. I. Pakunlu, A. Brannan, F. Bates, T. Minko and D. E. Discher, *Journal of Controlled Release*, 2006, **116**, 150-158.
109. P. P. Ghoroghchian, J. J. Lin, A. K. Brannan, P. R. Frail, F. S. Bates, M. J. Therien and D. A. Hammer, *Soft Matter*, 2006, **2**, 973-980.
110. K. Kataoka, T. Matsumoto, M. Yokoyama, T. Okano, Y. Sakurai, S. Fukushima, K. Okamoto and G. S. Kwon, *Journal of Controlled Release*, 2000, **64**, 143-153.
111. Y. Zhang, H. F. Chan and K. W. Leong, *Advanced Drug Delivery Reviews*, 2013, **65**, 104-120.
112. N. D. James, R. J. Coker, D. Tomlinson, J. R. W. Harris, M. Gompels, A. J. Pinching and J. S. W. Stewart, *Clinical Oncology*, 1994, **6**, 294-296.
113. T. Schluep, J. Hwang, J. Cheng, J. D. Heidel, D. W. Bartlett, B. Hollister and M. E. Davis, *Clinical Cancer Research*, 2006, **12**, 1606-1614.
114. C. Young, T. Schluep, J. Hwang and S. Eliasof, *Current Bioactive Compounds*, 2011, **7**, 8-14.
115. K. Cho, X. Wang, S. Nie and D. M. Shin, *Clinical Cancer Research*, 2008, **14**, 1310-1316.
116. L. W. Seymour, D. R. Ferry, D. J. Kerr, D. Rea, M. Whitlock, R. Poyner, C. Boivin, S. Hesslewood, C. Twelves and R. Blackie, *International Journal of Oncology*, 2009, **34**, 1629-1636.
117. J. W. Hopewell, R. Duncan, D. Wilding and K. Chakrabarti, *Human & Experimental Toxicology*, 2001, **20**, 461-470.

118. O. Soepenberg, M. J. de Jonge, A. Sparreboom, P. de Bruin, F. A. Eskens, G. de Heus, J. Wanders, P. Cheverton, M. P. Ducharme and J. Verweij, *Clinical Cancer Research*, 2005, **11**, 703-711.
119. R. Bhatt, P. de Vries, J. Tulinsky, G. Bellamy, B. Baker, J. W. Singer and P. Klein, *Journal of Medicinal Chemistry*, 2003, **46**, 190-193.
120. A. Patnaik, K. Papadopoulos, A. Tolcher, M. Beeram, S. Urien, L. Schaaf, S. Tahiri, T. Bekaii-Saab, F. Lokiec, K. Rezaï and A. Buchbinder, *Cancer Chemotherapy and Pharmacology*, 2013, **71**, 1499-1506.
121. U. Hoch, C.-M. Staschen, R. K. Johnson and M. A. Eldon, *Cancer Chemotherapy and Pharmacology*, 2014, **74**, 1125-1137.
122. D. W. Kim, S. Y. Kim, H. K. Kim, S. W. Kim, S. W. Shin, J. S. Kim, K. Park, M. Y. Lee and D. S. Heo, *Annals of Oncology*, 2007, **18**, 2009-2014.
123. K. Lee, H. Chung, S. Im, Y. Park, C. Kim, S.-B. Kim, S. Rha, M. Lee and J. Ro, *Breast Cancer Research and Treatment*, 2008, **108**, 241-250.
124. R. Duncan, M. Vicent, F. Greco and R. Nicholson, *Endocrine-Related Cancer*, 2005, **12**, S189-S199.
125. Y. Matsumura, T. Hamaguchi, T. Ura, K. Muro, Y. Yamada, Y. Shimada, K. Shirao, T. Okusaka, H. Ueno, M. Ikeda and N. Watanabe, *British Journal of Cancer*, 2004, **91**, 1775-1781.
126. T. Hamaguchi, Y. Matsumura, M. Suzuki, K. Shimizu, R. Goda, I. Nakamura, I. Nakatomi, M. Yokoyama, K. Kataoka and T. Kakizoe, *British Journal of Cancer*, 2005, **92**, 1240-1246.
127. A. Madaan, P. Singh, A. Awasthi, R. Verma, A. Singh, M. Jaggi, S. Mishra, S. Kulkarni and H. Kulkarni, *Clinical and Translational Oncology*, 2013, **15**, 26-32.
128. J. Valle, A. Armstrong, C. Newman, V. Alakhov, G. Pietrzynski, J. Brewer, S. Campbell, P. Corrie, E. Rowinsky and M. Ranson, *Investigational New Drugs*, 2011, **29**, 1029-1037.
129. J. Iglesias, *Breast Cancer Research*, 2009, **11**, S21.
130. L. H. Reddy and P. Couvreur, *Journal of Hepatology*, 2011, **55**, 1461-1466.
131. J. D. Heidel and T. Schluep, *Journal of Drug Delivery*, 2012, DOI: 10.1155/2012/262731, 1-17.
132. M. Elsabahy and K. L. Wooley, *Chemical Society Reviews*, 2012, **41**, 2545-2561.
133. S. M. Moghimi, A. C. Hunter and J. C. Murray, *Pharmacological reviews*, 2001, **53**, 283-318.
134. D. E. Owens I and N. A. Peppas, *International journal of pharmaceutics*, 2006, **307**, 93-102.

135. M. Gaumet, A. Vargas, R. Gurny and F. Delie, *European Journal of Pharmaceutics and Biopharmaceutics*, 2008, **69**, 1-9.
136. S. K. Hobbs, W. L. Monsky, F. Yuan, W. G. Roberts, L. Griffith, V. P. Torchilin and R. K. Jain, *Proceedings of the National Academy of Sciences*, 1998, **95**, 4607-4612.
137. N. Jawahar and S. Meyyanathan, *International Journal of Health & Allied Sciences*, 2012, **1**, 217.
138. V. G. Kadajji and G. V. Betageri, *Polymers*, 2011, **3**, 1972-2009.
139. F. M. Veronese and G. Pasut, *Drug discovery today*, 2005, **10**, 1451-1458.
140. K. Jankova, X. Chen, J. Kops and W. Batsberg, *Macromolecules*, 1998, **31**, 538-541.
141. J. M. Harris, N. Martin and M. Modi, *Clinical Pharmacokinetics*, 2001, **40**, 539-551.
142. G. Sun, A. Hagooly, J. Xu, A. M. Nyström, Z. Li, R. Rossin, D. A. Moore, K. L. Wooley and M. J. Welch, *Biomacromolecules*, 2008, **9**, 1997-2006.
143. K. Fukukawa, R. Rossin, A. Hagooly, E. D. Pressly, J. N. Hunt, B. W. Messmore and C. J. Hawker, *Biomacromolecules*, 2008, **115**, 1329-1339.
144. E. D. Pressly, R. Rossin, A. Hagooly, K. Fukukawa, B. W. Messmore, M. J. Welch, K. L. Wooley, M. S. Lamm, R. A. Hule, D. J. Pochan and C. J. Hawker, *Biomacromolecules*, 2007, **8**, 3126-3134.
145. S. Jevševar, M. Kunstelj and V. G. Porekar, *Biotechnology Journal*, 2010, **5**, 113-128.
146. R. Webster, E. Didier, P. Harris, N. Siegel, J. Stadler, L. Tilbury and D. Smith, *Drug Metabolism and Disposition*, 2007, **35**, 9-16.
147. F. M. Veronese, A. Mero and G. Pasut, *Protein PEGylation, basic science and biological applications*, Birkhäuser Basel, 2009.
148. Y. Hu, X. Jiang, Y. Ding, H. Ge, Y. Yuan and C. Yang, *Biomaterials*, 2002, **23**, 3193-3201.
149. L. E. van Vlerken, T. K. Vyas and M. M. Amiji, *Pharmaceutical Research*, 2007, **24**, 1405-1414.
150. M. R. Prausnitz and R. Langer, *Nature Biotechnology*, 2008, **26**, 1261-1268.
151. S. K. Lai, Y.-Y. Wang and J. Hanes, *Advanced Drug Delivery Reviews*, 2009, **61**, 158-171.
152. M. T. Brown and J. K. Bussell, *Mayo Clinic Proceedings*, 2011, **86**, 304-314.
153. H. Fischer, R. Gottschlich and A. Seelig, *The Journal of Membrane Biology*, 1998, **165**, 201-211.
154. W. M. Pardridge, *Molecular Interventions*, 2003, **3**, 90.

155. J. M Rabanel, V. Aoun, I. Elkin, M. Mokhtar and P. Hildgen, *Current Medicinal Chemistry*, 2012, **19**, 3070-3102.
156. T. Iversen, T. Skotland and K. Sandvig, *Nano Today*, 2011, **6**, 176-185.
157. G. Sahay, D. Y. Alakhova and A. V. Kabanov, *Journal of Controlled Release* 2010, **145**, 182-195.
158. H. Hillaireau and P. Couvreur, *Cellular and Molecular Life Sciences*, 2009, **66**, 2873-2896.
159. A. Aderem and D. M. Underhill, *Annual Review of Immunology*, 1999, **17**, 593-623.
160. M. Rabinovitch, *Trends in cell biology*, 1995, **5**, 85-87.
161. L. Illum and S. S. Davis, *FEBS Letters*, **167**, 79-82.
162. O. C. Farokhzad and R. Langer, *ACS Nano*, 2009, **3**, 16-20.
163. Y. Matsumura and H. Maeda, *Cancer research*, 1986, **46**, 6387-6392.
164. L. W. Seymour, K. Ulbrich, P. S. Steyger, M. Brereton, V. Subr, J. Strohalm and R. Duncan, *British Journal of Cancer*, 1994, **70**, 636-641.
165. A. A. Gabizon, H. Shmeeda and S. Zalipsky, *Journal of Liposome Research*, 2006, **16**, 175-183.
166. T. Nakanishi, S. Fukushima, K. Okamoto, M. Suzuki, Y. Matsumura, M. Yokoyama, T. Okano, Y. Sakurai and K. Kataoka, *Journal of Controlled Release*, 2001, **74**, 295-302.
167. I. Brigger, C. Dubernet and P. Couvreur, *Advanced Drug Delivery Reviews*, 2002, **54**, 631-651.
168. H. Maeda, *Advances in Enzyme Regulation*, 2001, **41**, 189-207.
169. H. Maeda, *Bioconjugate Chemistry*, 2010, **21**, 797-802.
170. K. F. Pirollo and E. H. Chang, *Trends in Biotechnology*, **26**, 552-558.
171. D. B. Kirpotin, D. C. Drummond, Y. Shao, M. R. Shalaby, K. Hong, U. B. Nielsen, J. D. Marks, C. C. Benz and J. W. Park, *Cancer Research*, 2006, **66**, 6732-6740.
172. E. Ruoslahti, S. N. Bhatia and M. J. Sailor, *The Journal of Cell Biology*, 2010, **188**, 759-768.
173. www.bindtheraputics.com/about/overview, June 2015.
174. F. L. Hatton, L. M. Tatham, L. R. Tidbury, P. Chambon, T. He, A. Owen and S. P. Rannard, *Chemical Science*, 2015, **6**, 326-334.

Chapter 2

Synthesis and Characterisation of *p*(HPMA) for Investigation and Optimisation of Nanoprecipitation Conditions and Introduction to Co-nanoprecipitation

Publication from this research chapter

'Multiple and co-nanoprecipitation studies of branched hydrophobic copolymers and A−B amphiphilic block copolymers, allowing rapid formation of sterically stabilized nanoparticles in aqueous media'

Jane Ford, Pierre Chambon, Jocelyn North, Fiona L. Hatton, Marco Giardiello, Andrew Owen and Steve P. Rannard.

Macromolecules 2015, 48, 1883-1893.

2.1 Introduction

The first nanoprecipitation of hydrophobic branched copolymers comprised predominantly of poly(2-hydroxypropyl methacrylate) (HPMA) and a low molar concentration of ethylene glycol dimethacrylate (EGDMA) (*p*(HPMA$_x$-*co*-EGDMA$_y$)) were reported by Rannard and co-workers. These high molecular weight soluble architectures[1-3] produced stable nanoparticles without the need for stabilisers. These reports utilised atom transfer radical polymerisation (ATRP) to synthesise both linear and branched statistical copolymers containing either ethyl functionality at the chain ends or ideally branched dendrons of varying generation. When linear-dendritic hybrid polymers are branched, the resulting materials have been termed hyperbranched polydendrons (*hyp*-polydendrons). In most cases, uniform polymer nanoparticles were generated *via* nanoprecipitation into water, from rapidly assembling collapsed branched copolymers, which yielded diameters ranging from 60 to 800 nm.

When designing polymer nanoparticles for drug delivery applications, it is important that they can endure various biological environments, including salts and buffers, which are present in the human body. Unfortunately, nanoparticles previously prepared from *p*(HPMA$_x$-*co*-EGDMA$_y$) were charge stabilised and therefore precipitated during NaCl addition. Charge stabilised colloids can be easily de-stabilised by addition of electrolytes, due to the screening of repulsive charges by the ions present, which ultimately leads to polymer precipitation.[4] The lack of colloidal stability in electrolyte solutions has delayed the use of these systems and relatively complex synthetic strategies have sought to overcome this problem. Steric stabilisation can be achieved through the incorporation of a hydrophilic moiety to the nanoparticle, usually a hydrophilic polymer.[5] Typical hydrophilic polymers which have been used as such to stabilise hydrophobic aqueous nanoparticles include; polyethylene glycol (PEG), polycyclodextrin, polyglutamate, PLA PLGA.[6]

Nanoprecipitation of hydrophobic polymers into aqueous media is still a relatively poorly understood concept, therefore the initial studies presented in this research chapter will seek to investigate the optimum conditions for the preparation of *p*(HPMA$_x$-*co*-EGDMA$_y$) nanoparticles. To date, there have been no reports of nanoprecipitation of a branched hydrophobic polymer and A-B block copolymer to produce sterically stabilised nanoparticles. Therefore, this research aims to investigate the nanoprecipitation of the

hydrophobic copolymer *p*(HPMA$_x$-*co*-EGDMA$_y$) and a range of PEG A-B block copolymers to assess if steric stabilisation can be achieved *via* this method.

2.2 Controlled polymer synthesis

Conventional free radical polymerisation (FRP) has many advantages over other polymerisation methods, including less stringent conditions, wide range of solvents (including water) and polymerisation of an extensive range of vinyl monomers. Hence, nearly ~50% of all commercial synthetic polymers are synthesised by FRP, providing a wide range of polymers for varying applications.[7] However, the major limitations of FRP include; the poor control of the molecular weight, broad molecular weight distribution, and the difficulty (or even impossibility) of preparing well-defined copolymers or polymers with a predetermined functionality. During the last two decades, various controlled radical polymerisation (CRP) techniques have been developed that enables FRP to offer some of the benefits of 'living' polymerisations.

2.2.1 Atom transfer radical polymerisation

ATRP is among the most effective and most widely used CRP methods. This technique was first reported independently by Wang and Matyjaszewski[8] and Sawamoto[9] and co-workers during 1995. Since then, there has been a vast amount of research within this area and ATRP has become a very useful technique towards the preparation of functional polymers[10, 11] and, contrasting to FRP, ATRP enables the control of polymer molecular weight and architecture.

The general mechanism for ATRP is shown in Scheme 2.1 and a typical reaction includes a halogen initiating species (R-X), monomer and a transition metal complex (Mt^n/L). The initiating species (R-X) is abstracted by the transition metal catalyst to form both X-Mt^{n+1}/L and the initiating radical species $R^\bullet$, which occur with a rate of activation (k_{act}). During this process, the halogen undergoes a one electron redox reaction with the transition metal catalyst. The transition metal catalyst is added to the reaction in a lower oxidation state and forms the reactive species and catalyst complex in the higher oxidation state, which can then deactivate the propagating radical. The initiating radical species, $R^\bullet$ reacts with the vinyl group of the monomer *via* a radical mechanism resulting in R-$M^\bullet$ which subsequently propagates with the rate constant k_p, by further reaction with monomer units. This process reduces the concentration of active chain ends by establishing a dynamic equilibrium between the radical and the dormant species. The

equilibrium lies heavily towards the dormant species (the rate of this step is denoted as k_{deact}), therefore reducing the number of reactive chain ends present at any one time and so reducing the possibility of unwanted side reactions, which would result in higher molecular weights and broader molecular weight distributions. The mechanism of ATRP allows for the preparation of more precisely controlled polymer molecular weights with a low dispersity ($Đ$ <1.3). Termination reactions may also occur, usually as coupling or disproportionation, and the rate is denoted as k_t, however they are minimal during the reaction. Due to the presence of radicals and a transition metal catalyst, care must be taken to ensure no oxygen is present, which would scavenge radicals, terminate the polymerisation and oxidise the copper catalyst.

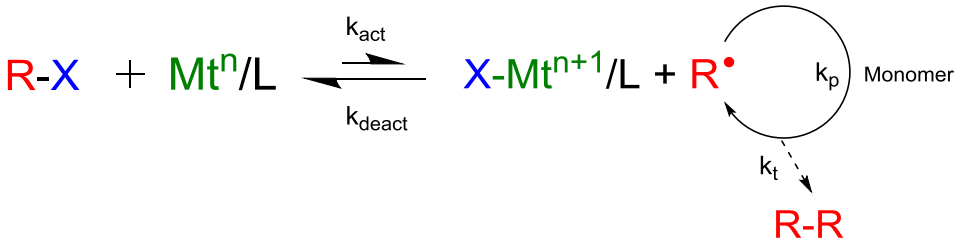

Scheme 2.1 General mechanism for ATRP.

ATRP has attracted both research and commercial interests for the following reasons; (1) relatively straight forward experimental setup, (2) compatibility with a wide range of different solvents and solvent mixtures, including water which is attractive for biomedical applications, (3) polymers can be prepared over a range of temperatures without the formation of side products, (4) use of readily available and inexpensive catalyst components and (5) commercially available or easily prepared initiators or macroinitiators, depending on the desired composition and application.[12]

2.2.2 Preparation of amphiphilic block copolymers *via* ATRP

As briefly discussed in Chapter 1 (Section 1.2.1), the self assembly of block copolymers has been extensively researched for the development of drug delivery vehicles. Block copolymers can consist of two or more distinct monomers and can have various architectures such as linear block copolymer (A-B), triblock (A-B-A), multiblock or segmented polymers (A_x-B_y) and can be prepared *via* ATRP.[13-15] Due to its radical nature, the topology of the polymer (linear, branched etc.) and the composition of the polymeric chains (statistical, grafts, block copolymers etc.) can be varied depending on the intended application. ATRP allows for the incorporation of the initiator functionality at every primary polymer chain end, which can enable functionalities such as vinyl, cyano,

hydroxyl and other groups at one end of the polymer chain, whilst the other chain end remains an alkyl halide, under ideal conditions.[16]

A wide range of well defined, near monodisperse amphiphilic block copolymers have been prepared for many applications, including drug delivery nanocarriers,[17] (Chapter 1, Section 1.2), which are the main focus of this research project. Many examples of amphiphilic block copolymers incorporate PEG as the hydrophilic component, due to its previously discussed biocompatibility and versatility with hydrophobic monomers.[18] The synthesis of polymers from a PEG isobutyryl bromide macroinitiator has been a successful route for the preparation of A-B block copolymer.[19] Some examples of monomers used for A-B and A-B-A block copolymer include (but not limited to); 2-hydroxyl ethyl methacrylate,[20] styrene,[19] *N*-isopropylacrylamide,[21] *tert*-butyl methacrylate and 2-(dimethylamino)ethyl methacrylate.[22]

2.2.3 Branched polymers *via* ATRP

Branched vinyl polymerisation has been utilised to produce various branched copolymers with varying compositions. Examples of structures achieved include; branched homopolymers, branched block copolymers, branched statistical copolymers, branched graft-copolymers and more complex structures such as shaped branched amphiphilic copolymers.[23] Various polymerisation techniques have been employed to produce branched copolymers and include; chain transfer agent mediated free radical polymerisation (Strathclyde approach),[24] atom transfer radical polymerisation (ATRP),[25] and reversible addition-fragmentation chain-transfer (RAFT) polymerisation.[26]

The use of ATRP to produce branched copolymers is most relevant to the research project and the copolymerisation of a vinyl and a divinyl monomer using ATRP was first reported during 2001.[27] Branched architectures can be prepared by incorporation of a vinyl and divinyl monomer during the polymerisation. The intention of this research was to form soluble branched copolymers as opposed to insoluble gels. During 2004, Isaure *et al.* reported the preparation of branched soluble polymers *via* ATRP,[25] utilising methyl methacrylate (MMA) and the divinyl monomer, EGDMA, to form branched *p*(MMA_x-*co*-$EGDMA_y$). Further examples of branched copolymers reported include *p*($HPMA_x$-*co*-$EGDMA_y$)[28] and polystyrene, ***p*(styrene-co-divinylbenzene)**.[29] This useful one-pot reaction has provided a route to synthesise new material architectures, including amphiphilic blocks and graft copolymers.[30] Utilising ATRP for the formation of branched copolymers produces architectures similar to those expected *via* the Strathclyde

approach,[24] however, ATRP allows for the incorporation of the initiator functionality at every primary polymer chain end.

During the early stages of a branched copolymerisation *via* ATRP, the divinyl monomer and monomer behave almost identically and the divinyl monomer incorporates into the polymer chain leaving pendant unreacted double bonds (Figure 2.1). At low monomer conversion, the ratio is so highly biased towards unreacted monomer, therefore it is not until high conversions, when the number of unreacted monomers and pendant vinyl groups becomes comparable, which results in the onset of intermolecular coupling of polymer chains. At this point, the probability of the growing chains incorporating a pendant vinyl group of another polymer chain increases, hence a large increase in molecular weight and broad molecular weight distribution. For effective initiation, experimentally the ratio of divinyl monomer/initiator should be ≤ 1, if not, then the polymer formed will be an insoluble crosslinked material or microgel.

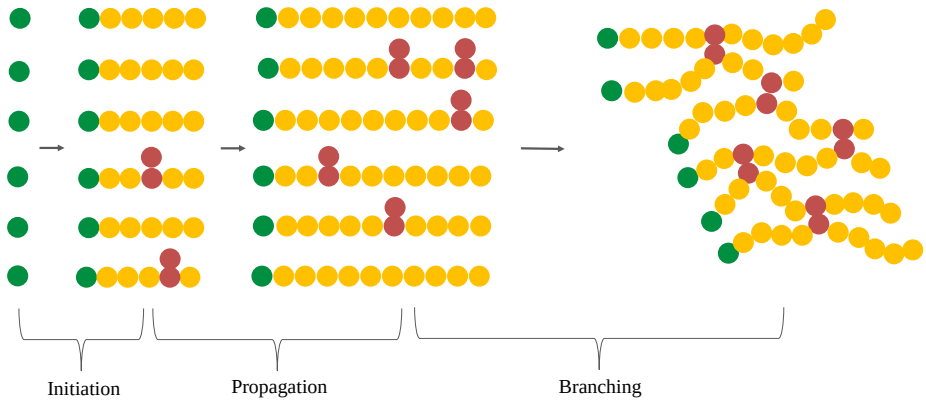

Figure 2.1 Schematic representation of a branched copolymerisation *via* ATRP. *Adapted from ref*[28]

The aims of this research chapter is to synthesise HPMA polymers based upon previous reports[1] and assess their nanoprecipitation behaviour in detail. Nanoparticles composed of HPMA alone are charge stabilised, therefore, it was of interest for the research project to investigate if steric stabilisation could be introduced *via* addition of a PEG A-B block copolymer. The synthesis of the branched copolymer, *p*(HPMA$_x$-*co*-EGDMA$_y$) and a range of varying PEG A-B block copolymers will be conducted *via* ATRP, and the properties of the resulting nanoparticles formed *via* nanoprecipitation will be investigated.

2.3 Synthesis of linear *p*(HPMA$_x$) and the branched copolymer *p*(HPMA$_x$-*co*-EGDMA$_y$)

Both linear and branched HPMA polymers (Scheme 2.2) were synthesised for the following study *via* previously reported copper catalysed methanolic ATRP chemistry.[28] HPMA was the selected monomer for further studies as previous research within the Rannard group had determined the optimum polymerisation conditions *via* ATRP, the subsequent preparation of nanoparticles from varying polymeric architectures, resulting in nanoparticle stability for extended periods of time. The polymerisations and copolymerisations of HPMA with a targeted number average degree of polymerisation (DP_n) of 50, and for the branched copolymer, the DP_n targeted is based upon the primary chain length only. The polymerisations were carried out at 30°C in methanol with CuCl:bipyridyl (bpy) (1:2), as the catalytic system. The initiator, ethyl bromo isobutyrate (EBiB) (**1**), presented in Scheme 2.2 was utilised for both polymerisations due to previous success during ATRP reactions and commercial availability. The formation of branched HPMA was achieved by addition of EGDMA (**2**) to yield, *p*(HPMA$_{50}$-*co*-EGDMA$_{0.9}$) (**3**). The molar ratio of initiator:divinyl monomer (EBiB:EGDMA) is crucial to ensure the formation of a soluble high molecular weight polymer, therefore in order to avoid gelation a ratio of 1:0.9 was employed.

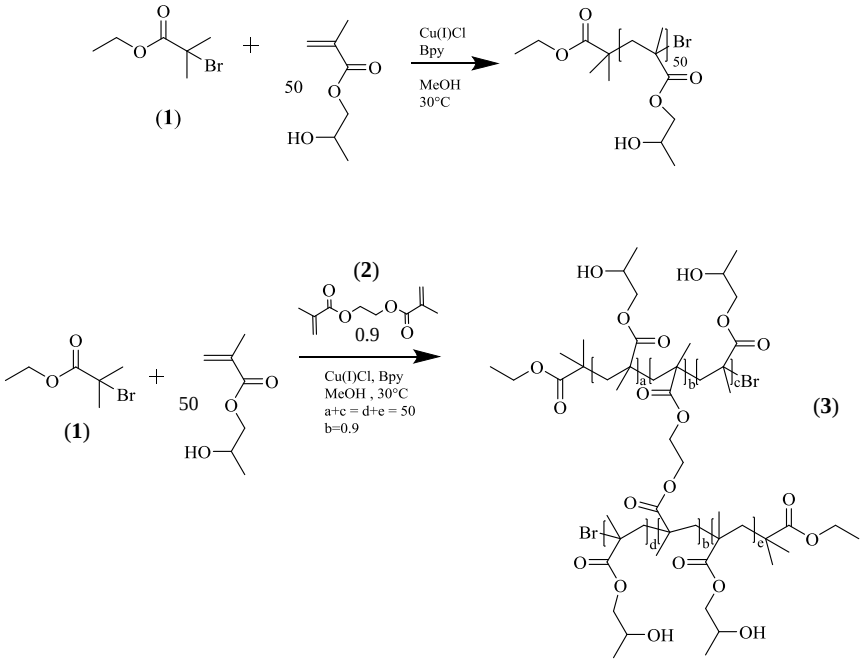

Scheme 2.2 Polymer synthesis. A) linear *p*(HPMA$_{50}$), B) branched *p*(HPMA$_{50}$-*co*-EGDMA$_{0.9}$).

Triple detection gel permeation chromatography (GPC) was used to determine molecular weights and dispersities of the synthesised polymers; the targeted number average molecular weight (M_n) for the linear *p*(HPMA$_{50}$) homopolymer was 7200 g/mol. A higher than expected M_n of 9900 g/mol was obtained by GPC, which may be due to the initiating efficiency of EBiB. The weight-average molecular weight (M_w) was 12400 g/mol with a dispersity (*Đ*) of 1.25. The branched copolymer, *p*(HPMA$_{50}$-*co*-EGDMA$_{0.9}$) exhibited a much higher molecular weight; M_n = 24200 g/mol, M_w = 251400 g/mol and *Đ* = 10.4, as a result of the presence of the EGDMA during the polymerisation. The HPMA monomer conversion for both polymers was determined using ^{1}H NMR analysis, by integration of the vinyl protons to an internal reference (anisole) (Appendix, Fig. A1) and both polymers reached high monomer conversion (>98%). The GPC overlays for *p*(HPMA$_{50}$) highlight the differences between both linear and branched architectures *via* the refractive index (RI) (Figure 2.2A) and right angle light scattering (RALS) (Figure 2.2B) chromatograms. The RI detector response is dependent upon the concentration of the polymer, whilst the RALS detector response is dependent upon the size of the polymeric material present in solution. The RI overlay, illustrates a narrow monomodal and broad, multi-modal molecular weight distribution for the linear *p*(HPMA$_{50}$) polymer and branched *p*(HPMA$_{50}$-*co*-EGDMA$_{0.9}$) copolymer respectively. Due to the statistical nature of EGDMA incorporation, a broad and multi-modal molecular weight distribution suggests polymer species that range across linear, lightly branched and highly branched architectures, which is typical of branched copolymers formed *via* this mechanism.[1] It is useful to compare both RI and RALS chromatograms because although a small RI response for branched *p*(HPMA$_{50}$-*co*-EGDMA$_{0.9}$) is detected between a retention volume of 14 - 15.5 mL, the RALS detector response (Figure 2.2B) is much larger between these retention volumes as the highly branched copolymer scatters significantly more light than the small polymer molecules. ^{1}H nuclear magnetic resonance (NMR) analysis of the final polymer can also be used to determine the DP_n of the primary chains but unfortunately for the linear *p*(HPMA$_{50}$), the proton environments of the initiating chain end overlap with the polymer peaks so this value cannot be calculated. However, the main proton environments can be depicted by ^{1}H NMR for both linear *p*(HPMA$_{50}$) and branched *p*(HPMA$_{50}$-*co*-EGDMA$_{0.9}$), Appendix, Fig. A2 & A3.

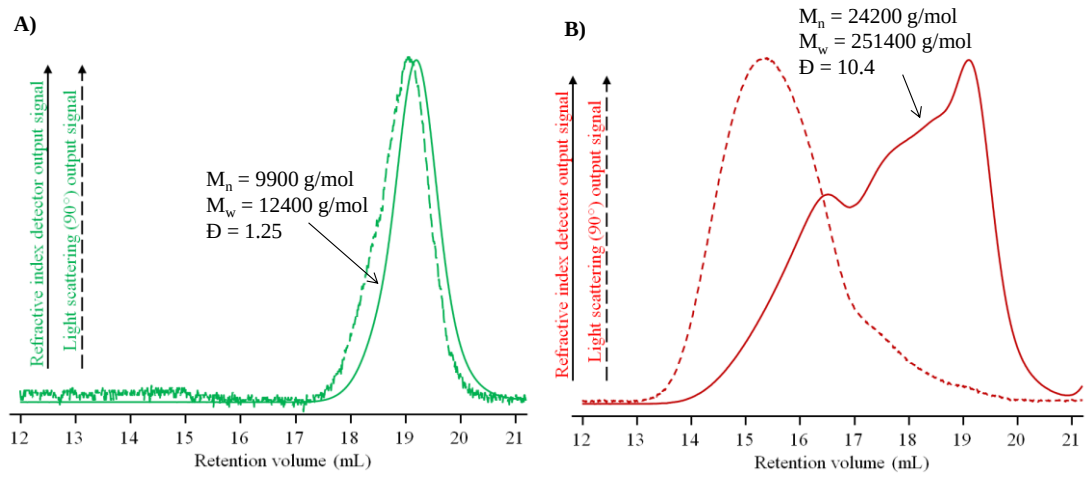

Figure 2.2 GPC chromatogram overlays of linear *p*(HPMA$_{50}$) and branched *p*(HPMA$_{50}$-*co*-EGDMA$_{0.9}$). A) refractive index, B) right angle light scattering detectors.

2.4 Aqueous nanoprecipitation studies

2.4.1 Aqueous nanoprecipitation studies of linear *p*(HPMA$_{50}$) and branched copolymer *p*(HPMA$_{50}$-*co*-EGDMA$_{0.9}$)

Although the nanoprecipitation of polymers has been studied for several decades, some aspects of the mechanism are not fully understood or studied in detail. As previously discussed, there are different approaches towards nanoprecipitation but prior studies within the Rannard research group have employed rapid addition of polymer solutions to volumes of stirring water,[1-3] therefore continuation of this method will allow a direct comparison and broaden our understanding of the process. A series of experiments were conducted, whereby a consistent mass of polymer was nanoprecipitated into a set volume of water with increasing amounts of good solvent. Maintaining a constant mass of polymer during the different nanoprecipitations was important to evaluate the quality of the mixed solvent environments.

A schematic representation of nanoprecipitation is represented in Figure 2.3 and for the following studies, previously synthesised *p*(HPMA$_{50}$) and *p*(HPMA$_{50}$-*co*-EGDMA$_{0.9}$) were dissolved in either tetrahydrofuran (THF) or acetone, as recent literature has shown that the nature of the good solvent can affect nanoprecipitation outcomes, therefore testing within two different solvents was considered important for the study.[31] From this point onwards, the organic solvent will be described as the good solvent, as this readily solubilises the polymers. The term anti-solvent will be used to describe the solvent in

which the polymers are nanoprecipitated into and for the purpose of this research and often used within the literature, this anti-solvent is water (the bad solvent for the polymers). The polymers were dissolved at specific concentrations from 25 to 1.5625 mg/mL and varying volumes of each solution ranging from 0.5 mL of the 25 mg/mL solution to 8 mL of the 1.5625 mg/mL solution were added to 5 mL of water. This system ensured that a consistent fixed mass (12.5 mg) of each polymer was precipitated into a set volume of water under varying solvent conditions (Table 2.1). A constant mass of polymer during each nanoprecipitation experiment was important to determine if increasing volumes of good solvent can prevent the formation of stabilised nanoparticles.

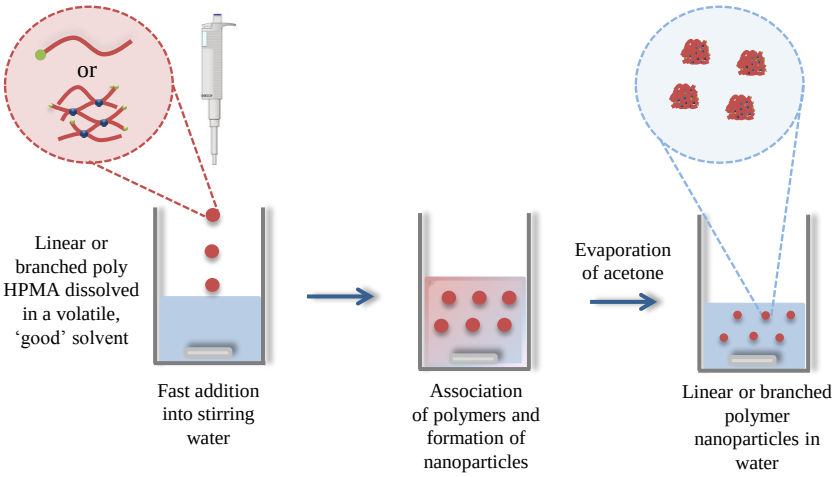

Figure 2.3 Schematic representation of the nanoprecipitation process.

Table 2.1 The conditions for nanoprecipitation experiments of both linear *p*(HPMA$_{50}$) and *p*(HPMA$_{50}$-*co*-EGDMA$_{0.9}$). Mass of polymers dissolved in good solvent (kept constant at 12.5 mg), during each nanoprecipitation.

Volume of good solvent (acetone or THF + polymer (mL)	Concentration of polymer in good solvent (mg/mL)	Volume of water (mL)	Volume fraction of good solvent
0.5	25	5	0.0909
1	12.5	5	0.1667
2	6.25	5	0.2857
3	4.167	5	0.3750
4	3.125	5	0.4444
5	2.5	5	0.5000
8	1.5625	5	0.6154

The following nanoprecipitation experiments aim to investigate if there is an advantage of using branched *p*(HPMA$_{50}$-*co*-EGDMA$_{0.9}$) copolymers rather than linear *p*(HPMA$_{50}$), when seeking to achieve narrow, monomodal polymer nanoparticle distributions. Nanoparticles prepared during this study were analysed using dynamic light scattering (DLS). DLS analysis of nanoparticles can be used to determine parameters such as the z-average diameter (D_z) (d. nm) and polydispersity index (PdI), which is a measure of the width of the size distribution. The derived count rate, measured in kilo counts per second (kcps) is also a calculated parameter, which is the number of photons detected and is and takes into account the attenuation factor used. Light scattered is directly proportional to the size and number of particles present in a sample, therefore the derived count rate can be used to indicate the presence of nanoscale objects. Unless otherwise stated, an average of 3 repeat measurements were taken for each nanoparticle sample. During the nanoprecipitation of linear *p*(HPMA$_{50}$) (Figure 2.4A), no clear trends were observed using DLS, when measuring the samples immediately after addition or after complete evaporation of the good solvent phase.

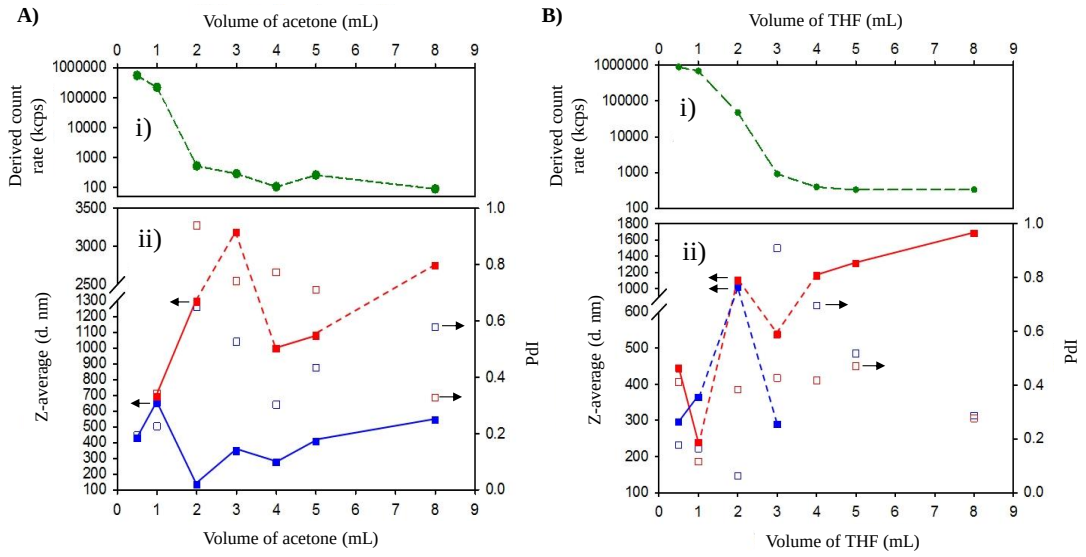

Figure 2.4 DLS analysis of linear *p*(HPMA$_{50}$). A) nanoprecipitation from acetone, B) nanoprecipitation from THF, A, B) i) derived count rate from samples immediately after addition of the acetone or THF solution into water, using a constant mass (12.5 mg) of polymer and A, B) ii) z-average diameter (nm) (closed symbols) and PdI (open symbols) of the samples in the acetone/water mixture (blue symbols) and in water (red symbols) after acetone or THF evaporation.

A very high intensity of light scattering was only observed when <1 mL of either acetone or THF was present within the anti-solvent (Figure 2.4 Ai & Bi). When >1 mL of good

solvent was introduced, the derived count rate rapidly decreased, suggesting a very low concentration of nanoscale objects present upon increasing volumes of good solvent. The DLS results show that for linear *p*(HPMA$_{50}$), there is a large increase in size (>500 nm) during removal of acetone and THF and PdI values exceed 0.3, suggesting the formation of large unstable aggregates.

The nanoprecipitation of branched *p*(HPMA$_{50}$-*co*-EGDMA$_{0.9}$) demonstrated considerably different behaviour (Figure 2.5). Highly significant light scattering intensities were obtained when the branched copolymer solutions were added to water when dissolved in up to 3 mL of good solvent (Figure 2.5 Ai & Bi), and similarly, nanoparticles with a D_z less than 250 nm were readily observed (Figure 2.5 Aii & Bii). After evaporation of the good solvent, the measured D_z values of the nanodispersion were lower than D_z values obtained in the presence of the good solvent. This is due to the desolvation of assemblies resulting in a slight decrease in hydrodynamic diameter. The nanoprecipitated particles also exhibited a uniform size distribution (PdI values <0.1) which was maintained after evaporation of the good solvent (Appendix, Table A1). As may be expected, when volumes >3 mL of each acetone solution were used in the nanoprecipitation, a sudden decrease in the light scattering intensity was seen, with a concomitant loss of quality within the correlation functions, within the samples measured immediately after acetone solution addition (Figure 2.5 Ai). A corresponding decrease was observed in the measured D_z values; however, after solvent evaporation, particles with D_z values >1 μm were observed (Figure 2.5 Aii) with broad PdIs (>0.3); the slow formation of particles during evaporation of acetone is clearly not controlled. An identical trend was seen when using THF as the good solvent phase, but up to 4 mL volumes of polymer solution were able to generate nanoprecipitates immediately after addition and the sudden decrease in light scattering of samples containing good solvent and anti-solvent was observed at volumes > 4 mL (Figure 2.5 Bi & ii). The solvent swollen nanoprecipitates formed immediately after THF addition were significantly larger than those derived from acetone solutions, and this increased size was also seen within the nanoparticles after solvent evaporation. The nanoparticle sizes were generally larger during mixing of the solvents, which could be due to swelling of the nanoprecipitates in the solvent mixture during the evaporation stages and THF appears to be a better solvent for *p*(HPMA$_{50}$-*co*-EGDMA$_{0.9}$). Therefore, after complete solvent removal there is an overall decrease in size. From this study, it is unclear whether these differences indicate considerable or slight differences in the solubility of branched *p*(HPMA$_{50}$-*co*-EGDMA$_{0.9}$) in these aqueous solvent environments.

The larger swollen nanoprecipitates, and resulting solvent-free aqueous dispersions, do suggest different factors controlling the nucleation and growth mechanism when using these two different solvents. It appears that branched chains can effectively collapse to form relatively large nuclei that assemble to form the larger, colloidally stable nanoparticles.

The investigation of a good solvent/anti-solvent phase ratio, suggests that during the addition of large volumes of good solvent to the anti-solvent phase, the nanoprecipitation process is prevented due to the saturated environment. It is apparent from the obtained derived count rate values, that nanoparticles are formed very quickly on mixing and will be present within the mixed solvent/anti-solvent environment during solvent evaporation stages, rather than being formed slowly from a dissolved state as the good solvent is removed.

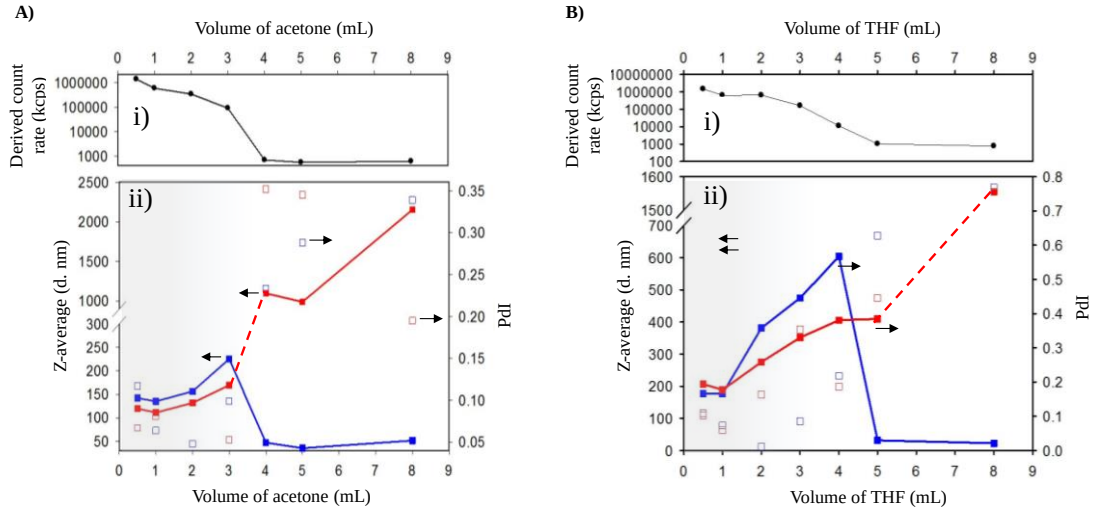

Figure 2.5 DLS analysis of branched *p*(HPMA$_{50}$-*co*-EGDMA$_{0.9}$) (A) nanoprecipitation from acetone, B) nanoprecipitation from THF, i) derived count rate from samples immediately after addition of the acetone or THF solution into water, using a constant mass (12.5 mg) of polymer and ii) z-average (d. nm) (closed symbols) and PdI (open symbols) of the samples in the acetone/water mixture (blue symbols) and in water (red symbols) after acetone or THF evaporation.

2.4.2 Multiple nanoprecipitation studies

The formation of colloidally stable nanoparticles *via* nanoprecipitation has the potential to allow additional subsequent nanoprecipitations into the same anti-solvent mixture, after removal of good solvent, assuming the mixed good/anti-solvent environment does not pass the nanoprecipitation boundary. It was hypothesised, that during a multiple nanoprecipitation experiment i.e. addition of polymer in good solvent (i_5-f_1) to already

formed nanoparticles, one of the two following outcomes could occur; (i) the growth of existing nanoparticles will continue and an increase in D_z would be observed or, (ii) the formation of new nanoparticles of identical D_z. A schematic representation of a the proposed multiple nanoprecipitation process is outlined in Figure 2.6, and the details of each step are as follows; (i) addition of polymer dissolved in a good solvent to the aqueous anti-solvent, (ii) removal of good solvent to generate stable nanoparticles in water, and (iii) a second and identical addition of polymer solution in a good solvent to the aqueous nanoparticle dispersion, with (iv) removal of the second volume of good solvent to create a greater number of nanoparticles whose size increases or matches the original distribution.

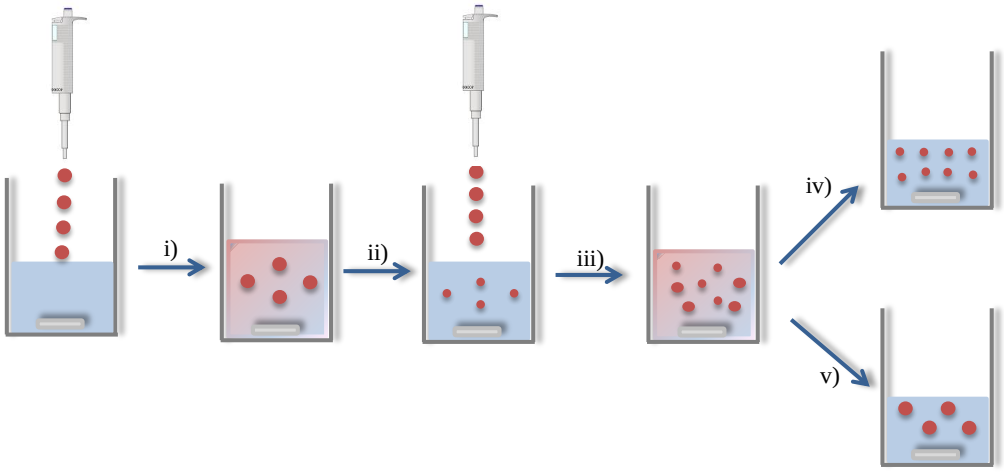

Figure 2.6 Schematic representation of multiple nanoprecipitations of branched copolymers: (i) addition of polymer in good solvent to water, (ii) formation of particles in mixed solvent/water, (iii) evaporation of good solvent and desolvation to generate aqueous nanoparticle dispersion and second addition of polymer solution, (iv) formation of new particles of identical size, (v) growth of existing particle diameters.

Acetone and THF solutions of *p*(HPMA$_{50}$-*co*-EGDMA$_{0.9}$) were prepared at a concentration of 5 mg/mL, and varying volumes of the solutions from 0.5 to 4 mL were rapidly added to 5 mL of water with vigorous stirring; samples were studied by DLS after solvent evaporation. As can be seen from Table 2.2 and Figure 2.7, for repeated additions of the branched copolymer solution up to 2 mL of acetone addition, the recorded D_z values of the nanoprecipitated particles are almost identical and only slight changes in PdI are observed, as would be expected if no perturbation of the initial nanodispersion occurred and the existing nanoparticles do not act as nuclei for further growth. When repeating additions of volumes >3 mL, the nanoparticles formed from *p*(HPMA$_{50}$-*co*-EGDMA$_{0.9}$)

varied considerably after the second addition and subsequent evaporation of good solvent; repeated addition of 3 and 4 mL of the polymer solution in acetone and THF led to considerable phase separation, for DLS analysis see Appendix, Table A2.

When using THF as the good solvent phase, similar behaviour was observed but repeated nanoprecipitations only tolerated volumes of <2 mL; higher volumes generated appreciable variation in D_z or observable precipitates on second addition. This suggests that the mixed THF/water environments formed during the second sample addition were more capable of perturbing the initial nanoparticles, potentially solvating them to a point where they were able to aggregate or able to act as nuclei for additional growth.

Table 2.2 DLS results for multiple nanoprecipitations from both acetone and THF polymer solutions.

Volume of Polymer Solution Added (mL)	**Addition no.**	**D_z (nm)**	**PdI**	**Derived count rate (kcps)**
Acetone				
0.5	1	72	0.119	66551
	2	75	0.193	176697
1	**1**	**79**	**0.075**	**254902**
	2	**83**	**0.099**	**442959**
2	1	105	0.113	1049237
	2	112	0.081	1451725
3	1	162	0.054	1443879
	2	293	0.156	1369080
THF				
0.5	1	83	0.107	106516
	2	81	0.118	276651
1	**1**	**91**	**0.08**	**356127**
	2	**92**	**0.103**	**629711**
2	1	107	0.083	1318163
	2	130	0.080	1531601

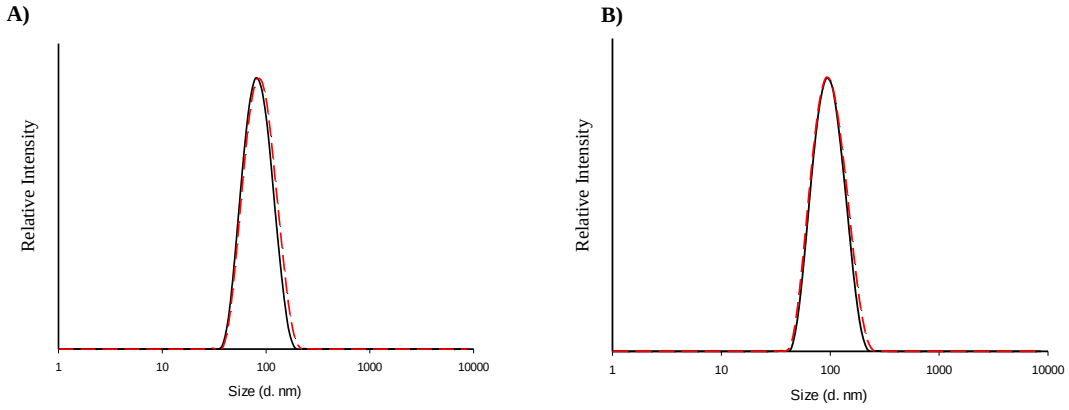

Figure 2.7 DLS overlays for the multiple nanoprecipitations of branched *p*(HPMA$_{50}$-*co*-EGDMA$_{0.9}$) A) Overlay of DLS data for multiple nanoprecipitations of *p*(HPMA$_{50}$-*co*-EGDMA$_{0.9}$) from acetone B) Overlay of DLS data for multiple nanoprecipitations of *p*(HPMA$_{50}$-*co*-EGDMA$_{0.9}$) from THF. For (A) and (B), first nanoprecipitation (black trace) followed by the second nanoprecipitation (red dashed trace).

The derived count rates obtained by DLS after each nanoprecipitation varied in a very consistent manner across the two solvent systems studied. When using either acetone or THF as the good solvent phase, an approximate 2.6-fold increase was seen during the second addition of 0.5 mL of polymer solution, which, in conjunction with the similarity of D_z, would suggest an approximate doubling of the number of nanoparticles within the aqueous phase after good solvent evaporation (Figure 2.6 iv). The comparisons of derived count rates after the first and second nanoprecipitations when using 1 mL addition were also similar across the two good solvents. Generally, an increase in scattering was observed during each subsequent addition of polymer dissolved in good solvent and similar D_z values were obtained. This suggests that after the second addition of polymer in good solvent, additional nanoparticles of the same size are present as well as the existing nanoparticles in the aqueous dispersion. An exception to the general trend was for the multiple addition of 3 mL of polymer dissolved in acetone, where the D_z almost doubled and a slight decrease in scattering was observed. This may suggest that for the increasing addition of polymer in good solvent, the growth of existing nanoparticles can result, as opposed to the formation of a new particle distribution. In terms of drug delivery nanocarriers, the ability to instantly increase the concentration of polymer nanoparticles *via* low volume additions is very appealing for increasing the concentration of therapeutic drug molecules whilst maintaining a constant volume.

2.4.3 Variation of concentration and temperature

So far, the mass of polymer has been kept constant during the nanoprecipitation experiments, in order to evaluate the effects of increasing volume additions from both acetone and THF. The following experiments aimed to determine if the concentration of polymer within the good solvent would affect the D_z values if varied. In order to investigate this, nanoprecipitation experiments of *p*(HPMA$_{50}$-*co*-EGDMA$_{0.9}$) were conducted using fixed volumes of solutions with polymer concentrations varying from 25, 10, and 5 mg/mL. Irrespective of good solvent choice, solutions containing the branched copolymer at 5 mg/mL consistently produced smaller nanoparticles. Nanoprecipitations using >1mL of these solutions (acetone or THF) conducted at the higher concentrations of 10 mg/mL and 25 mg/mL, resulted in the formation of large unstable aggregates (Figure 2.8). During an increase in polymer concentration, the DLS results suggest that the growth of the nanoparticles becomes limited by the poor diffusion of the polymer molecules to the nuclei surface. An increased number of nuclei will limit the diffusion into the anti-solvent and the growth of nanoparticles will occur through random collisions of existing particles and most likely result in aggregation.[32]

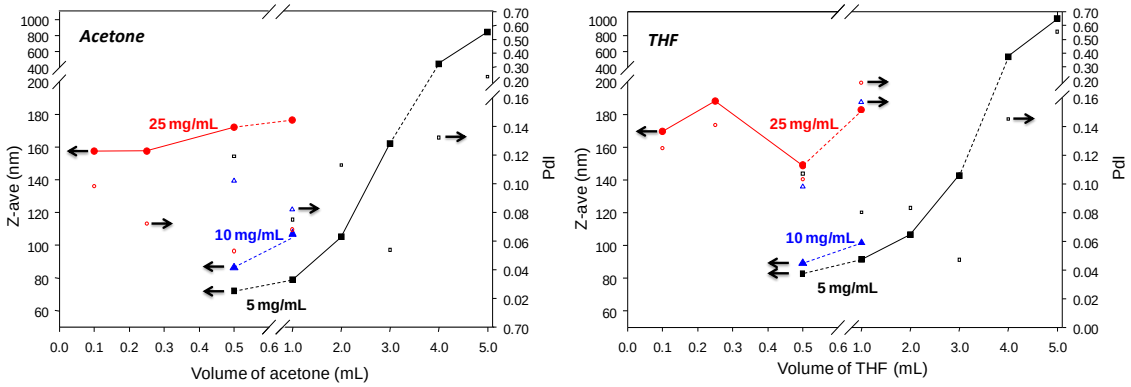

Figure 2.8 DLS analysis of nanoprecipitation of *p*(HPMA$_{50}$-*co*-EGDMA$_{0.9}$) dissolved within either acetone (left) or THF (right) using varying volumes of three different solution concentrations (25 mg/mL – red circle, 10mg/mL – blue triangle and 5 mg/mL – black square. (Each volume was added to 5 mL of water and the solvent was evaporated prior to measurement).

In summary, the nanoprecipitation experiments of *p*(HPMA$_{50}$-*co*-EGDMA$_{0.9}$) from acetone generally gave lower PdI and smaller D_z values prior to, and after, good solvent removal; therefore, THF was not selected for further study. Acetone also has the practical advantage of a lower boiling point to aid removal. Therefore, based on these experimental results, all nanoparticles from this point onwards (unless otherwise stated) will be prepared from 1 mL of a 5 mg/mL polymer solution nanoprecipitated from acetone into 5

mL of water. The initial and final concentration of samples prepared by aqueous nanoprecipitation will be described as i_x-f_y, where x represents the initial concentration and $\boldsymbol{y}$ the final concentration in mg/mL, therefore unless otherwise stated; the conditions will be i_5-f_1.

In order to study the effect of the water temperature during the nanoprecipitation of *p*(HPMA$_{50}$-*co*-EGDMA$_{0.9}$), experiments were conducted at both ambient and elevated temperatures of 50°C (Figure 2.9). From previous experiments, it is evident that up to a 3 mL addition of acetone, there is a very small effect on the nanoparticle dispersion, which suggests any sudden increase in temperature will have negligible effects on the formation of the nanoparticles' size and dispersity.

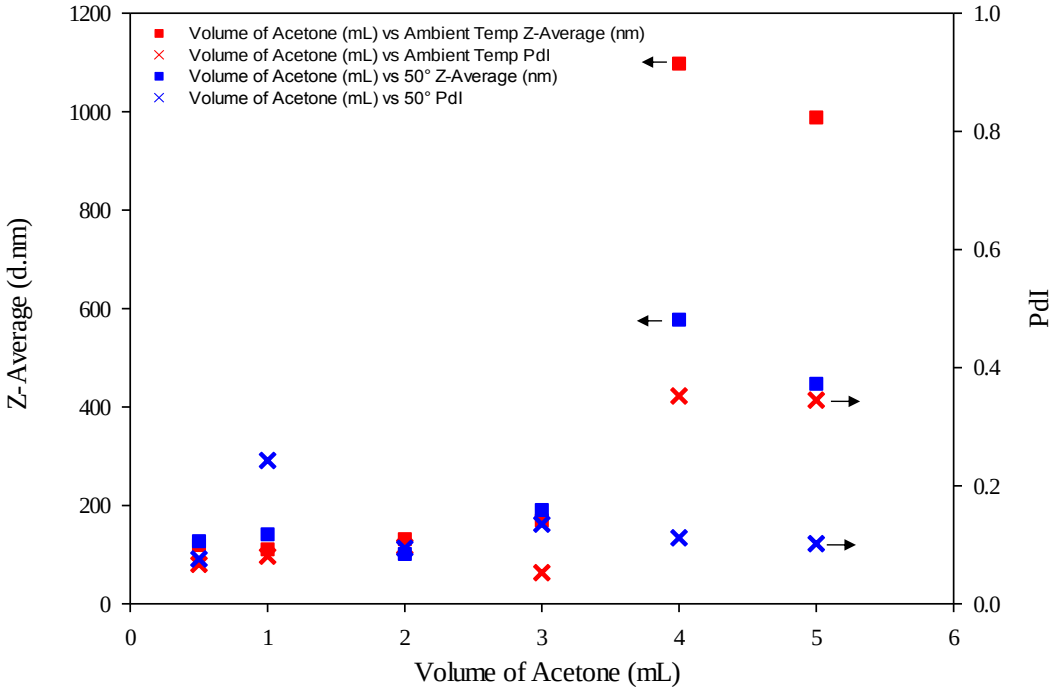

Figure 2.9 The formation of *p*(HPMA$_{50}$-*co*-EGDMA$_{0.9}$) polymer nanoparticles into both ambient and 50°C water, red square = volume of acetone (mL) *vs* ambient temp z-average (nm), red cross = volume of acetone (mL) *vs* ambient temperature PdI, blue square = volume of acetone (mL) *vs* 50°C z-average (nm), blue cross = volume of acetone (mL) vs 50°C PdI.

The nanoprecipitation conditions which have been carried out support the previous research that there are clear advantages to using *p*(HPMA$_{50}$-*co*-EGDMA$_{0.9}$) copolymers rather than linear homopolymers for formation of nanoparticles which have narrow, monomodal size distributions. The direct observations that (a) nanoparticles are formed immediately after addition of the polymer within a good solvent to the anti-solvent, (b)

the addition of large volumes of good solvent can prevent nanoprecipitation, and (c) repeated nanoprecipitations into the same anti-solvent sample led to increased numbers of particles that match previous nanoprecipitations and also support the nucleation and growth mechanism that has been proposed.[2, 32] Unfortunately, nanoparticles formed from branched *p*(HPMA$_{50}$-*co*-EGDMA$_{0.9}$) are charge stabilised as they exhibit high negative zeta potentials (~ -40 mV), and are, therefore, unstable during addition of small amounts of buffer/NaCl. As set out in the initial aims of the project, it would be desirable to introduce steric stabilisation into the system for nanoparticles to be considered for potential drug delivery applications. In order to do this, the next part of the research will describe the synthesis of A-B amphiphilic block copolymers and subsequent nanoprecipitation and co-nanoprecipitation studies.

2.5 Synthesis and characterisation of A-B block copolymers

2.5.1 A-B block copolymer compositions

As discussed, the charge stabilisation of branched *p*(HPMA$_{50}$-*co*-EGDMA$_{0.9}$) nanoparticles limits their development for use as drug delivery nanocarriers. To improve the properties of these hydrophobic nanoparticles, it has been hypothesised that the synthesis of PEG containing A-B block copolymers and their inclusion within the nanoprecipitation process, could introduce steric stabilisation. After the nanoprecipitation of both *p*(HPMA$_{50}$-*co*-EGDMA$_{0.9}$) and *p*(PEG$_y$-*b*-HPMA$_x$) A-B block copolymers, it has been hypothesised that there are several potential outcomes which could occur and this is presented schematically in Figure 2.10 suggesting either; i) the HPMA chain from the A-B block copolymer could become adsorbed onto the *p*(HPMA$_{50}$-*co*-EGDMA$_{0.9}$) nanoparticle surface resulting in a pendant PEG chain, ii) the incorporation of hydrophobic HPMA of the A-B block copolymer within the nanoparticle core and PEG chains existing at the surface, iii) entrapment of the A-B block copolymer within the branched nanoparticle core, iv) formation of two or more different nanoscale objects of *p*(HPMA$_{50}$-*co*-EGDMA$_{0.9}$) nanoparticles and micellar structures from *p*(PEG$_y$-*b*-HPMA$_x$) A-B block copolymers.

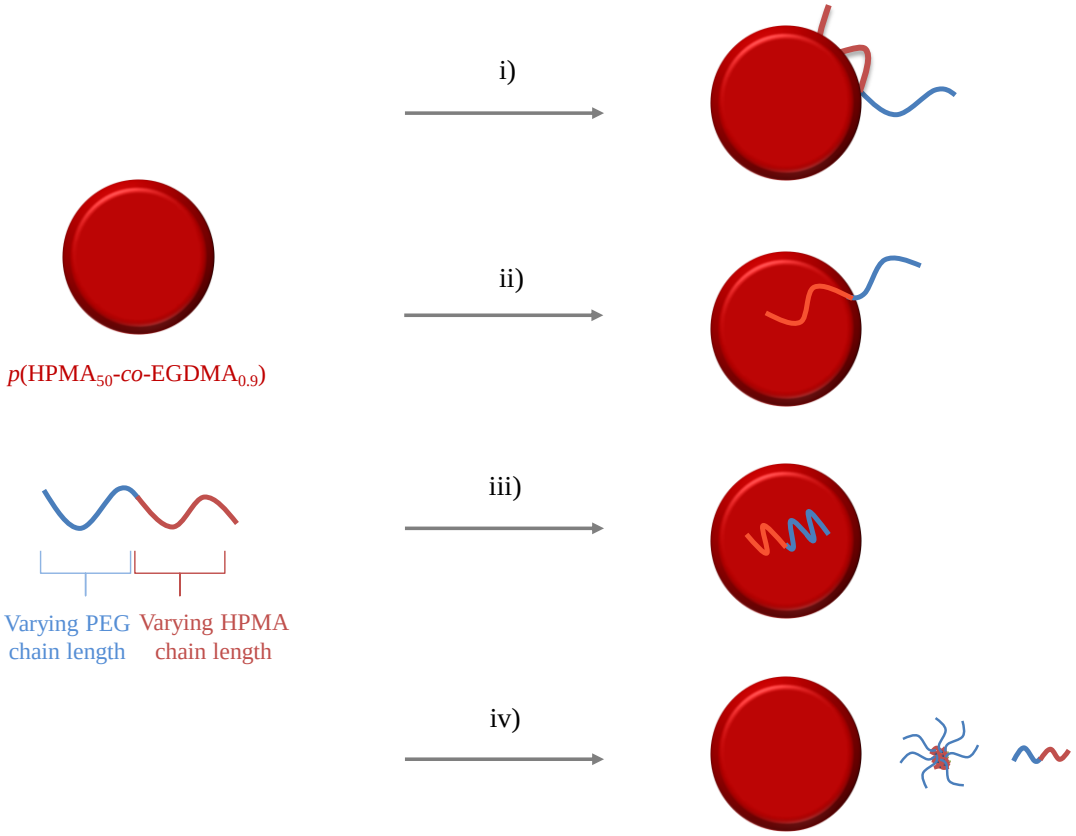

Figure 2.10 Schematic representation of potential outcomes of the formation of nanoparticles during addition of *p*(HPMA$_{50}$-*co*-EGDMA$_{0.9}$) and an A-B block copolymer; i) adsorption of the A-B block copolymer on the surface of *p*(HPMA$_{50}$-*co*-EGDMA$_{0.9}$) nanoparticles resulting in a pendant PEG chain, ii) incorporation of hydrophobic HPMA into the nanoparticle core and PEG chains at the surface, iii) entrapment of the A-B block copolymer within the branched nanoparticle core, iv) formation of two or more different nanoscale objects of *p*(HPMA$_{50}$-*co*-EGDMA$_{0.9}$) nanoparticles and micellar structures from *p*(PEG$_y$-*b*-HPMA$_x$) A-B block copolymers.

The choice of macroinitiator, monomer and subsequent A-B block copolymers is demonstrated in Figure 2.11. The molecular weight of the macroinitiators (PEG$_{45}$-Br or PEG$_{114}$-Br) and targeted DP$_n$ of HPMA were varied in order to investigate the effects of different PEG$_y$ *vs* HPMA$_x$ block lengths. The synthesis and characterisation of the macroinitiators and copolymers will be discussed below.

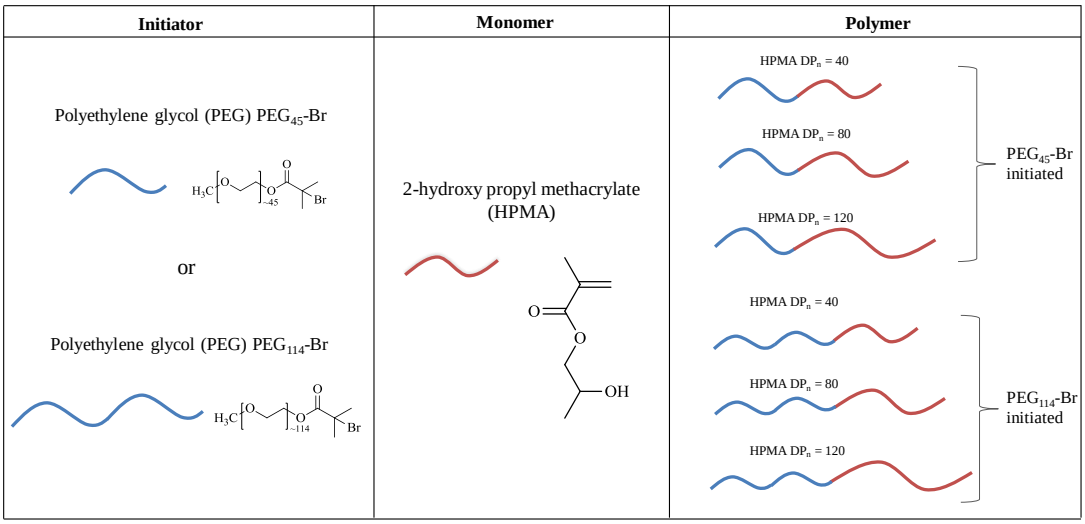

Figure 2.11 Schematic representation of targeted PEG_y-$HPMA_x$ A-B block copolymers *via* ATRP.

2.5.2 PEG_{45}-Br and PEG_{114}-Br macroinitiator synthesis

The PEG_{45}-Br macroinitiator (**4**), was synthesised as previously reported[19] *via* an esterification reaction from poly(ethylene glycol) monomethyl ether (average molecular weight ~2000 g/mol) and α-bromoisobutyryl bromide as shown below in Scheme 2.3A.

The monomethoxy PEG, MeO-PEG_{45}-OH (M_n ~2000 g/mol) was dissolved in toluene with the addition of triethylamine, 4-dimethyl-aminopyridine (DMAP) and degassed with N_2 for 20-30 minutes. The α-bromoisobutyryl bromide was added drop wise over 30 minutes to the reaction vessel which was cooled to 0°C. The rapid formation of a white precipitate (triethylamine salt $Et_3NH^+Br^-$) indicated progress of the reaction. The reaction medium was left to stir for 24 hours at room temperature under N_2. The precipitate was filtered and the solvent was concentrated *in vacuo*. The resulting product was diluted in acetone and purified by precipitation into cold petroleum ether (40-60°C). This last step was repeated and the product was finally dried under vacuum at 40°C for 24 hours.

The formation of **4** was confirmed by ^{1}H NMR spectroscopy, as shown in Figure 2.12. The integration ratios for proton environments **h:a** are 6:3 respectively, which corresponds to the proposed structure and environments **b**, **c**, **d**, **e**, & **f** integrate to give a value of 180 which is representative of a PEG repeat unit with an M_n ~2000 g/mol. Proton environment **g**, results from the formation of the ester bond, as this peak does not appear in the original mono methoxy alcohol ^{1}H NMR. For further confirmation, the mass spectrometric analysis MALDI-TOF is shown in the Appendix (Fig. A4).

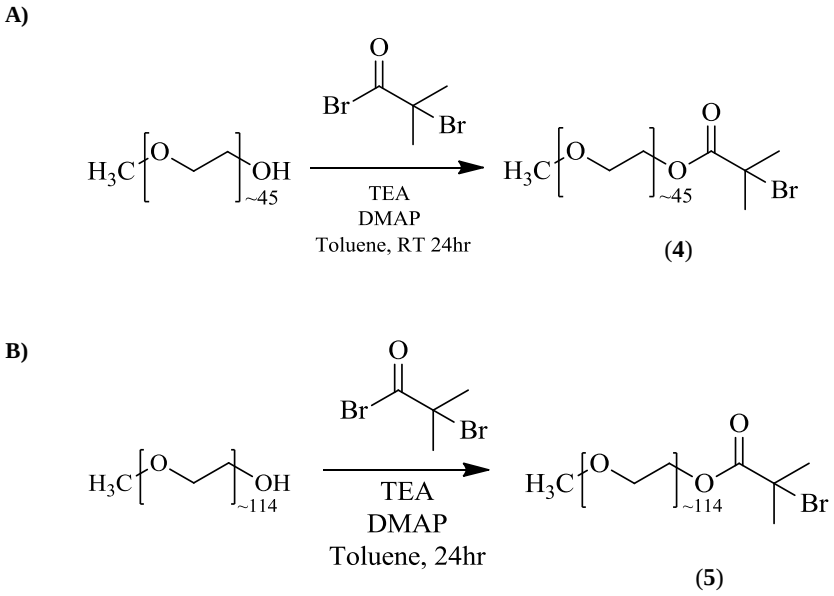

Scheme 2.3 Synthesis of MeO-PEG$_y$-Br macroinitiators, A) MeO-PEG$_{45}$-Br, B) MeO-PEG$_{114}$-Br.

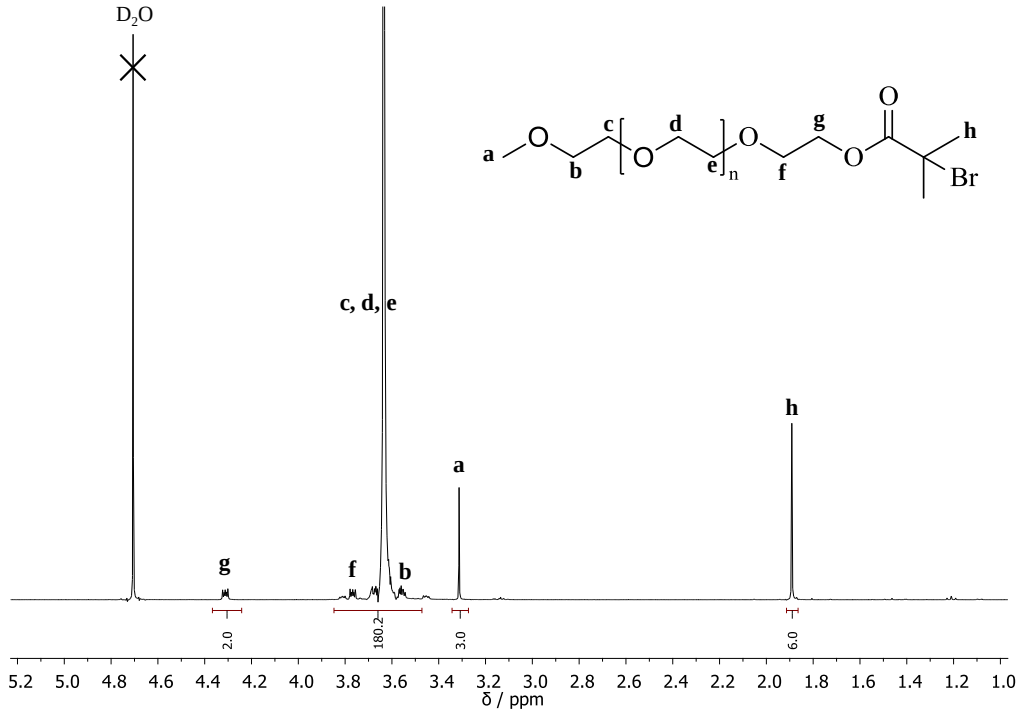

Figure 2.12 ^{1}H NMR (D_2O, 400MHz) of the mono-functional ATRP macroinitiator, MeO-PEG$_{45}$-Br.

The MeO-PEG$_{114}$-Br macroinitiator (**5**) (Scheme 2.3B) was synthesised using a monomethoxy PEG M_n ~5000 g/mol under the same conditions as the esterification reaction discussed above for the MeO-PEG$_{45}$-Br macroinitiator. The formation of **5** was confirmed by ^{1}H NMR spectroscopy (Appendix, Fig. A5). The integration value obtained for the MeO-PEG$_{114}$-Br repeat unit was 455, which is expected for a ~5000 g/mol MeO-PEG$_{114}$-Br macroinitiator.

2.5.3 Synthesis of linear A-B block copolymers

The ATRP polymerisations of HPMA initiated by the PEG macroinitiators (PEG$_{45}$-Br or PEG$_{114}$-Br) with a targeted DP_n of 40, 80 and 120 were carried out at 30°C in methanol utilising the same catalytic system of CuCl:bpy (1:2) discussed in Section 2.3. A generalised reaction scheme for the polymerisations is illustrated in Scheme 2.4 below.

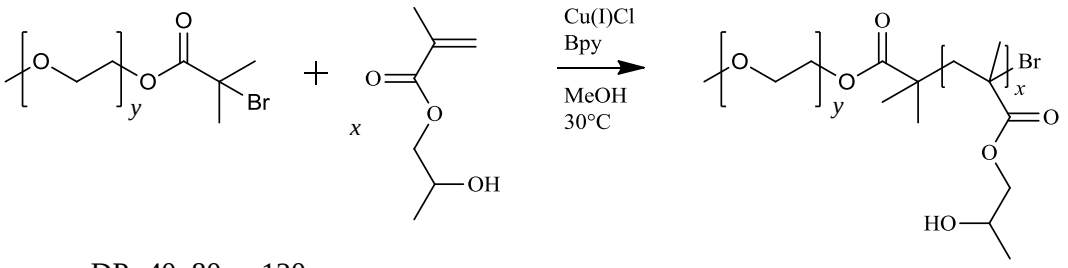

x = DP_n 40, 80 or 120
y = 45, 114

Scheme 2.4 Generic reaction scheme for the ATRP synthesis of *p*(PEG$_y$-*b*-HPMA$_x$) A-B block copolymers.

Confirmation of the DP_n using ^{1}H NMR was possible due to the presence of the methyl end group on the PEG chain and high molecular weight of the macroinitiator. The targeted DP_n for this polymerisation was 40 monomer units. The ^{1}H NMR spectrum presented in Figure 2.13 shows that environment **d** has been calibrated to 3 protons and the corresponding **b**, **b'**, **e** and **e'** integrate to ~242, which when divided by 6 equals ~40 which would be expected for this polymerisation. The ^{1}H NMR spectra for all other amphiphilic copolymers are assigned and located in the Appendix (Fig. A6-A10) and the DP_n values by ^{1}H NMR for all A-B block copolymers are reported in Table 2.3. Kinetic experiments were carried out for *p*(PEG$_{45}$-*b*-HPMA$_{40}$) and *p*(PEG$_{114}$-*b*-HPMA$_{40}$) to confirm that each polymerisation followed first order kinetics with respect to monomer concentration (Appendix, Fig. A11 & A12).

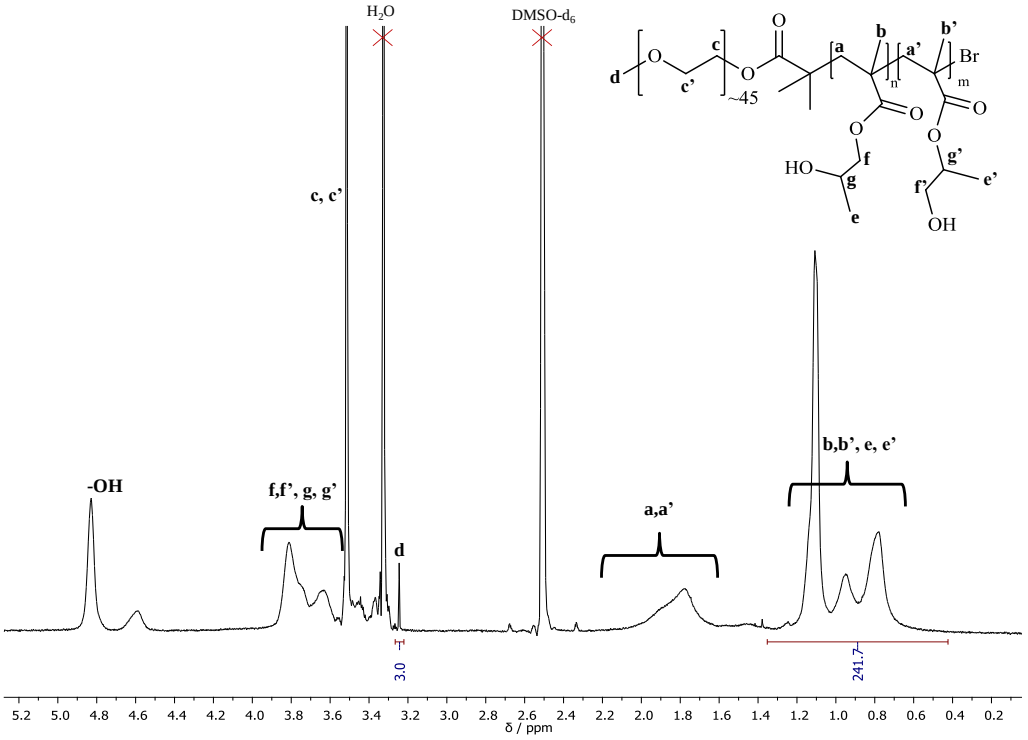

Figure 2.13 ^{1}H NMR spectrum of *p*(PEG$_{45}$-*b*-HPMA$_{40}$) (DMSO-d$_6$, 400 MHz).

The GPC and ^{1}H NMR analysis for the linear A-B block copolymers synthesised from both macroinitiators is presented below (Table 2.3). The DP_n values calculated by ^{1}H NMR spectroscopy were lower than the values obtained by GPC for all A-B block copolymers. These differences are most likely due to the initiator efficiency of the PEG macroinitiators being less than 100%. It is also worth taking into consideration that the ^{1}H NMR evaluation may include unreacted initiator, resulting in calculations of polymer chains that are shorter than reported than GPC analysis and is discussed in the literature.[33, 34] The GPC RI overlays for the macroinitiators and linear A-B block copolymers demonstrate monomodal distributions for all polymers (Figure 2.14 A&B). The height of each peak has been normalised, so does not reflect the true differences in detector response.

Table 2.3 GPC and ^{1}H NMR data for MeO-PEG$_{45}$-Br and MeO-PEG$_{114}$-Br initiated A-B block copolymers.

Target Polymer Composition	GPC (DMF)					^{1}H NMR[a]	
	M_n Theory (g/mol)	M_n (g/mol)	M_w (g/mol)	Đ	DP_n	DP_n	Conversion (%)
MeO-PEG$_{45}$-Br	~2000	2100	2200	1.05	-	-	-
MeO-PEG$_{114}$-Br	~5000	5800	5840	1.01	-	-	-
p(PEG$_{45}$-*b*-HPMA$_{40}$)	7800	9250	11200	1.21	58	40	98
p(PEG$_{45}$-*b*-HPMA$_{80}$)	13500	18800	24400	1.29	110	82	98
p(PEG$_{45}$-*b*-HPMA$_{120}$)	19300	20300	25000	1.23	130	91	98
p(PEG$_{114}$-*b*-HPMA$_{40}$)	10800	16500	21000	1.27	79	39	98
p(PEG$_{114}$-*b*-HPMA$_{80}$)	16500	20000	25200	1.26	104	78	98
p(PEG$_{114}$-*b*-HPMA$_{120}$)	22300	25000	31350	1.25	139	113	98

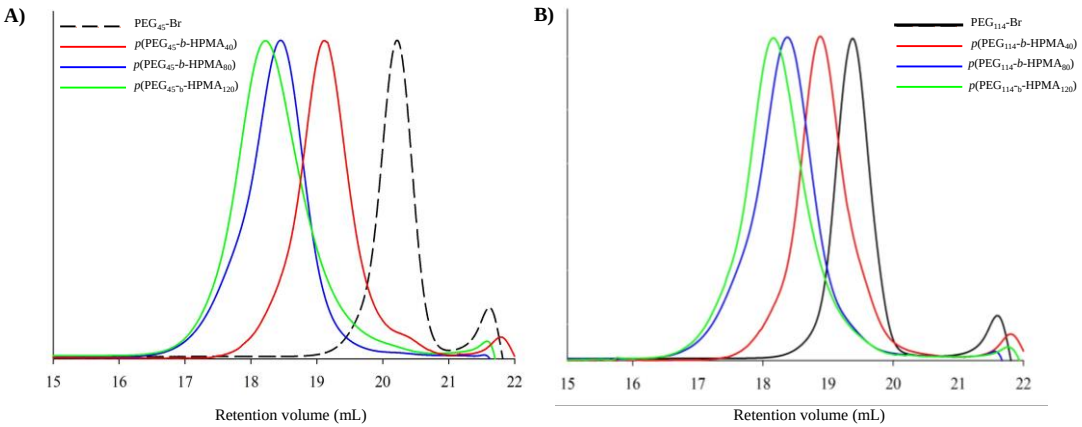

Figure 2.14 GPC analysis of *p*(PEG$_y$-*b*-HPMA$_x$) A-B block polymers. A) GPC RI chromatogram overlays of PEG$_{45}$-Br initiated A-B block copolymers B) GPC RI chromatogram overlays of PEG$_{114}$-Br initiated A-B block copolymers.

2.6 Introduction to co-nanoprecipitation

2.6.1 Aqueous nanoprecipitation studies of linear A-B block copolymers

In order to assess whether the *p*(PEG$_y$-*b*-HPMA$_x$) A-B block copolymers could provide stability during addition to the nanoprecipitation process of branched *p*(HPMA$_{50}$-*co*-EGDMA$_{0.9}$) nanoparticles, it was firstly important to nanoprecipitate both the A-B block copolymers and branched *p*(HPMA$_{50}$-*co*-EGDMA$_{0.9}$) individually to study their behaviour. The nanoprecipitation of the A-B block copolymers is an essential control

experiment before carrying out the co-nanoprecipitation experiments, to see if nanoscale objects (if any) are formed. The A-B block copolymers were individually dissolved in acetone at 5 mg/mL and nanoprecipitated into 5 mL of water to give a final concentration of polymer in water of 1 mg/mL. The DLS size by intensity traces for the nanoprecipitation of solutions solely containing the A-B block copolymers are presented in Figure 2.15. A multi-modal peak was observed for *p*(PEG_{45}-*b*-$HPMA_{40}$) suggesting the sample consisted of two different size distributions after nanoprecipitation of this A-B block copolymer in water. In addition to this, a very low derived count rate (Table 2.4) and high attenuation value of 9 was observed, which suggests a low concentration of nanoscale objects present and an appreciable solubility of the A-B copolymer solubility in water. The nanoprecipitation of the higher molecular weight A-B copolymer, *p*(PEG_{45}-*b*-$HPMA_{80}$) gave a monomodal peak when analysed by DLS and although the PdI obtained was reasonably broad, there was an increase in derived count rate when compared with *p*(PEG_{45}-*b*-$HPMA_{40}$). As *p*(PEG_{45}-*b*-$HPMA_{80}$) is insoluble in water, it would be expected that the amphiphilic nature of the polymer would result in formation of micellar objects within this environment. It is worth noting that the DLS results for two of three block copolymers, *p*(PEG_{45}-*b*-$HPMA_{40}$) and *p*(PEG_{45}-*b*-$HPMA_{80}$), did not provide reliable scattering data. The most hydrophobic A-B block copolymer of the PEG_{45} series, *p*(PEG_{45}-*b*-$HPMA_{120}$), as expected, was also insoluble in water and a monomodal peak was observed during nanoparticle analysis by DLS. The nanoscale objects formed gave a large D_z of 372 nm, with a moderately low PdI, and the scattering of large objects was confirmed by the increased derived count rate.

The *p*(PEG_{114}-*b*-$HPMA_x$) A-B block copolymer series were all water soluble due to the increased length of the hydrophilic PEG block (5000 g/mol); this increase in hydrophilicity becomes apparent when attempts are made to nanoprecipitate the polymers into water from acetone. Again, the DLS results obtained for *p*(PEG_{114}-*b*-$HPMA_{40}$) and *p*(PEG_{114}-*b*-$HPMA_{80}$) gave low quality data and the low derived count rates also confirmed their solubility in water. The highest molecular weight A-B block copolymer of the *p*(PEG_{114}-*b*-$HPMA_x$) series appeared to form small nanoscale objects, however multi-modal peaks were observed for the z-average size distribution and the large PdI value would not be ideal if we were to use these nanodispersions for further applications.

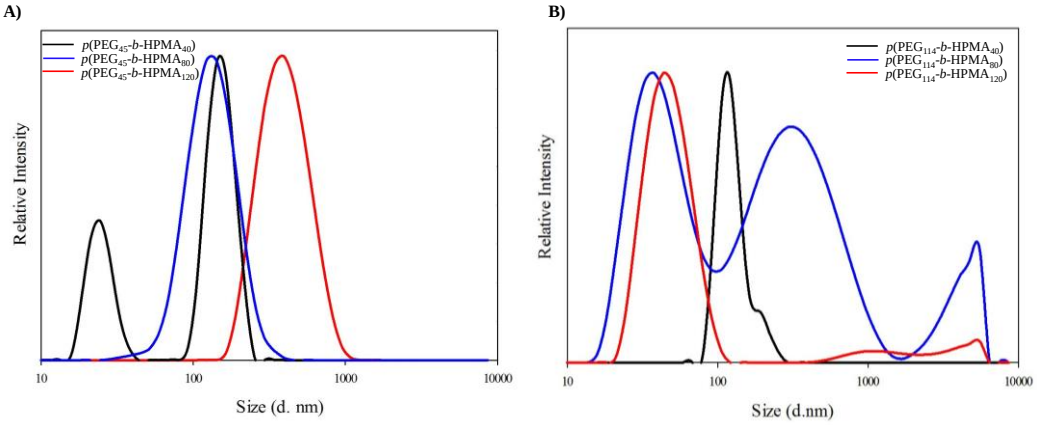

Figure 2.15 DLS D_z overlays of the nanoprecipitation of A-B block copolymers from acetone into water. (i_5-f_1) A) p(PEG$_{45}$-b-HPMA$_x$), B) p(PEG$_{114}$-b-HPMA$_x$).

Table 2.4 DLS results for the nanoprecipitation of linear p(PEG$_y$-b-HPMA$_x$) A-B block copolymers (1 mg/mL).

Polymer	$\boldsymbol{D_z}$ (nm)	**PdI**	$\boldsymbol{D_n}$(nm)	**Derived Count Rate** (kcps)
p(PEG$_{45}$-b-HPMA$_{40}$)*	268 (153 79%, 25 21%)	0.338	21	1850
p(PEG$_{45}$-b-HPMA$_{80}$)*	131	0.227	75	71500
p(PEG$_{45}$-b-HPMA$_{120}$)	372	0.145	340	50300
p(PEG$_{114}$-b-HPMA$_{40}$)*	317	0.373	109	2280
p(PEG$_{114}$-b-HPMA$_{80}$)*	88 (320 49%, 45 39%, 4000 12%)	0.738	23	3720
p(PEG$_{114}$-b-HPMA$_{120}$)	49 (49 90%, 921 5%, 4657 4%)	0.265	30	10020

* Inadequate scattering data

Overall, this control experiment has shown that when the A-B block copolymers are nanoprecipitated individually, nanoscale objects were formed for two of the polymeric materials. Interestingly, the polymers which gave reliable results when measured by DLS, were water insoluble p(PEG$_{45}$-b-HPMA$_{120}$) and soluble p(PEG$_{114}$-b-HPMA$_{120}$) polymers, which are both the most hydrophobic polymers, due to the highest compositions of HPMA within each respective p(PEG$_y$-b-HPMA$_x$) series. The scattering data obtained for p(PEG$_{45}$-b-HPMA$_{80}$) also demonstrated the formation of nanoscale objects, however,

inconsistent data from DLS analysis limited the reliability of the results. These control experiments will be important when studying the co-nanoprecipitation system, which will be discussed further in section 2.6.3.

2.6.2 Aqueous nanoprecipitation studies of branched *p*(HPMA$_{50}$-*co*-EGDMA$_{0.9}$)

Although the nanoprecipitation of branched *p*(HPMA$_x$-*co*-EGDMA$_y$) has been previously discussed and recently reported,[1] it is important to nanoprecipitate the branched copolymer as a control, before carrying out the subsequent co-nanoprecipitation experiments. Due to complete consumption of the previous sample, a new batch of *p*(HPMA$_{50}$-*co*-EGDMA$_{0.9}$) was synthesised as previously described in section 2.3. The GPC analysis of the original sample exhibited an M_n = 24200 g/mol, M_w = 251400 g/mol and a *Đ* of 10.4. The GPC data below (Figure 2.16A) shows the RI chromatogram for the new sample of *p*(HPMA$_{50}$-*co*-EGDMA$_{0.9}$) and the molecular weight values were comparable with the original sample as a broad molecular weight distribution was obtained as observed previously (M_n = 39100 g/mol, M_w = 293100 g/mol and a *Đ* of 7.49). To ensure all nanoparticle dispersions were comparable, the nanoparticles were prepared under the same conditions as previously described, i_5-f_1 from acetone into water. The DLS analysis for aqueous *p*(HPMA$_{50}$-*co*-EGDMA$_{0.9}$) nanoparticles *via* nanoprecipitation of the newly synthesised sample (Figure 2.16B) gave a monomodal peak with a D_z of 148 nm (PdI 0.080). This correlates accordingly with the nanoparticles prepared in Section 2.4.1 from the original sample (D_z = 111, PdI = 0.081) and *p*(HPMA$_{50}$-*co*-EGDMA$_{0.9}$) nanoparticles prepared by Slater *et al* with a D_z of 146 nm (PdI 0.034), so although there are differences in polymer molecular weights, similar nanoparticle sizes were obtained. Generally, nanoparticles prepared from *p*(HPMA$_{50}$-*co*-EGDMA$_{0.9}$) under these conditions, range within the size range of 110-150 nm and from this point onwards all nanoprecipitation experiments will be conducted using the new sample of *p*(HPMA$_{50}$-*co*-EGDMA$_{0.9}$). The presence of spherical nanoparticles consisting of *p*(HPMA$_{50}$-*co*-EGDMA$_{0.9}$) were further confirmed by scanning electron microscopy (SEM) (Figure 2.16C) and the number average diameter (D_n) size value from DLS correlates closely with the D_n calculated from SEM (D_{SEM}). The D_{SEM} value obtained, was averaged over a sample of 220 nanoparticles. During the project, various batches of aqueous *p*(HPMA$_{50}$-*co*-EGDMA$_{0.9}$) nanoparticles were prepared and the DLS analysis for the various batches are presented in the Appendix (Table. A3).

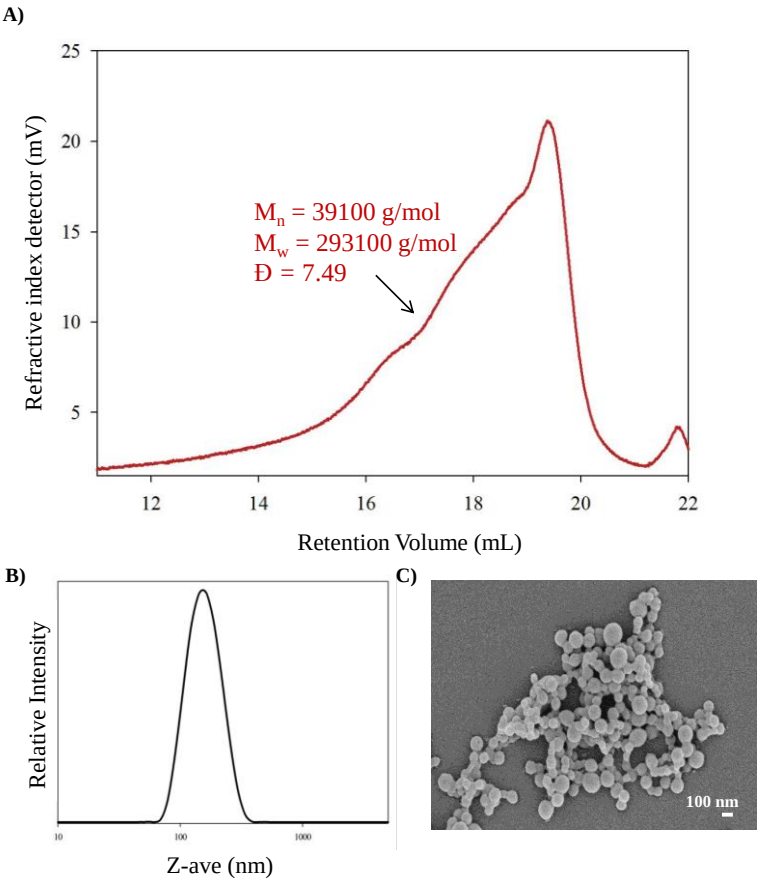

Figure 2.16 Branched *p*(HPMA$_{50}$-*co*-EGDMA$_{0.9}$) analysis and subsequent nanoparticle preparation A) GPC RI chromatogram of *p*(HPMA$_{50}$-*co*-EGDMA$_{0.9}$), B) DLS analysis of *p*(HPMA$_{50}$-*co*-EGDMA$_{0.9}$) aqueous nanoparticles (i_5-f_1), C) SEM image of *p*(HPMA$_{50}$-*co*-EGDMA$_{0.9}$) nanoparticles (diluted to 0.1 mg/mL for imaging).

2.6.3 Co-nanoprecipitation studies of branched *p*(HPMA$_{50}$-*co*-EGDMA$_{0.9}$) and A-B block copolymers

Before conducting the following co-nanoprecipitation experiments, it was hypothesised that the nanoprecipitation of these two architecturally different polymers could result in different outcomes, as shown in Figure 2.10, Section 2.5.1. Ideally, the hydrophobic branched copolymer, *p*(HPMA$_{50}$-*co*-EGDMA$_{0.9}$) and A-B block copolymer, *p*(PEG$_y$-*b*-HPMA$_x$) would associate when nanoprecipitated simultaneously. It may be expected that the hydrophobic *p*(HPMA) segment from the A-B block copolymer would become incorporated within the core and the hydrophilic PEG chain would reside on the nanoparticle surface (Figure 2.10ii). It is also likely that either; the A-B block copolymer would adsorb onto the surface of *p*(HPMA$_{50}$-*co*-EGDMA$_{0.9}$) nanoparticles resulting in a pendant PEG chains (Figure 2.10i), entrapment of the A-B block copolymer within the hydrophobic *p*(HPMA$_{50}$-*co*-EGDMA$_{0.9}$) nanoparticles could occur; (Figure 2.10iii) or

individual objects would form from both the *p*(HPMA$_{50}$-*co*-EGDMA$_{0.9}$) and *p*(PEG$_y$-*b*-HPMA$_x$) resulting in two distinct size populations (Figure 2.10iv). This latter result could occur due to both polymers being able to stabilise themselves independently.

During a typical co-nanoprecipitation experiment, the branched *p*(HPMA$_{50}$-*co*-EGDMA$_{0.9}$) and A-B block copolymer were both dissolved in the good solvent at various ratios for 12-24 hours to ensure complete solubilisation of both polymers. Conditions for the nanoprecipitation experiments were as described in Section 2.4.3, therefore, acetone was employed as the good solvent, water as the anti-solvent and concentrations of i_5-f_1 were maintained, in order to ensure consistency and allow comparison between different polymers and nanoprecipitations in the absence of an A-B block copolymer. The amount of branched copolymer and A-B block copolymer were varied between the ratios of 100:0 to 0:100 wt % respectively. Experimentally, this is a relatively straightforward method and is presented schematically in Figure 2.17.

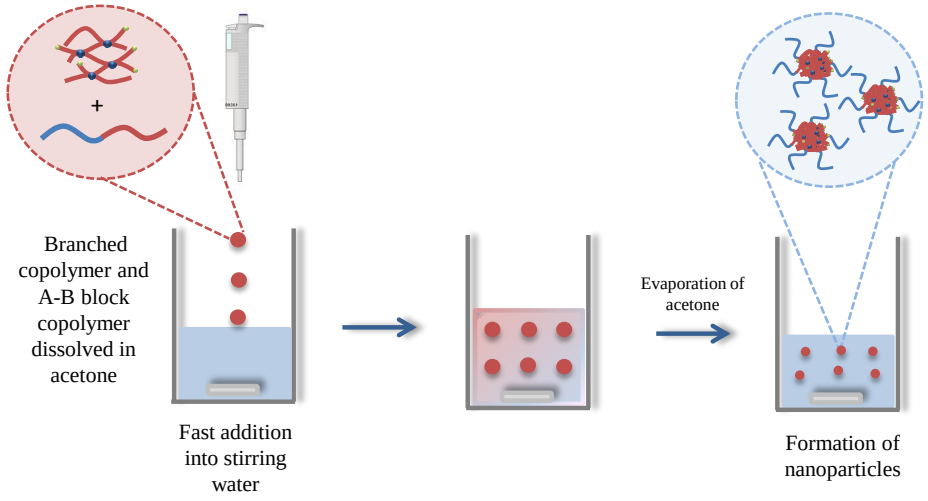

Figure 2.17 Schematic representation of a typical co-nanoprecipitation experiment.

During the nanoprecipitation of solutions containing only A-B block copolymer, four of the six nanodispersions did not provide adequate scattering data. As expected, the nanoprecipitation of branched *p*(HPMA$_{50}$-*co*-EGDMA$_{0.9}$) gave stable spherical nanoparticles but as discussed previously, they were charge stabilised which is supported by a highly negative zeta potential (ζ) of -41 mV. Charge stabilised nanoparticles can easily be de-stabilised by addition of electrolytes, such as NaCl, due to the screening of the repulsive forces by the Na^+ and Cl^- ions.[4] Therefore, a co-nanoprecipitation study was conducted to establish whether the inclusion of an A-B block copolymer could introduce steric stabilisation and provide benefits. It was also important to determine how the

varying chemical compositions of the A-B block copolymer (i.e. ratio of PEG_y:$HPMA_x$) could affect the resulting nanoparticles in terms of size (D_z), PdI and morphology.

2.6.3.1 Co-nanoprecipitation of *p*(HPMA$_{50}$-*co*-EGDMA$_{0.9}$) and *p*(PEG$_{45}$-*b*-HPMA$_x$)

The DLS analysis including D_z, PdI, ζ and D_n for the *p*(PEG_{45}-*b*-$HPMA_x$) A-B block copolymer series is shown in Table 2.5. In almost all cases, the co-nanoprecipitation experiments successfully generated uniform, monomodal particle distributions without sample filtration. It is worth noting that the ratios discussed below correspond to branched copolymer:A-B block copolymer respectively. The sample which did not follow this trend was *p*($HPMA_{50}$-*co*-$EGDMA_{0.9}$):*p*(PEG_{45}-*b*-$HPMA_{80}$) 10:90 wt %, which may be due to the very low wt % of *p*($HPMA_{50}$-*co*-$EGDMA_{0.9}$), therefore poor association occurs between the polymers during the early stages of the nanoprecipitation. The D_z values of the nanoprecipitated particles for *p*(PEG_{45}-*b*-$HPMA_x$) block copolymers between the ratios of 90:10 to 50:50 wt %, varied between 94–127 nm. As the *p*(PEG_{45}-*b*-$HPMA_x$) content was increased beyond 50 wt %, nanoparticles containing *p*(PEG_{45}-*b*-$HPMA_{40}$) and *p*(PEG_{45}-*b*-$HPMA_{80}$) decreased in size (56-78 nm) and interestingly the PdI values for the samples increased after 50:50 wt %. Therefore, to maintain a size ~ 100 nm and a narrow PdI, the optimum wt % during inclusion of both A-B block copolymers was 10–50 wt %. On the other hand, the nanoparticles containing >50 wt % for *p*(PEG_{45}-*b*-$HPMA_{120}$), witnessed an increase in D_z. The *p*(PEG_{45}-*b*-$HPMA_{120}$) is the most hydrophobic across the A-B block copolymer series (<0.13 mg/mL solubility) and the co-nanoprecipitation experiments suggest an optimum wt % range in which the which the *p*(PEG_{45}-*b*-$HPMA_{120}$) associates with the branched copolymer. Although during addition of 20 wt % of *p*(PEG_{45}-*b*-$HPMA_{120}$), nanoparticles were slighter larger, they were consistent with sizes obtained for the varying ratios throughout the series and narrow PdI values were maintained (<0.068). The presence of only 10 wt % *p*($HPMA_{50}$-*co*-$EGDMA_{0.9}$) i.e. inclusion of > 90 wt % of this A-B block copolymer, resulted in an increase for both D_z and PdI, therefore suggesting the optimum amount of *p*(PEG_{45}-*b*-$HPMA_{120}$) for a successful co-nanoprecipitation was 10–80 wt %.

As previously discussed, a strongly negative zeta potential was obtained for charge stabilised *p*($HPMA_{50}$-*co*-$EGDMA_{0.9}$) polymer nanoparticles (-41 mV), however during addition of the varying ratios of *p*(PEG_y-*b*-$HPMA_x$), a decrease in ζ across all co-nanoprecipitates was observed. For example, the addition of only 10 wt % stabilising

p(PEG$_{45}$-*b*-HPMA$_{120}$) block copolymer into the acetone solution with *p*(HPMA$_{50}$-*co*-EGDMA$_{0.9}$), led to a considerable decrease in ζ from -41 mV to -19 mV, suggesting the presence of PEG$_y$ chains on the nanoparticle surface, which is consistent with PEG stabilised nanoparticles or micelles.[35, 36]

The sizes of the co-nanoprecipitated particles, obtained from SEM, were measured and used to calculate a number average, which could be compared to the number average measured by DLS. The SEM images for *p*(HPMA$_{50}$-*co*-EGDMA$_{0.9}$):*p*(PEG$_{45}$-*b*-HPMA$_{120}$) (100:0 – 50:50 wt%) are presented in Figure 2.18A-H and provide evidence of spherical nanoparticle formation. The D_n values determined for the co-nanoprecipitated particles by DLS were consistent with the same assessment by SEM (Table 2.5 & Figure 2.19) (220 particles per reported D_{SEM} value, for histogram analysis see Appendix Fig. A13). Although evidence of nanoparticle formation was observed, determination of D_{SEM} by SEM analysis became increasingly difficult with increasing amounts of A−B block copolymer, due to possible film formation and the presence of objects resembling flattened vesicles at higher ratios (Figure 2.18I-K). The DLS analysis overlays for all co-nanoprecipitates including *p*(HPMA$_{50}$-*co*-EGDMA$_{0.9}$):*p*(PEG$_{45}$-*b*-HPMA$_x$) are presented in the Appendix (Fig. A14).

Table 2.5 DLS and SEM characterisation of nanoparticles comprising of either *p*(HPMA$_{50}$-*co*-EGDMA$_{0.9}$), *p*(PEG$_{45}$-*b*-HPMA$_x$) or varying ratios of *p*(HPMA$_{50}$-*co*-EGDMA$_{0.9}$):*p*(PEG$_{45}$-*b*-HPMA$_x$) both *via* co-nanoprecipitation from acetone (5 mg/mL) into water (Final concentration = 1 mg/mL).

***p*(HPMA$_{50}$-*co*-EGDMA$_{0.9}$):*p*(PEG$_{45}$-*b*-HPMA*x*) Weight ratio (%)**	**100:0**	**90:10**	**80:20**	**70:30**	**60:40**	**50:50**	**40:60**	**30:70**	**20:80**	**10:90**	**0:100**
***p*(HPMA$_{50}$-*co*-EGDMA$_{0.9}$):*p*(PEG$_{45}$-*b*-HPMA$_{40}$)**											
D_z (nm)	148	113	94	106	115	109	75	75	78	77	268*
PdI	0.080	0.067	0.123	0.029	0.047	0.048	0.152	0.166	0.111	0.163	0.338*
ζ (mV)	-41	-30	-31	-19	-25	-32	-23	-25	-20	-24	-15
D_n (nm)	112	87	67	87	94	85	57	54	58	54	21
***p*(HPMA$_{50}$-*co*-EGDMA$_{0.9}$):*p*(PEG$_{45}$-*b*-HPMA$_{80}$)**											
D_z (nm)	148	114	127	115	111	115	76	69	56	76	131*
PdI	0.080	0.045	0.061	0.053	0.037	0.055	0.113	0.122	0.126	0.717	0.227*
ζ (mV)	-41	-28	-28	-26	-23	-27	-26	-19	-18	-20	-23
D_n (nm)	112	91	101	91	91	85	55	49	38	40	75
***p*(HPMA$_{50}$-*co*-EGDMA$_{0.9}$):*p*(PEG$_{45}$-*b*-HPMA$_{120}$)**											
D_z (nm)	148	120	111	108	103	109	95	114	159	217	372
PdI	0.080	0.066	0.033	0.037	0.069	0.032	0.051	0.061	0.068	0.167	0.145
ζ (mV)	-41	-19	-24	-21	-22	-20	-17	-14	-12	-17	-11
D_n (nm)	112	92	89	88	80	88	74	89	135	157	340
D_{SEM} (nm)	117	81	105	117	88	110	-	-	-	-	-

* Inadequate scattering data

Figure 2.19 SEM images of nanoprecipitates and co-nanoprecipitates produced using varying *p*(HPMA$_{50}$-*co*-EGDMA$_{0.9}$):*p*(PEG$_{45}$-*b*-HPMA$_{120}$) ratios: (A) 100:0, (B) 90:10, (C) 80:20, (D) 70:30, (E) 60:40, (F) 50:50, (G) 40:60, (H) 30:70, (I) 20:80, (J) 10:90, (K) 0:100 wt %.

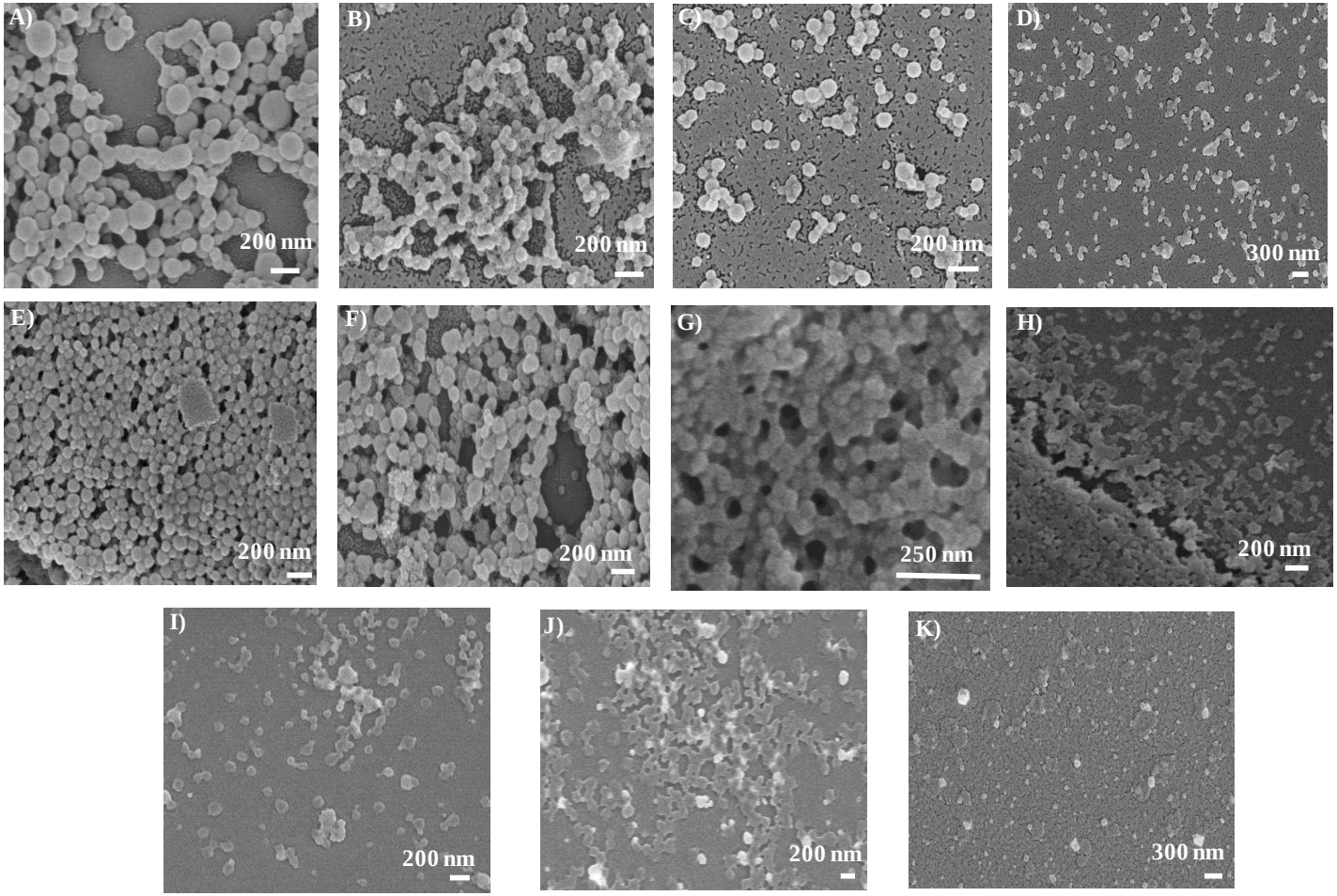

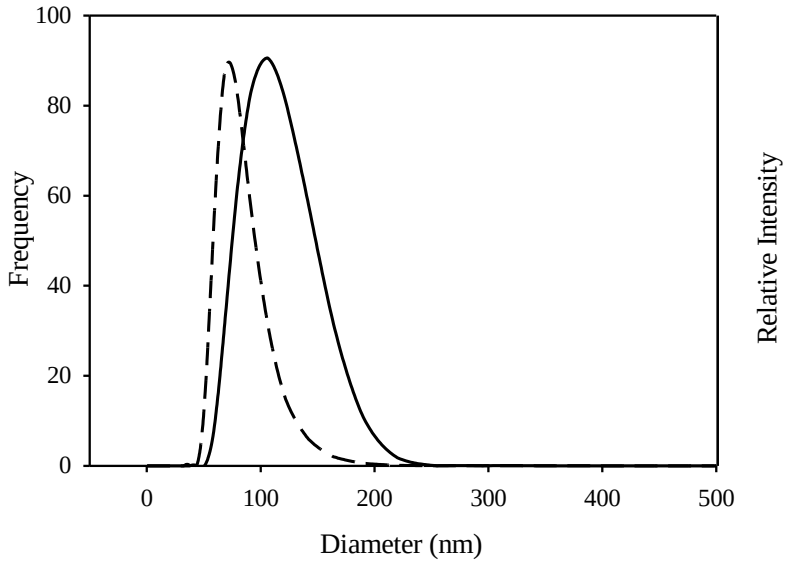

Figure 2.18 Histogram analysis of nanoparticles *via* SEM imaging (average of 220 particles) (grey bar chart) overlaid with the DLS size distribution by intensity (black solid line) and number traces (black dashed line) for *p*(HPMA$_{50}$-*co*-EGDMA$_{0.9}$):*p*(PEG$_{45}$-*b*-HPMA$_{120}$) 60:40 wt %.

2.6.3.2 Co-nanoprecipitation of *p*(HPMA$_{50}$-*co*-EGDMA$_{0.9}$) and *p*(PEG$_{114}$-*b*-HPMA$_x$)

To enhance the steric stabilisation, the following nanoprecipitation experiments were conducted including the A-B block copolymers previously synthesised with an increased PEG chain length (5000 g/mol). As observed with the *p*(PEG$_{45}$-*b*-HPMA$_x$) block copolymer series, the majority of these newly formed co-nanoprecipitates from *p*(HPMA$_{50}$-*co*-EGDMA$_{0.9}$):*p*(PEG$_{114}$-*b*-HPMA$_{40}$), generated monomodal particle distributions without sample filtration. The DLS analysis including; D_z, PdI, ζ and D_n is presented in Table 2.6. It is worth noting that the ratios discussed below correspond to branched copolymer:A-B block copolymer respectively.

The inclusion of *p*(PEG$_{114}$-*b*-HPMA$_{40}$) and *p*(PEG$_{114}$-*b*-HPMA$_{80}$) with *p*(HPMA$_{50}$-*co*-EGDMA$_{0.9}$), between the ratios of 90:10 to 50:50 wt % produced nanoparticles within the range of 103-117 nm. When 50-90 wt % of A-B block copolymer was present, the nanoparticle D_z values decreased (~56-84 nm) and the PdI values for the nanoparticles increased up to a value of 0.332. This decrease in size along with broader PdI values suggests loss of control and the formation of smaller nanoscale objects, possibly micelles or flattened vesicles from the self assembly of the A-B block copolymers. The inclusion of *p*(PEG$_{114}$-*b*-HPMA$_{120}$), resulted in the narrowest distribution of the six A-B block

copolymers selected for the study. The co-nanoprecipitates obtained upon inclusion of this A-B block copolymer from 40:60 to 10:90 wt % were generally less affected by an increase in A-B block copolymer as narrow PdI values were obtained throughout. The overall decrease in size with increasing amount of A-B block copolymer observed for all *p*(PEG_{114}-*b*-$HPMA_x$) A-B block copolymers suggests that a lower ratio of *p*($HPMA_{50}$-*co*-$EGDMA_{0.9}$) encourages colloidal stability and the ratio of branched copolymer:A-B block copolymer does have an effect on the co-nanoprecipitation process. The DLS size value overlays for *p*($HPMA_{50}$-*co*-$EGDMA_{0.9}$):*p*(PEG_{114}-*b*-$HPMA_x$) are presented in the Appendix, Fig. A15.

Introduction of a *p*(PEG_{114}-*b*-$HPMA_x$) block copolymer, again, as witnessed with *p*(PEG_{45}-*b*-$HPMA_x$) association, produces a decrease in ζ across all co-nanoprecipitates, suggesting presence of PEG_y chains on the surface.

To determine the morphology of the *p*($HPMA_{50}$-*co*-$EGDMA_{0.9}$):*p*(PEG_{114}-*b*-$HPMA_{120}$) nanoparticles, nanodispersions containing *p*(PEG_{114}-*b*-$HPMA_{120}$) block copolymer were analysed by SEM, which confirmed the presence of spherical nanoparticles (Figure 2.20A-G). D_n values determined by DLS were consistent with the same assessment by SEM, Table 2.6 & Appendix A16. As reported for *p*($HPMA_{50}$-*co*-$EGDMA_{0.9}$):*p*(PEG_{114}-*b*-$HPMA_{120}$) nanoparticles, the D_{SEM} values were obtained from a sample of 220 particles. Although SEM has provided evidence of nanoparticle formation, the analysis became increasingly difficult with increasing amounts of A−B block copolymer, possibly due to PEG film formation and hence the detailed analysis of 100:0 to 50:50 wt % ratios only.

Table 2.6 DLS and SEM characterisation of nanoparticles comprising of either *p*(HPMA$_{50}$-*co*-EGDMA$_{0.9}$), *p*(PEG$_{114}$-*b*-$_{HPMAx}$) or varying ratios of *p*(HPMA$_{50}$-*co*-EGDMA$_{0.9}$):*p*(PEG$_{114}$-*b*-HPMA$_x$) both *via* co-nanoprecipitation from acetone (5 mg/mL) into water (Final concentration = 1 mg/mL).

***p*(HPMA$_{50}$-*co*-EGDMA$_{0.9}$):p(PEG$_{114}$-*b*-HPMA*x*) Weight ratio (%)**	**100:0**	**90:10**	**80:20**	**70:30**	**60:40**	**50:50**	**40:60**	**30:70**	**20:80**	**10:90**	**0:100**
***p*(HPMA$_{50}$-*co*-EGDMA$_{0.9}$):*p*(PEG$_{114}$-*b*-HPMA$_{40}$)**											
D_z (nm)	148	111	103	121	107	117	76	75	75	73	317*
PdI	0.080	0.055	0.152	0.061	0.028	0.088	0.178	0.224	0.212	0.254	0.373*
ζ (mV)	-41	-30	-27	-28	-28	-32	-30	-26	-26	-25	-15
D_n (nm)	112	88	72	96	87	129	53	49	49	48	105
***p*(HPMA$_{50}$-*co*-EGDMA$_{0.9}$):*p*(PEG$_{114}$-*b*-HPMA$_{80}$)**											
D_z (nm)	148	112	106	106	103	111	84	71	67	56	88*
PdI	0.080	0.045	0.118	0.124	0.045	0.081	0.332	0.096	0.140	0.184	0.738*
ζ (mV)	-41	-27	-29	-29	-28	-21	-24	-22	-16	-14	-20
D_n (nm)	112	90	74	74	79	112	54	54	46	33	23
***p*(HPMA$_{50}$-*co*-EGDMA$_{0.9}$):*p*(PEG$_{114}$-*b*-HPMA$_{120}$)**											
D_z (nm)	148	132	127	113	117	103	70	62	56	46	49
PdI	0.080	0.059	0.043	0.069	0.059	0.051	0.085	0.085	0.075	0.152	0.265
ζ (mV)	-41	-13	-21	-23	-17	-15	-15	-10	-15	-13	-15
D_n (nm)	112	90	74	74	79	82	54	54	46	33	30
D_{SEM} (nm)	117	101	85	88	82	95	-	-	-	-	-

* Inadequate scattering data

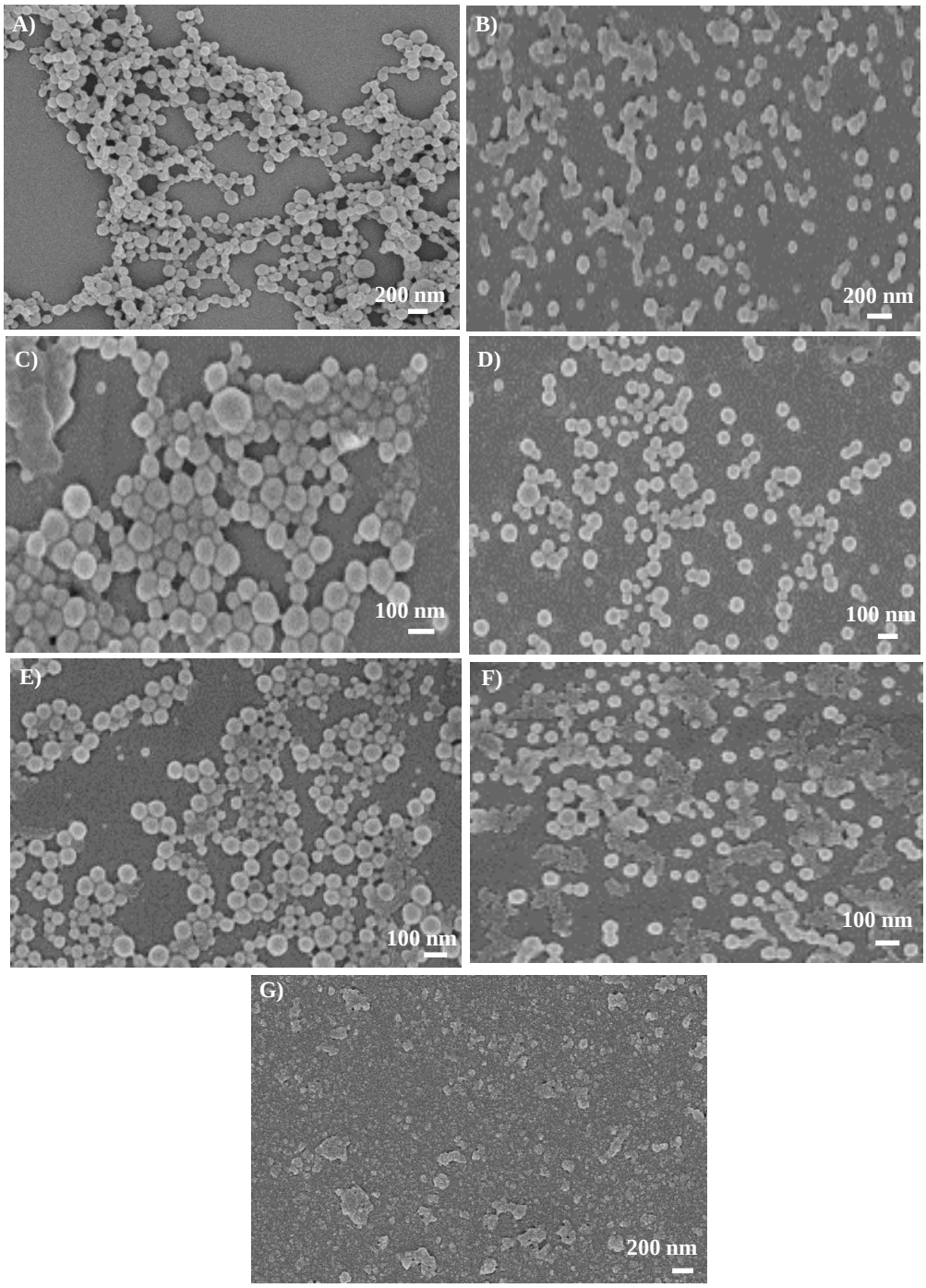

Figure 2.20 SEM images of nanoprecipitates and co-nanoprecipitates produced using varying *p*(HPMA$_{50}$-*co*-EGDMA$_{0.9}$):*p*(PEG$_{114}$-*b*-HPMA$_{120}$) weight ratios: (A) 100:0, (B) 90:10, (C) 80:20, (D) 70:30, (E) 60:40, (F) 50:50, (G) 0:100 wt %.

Overall, the nanoparticles obtained *via* co-nanoprecipitation from the association of *p*(PEG$_{45}$-*b*-HPMA$_x$)/*p*(PEG$_{114}$-*b*-HPMA$_x$) A-B block copolymers with *p*(HPMA$_{50}$-*co*-EGDMA$_{0.9}$) were within the ideal size range to be considered as drug delivery nanocarriers. It should be highlighted that none of the nanoparticle dispersions required filtration in order to obtain a narrow monomodal distribution. Generally, the D_z values remained around ~100 nm between the ratios of 90:10 to 50:50 wt % *p*(HPMA$_{50}$-*co*-EGDMA$_{0.9}$):*p*(PEG$_y$-*b*-HPMA$_x$) respectively. This was followed by a noticeable decrease from 40:60 wt % onwards, which could be due to nanoparticles reaching colloidal stability at a smaller size and competition of the A-B block copolymer. Interestingly, the increasing wt % of the two most hydrophobic A-B block copolymers of each series, *p*(PEG$_{45}$-*b*-HPMA$_{120}$) and *p*(PEG$_{114}$-*b*-HPMA$_{120}$), resulted in nanoparticles which maintained narrow PdI values throughout the variations of ratios. These trends observed are presented schematically in Figure 2.21. An exception of the general trend was recognised for *p*(PEG$_{45}$-*b*-HPMA$_{120}$), where minor deviations in size were observed at high wt % A-B block copolymer, contrasting to all the other A-B block copolymers. The D_z and narrow PdI values obtained for up to 80 wt % of this particular A-B block copolymer, suggest the mechanism of nanoparticle formation is less affected when an insoluble A-B block copolymer is utilised and may imply that there is less competition between the A-B block copolymer and *p*(HPMA$_{50}$-*co*-EGDMA$_{0.9}$) branched copolymer.

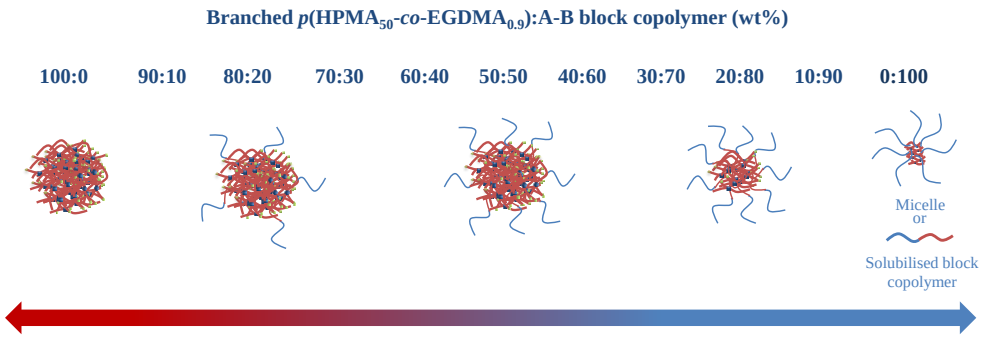

Figure 2.21 Schematic representation of the nanoparticles formed *via* nanoprecipitation and co-nanoprecipitation of branched *p*(HPMA$_{50}$-*co*-EGDMA$_{0.9}$) and an A-B block copolymer.

2.6.3.3 Aqueous nanoprecipitation of branched *p*(HPMA$_{50}$-*co*-EGDMA$_{0.9}$) into an aqueous solution of water soluble A-B block copolymers

Previous research studies of the preparation of polymer nanoparticles *via* nanoprecipitation often include commercial surfactants such as Tween 20 and polyvinyl alcohol to stabilise the polymer within the aqueous phase (see Chapter 1, Table 1.1). The

aim of the following experiments was to investigate if it was possible to form stable nanoparticles after addition of branched *p*(HPMA$_{50}$-*co*-EGDMA$_{0.9}$) into aqueous solutions of the four soluble A-B block copolymers; *p*(PEG$_{45}$-*b*-HPMA$_{40}$), *p*(PEG$_{114}$-*b*-HPMA$_{40}$), *p*(PEG$_{114}$-*b*-HPMA$_{80}$) and *p*(PEG$_{114}$-*b*-HPMA$_{120}$). If so, it was of interest to see if a difference in size was observed when using this method compared with the co-nanoprecipitation, and the process is represented graphically in Figure 2.21. The nanoprecipitation was conducted by preparing a stock solution of *p*(HPMA$_{50}$-*co*-EGDMA$_{0.9}$) (2.5 mg/mL) in acetone and 1 mL of this solution was added to one of the four A-B block copolymers solubilised in H_2O (0.1 mg/mL in 5 mL H_2O). The same final concentration of both polymers (1 mg/mL) was maintained in order to draw direct comparisons with the simultaneous addition experiments and the ratio of branched copolymer:A-B block copolymer studied was 50:50 wt %.

It was hypothesised that the addition of *p*(HPMA$_{50}$-*co*-EGDMA$_{0.9}$) into a solution of solubilised A-B block copolymer may have resulted in two or more different nanoparticle size distributions, due to the association of both the branched copolymer with the A-B block copolymer and formation of nanoscale objects composed of A-B block copolymer only (DLS results for the solubilisation of the A-B block copolymers in water, Appendix, Fig. A17 & Table A4), however this was not the case. The data presented in Table 2.7, shows that for all nanoprecipitation experiments involving the addition of *p*(HPMA$_{50}$-*co*-EGDMA$_{0.9}$) into aqueous solutions of water soluble A-B block copolymer, single size distributions were obtained, as well as a noticeable decrease in size when compared with simultaneous addition. This decrease in size could be due to the large differences in concentration of polymers during the nanoprecipitation experiment. The dropwise addition of *p*(HPMA$_{50}$-*co*-EGDMA$_{0.9}$) into an excess aqueous solution of *p*(PEG$_y$-*b*-HPMA$_x$) A-B block copolymer could result in the A-B block copolymers concentrating at the particle surface to stabilise *p*(HPMA$_{50}$-*co*-EGDMA$_{0.9}$) nanoparticles. This suggests adsorption of the A-B block copolymers onto the surface and as seen previously with simultaneous addition, the PdI values obtained were <0.101, which is evident of a controlled nanoprecipitation. The monomodal distributions observed (Figure 2.22) suggest that the A-B block copolymers are becoming incorporated during the nanoprecipitation of *p*(HPMA$_{50}$-*co*-EGDMA$_{0.9}$), and if this was not the case, two different size populations would have been observed for both *p*(HPMA$_{50}$-*co*-EGDMA$_{0.9}$) and the A-B block copolymer present in the water. These experiments provide further evidence that the HPMA chain from the A-B block copolymer becomes either associated/adsorbed

onto *p*(HPMA$_{50}$-*co*-EGDMA$_{0.9}$) (Figure 2.10i) or incorporated into the *p*(HPMA$_{50}$-*co*-EGDMA$_{0.9}$) nanoparticle during the nanoprecipitation (Figure 2.10ii). If successful, the electrolyte stability of these nanoparticles will be explored in section 2.7.1 to further evaluate the nanoparticle behaviour and how this compares to nanoparticles prepared during simultaneous addition. It is worth noting that the addition of all branched *p*(HPMA$_{50}$-*co*-EGDMA$_{0.9}$) polymer solutions into A-B block copolymer aqueous dispersions, were conducted under the same conditions and during the same day to ensure consistency.

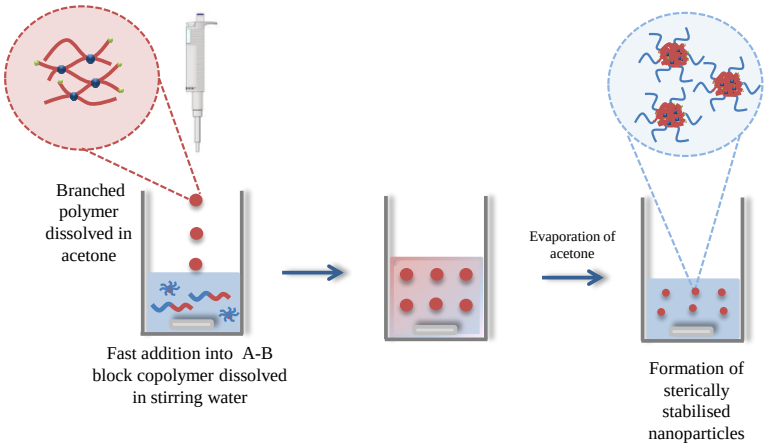

Figure 2.21 Graphical representation of the formation of co-nanoprecipitated nanoparticles by addition of branched *p*(HPMA$_{50}$-*co*-EGDMA$_{0.9}$) to a solution of a water soluble A-B block copolymer. (Final concentration of total polymer 1 mg/mL in H_2O).

Table 2.7 Comparison of DLS results for branched *p*(HPMA$_{50}$-*b*-EGDMA$_{0.9}$) and A-B block copolymer added co-nanoprecipitated *vs* nanoprecipitation of *p*(HPMA$_{50}$-*co*-EGDMA$_{0.9}$) into aqueous solutions of water soluble A-B block copolymer. All ratios were fixed at 50 wt % of each polymer.

Sample (50:50 wt %)		**D_z** (nm)	**PdI**	**D_n** (nm)
Nanoprecipitation	Addition of *p*(HPMA$_{50}$-*co*-EGDMA$_{0.9}$) into an aqueous solution of *p*(PEG$_{45}$-*b*-HPMA$_{40}$)	80	0.073	64
	Addition of *p*(HPMA$_{50}$-*co*-EGDMA$_{0.9}$) into an aqueous solution of *p*(PEG$_{114}$-*b*-HPMA$_{40}$)	83	0.069	63
	Addition of *p*(HPMA$_{50}$-*co*-EGDMA$_{0.9}$) into an aqueous solution of *p*(PEG$_{114}$-*b*-HPMA$_{80}$)	89	0.101	67
	Addition of *p*(HPMA$_{50}$-*co*-EGDMA$_{0.9}$) into an aqueous solution of *p*(PEG$_{114}$-*b*-HPMA$_{120}$)	90	0.055	70
Co-nanoprecipitation	Simultaneous addition of *p*(HPMA$_{50}$-*co*-EGDMA$_{0.9}$) and *p*(PEG$_{45}$-*b*-HPMA$_{40}$)	109	0.048	85
	Simultaneous addition of *p*(HPMA$_{50}$-*co*-EGDMA$_{0.9}$) and *p*(PEG$_{114}$-*b*-HPMA$_{40}$)	117	0.088	129
	Simultaneous addition of *p*(HPMA$_{50}$-*co*-EGDMA$_{0.9}$) and *p*(PEG$_{114}$-*b*-HPMA$_{80}$)	111	0.081	84
	Simultaneous addition of *p*(HPMA$_{50}$-*co*-EGDMA$_{0.9}$) and *p*(PEG$_{114}$-*b*-HPMA$_{120}$)	103	0.045	82

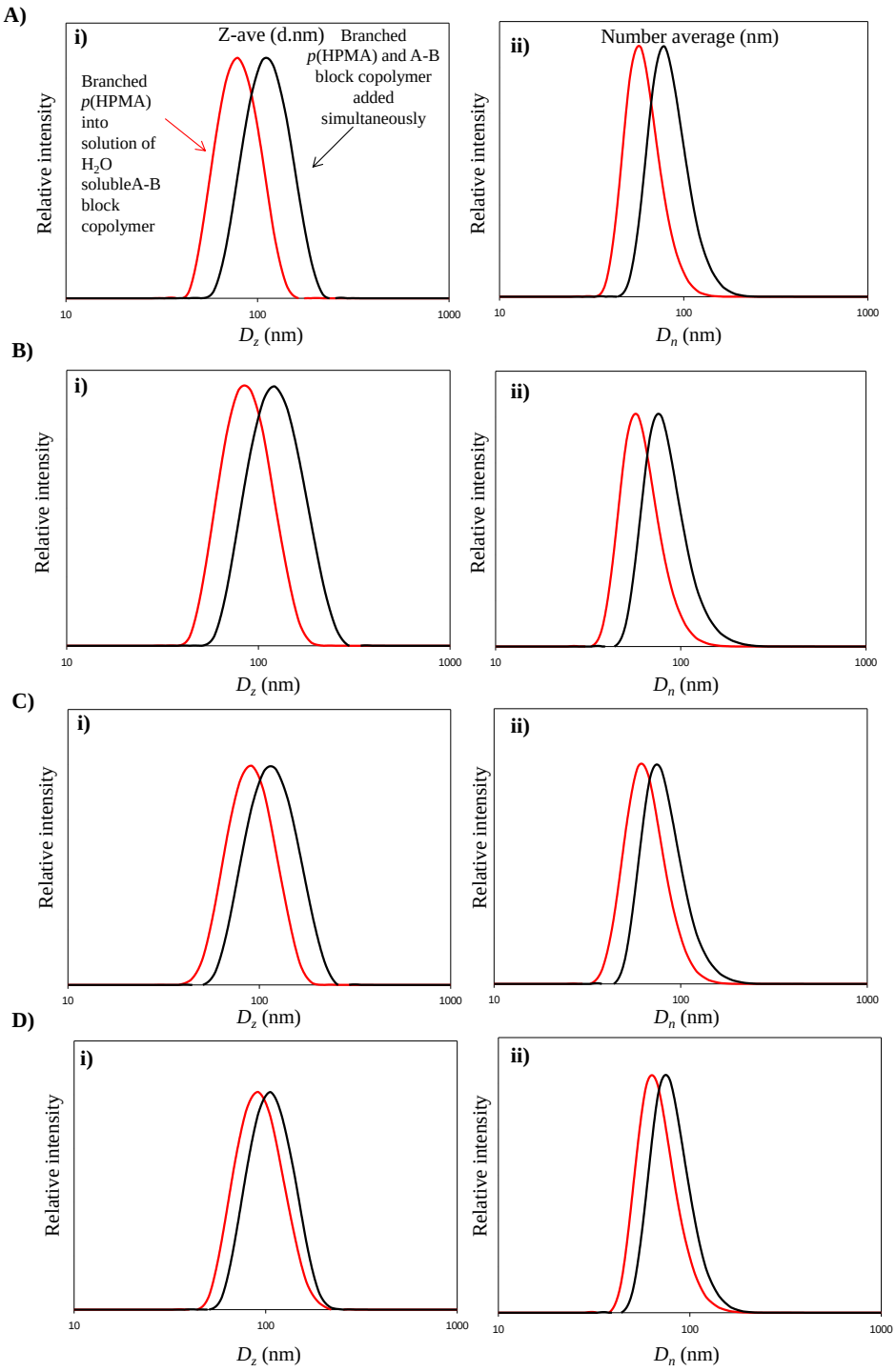

Figure 2.22 DLS trace overlays A) i) Z-average sizes for branched *p*(HPMA$_{50}$-*co*-EGDMA$_{0.9}$) added simultaneously (black trace), *p*(HPMA$_{50}$-*co*-EGDMA$_{0.9}$) added to *p*(PEG$_{45}$-*b*-HPMA$_{40}$) dissolved in H_2O (red trace), ii) Number average sizes for *p*(HPMA$_{50}$-EGDMA$_{0.9}$) and *p*(PEG$_{45}$-*b*-HPMA$_{40}$) added simultaneously (black trace), *p*(HPMA$_{50}$-*co*-EGDMA$_{0.9}$) added to *p*(PEG$_{45}$-*b*-HPMA$_{40}$) dissolved in H_2O (red trace) and B), C) & D) have the same labelling system. B) *p*(HPMA$_{50}$-EGDMA$_{0.9}$):*p*(PEG$_{114}$-*b*-HPMA$_{40}$) C) *p*(HPMA$_{50}$-*co*-EGDMA$_{0.9}$):*p*(PEG$_{114}$-*b*-HPMA$_{80}$) D) *p*(HPMA$_{50}$-*co*-EGDMA$_{0.9}$):*p*(PEG$_{114}$-*b*-HPMA$_{120}$), all 50:50 wt % ratios.

The shape of the aqueous nanoparticles prepared by addition of *p*(HPMA$_{50}$-*co*-EGDMA$_{0.9}$) into aqueous solutions of the A-B block copolymers; *p*(PEG$_{45}$-*b*-HPMA$_{40}$), *p*(PEG$_{114}$-*b*-HPMA$_{40}$), *p*(PEG$_{114}$-*b*-HPMA$_{80}$) and *p*(PEG$_{114}$-*b*-HPMA$_{120}$) *via* nanoprecipitation, were also analysed by SEM and spherical nanoparticles were observed for each sample (Figure 2.23 A-D). The nanoparticle dispersions did not exhibit any sign of polymer precipitation (Figure 2.23 E) and did not require further filtration. The NaCl stability of these nanodispersions will be investigated in Section 2.7.4, in order to gain a further insight into this nanoprecipitation process.

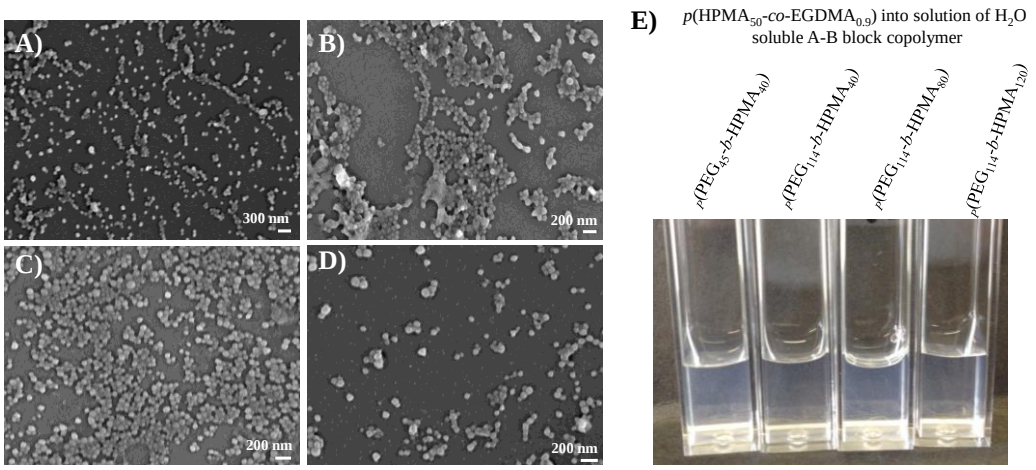

Figure 2.23 SEM images for branched *p*(HPMA$_{50}$-*co*-EGDMA$_{0.9}$) nanoprecipitated into water soluble A-B block copolymers 50:50 wt% (Nanoparticle dispersions diluted to 0.1 mg/mL for imaging) A) *p*(PEG$_{45}$-*b*-HPMA$_{40}$), B) *p*(PEG$_{114}$-*b*-HPMA$_{40}$), C) *p*(PEG$_{114}$-*b*-HPMA$_{80}$), D) *p*(PEG$_{114}$-*b*-HPMA$_{120}$), E) Photograph to show nanoparticle dispersions after nanoprecipitation of *p*(HPMA$_{50}$-*co*-EGDMA$_{0.9}$) into A-B block copolymers. For all co-nanoprecipitation experiments, the ratio for all experiments was 50:50 wt %.

2.7 Stability studies of aqueous co-nanoprecipitated particle dispersions

2.7.1 Stability of co-nanoprecipitated nanoparticles in the presence of NaCl

To be considered as a potential drug delivery vehicle, it is important for the nanoparticles to remain stable under physiologically relevant conditions. During a typical NaCl addition experiment, aliquots (20 μL) of an aqueous 0.5 M NaCl solution were added to 1 mL samples of the aqueous nanoparticle dispersions, and D_z and PdI values were measured during a 21 day period at ambient temperature. It is worth noting that an aliquot of NaCl was added to ensure any dilution effects were minimised and a final concentration of NaCl was kept constant at 0.01M for all samples. After evaporation of the good solvent, DLS

measurements were conducted and the solution was agitated before addition to a disposable sizing cuvette (D_z, D_n and ζ values were taken as the average of 3 repeated measurements per sample). The nanodispersion was returned to the original sample vial and stored at ambient temperature for the 1, 7 and 21 day measurements, and studies were carried out as described above.

As previously discussed, it is desirable to produce nanoparticles which would be sterically stabilised, rather than charge stabilised, to afford stability in physiological conditions. Nanoparticles composed solely of branched *p*(HPMA$_{50}$-*co*-EGDMA$_{0.9}$), can be easily de-stabilised by addition of electrolytes, due to the screening of repulsive charges by the ions present. The screening of charges reduces the repulsive forces between the nanoparticles and as a result attractive forces dominate, bringing the particles closer together causing aggregation and ultimately precipitation. Branched *p*(HPMA$_{50}$-*co*-EGDMA$_{0.9}$) nanoparticles are stable for long periods of time and have shown no increase in D_z after 1 month under ambient storage conditions (Figure Bi&ii). However, during NaCl addition the polymer nanoparticles become destabilised and precipitation was observed. This was expected for the charge stabilised particles and the precipitation of the polymer is illustrated in Figure 2.24C.

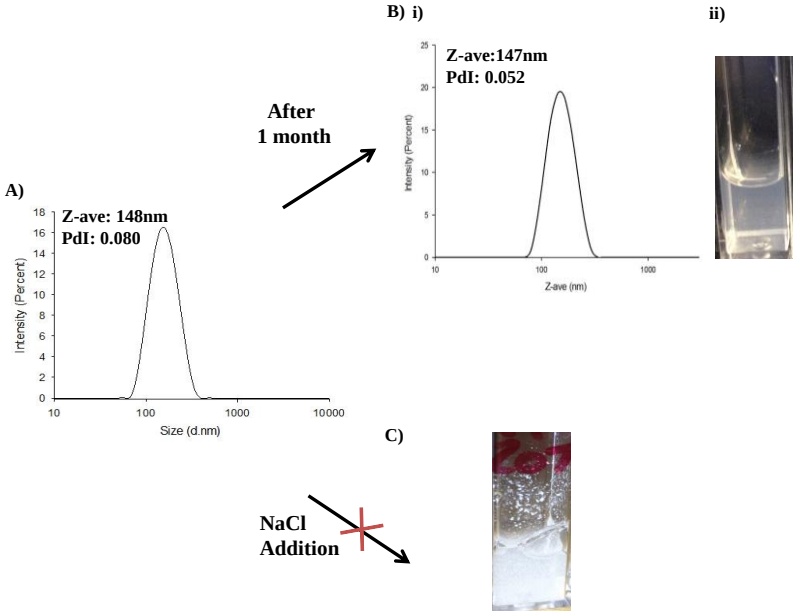

Figure 2.24 Stability of aqueous branched *p*(HPMA$_{50}$-*co*-EGDMA$_{0.9}$) nanoparticles. A) DLS analysis of branched *p*(HPMA$_{50}$-*co*-EGDMA$_{0.9}$) nanoparticles, B) i) DLS analysis of branched *p*(HPMA$_{50}$-*co*-EGDMA$_{0.9}$) nanoparticles after 1 month, ii) Photograph of a stable *p*(HPMA$_{50}$-*co*-EGDMA$_{0.9}$) nanodispersion, C) Photograph of NaCl addition to a *p*(HPMA$_{50}$-*co*-EGDMA$_{0.9}$) nanodispersion (20 µL of 0.5M NaCl to 1 mL of 1 mg/mL dispersion).

The DLS measurements for the nanoprecipitation of solutions composed solely of *p*(PEG$_{45}$-*b*-HPMA$_{120}$) and *p*(PEG$_{114}$-*b*-HPMA$_{120}$) generated accurate, meaningful data and interestingly both A-B block copolymers were composed of the longest hydrophobic HPMA chains. The DLS results obtained for the nanoprecipitation of 100 wt % of the remaining four A-B block copolymers were inconclusive due to inadequate light scattering. Therefore, the NaCl stability experiments were only conducted for *p*(PEG$_{45}$-*b*-HPMA$_{120}$) and *p*(PEG$_{114}$-*b*-HPMA$_{120}$). For *p*(PEG$_{45}$-*b*-HPMA$_{120}$), after 1 day exposure to NaCl, the nanoparticle D_z values showed a decrease of 148 from 404 nm (instant addition measurement), as introduction of the electrolyte had greatly affected the nanoscale objects (Figure 2.25A). To rationalise this effect, it has been reported that the introduction of electrolyte solution disturbs the water structure around PEG and can cause shrinking of PEG$_y$ chains at the nanoparticle surface.[37] The decrease in size was further confirmed by comparing the average D_n values for this sample as an additional smaller size population was observed (Figure 2.26 A). An increase in size was observed between the 1 and 21 day NaCl addition measurements; up to a final D_z of 466 nm and the number average traces also highlight this (Figure 2.26 B&C). These results suggest that after 1 day, the nanoscale objects associated together to form larger objects and although the PEG chains on the surface have decreased in size due to NaCl addition, they are still sufficient to provide steric stabilisation and therefore prevent aggregation.

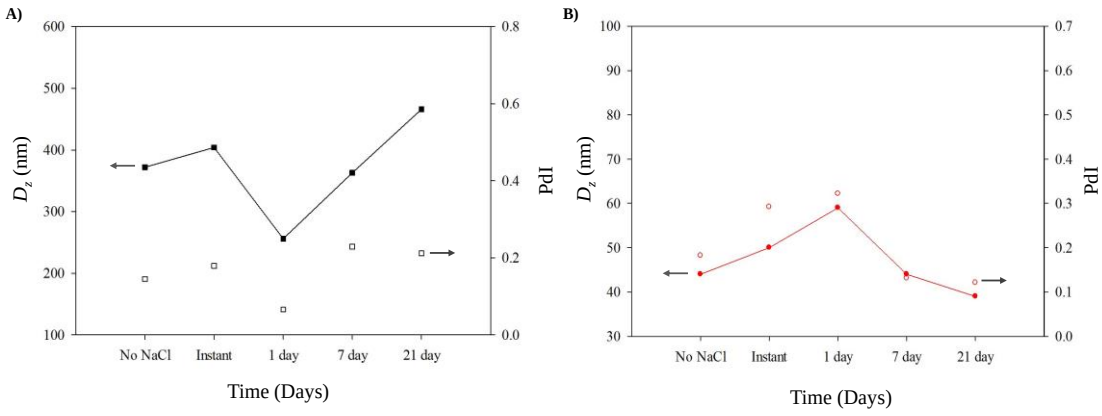

Figure 2.25 Stability of nanodispersion of A-B block copolymer in the presence of NaCl during a 0-21 day period. A) *p*(PEG$_{45}$-*b*-HPMA$_{120}$), B) *p*(PEG$_{114}$-*b*-HPMA$_{120}$).

A small decrease in D_z (~10 nm) was observed for *p*(PEG$_{114}$-*b*-HPMA$_{120}$) A-B block copolymer after 21 days when compared to the original nanodispersion (Figure 2.25 B). During the first 24 hours the nanoscale objects increased ~15 nm, suggesting the association of nanoscale objects in order to minimise the effects of the addition of NaCl.

The decrease observed between 7-21 day, again as seen previously with *p*(PEG$_{45}$-*b*-HPMA$_{120}$), the presence of NaCl can result in a shrinking of PEG chains at the surface and therefore a smaller size, but not enough to cause precipitation of the polymer. The D_n trace overlays (Appendix, Fig. A18), also show the small changes in size observed throughout the study. Although both nanodispersions of the A-B block copolymers remained stable to NaCl throughout the 21 day test period, there were large variations in sizes within this study and PdI values which often exceeded > 0.2.

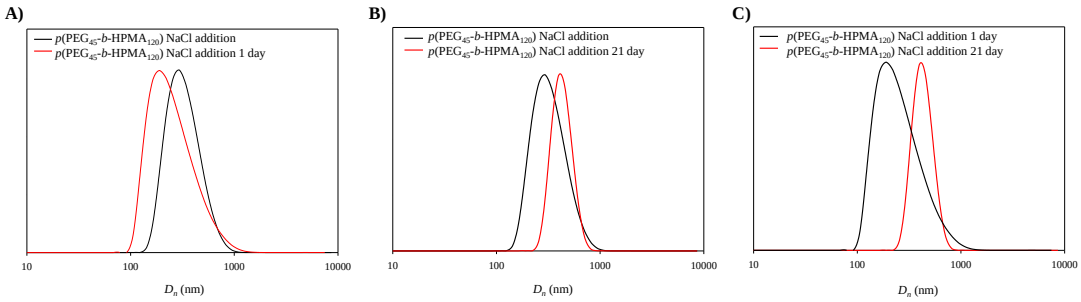

Figure 2.26 D_n analysis by DLS after NaCl addition. A) *p*(PEG$_{45}$-*b*-HPMA$_{120}$) in the absence of NaCl (black line), *p*(PEG$_{45}$-*b*-HPMA$_{120}$) 1 day NaCl addition (red line), B) *p*(PEG$_{45}$-*b*-HPMA$_{120}$) in the absence of NaCl (black line), *p*(PEG$_{45}$-*b*-HPMA$_{120}$) 21 day NaCl addition (red line), C) *p*(PEG$_{45}$-*b*-HPMA$_{120}$) 7 day NaCl addition (black line), *p*(PEG$_{45}$-*b*-HPMA$_{120}$) 21 day NaCl addition (red line).

2.7.2 Stability of *p*(PEG$_{45}$-*b*-HPMA$_x$) A-B block copolymer aqueous co-nanoprecipitated particles

Up to now, it is evident that NaCl addition to nanoparticles composed solely of *p*(HPMA$_{50}$-*co*-EGDMA$_{0.9}$), results in de-stabilisation and precipitation of the polymer. Although stable to NaCl, the nanoscale objects of *p*(PEG$_y$-*b*-HPMA$_{120}$) A-B block copolymers demonstrated large size deviations throughout the 21 day study period and final sizes of nanoparticles obtained were not ideal. To further investigate the co-nanoprecipitation process, it was of interest to conduct NaCl stability studies across the varying ratios of *p*(HPMA$_{50}$-*co*-EGDMA$_{0.9}$):*p*(PEG$_y$-*b*-HPMA$_x$), to provide a greater understanding of how the A-B block copolymer becomes involved during the nanoprecipitation. As previously discussed and schematically presented in Figure 2.10, there are four potential outcomes, which could occur during a co-nanoprecipitation experiment. Up to now, the hypothesis which suggested the formation of various sized nanoscale objects (Figure 2.10iv) is unlikely due to the results obtained from previous co-nanoprecipitation studies (monomodal size distributions and narrow PdI values). It is more

likely that the A-B block copolymer is either; adsorbing loosely onto the *p*(HPMA$_{50}$-*co*-EGDMA$_{0.9}$) nanoparticle with pendant PEG chains on the surface (Figure 2.10i), the HPMA segment from the A-B block copolymer becomes incorporated into *p*(HPMA$_{50}$-*co*-EGDMA$_{0.9}$), with PEG chains on the surface (Figure 2.10ii) or entrapment of the A-B block copolymer within the *p*(HPMA$_{50}$-*co*-EGDMA$_{0.9}$) core (Figure 2.10iii). If the co-nanoprecipitates were behaving as suggested in Figure 2.10iii, then it would be expected that the resulting nanoparticles would behave identically to nanoparticles composed only of *p*(HPMA$_{50}$-*co*-EGDMA$_{0.9}$) i.e. charge stabilised and precipitate upon NaCl addition. The varying chemical compositions of the A-B block copolymers are expected to have a large effect on the stability of co-nanoprecipitates (i.e. PEG$_y$ to HPMA$_x$ content), therefore it may be observed that different mechanisms are adopted during incorporation of the varying A-B block copolymers. It would be anticipated that the *p*(PEG$_{114}$-*b*-HPMA$_x$) A-B block copolymer series should offer an increased resistance to NaCl, due the increased PEG$_y$ chain length (~ 5000 g/mol).

So far, the low ζ values obtained from the co-nanoprecipitation experiments of an A-B block copolymer and *p*(HPMA$_{50}$-*co*-EGDMA$_{0.9}$) have demonstrated an overall decrease in surface charge when compared with branched *p*(HPMA$_{50}$-*co*-EGDMA$_{0.9}$). The reduced ζ values obtained during the inclusion of the A-B block copolymer suggests that the PEG chains from the A-B block copolymer are situated on the outer surface of the nanoparticles, and should therefore offer a level of resistance to salt addition due to steric stabilisation. In order to investigate the effect of A-B block copolymer concentration required to stabilise *p*(HPMA$_{50}$-*co*-EGDMA$_{0.9}$) during exposure to NaCl, the experiments were carried out for the ratios between 90:10-10:90 wt %, *p*(HPMA$_{50}$-*co*-EGDMA$_{0.9}$):*p*(PEG$_y$-*b*-HPMA$_x$) respectively.

The addition of 10 and 20 wt % of *p*(PEG$_{45}$-*b*-HPMA$_{40}$) A-B block copolymer had no meaningful effect on the salt stability of the co-nanoprecipitates, as demonstrated by a large increase in D_z values and precipitation after 1 day for both samples (Figure 2.26A). However, 30 wt % addition led to an increase in stability during the 7 day test period, yet a large D_z increase (>300 nm) was observed. The 21 day test measurement was not conducted on this sample due to polymer precipitation (Figure 2.26B). Further increase in A−B block copolymer content within the co-nanoprecipitates (60:40-20:80 wt %), led to increasing stability and no visible precipitate after the 21 day study period was observed. The size and PdI values of nanodispersions 40:60, 30:70 and 20:80 wt % were least affected by NaCl addition during the 21 day period. For samples >40:60 wt % there was

an observed decrease ~75 nm from previous values >100 nm. After instantaneous NaCl addition, the co-nanoprecipitates including *p*(HPMA$_{50}$-*co*-EGDMA$_{0.9}$):*p*(PEG$_{45}$-*b*-HPMA$_{40}$) 10:90 wt %, did not provide reliable DLS data. This behaviour suggests that although there is a huge excess of stabilising PEG chains from the A-B block copolymer, the ratio of both polymers is not favourable and results in an unstable dispersion.

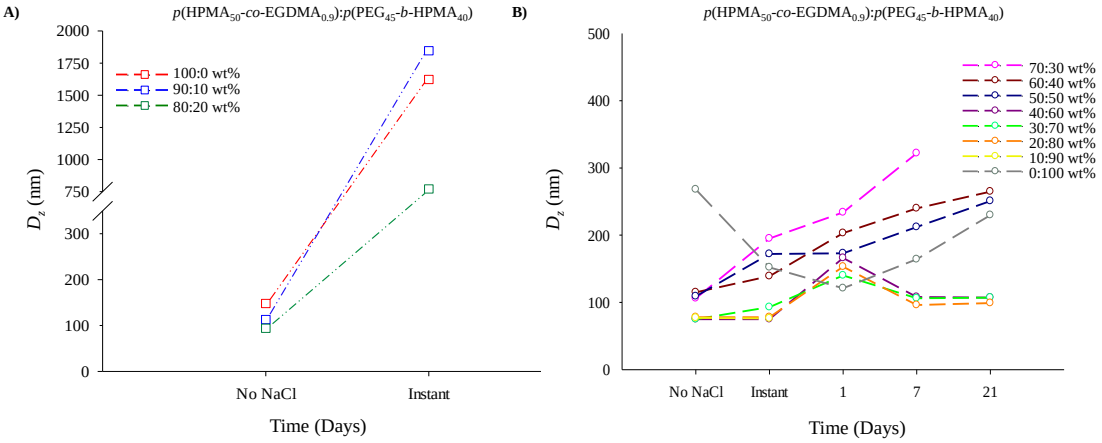

Figure 2.26 Stability of *p*(HPMA$_{50}$-*co*-EGDMA$_{0.9}$):*p*(PEG$_{45}$-*b*-HPMA$_{40}$) to NaCl during a 21 day period. A) Dashed line open squares, 100:0 = red, 90:10 = blue, 80:20 = dark green, B) Dashed line open circles, 70:30 = pink 60:40 = dark red, 50:50 = dark blue, 40:60 = dark purple, 30:70 = light green = 30:70, orange = 20:80, yellow = 10:90, grey = 0:100 wt %*. (*Inadequate light scattering data obtained)

There are notable differences in stability when the DP$_n$ of HPMA of *p*(PEG$_{45}$-*b*-HPMA$_x$) A-B block copolymer is increased from 40 to 80 monomer units. The co-nanoprecipitates between 90:10-50:50 wt % ratios remained stable during the 21 day test period and contrasting to *p*(PEG$_{45}$-*b*-HPMA$_{40}$), the lower ratios of 10 and 20 wt % A-B block copolymer were stabilised (Figure 2.27). The effects on D_z were minimal during addition of NaCl to the 80:20 wt % ratio, as there is almost no difference between the blank *vs* 21 day sample. The 40:60 and 30:70 wt % ratios became unstable between instant and 1 day measurement, whilst 20:80 and 10:90 wt % remained stable, yet, large changes in D_z were observed throughout the 21 day test period. Apart from 40:60 and 30:70 wt % and some observed increases in D_z, all co-nanoprecipitated dispersions including *p*(PEG$_{45}$-*b*-HPMA$_{40}$) were stable to NaCl during the 21 day period.

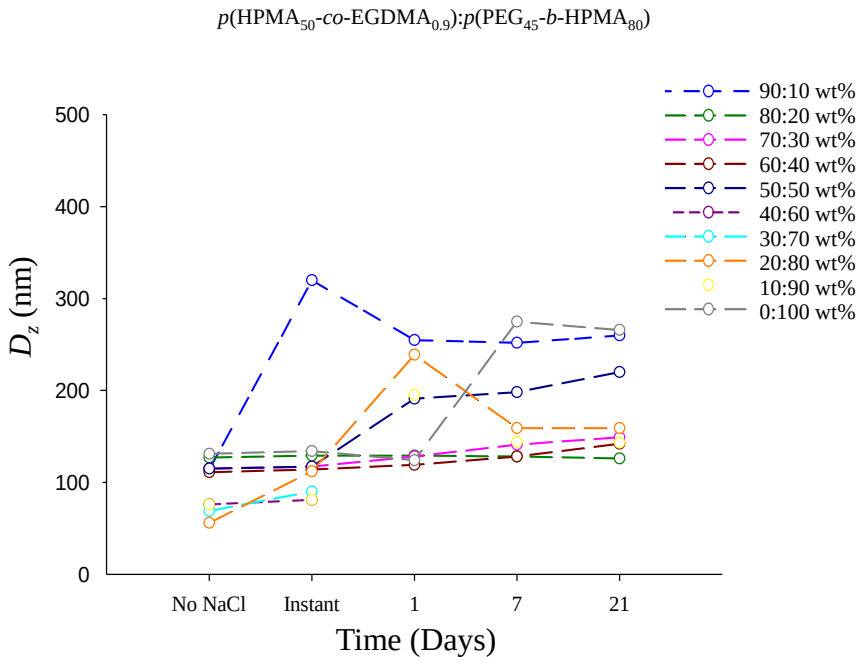

Figure 2.27 Stability of *p*(HPMA$_{50}$-*co*-EGDMA$_{0.9}$):*p*(PEG$_{45}$-*b*-HPMA$_{80}$) to NaCl during a 21 day period, 90:10-0:100 wt %. Dashed line open circles, 90:10 = blue, 80:20 = dark green, 70:30 = pink 60:40 = dark red, 50:50 = dark blue, 40:60 = dark purple, 30:70 = light green = 30:70, orange = 20:80, yellow = 10:90, grey = 0:100 wt %*. (*Inadequate light scattering data obtained).

The results for NaCl addition to the co-nanoprecipitates including *p*(PEG$_{45}$-*b*-HPMA$_{120}$) A-B block copolymer are presented in Figure 2.28. The incorporation of 10 wt % of the A−B block copolymer had no meaningful effect on the salt stability of the co-nanoprecipitates (Figure 2.28A), however, 20 wt % incorporation led to stability over the 21 day test period. An immediate approximate doubling in D_z was seen on addition of salt (110 to 190 nm), and a small variation was observed from this point (Figure 2.28B). Further increases in A−B block copolymer led to increasing stability as demonstrated by a decreasing impact on D_z immediately after salt addition, low D_z values on storage, and maintenance of low PdI values (<0.085) throughout 7 days, after which precipitation was observed for 70:30 and 50:50 wt %. Interestingly, this benefit was seen to decrease after the 50:50 ratio of *p*(HPMA$_{50}$-*co*-EGDMA$_{0.9}$):*p*(PEG$_{45}$-*b*-HPMA$_{120}$), and nanoparticles comprising more than 60 wt % A−B block copolymer were progressively less stable and unable to avoid aggregation after 1 day. The only exception was the co-nanoprecipitates formed from a 10:90 wt % ratio. This behaviour may be due to the lack of an efficient co-nanoprecipitation at high levels of the stabilising block copolymer leading to a non-uniform A−B incorporation within the nanoparticle distribution; the optimum composition appeared to be a 60:40 wt % ratio of *p*(HPMA$_{50}$-*co*-EGDMA$_{0.9}$) and *p*(PEG$_{45}$-*b*-

HPMA$_{120}$). The ability of the co-nanoprecipitates to tolerate salt was in marked contrast to the behaviour of the branched copolymer *p*(HPMA$_{50}$-co-EGDMA$_{0.9}$) nanoprecipitated in the absence of the A−B block copolymer. The size and PdI values obtained for the PEG$_{45}$ series are located in the Appendix (Table A5).

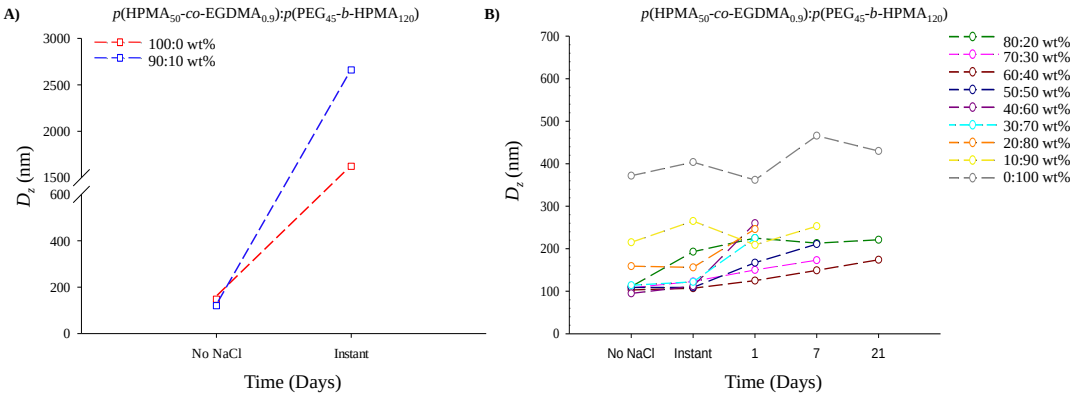

Figure 2.28 Stability of *p*(HPMA$_{50}$-*co*-EGDMA$_{0.9}$):*p*(PEG$_{45}$-*b*-HPMA$_{120}$) to NaCl during a 21 day period. A) Dashed line open squares, 100:0 = red, 90:10 = blue, B) Dashed line open circles, 80:20 = dark green, 70:30 = pink 60:40 = dark red, 50:50 = dark blue, 40:60 = dark purple, 30:70 = light green = 30:70, orange = 20:80, yellow = 10:90, grey = 0:100 wt %.

During the variation of the A-B block copolymer composition, different results were obtained during NaCl addition. Overall, the addition of *p*(PEG$_{45}$-*b*-HPMA$_{40}$) with *p*(HPMA$_{50}$-*co*-EGDMA$_{0.9}$) led to stability when >70 wt % A-B block copolymer was added, yet, large deviations in size during the 21 day study period were observed. An increase in DP$_n$ of HPMA from 40 to 80 monomer units i.e. *p*(PEG$_{45}$-*b*-HPMA$_{80}$), improved the stability, as only 10 wt % was required to stabilise *p*(HPMA$_{50}$-*co*-EGDMA$_{0.9}$). Generally, the dispersions remained relatively stable during 21 days but for increasing amounts of A-B block copolymer, large fluctuations in size were observed. A further increase in the HPMA chain length for the A-B block copolymer *p*(PEG$_{45}$-*b*-HPMA$_{120}$), did not appear to increase the stability, as addition of 10 wt % resulted in precipitation upon instant NaCl addition and the majority of samples started to precipitate <7 days.

Although stability to a set concentration of NaCl is of interest, it was also important to establish the impact of varying salt concentrations over a relatively short period of time, for example after injection or during formulation with other ingredients. As such, an evaluation of the behaviour of fresh samples of the varying co-nanoprecipitates consisting of *p*(HPMA$_{50}$-*co*-EGDMA$_{0.9}$):*p*(PEG$_{45}$-*b*-HPMA$_{120}$) was studied, as successive aliquots

of the 0.5 M NaCl solution were added to 1 mL samples (Figure 2.30); again, DLS measurement was used to study the D_z and PdI of the nanoparticles. As seen previously, the nanoparticle samples comprising 100:0 and 90:10 wt % ratios of the *p*(HPMA$_{50}$-*co*-EGDMA$_{0.9}$):*p*(PEG$_{45}$-*b*-HPMA$_{120}$) polymers showed significant aggregation after low concentrations (0.01M) of added aqueous NaCl. Interestingly, all other *p*(HPMA$_{50}$-*co*-EGDMA$_{0.9}$):*p*(PEG$_{45}$-*b*-HPMA$_{120}$) co-nanoprecipitates were stable up to 2 mL addition; however, only the co-nanoprecipitates containing 30, 40, 80, and 90 wt % A−B block copolymer were able to maintain PdI values <0.090, with the 60:40 wt % material showing only a 13 % variance from its initial D_z value and a PdI = 0.039 after the addition of 2 mL of salt solution. The PdI value obtained for 50:50 wt % increased up to 0.161 after 2 mL addition.

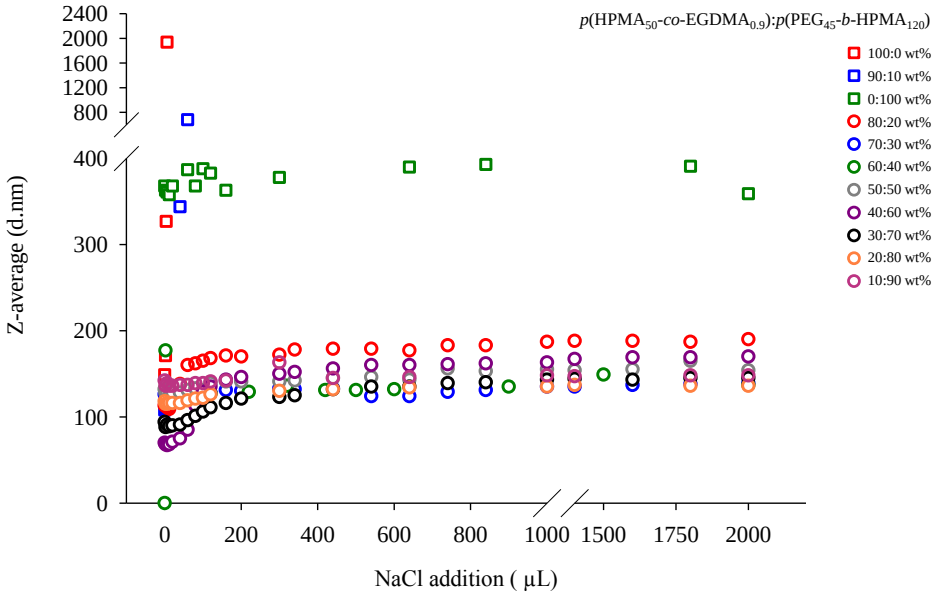

Figure 2.30 Analysis of co-nanoprecipitated particles with varying *p*(HPMA$_{50}$-*co*-EGDMA$_{0.9}$):*p*(PEG$_{45}$-*b*-HPMA$_{120}$) wt % ratios after sequential addition of aliquots of aqueous 0.5 M NaCl to a 1 mL sample of nanoparticles at 1 mg/mL. D_z variation of samples is shown. Open squares: red = 100:0, blue = 90:10, green = 0:100. Open circles: red = 80:20, blue = 70:30, green = 60:40, gray = 50:50, purple = 40:60, black = 30:70, orange = 20:80, dark pink = 10:90.

2.7.3 Stability of *p*(PEG$_{114}$-*b*-HPMA$_x$) A-B block copolymer aqueous co-nanoprecipitated particles

To assess if an increase of the hydrophilic PEG chain length (5000 g/mol) enhances the stability, NaCl addition experiments were also conducted for *p*(HPMA$_{50}$-*co*-EGDMA$_{0.9}$):*p*(PEG$_{114}$-*b*-HPMA$_x$) co-nanoprecipitated particles. It would be expected that

an increase in PEG length from PEG_{45} to PEG_{114} for the A-B block copolymers would provide additional steric stabilisation to the nanoparticles and as a result, be less affected when exposed to NaCl.

The NaCl stability plots are shown in Figure 2.31 for the *p*($HPMA_{50}$-*co*-$EGDMA_{0.9}$):*p*(PEG_{114}-*b*-$HPMA_x$). The addition of 10 wt % of the A-B block copolymer had no meaningful effect on the NaCl stability of the co-nanoprecipitates and precipitation was observed instantly. Whilst there was some stability, the addition of NaCl to the 80:20 wt % nanodispersion resulted in broad PdI values (>0.3) and D_z which were triple their original value. This suggests that for both 90:10 and 80:20 wt % ratios, there is an insufficient amount of PEG chains present to stabilise *p*($HPMA_{50}$-*co*-$EGDMA_{0.9}$). However, the varying ratios between 70:30-50:50 wt % demonstrated an increased stability after NaCl addition. After 21 days, all PdI values remained <0.037, although a 127 % and 120 % increase in size was observed for 70:30 and 60:40 wt % respectively, the polymers did not precipitate. Within the 21 day period, the 50:50 wt % nanoparticles increased by a negligible amount of 17 nm and resulting PdI of 0.018. Above 50 wt % A-B block copolymer, a general decrease in size was observed. For 40:60, 20:80 and 10:90 wt %, the nanoparticles were generally stable for 7 days, after which, DLS data became unreliable for both 20:80 and 10:90 wt %. The nanoparticles formed from a 30:70 wt % ratio, increase slightly but up to 21 days period gave a final size of 104 nm and PdI <0.082.

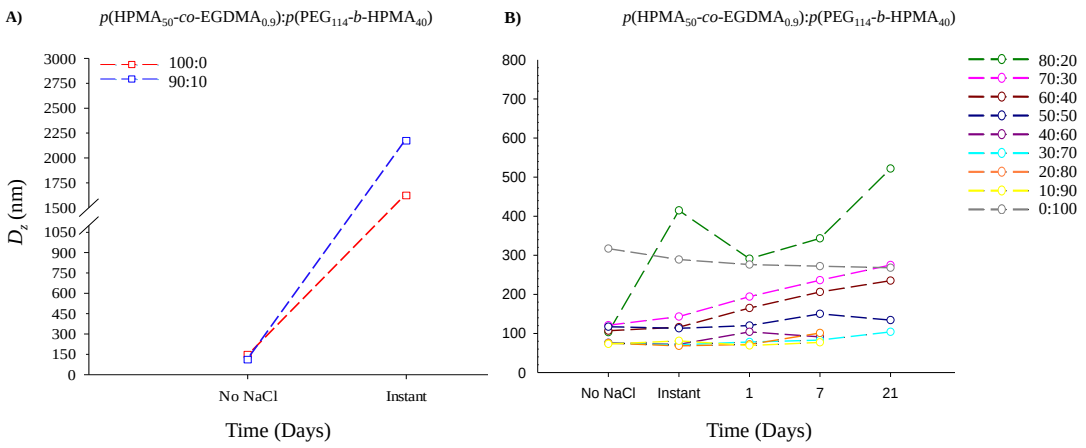

Figure 2.31 Stability of branched *p*($HPMA_{50}$-*co*-$EGDMA_{0.9}$):*p*(PEG_{114}-*b*-$HPMA_{40}$) A-B block copolymer to NaCl during a 21 day period. A) Dashed line open squares, 100:0 = red, 90:10 = blue, B) Dashed line open circles, 80:20 = dark green, 70:30 = pink 60:40 = dark red, 50:50 = dark blue, 40:60 = dark purple, 30:70 = light green = 30:70, orange = 20:80, yellow = 10:90, grey = 0:100 wt %*. (*Inadequate light scattering data obtained).

In comparison with *p*(PEG$_{114}$-*b*-HPMA$_{40}$), the increase in DP$_n$ of HPMA to 80 monomer units did appear to result in an overall increase in stability of the nanoparticles in the NaCl environment, in particular for the 80:20 wt % ratio (Figure 2.32). The ratios between 90:10-50:50 wt % were stable during 21 days and although for 90:10, 80:20 and 60:40 wt % the PdI values remained below 0.057, a slight increase was observed to ~0.19 for 80:20 and 50:50 wt %. The nanoparticle dispersions which were least effected after NaCl addition were 70:30, 60:40 and 50:50 wt %. From 40:60 wt % there is a general decrease in size of the nanoparticles and instability after 7 days is observed for 40:60, 30:70, 20:80 and 10:90 wt % as all 21 day measurements were considered unreliable by DLS analysis. There was no visible precipitate after 7 days but an increase in PdI for 40:60 20:80 and 10:90 wt % and PdI values remained below 0.2.

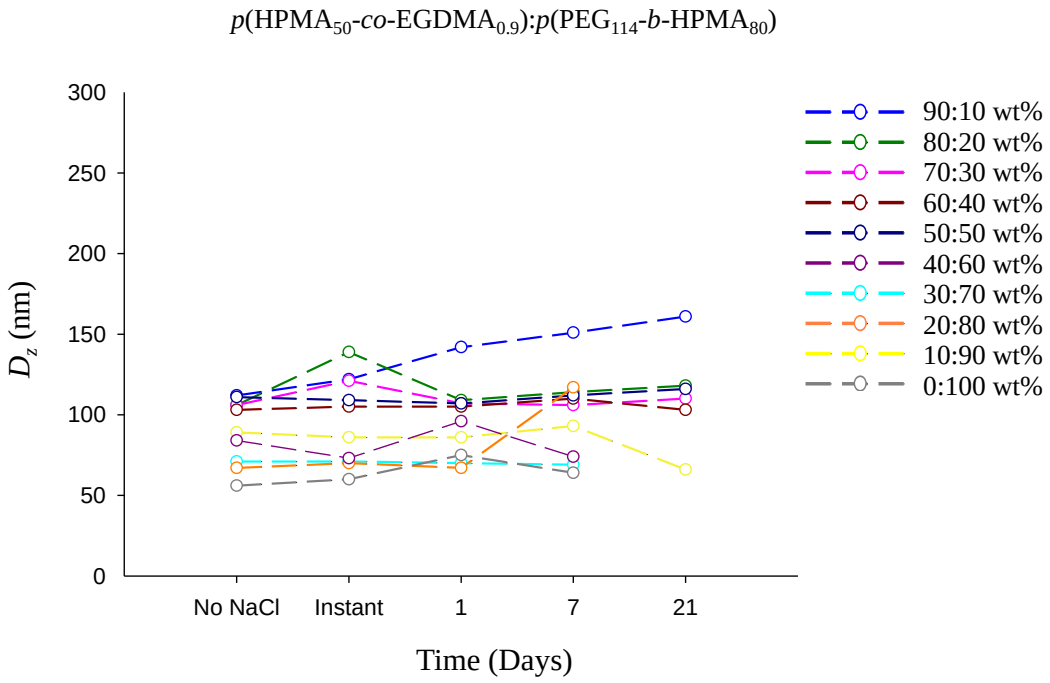

Figure 2.32 Stability of *p*(HPMA$_{50}$-*co*-EGDMA$_{0.9}$):*p*(PEG$_{114}$-*b*-HPMA$_{80}$) to NaCl during a 21 day period, 90:10-0:100 wt %. Dashed line open circles, 90:10 = blue, 80:20 = dark green, 70:30 = pink 60:40 = dark red, 50:50 = dark blue, 40:60 = dark purple, 30:70 = light green = 30:70, orange = 20:80, yellow = 10:90, grey = 0:100 wt %*. (*Inadequate light scattering data obtained).

The *p*(PEG$_{114}$-*b*-HPMA$_x$) A-B block copolymer with the highest HPMA content (DP$_n$ = 120), showed a higher stability when compared with the other *p*(PEG$_{114}$-*b*-HPMA$_x$) polymers. The D_z values for the varying ratios of *p*(HPMA$_{50}$-*co*-EGDMA$_{0.9}$):*p*(PEG$_{114}$-*b*-HPMA$_x$) during the 21 day test period are presented in Figure 2.33 and interestingly, as the mass of A-B block copolymer is increased the starting size decreases almost

systematically. The nanoparticles experienced negligible changes between the ratios of 90:10-50:50 wt % during the 21 day NaCl addition test period. The addition of 80 wt % A-B block copolymer resulted in a nanodispersion which was stable for 21 days, however the PdI increased to 0.249. The co-nanoprecipitate ratios of 40:60, 30:70 and 10:90 wt % were stable up until 7 days, and although there was no visible precipitate, the DLS data was not reliable and therefore not included as part of the stability plot. It is evident that an increase in the DP_n of HPMA for the A-B block copolymer does in fact increase the stability of the PEG_{114} nanoparticles and the optimum weight % ratios for stability are between 90:10 and 50:50 wt %. The size and PdI values obtained for the PEG_{114} series are located in the Appendix (Table A6).

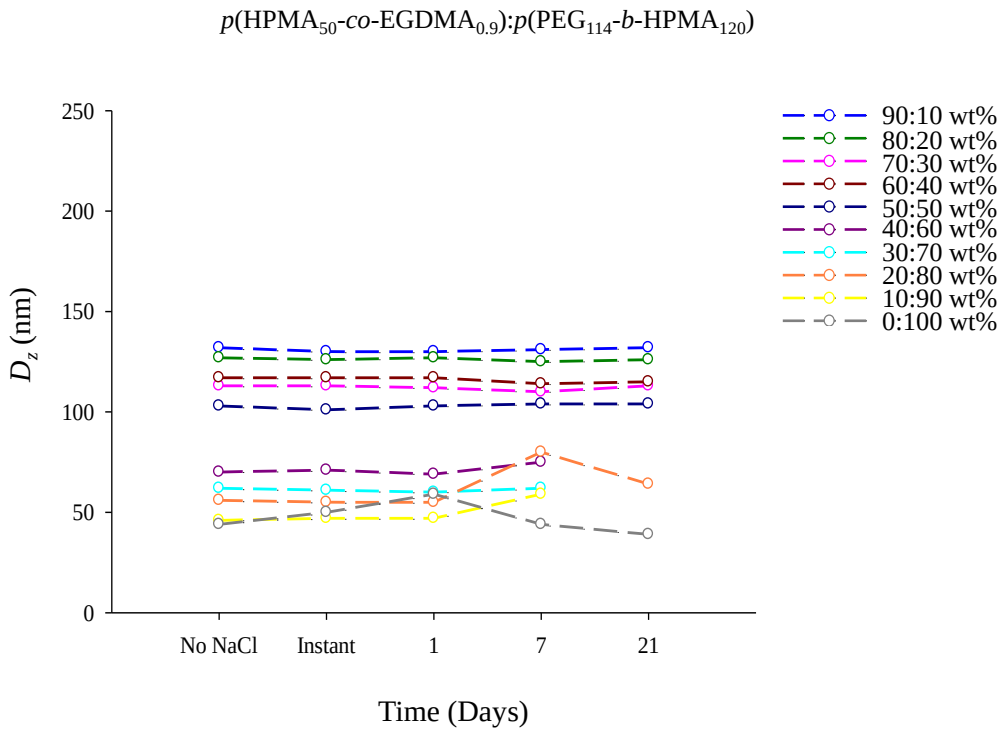

Figure 2.33 Stability of branched *p*(HPMA$_{50}$-*co*-EGDMA$_{0.9}$):*p*(PEG$_{114}$-*b*-HPMA$_{120}$) A-B block copolymer to NaCl during a 21 day period, 90:10-0:100 wt %. Dashed line open circles, 90:10 = blue, 80:20 = dark green, 70:30 = pink 60:40 = dark red, 50:50 = dark blue, 40:60 = dark purple, 30:70 = light green = 30:70, orange = 20:80, yellow = 10:90, grey = 0:100 wt %.

Overall, the NaCl stability studies have shown that the length of both the PEG_y and $HPMA_x$ chain of the A-B block copolymer when nanoprecipitated with *p*(HPMA$_{50}$-*co*-EGDMA$_{0.9}$), greatly affects the stability. There are clear trends during the inclusion of *p*(PEG$_{114}$-*b*-HPMA$_x$) A-B block copolymers when compared to the *p*(PEG$_{45}$-*b*-HPMA$_x$) series. The A-B block copolymer which maintained the greatest level of stability was

p(PEG$_{114}$-*b*-HPMA$_{120}$), due to the very minor changes in size between 10-50 wt % addition of A-B block copolymer to *p*(HPMA$_{50}$-*co*-EGDMA$_{0.9}$).

When considering the original hypothesis, if the A-B block copolymer was loosely absorbed onto the surface (Figure 2.10i), it would be expected that destabilisation would occur during NaCl addition. Although some nanodispersions did precipitate upon NaCl addition, many remained stable, particularly those including *p*(PEG$_{45}$-*b*-HPMA$_{80}$) and *p*(PEG$_{114}$-*b*-HPMA$_{x}$) A-B block copolymers. These results suggest the HPMA chain from the A-B block copolymer is most likely incorporated into the *p*(HPMA$_{50}$-*co*-EGDMA$_{0.9}$) branched core, hence, steric stabilisation is provided by the residing PEG chains on the surface (Figure 2.34).

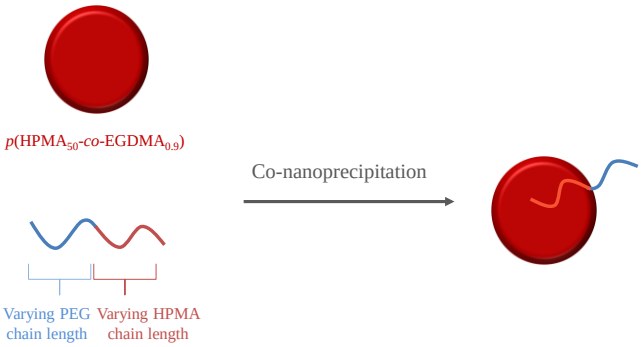

Figure 2.34 Schematic representation of the proposed co-nanoprecipitation approach.

As discussed, the *p*(HPMA$_{50}$-*co*-EGDMA$_{0.9}$):*p*(PEG$_{114}$-*b*-HPMA$_{120}$) co-nanoprecipitated system demonstrated the highest tolerance during exposure to NaCl, therefore, it was of interest to establish the minimum amount of A-B block copolymer required to stabilise *p*(HPMA$_{50}$-*co*-EGDMA$_{0.9}$). As illustrated in Figure 2.34, the nanodispersion containing <10 wt % *p*(PEG$_{114}$-*b*-HPMA$_{120}$) was not stable and polymer precipitation was observed, suggesting insufficient PEG chains for steric stabilisation.

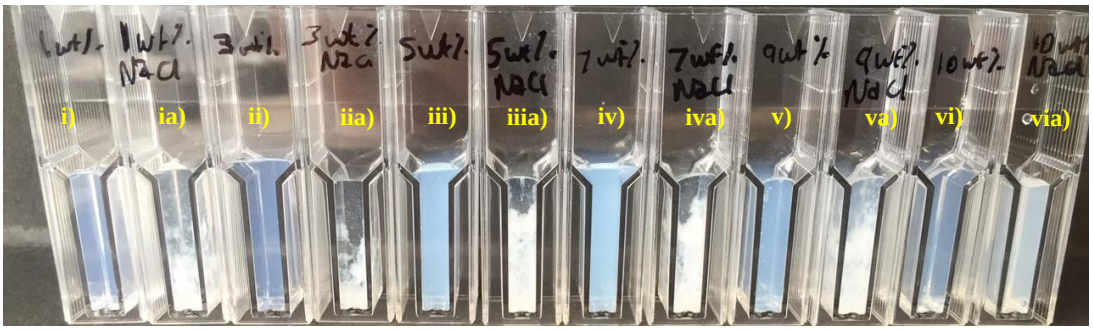

Figure 2.34 Photograph of co-nanoprecipitated nanodispersions *p*(HPMA$_{50}$-*co*-EGDMA$_{0.9}$):*p*(PEG$_{114}$-*b*-HPMA$_{120}$), left control nanodispersion, right NaCl addition. i) 99:1 wt %, ii) 97:3 wt %, iii) 95:5 wt %, iv) 97:3 wt %, v) 91:9 wt %, vi) 90:10 wt %.

2.7.4 Stability of nanodispersions of branched *p*(HPMA$_{50}$-*co*-EGDMA$_{0.9}$) into solutions of water soluble A-B block copolymer in the presence of NaCl

In order to compare the stability between a co-nanoprecipitation and the nanoprecipitation of *p*(HPMA$_{50}$-*co*-EGDMA$_{0.9}$) into solutions of water soluble A-B block copolymer, NaCl studies were conducted. The experimental conditions were as described previously, (20 µL, 0.5M NaCl to 1 mL of nanodispersion), in order to directly compare both methods. Interestingly, the addition of NaCl resulted in instant precipitation during inclusion of both *p*(PEG$_{45}$-*b*-HPMA$_{40}$) and *p*(PEG$_{114}$-*b*-HPMA$_{40}$) 50 wt %, which was not observed previously for simultaneous addition (Table 2.8). This suggests that for these particular A-B block copolymers, the HPMA chain was loosely bound onto the nanoparticle surface and not entrapped within the core, as destabilisation of the nanoparticles was observed. There is a clear improvement in NaCl stability when *p*(HPMA$_{50}$-*co*-EGDMA$_{0.9}$) is nanoprecipitated into both water soluble *p*(PEG$_{114}$-*b*-HPMA$_{80}$) and *p*(PEG$_{114}$-*b*-HPMA$_{120}$) 50 wt %, as sufficient stabilisation was observed during the 7 day test period. The presence of a longer hydrophobic chain on the A-B block copolymer appears to affect the stability during nanoprecipitation of *p*(HPMA$_{50}$-*co*-EGDMA$_{0.9}$) into the water soluble A-B block copolymers, as this behaviour was not observed when the polymers were added simultaneously during a co-nanoprecipitation.

Table 2.8 DLS results for the nanoparticles prepared *via* the nanoprecipitation of *p*($HPMA_{50}$-*co*-$EGDMA_{0.9}$) into solutions of H_2O soluble A-B block copolymers and simultaneous co-nanoprecipitation experiments and their stability to NaCl addition during a 7 day period.

Sample (50:50 wt %)		Blank		Instant		1 day		7 days	
		Z-ave (d.nm)	PdI	Z-ave (d.nm)	PdI	Z-ave (d.nm)	PdI	Z-ave (d.nm)	PdI
Nanoprecipitation	Addition of *p*($HPMA_{50}$-*co*-$EGDMA_{0.9}$) into an aqueous solution of *p*(PEG_{45}-*b*-$HPMA_{30}$)	80	0.062	514	X	X	X	X	X
	Addition of *p*($HPMA_{50}$-*co*-$EGDMA_{0.9}$) into an aqueous solution of *p*(PEG_{114}-*b*-$HPMA_{40}$)	86	0.048	1679	X	X	X	X	X
	Addition of *p*($HPMA_{50}$-*co*-$EGDMA_{0.9}$) into an aqueous solution of *p*(PEG_{114}-*b*-$HPMA_{80}$)	97	0.067	98	0.015	97	0.050	98	0.051
	Addition of *p*($HPMA_{50}$-*co*-$EGDMA_{0.9}$) into an aqueous solution of *p*(PEG_{114}-*b*-$HPMA_{120}$)	94	0.118	98	0.123	95	0.107	93	0.090
Co-nanoprecipitation	Simultaneous addition of *p*($HPMA_{50}$-*co*-$EGDMA_{0.9}$) and *p*(PEG_{45}-*b*-$HPMA_{30}$)	109	0.048	172	0.038	173	0.020	212	0.020
	Simultaneous addition of *p*($HPMA_{50}$-*co*-$EGDMA_{0.9}$) and *p*(PEG_{114}-*b*-$HPMA_{40}$)	117	0.048	113	0.079	120	0.029	150	0.031
	Simultaneous addition of *p*($HPMA_{50}$-*co*-$EGDMA_{0.9}$) and *p*(PEG_{114}-*b*-$HPMA_{80}$)	111	0.081	109	0.089	107	0.062	112	0.083
	Simultaneous addition of *p*($HPMA_{50}$-*co*-$EGDMA_{0.9}$) and *p*(PEG_{114}-*b*-$HPMA_{120}$)	103	0.045	101	0.050	103	0.060	104	0.043

X = Polymer precipitation

2.8 Mechanistic rationale for the role of the A-B block copolymer

The stability of colloidal materials in various media has been widely studied[38, 39] and many approaches utilise the initial principle, proposed by Derjaguin and Landau[40] and Verway and Overbeek[41] (DLVO), that suggests the total interaction energy (W_{total}) is the simple balance of van der Waals attractive interactions (W_{vdW}) and electrostatic repulsions ($W_{elect.}$). This DLVO theory has been questioned by several groups on the role of the so-called 'non-DLVO interactions' such as steric and hydrophobic interactions which are not included within classical DLVO approaches;[38, 42] the validity of the separate consideration of electrostatic and van der Waals interactions has also been questioned.[42] Classical DLVO theory has been used recently to study the factors governing the growth of nanoparticles during nanoprecipitation into aqueous electrolytes of different concentration and to understand the stability of the resulting particles.[43] Complicating factors for the estimation of W_{total} *via* DLVO theory include the calculation of the Hamaker constant for the study materials and the estimation of the surface potential of the nanoparticles for which, in experimental terms, the determination of ζ is more readily available. This is additionally complicated by the presence of stabilising ligands, but correlations do exist for ligand-coated inorganic nanoparticles.[44] The direct substitution of ζ values for surface potential,[45] and the selection of Hamaker constants[43] from previously published calculations of analogous materials, has been adopted by several groups to allow meaningful mechanistic insight into nanoparticle behaviour. The attractive van der Waals

interaction, repulsive electrostatic interaction, and the total interaction energies of two identical nanoparticles, substituting experimentally measured ζ values for surface potentials, are given by equations 1−3, respectively: where *A* is the Hamaker constant, *r* is the radius of the nanoparticles, *D* is the separation distance, ε_0 is the permittivity of free space, ε is the relative permittivity of the electrolyte medium, and κ is the reciprocal Debye length.

$$W_{vdW} = \frac{-Ar}{12D} \tag{1}$$

$$W_{elect.} = 2\pi\varepsilon\varepsilon_0 r\zeta^2 exp(-\kappa D) \tag{2}$$

$$W_{total} = W_{vdW} + W_{elect.} \tag{3}$$

The reciprocal Debye length κ may be calculated from eq. 4, where *k* is the Boltzmann constant, T is the absolute temperature, N_A is Avogadro's number, *e* is the elementary charge, and *I* is the ionic strength of the medium (mol m^{-3}).

$$\kappa^{-1} = \sqrt{\frac{\varepsilon_0 \varepsilon kT}{2N_A e^2 I}} \tag{4}$$

2.8.1 DLVO calculations for the A-B block copolymer *p*(PEG$_{45}$-*b*-HPMA$_{120}$)

The nanoparticles co-nanoprecipitated with the *p*(PEG$_{45}$-*b*-HPMA$_x$) materials showed a range of stability/instability rather than consistent stability seen for the *p*(PEG$_{114}$-*b*-HPMA$_x$) materials. Therefore, the study of *p*(PEG$_{45}$-*b*-HPMA$_x$) materials was more meaningful, as we could see a trend in some cases and determine at what wt % values the inclusion of the A-B material was not beneficial.

The D_n (DLS) values were used to calculate *r*, experimental ζ values were determined for the nanoparticles after addition of 0.5 M NaCl (20 μL to 1 mL of sample), κ was calculated as 3.32×10^8 m^{-1} at an ionic strength of 10 mol m^{-3} (0.01 M NaCl), and a Hamaker constant of 6.35×10^{-21} J was used due to the previous experimental determination of this value for methacrylate-based copolymer latex particles.[45] Figure 2.36A shows the

calculated W_{total} profile for the chosen co-nanoprecipitated particles immediately after salt addition.

The measured ζ value of −4.41 mV suggests considerable screening of nanoparticle charge, and this is reflected in a predicted attractive energy profile and would lead to an expectation of aggregation and instability in the presence of salt. The addition of the poorly water-soluble A−B block copolymer into the initial polymer solution (good solvent) does provide for the presence of a stabilising layer of PEG_{45} chains, assuming co-nanoprecipitation occurs.

The presence of water-soluble surfactants containing PEG chains of this length were also considered in recent classical DLVO analyses of latex particles.[45] PEG_{45} chains are reported to have a Flory radius of 3−3.5 nm,[45, 46] therefore acting as a steric barrier with a distance of approximately 6 nm from the overlapping stabilising layers, as the co-nanoprecipitates approach each other. A minimum value of W_{total} can be assumed to be attained from this overlap distance and has been mathematically determined as $-0.74kT$, considerably higher than the minimum $-5kT$ value that is reported to be indicative of an unstable dispersion.[45, 47] Although theoretical, calculations were also conducted to contrast the energy profile of the co-nanoprecipitate where its pre-salt addition ζ = −21.5 mV value was maintained. As can be seen, the increased ζ value would lead to a repulsive W_{total} until very small distances. The lack of stability of the co-nanoprecipitates from mixtures containing low wt % A−B block copolymer content was also mathematically investigated, as the presence of the PEG_{45} chains would have been expected to offer some stability.

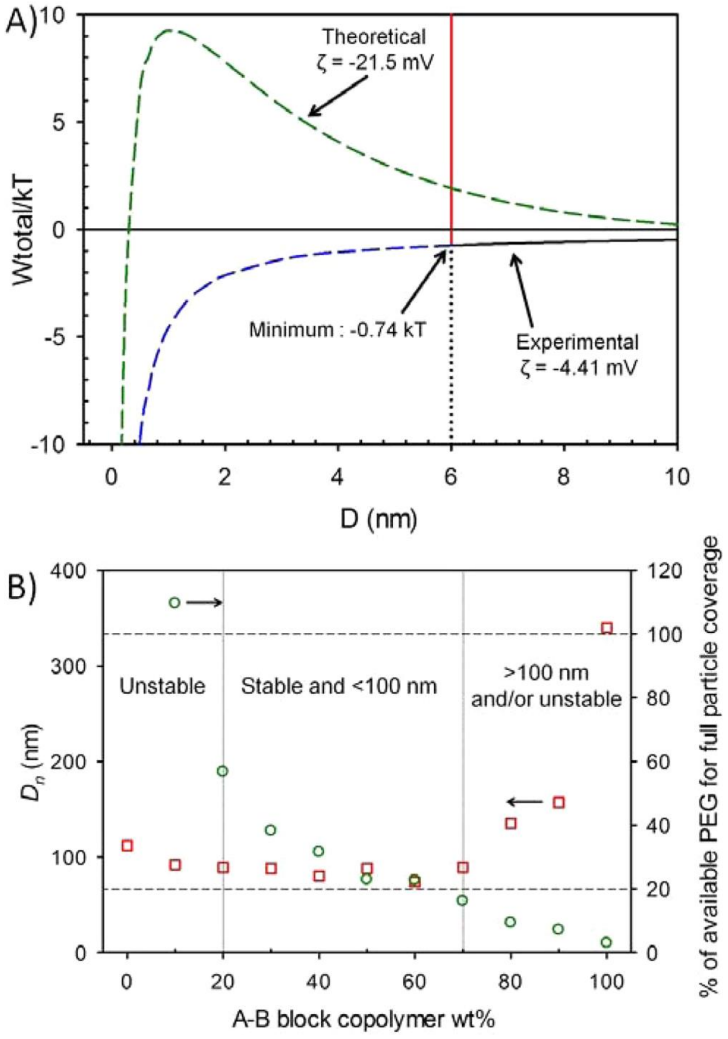

Figure 2.36 Mechanistic evaluation of *p*(HPMA$_{50}$-*co*-EGDMA$_{0.9}$):*p*(PEG$_{45}$-*b*-HPMA$_{120}$) co-nanoprecipitates. (A) DLVO calculation of total interaction energies for a co-nanoprecipitate comprising a 60:40 wt % ratio: calculated balance of attractive and repulsive interactions for the co-nanoprecipitate in 0.01 M NaCl and measured ζ = −4.41 mV (black solid and blue dashed line), aggregation barrier at 2 × PEG$_{45}$ chain length (red line), theoretical energy profile calculated for initial ζ value (green dashed line). B) Analysis of possible surface coverage of the co-nanoprecipitates with available PEG$_{45}$ chains within each nanoprecipitation experiment (>100 % indicates too few PEG$_{45}$ chains).

Previous reports of close-packed PEG$_{45}$ brushes on the surface of inorganic particles[46] have estimated that chains can pack within approximately 3.5 nm, therefore occupying a surface area of 12.25 nm^2 per chain. By taking the D_n (DLS) values, and assuming a density of 1 g cm^{-3} for the polymer nanoparticles (appropriate for polymethacrylates),[48] the mass and surface area of a single particle from each co-nanoprecipitate mass ratio was determined and a maximum theoretical number of PEG$_{45}$ chains required to cover each co-nanoprecipitate was therefore derived. Assuming a close-packed brush conformation,

the ability of each ratio to completely cover the nanoparticles formed was calculated by simply dividing this theoretical maximum number with the number of PEG_{45} chains available during each co-nanoprecipitation. Although this analysis is somewhat qualitative, it is interesting to see that the 90:10 wt % ratio of polymers requires >100 % of the available PEG_{45} chains (i.e., too few PEG_{45} chains were present) within the nanoprecipitation solution to generate complete coverage of the nanoparticle surfaces (Figure 2.36 B); this ratio was the only nanoprecipitate containing the A−B block copolymer that aggregated instantly on addition of NaCl. In addition, when the number of PEG_{45} chains required to cover the surfaces of the nanoparticles fell below 20 % of the available PEG_{45} chains within the polymer mixture, i.e. a large excess of A−B block copolymer is present, a loss of polymer size control and an indication of salt instability were seen. This may be another limit to successful co-nanoprecipitation as competitive nanoprecipitation of the poorly soluble A−B block copolymer may lead to in-homogeneity within the composition of the nanoparticles or the potential for vesicle and micelle formation.

2.9 Dialysis Studies of co-nanoprecipitated nanoparticles

During inclusion of the A-B block copolymer, *p*(PEG_{114}-*b*-$HPMA_{120}$) with *p*($HPMA_{50}$-*co*-$EGDMA_{0.9}$), stable nanoparticles and the highest tolerance to NaCl addition was observed, therefore this particular material was selected for the study. If the A-B block copolymer was only loosely associated with nanoprecipitates of branched *p*($HPMA_{50}$-*co*-$EGDMA_{0.9}$) after nanoprecipitation, i.e. adsorbed onto the nanoparticle surface (Figure 2.10i), then it would be expected that during dialysis of the nanodispersion against water, the A-B block copolymer would easily desorb and no longer sterically stabilise *p*($HPMA_{50}$-*co*-$EGDMA_{0.9}$). In order to investigate this, dialysis tubing with a molecular weight cut off (MWCO) of 100 kg/mol was used to conduct a dialysis experiment of a co-nanoprecipitated dispersion. This particular pore size was selected to ensure the highly branched *p*($HPMA_{50}$-*co*-$EGDMA_{0.9}$) polymer and any assembled nanoparticles remained within the tubing and the A-B block copolymer with a molecular weight <100 kg/mol was able to move freely across the membrane and equilibrate, if loose surface adsorption was the mechanism (Figure 2.10i).

This study was carried out using *p*($HPMA_{50}$-*co*-$EGDMA_{0.9}$):*p*(PEG_{114}-*b*-$HPMA_{120}$) co-nanoprecipitates at a ratio of 50:50 wt % and was prepared as previously discussed. The nanoprecipitation experiment was scaled up accordingly so the total polymer

concentration was 20 mg/mL. After DLS analysis of the nanodispersion, the particles were added to the dialysis tubing and left to stir at ambient temperature over a period of 128 hours, during which, samples were taken for analysis (Table 2.8 & Figure 2.37). As highlighted, the starting nanoparticle dispersion and 128 hour DLS D_z sizes are almost identical, suggesting the dialysis experiment has had very little effect on the nanodispersion. A DLS overlay of the nanoparticles before and after 128 hour dialysis emphasises how the D_z for both samples overlay almost exactly and almost identical sizes are obtained (Figure 2.37 B).

Table 2.8 DLS results for dialysis experiment of *p*(HPMA$_{50}$-*co*-EGDMA$_{0.9}$):*p*(PEG$_{114}$-*b*-HPMA$_{120}$) 50:50 wt % at increasing time intervals.

Time (hours)	D_z (nm)	**PdI**	D_n (nm)	**Derived count rate** (kcps)
0	**123**	**0.057**	**96**	**397200**
56	121	0.054	96	391750
80	120	0.045	95	463730
104	124	0.053	99	452240
128	**122**	**0.056**	**98**	**487180**

As previously discussed, the nanoprecipitation of *p*(HPMA$_{50}$-*co*-EGDMA$_{0.9}$) yields stable nanoparticles, but during addition of a small aliquot of NaCl they quickly precipitate. However, the inclusion of the A-B block copolymer, *p*(PEG$_{114}$-*b*-HPMA$_{120}$) introduces steric stabilisation and the addition of NaCl has minimal or no effects on the nanoparticles. In order to determine if the dialysed nanoparticles had maintained their steric stability, a 1 mL sample was taken from the dialysis solution inside the bag and NaCl (20 µL of 0.5M solution) was added. The process is outlined in Figure 2.38 and the final DLS measurement after 7 day NaCl addition, Figure 2.38iii, is almost identical to the initial nanodispersion measured before the dialysis experiment. The DLS sizes are reported in Table 2.9 and as highlighted, there are very small differences in comparison to the blank nanoparticle sample and it is worth noting that all PdI's remained narrow (<0.057) throughout the experiment. These results suggest that the HPMA from the A-B block copolymer is becoming fully incorporated with the branched *p*(HPMA$_{50}$-*co*-EGDMA$_{0.9}$) core and the PEG chain of the A-B block copolymer is remaining on the surface (Figure 2.10ii).

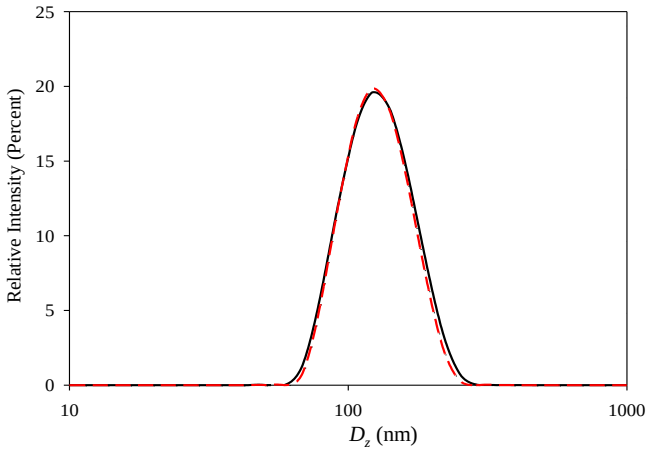

Figure 2.37 DLS overlay for dialysis experiment of *p*(HPMA$_{50}$-*co*-EGDMA$_{0.9}$):*p*(PEG$_{114}$-*b*-HPMA$_{120}$), before dialysis (black trace) and after 128 hours dialysis (red trace).

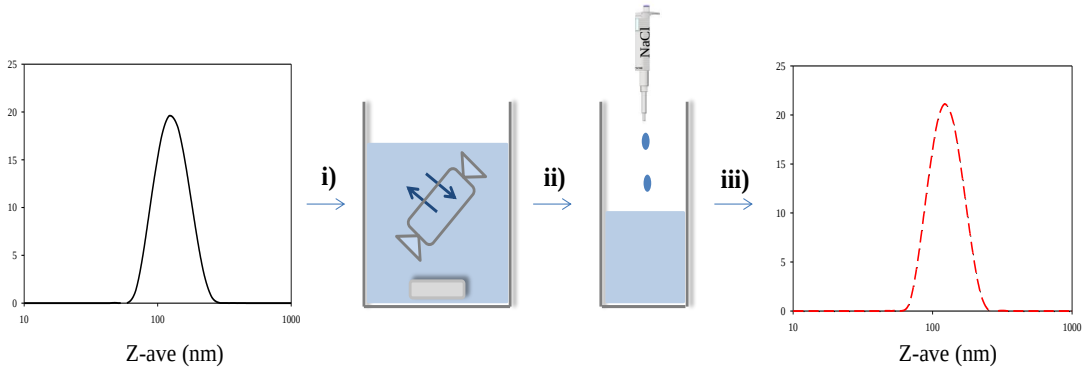

Figure 2.38 NaCl addition to dialysed nanoparticles, i) *p*(HPMA$_{50}$-*co*-EGDMA$_{0.9}$):*p*(PEG$_{114}$-*b*-HPMA$_{120}$) 50:50 wt % blank nanoparticles added to a dialysis bag ii) After 128 hours a 1 mL sample of this nanodispersion added to a vial and 20 µL NaCl is added iii) DLS trace after 7 day, NaCl addition result.

Table 2.9 DLS results comparing nanoparticle sizes before and after NaCl addition.

NaCl Addition Time (days)	D_z (nm)	**PdI**	D_n (nm)	**Derived count rate** (kcps)
Before Dialysis	**123**	**0.057**	**96**	**397200**
Instant	121	0.042	98	479406
1 day	115	0.033	93	346155
7 day	**120**	**0.036**	**98**	**273643**

In order to analyse the remaining polymeric material within and outside of the dialysis bag, the solutions were concentrated *in vacuo* and weighed for accurate triple detection GPC analysis. Unfortunately, after rotary evaporation of the solution outside of the dialysis bag, a brown material as well as polymer was present, which may be residual material from the pre-wetted dialysis membrane. The unknown material was not soluble in THF, therefore GPC analysis was not possible. However, the material present within the dialysis bag was readily solubilised in THF and analysed by GPC (Figure 2.39). Although similar retention volumes were obtained for *p*(HPMA$_{50}$-*co*-EGDMA$_{0.9}$) and the solution of polymers dialysed, both the RI and RALS GPC traces suggest there has been a change in molecular weight of the initial polymers, and further work would be required to determine the differences in the polymer mixture after dialysis. Although the GPC analysis was inconclusive, the DLS results discussed earlier do demonstrate that the co-nanoprecipitates are not affected when dialysed against a large excess of water for ~5 days and remain stable during NaCl addition during a 7 day period.

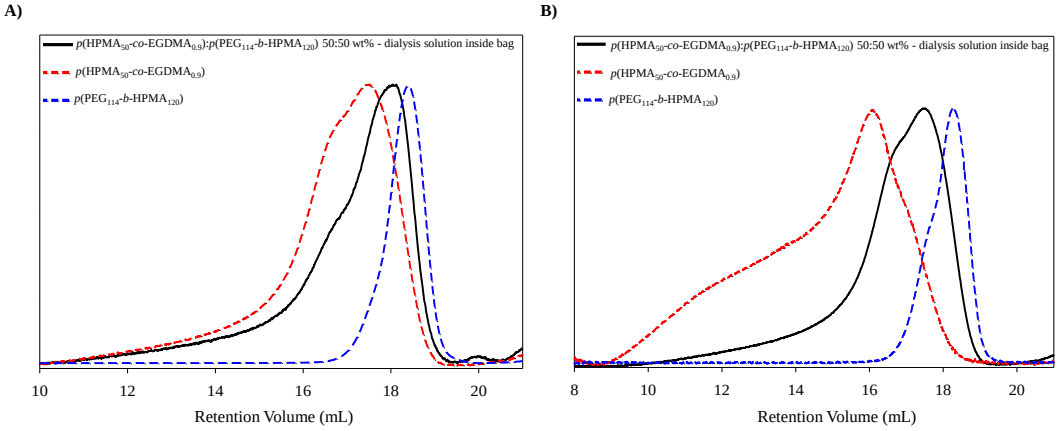

Figure 2.39 A) GPC RI trace overlay of *p*(HPMA$_{50}$-*co*-EGDMA$_{0.9}$):*p*(PEG$_{114}$-*b*-HPMA$_{120}$) 50:50 wt % dialysis solution inside the bag (black), *p*(HPMA$_{50}$-*co*-EGDMA$_{0.9}$) (red dash) and *p*(PEG$_{114}$-*b*-HPMA$_{120}$) (blue dash) B) GPC RALS trace overlay of *p*(HPMA$_{50}$-*co*-EGDMA$_{0.9}$):*p*(PEG$_{114}$-*b*-HPMA$_{120}$) 50:50 wt % dialysis solution inside the bag (black), *p*(HPMA$_{50}$-*co*-EGDMA$_{0.9}$) (red dash) and *p*(PEG$_{114}$-*b*-HPMA$_{120}$) (blue dash).

2.10 Probing the internal nanoparticle environment and co-nanoprecipitation mechanism using fluorescent guest molecule

The following experiments aim to investigate the encapsulation of a guest fluorescent molecule within nanoparticles to probe the physical properties of the internal environment. The results obtained from fluorimetry measurements can provide further indication as to

whether the PEG chains from the A-B block copolymer are incorporated internally or reside on the nanoparticle surface. A similar study has been previously conducted for *hyp*-polydendron nanoparticles, which are composed of varying amounts of PEG.[3]

Encapsulation can be achieved by dissolving the guest molecule within the polymer mixture in the good solvent (acetone) before addition to water. For the following studies the selected guest molecule was pyrene (Figure 2.40). Pyrene is a small hydrophobic molecule composed of four fused benzene rings and is soluble in a range of solvents, including acetone.

The fluorescence emission spectrum of pyrene is sensitive to solvent polarity, therefore can be used to probe the internal environment of nanoparticles. The emission spectrum of pyrene ($\pi^* \rightarrow \pi$) has five vibronic bands I-V. Peak I ($0 \rightarrow 0$ band) is strongly enhanced in polar solvents compared to peak III ($0 \rightarrow 2$ band). Thus, the ratio of the intensities of the first and third vibrational bands (the I_1/I_3 ratio) serves as a quantitative measure of solvent polarity. The I_1/I_3 ratio is one of the most widely used indicators of solvent polarity.[49] The reported value for pyrene in non-polar solvents such as hexane is ~0.61 whilst in polar solvents this value significantly increases; for example the I_1/I_3 value for water is reported within the range of 1.75 – 2.[50, 51]

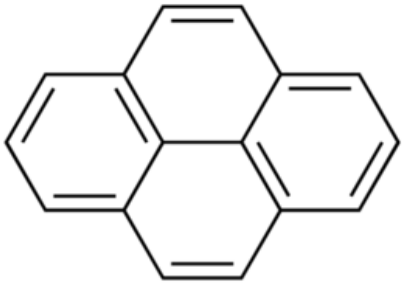

Figure 2.40 Chemical structure of pyrene.

The reported literature values for pyrene fluorescence were compared with experimental values obtained in different solvents (Figure 2.41). The results show that there are minor differences between reported and experimental values.

The encapsulation of pyrene into the polymer nanoparticles was conducted by dissolving pyrene in acetone to give a stock solution (0.1 mg/mL). The stock solution (300 µL) was added to an empty vial, and the acetone was allowed to evaporate to leave 30 µg of dye. During a typical 50:50 wt % co-nanoprecipitation, *p*($HPMA_{50}$-*co*-$EGDMA_{0.9}$), *p*(PEG_y-*b*-

HPMA$_{120}$) and acetone were added to the vial to give a final concentration of polymer 5 mg/mL and pyrene 5 µg/mL. The nanoparticles were prepared as previously described, by rapid addition of 1 mL of the solution into vigorously stirring distilled water (5 mL). The mixture was left for 24 hours at ambient temperature to ensure complete acetone evaporation, leading to a final polymer concentration in water of 1 mg/mL and 1 µg/mL pyrene in water.

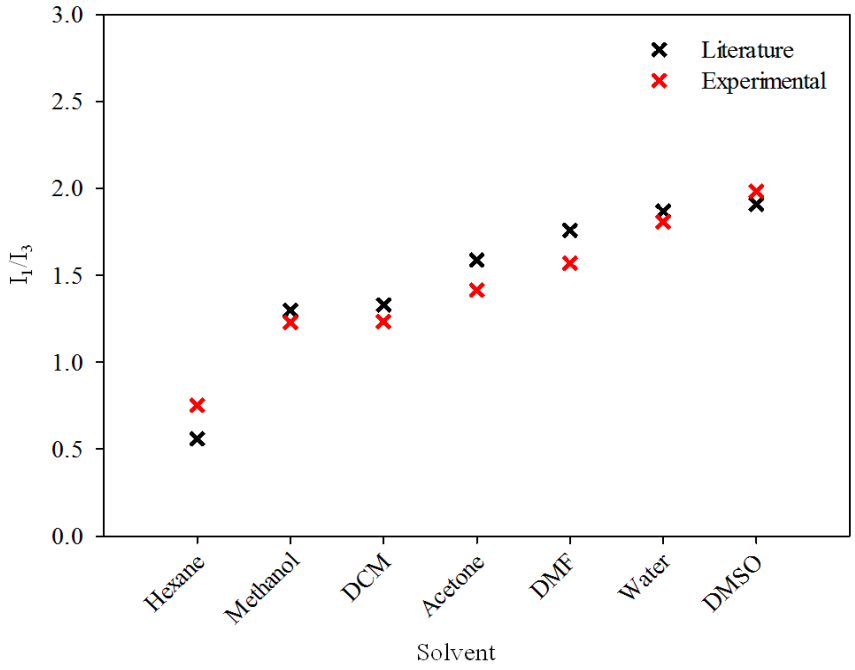

Figure 2.41 Comparison of literature and experimental values of pyrene dissolved in various solvents, literature (black cross) and experimental (red cross).

2.10.1 *p*(PEG$_{45}$-*b*-HPMA$_{120}$) pyrene studies

The size comparison of blank and pyrene encapsulated nanoprecipitates of branched *p*(HPMA$_{50}$-*co*-EGDMA$_{0.9}$) and *p*(PEG$_{45}$-*b*-HPMA$_{120}$) at various ratios is presented below (Figure 2.42) and shows there are only slight deviations from the size of the blank nanoparticles which appears to be within the normal error of nanoprecipitation. The D_z and PdI values are shown in the Appendix (Table A7).

The fluorescence emission spectra for blank and pyrene encapsulated nanoparticles is shown below in Figure 2.43 for *p*(HPMA$_{50}$-*co*-EGDMA$_{0.9}$):*p*(PEG$_{45}$-*b*-HPMA$_{120}$). For all results presented, the excitation wavelength was set to λ_{ex} = 335 nm. The emission spectrum in the absence of pyrene (Figure 2.43A) shows the absence of emission peaks for the blank nanoparticles when excited at 335 nm; this is expected as there are no

fluorophores present. For pyrene encapsulated nanoparticles (Figure 2.43B), the five vibronic bands are visible and I_1 and I_3 are highlighted.

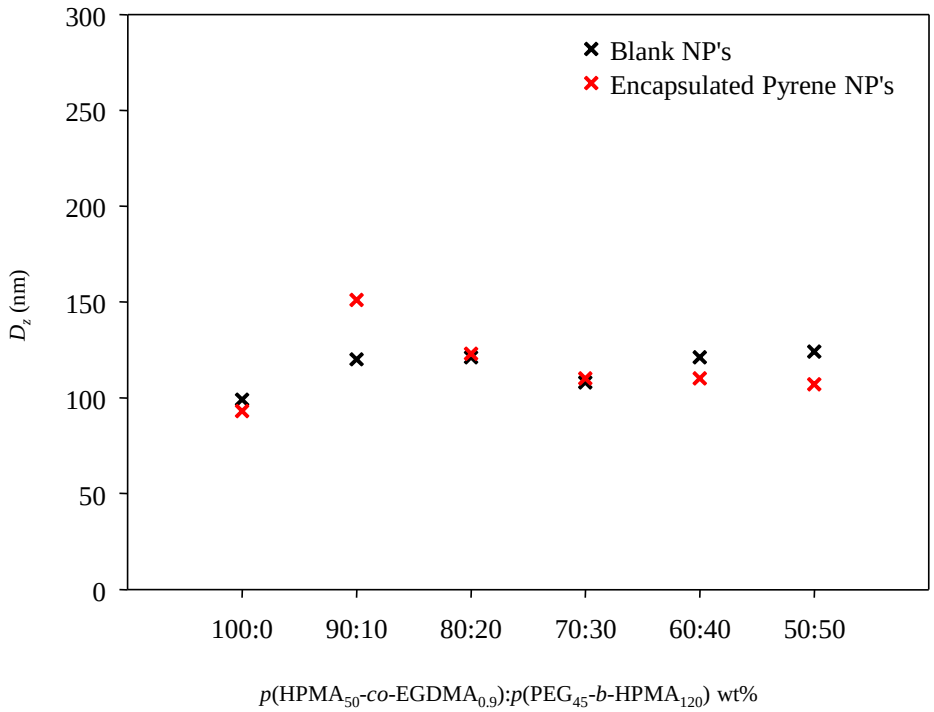

Figure 2.42 Nanoparticle sizes from DLS of blank nanoparticles (black crosses) and with 0.1 w/w % pyrene encapsulated (red crosses) for the p(PEG$_{45}$-b-HPMA$_{120}$) series.

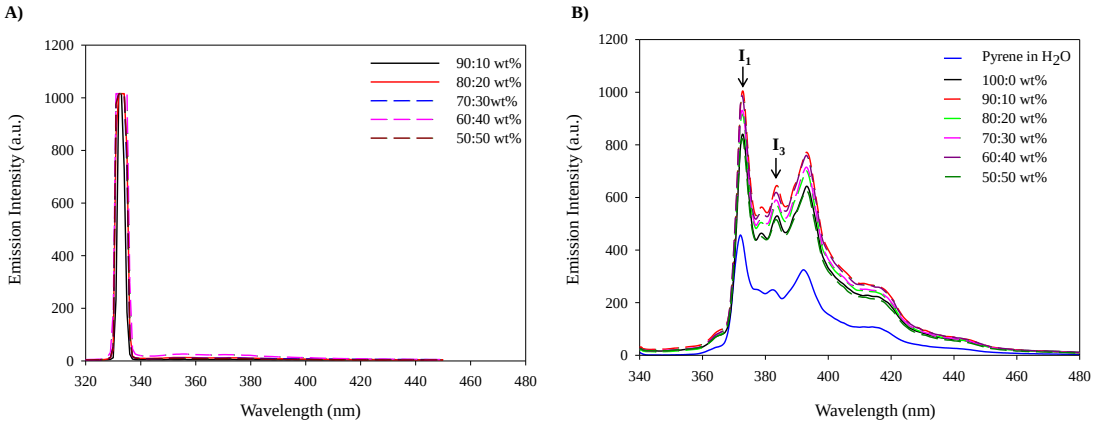

Figure 2.43 Fluorescence data for pyrene in water, p(HPMA$_{50}$-co-EGDMA$_{0.9}$) and p(HPMA$_{50}$-co-EGDMA$_{0.9}$):p(PEG$_{45}$-b-HPMA$_{120}$) co-nanoprecipitated nanoparticles at various ratios. A) fluorescence emission spectrum for blank polymeric nanoparticles, B) fluorescence emission spectrum for polymeric nanoparticles with encapsulation of 0.1 w/w % pyrene.

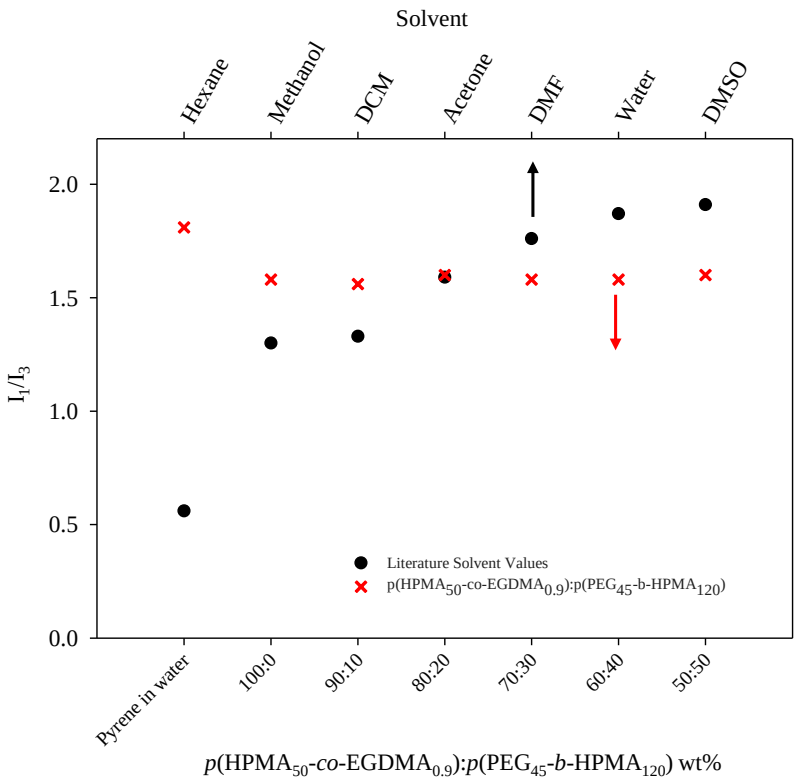

Figure 2.44 Fluorescence I_1/I_3 results for the *p*(HPMA$_{50}$-*co*-EGDMA$_{0.9}$):*p*(PEG$_{45}$-*b*-HPMA$_{120}$) series. I_1/I_3 ratio for series of nanoparticles with pyrene encapsulated (red crosses) and common solvents as a reference (black circles).

The pyrene encapsulated nanoparticles were prepared from *p*(HPMA$_{50}$-*co*-EGDMA$_{0.9}$):*p*(PEG$_{45}$-*b*-HPMA$_{120}$) between the varying ratios of 100:0 – 50:50 wt % and their I_1/I_3 values are presented in Figure 2.44A, as well as the literature solvent values. When pyrene was encapsulated within *p*(HPMA$_{50}$-*co*-EGDMA$_{0.9}$) nanoparticles, the I_1/I_3 value obtained was 1.58. Interestingly, the I_1/I_3 values across the co-nanoprecipitate ratios do not vary significantly (1.58-1.60), suggesting the core is composed mainly of hydrophobic *p*(HPMA$_{50}$-*co*-EGDMA$_{0.9}$) rather than containing additional (hydrophilic) PEG$_y$ chains (Table 2.10). Previous research within the Rannard research group has reported the pyrene nanoprecipitation studies of *hyp*-polydendrons composed of *p*(HPMA$_{50}$-*co*-EGDMA$_{0.9}$) with covalently bound PEG chains. The I_1/I_3 values obtained were higher for increasing PEG content which suggests that nanoprecipitation of the *hyp*-polydendron materials may result in a higher PEG content within the nanoparticle core.[3] For the co-nanoprecipitation system consisting of both branched *p*(HPMA$_{50}$-*co*-EGDMA$_{0.9}$) and an A-B block copolymer, the PEG chains are not covalently bound to the branched *p*(HPMA$_{50}$-*co*-EGDMA$_{0.9}$), therefore, the chance of PEG residing within the

nanoparticle core is minimised. The I_1/I_3 value obtained for highest ratio of A-B block copolymer (50 wt %) is 1.60, again, suggesting the core is composed mainly of branched *p*(HPMA$_{50}$-*co*-EGDMA$_{0.9}$) rather than PEG from the A-B block copolymer. Figure 2.45 shows a graphical representation of a branched copolymer with covalently bound PEG chains *vs* a branched/A-B block copolymer assembly along with each proposed internal environment.

Table 2.10 Summary of I_1/I_3 ratios across the varying ratios of the co-nanoprecipitated particles with encapsulated pyrene.

Sample	**Ratio**	**I_1/I_3**
Pyrene in H_2O	-	1.81
p(HPMA$_{50}$-*co*-EGDMA$_{0.9}$)	100:0	1.58
p(HPMA$_{50}$-*co*-EGDMA$_{0.9}$): p(PEG$_{45}$-*b*-HPMA$_{120}$)	90:10	1.56
p(HPMA$_{50}$-*co*-EGDMA$_{0.9}$): p(PEG$_{45}$-*b*-HPMA$_{120}$)	80:20	1.60
p(HPMA$_{50}$-*co*-EGDMA$_{0.9}$): p(PEG$_{45}$-*b*-HPMA$_{120}$)	70:30	1.58
p(HPMA$_{50}$-*co*-EGDMA$_{0.9}$): p(PEG$_{45}$-*b*-HPMA$_{120}$)	60:40	1.58
p(HPMA$_{50}$-*co*-EGDMA$_{0.9}$): p(PEG$_{45}$-*b*-HPMA$_{120}$)	50:50	1.60

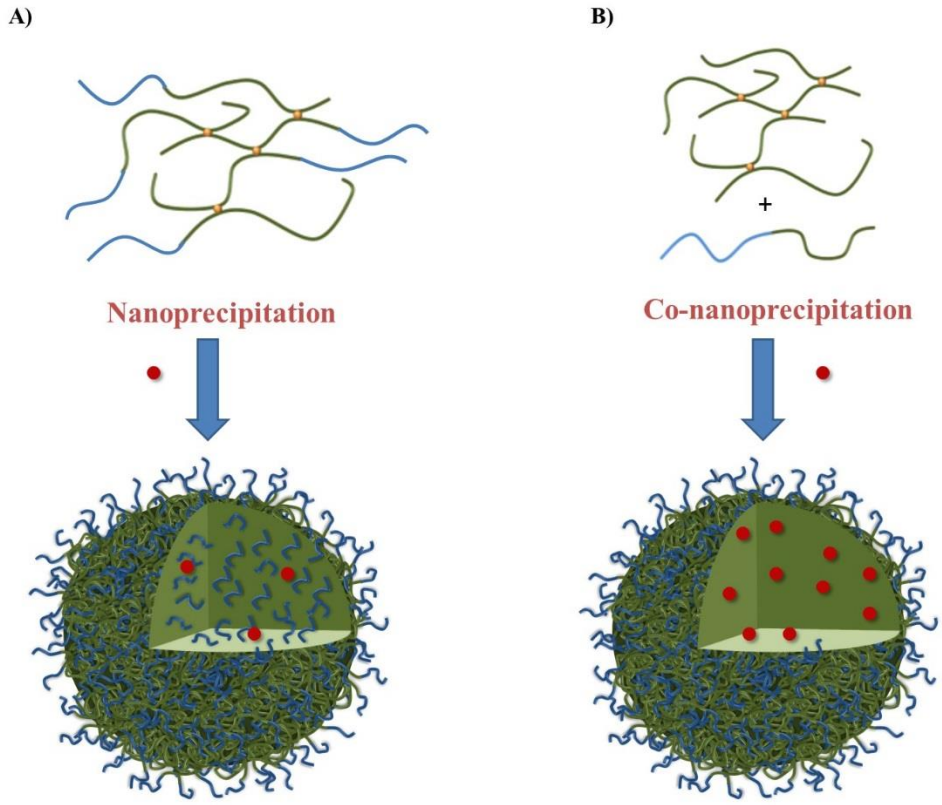

Figure 2.45 Graphical representation of pyrene encapsulation and comparison with previously prepared nanoparticles within the Rannard research group. A) *hyp*-polydendron nanoparticles, B) co-nanoprecipitated nanoparticles.

2.10.2 *p*(PEG$_{114}$-*b*-HPMA$_{120}$) pyrene studies

The excellent stability properties demonstrated by the *p*(PEG$_{114}$-*b*-HPMA$_{120}$) series were encouraging to study this system further. Also, it was of interest to determine how a water soluble A-B block copolymer could affect the core polarity. The blank *vs* pyrene encapsulated nanoparticles (Figure 2.46) demonstrated that there are again negligible differences between the nanoparticles sizes, which were discussed previously for the *p*(PEG$_{45}$-*b*-HPMA$_{120}$) series (Appendix, Table A8). The fluorescence data for blank and pyrene encapsulated nanoparticles are presented in the Appendix (Fig. A19).

The fluorimetry results for the *p*(HPMA$_{50}$-*co*-EGDMA$_{0.9}$):*p*(PEG$_{114}$-*b*-HPMA$_{120}$) nanoparticles at various ratios are generally higher than the I_1/I_3 values obtained for the *p*(HPMA$_{50}$-*co*-EGDMA$_{0.9}$):*p*(PEG$_{45}$-*b*-HPMA$_{120}$) series. The I_1/I_3 value for 100 % branched *p*(HPMA$_{50}$-*co*-EGDMA$_{0.9}$) was 1.64, so all following results were relative to this value, due to the absence of PEG chains (Figure 2.47). Overall, the reported I_1/I_3 values did not deviate much from 1.64, and for the 90 wt % *p*(PEG$_{114}$-*b*-HPMA$_{120}$) A-B

block copolymer, a minor decrease to 1.57 was observed. This fluorimetry data suggests that the hydrophobic core is composed mainly of HPMA and minimal or no PEG chains. This study further suggests that the A-B block copolymer HPMA chain becomes incorporated into the branched *p*(HPMA$_{50}$-*co*-EGDMA$_{0.9}$) core and PEG chains reside on the nanoparticle surface (Figure 2.10ii) .

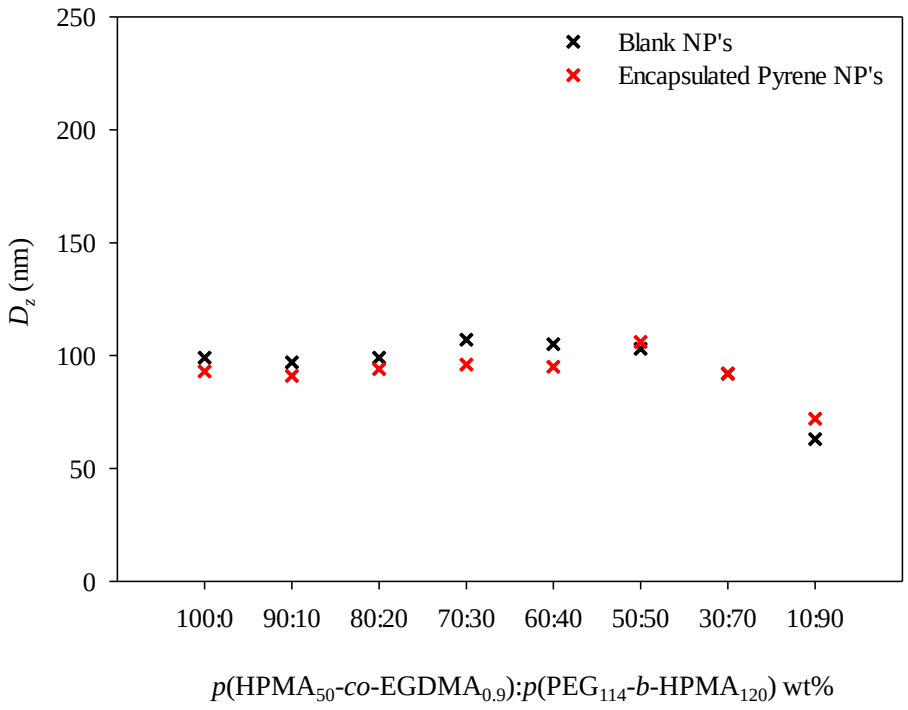

Figure 2.46 DLS results of blank nanoparticles (black crosses) and with 0.1 w/wt % pyrene encapsulated (red crosses) for the *p*(PEG$_{114}$-*b*-HPMA$_{120}$) series.

Considering both the I_1/I_3 ratios and low ζ values obtained previously, the results suggest that the PEG chains for both *p*(PEG$_{45}$-*b*-HPMA$_{120}$) and *p*(PEG$_{114}$-*b*-HPMA$_{120}$) A-B block copolymers are mainly located at the surface of the nanoprecipitates. The encapsulation of a hydrophobic organic molecule has highlighted the potential application of such materials as carriers of poorly soluble compounds and this study has utilised A−B block copolymers whilst varying their compositions. In addition, the process will be investigated to extend beyond the chemical compositions presented to enhance the properties of materials which have previously been overlooked as potential nanocarriers.

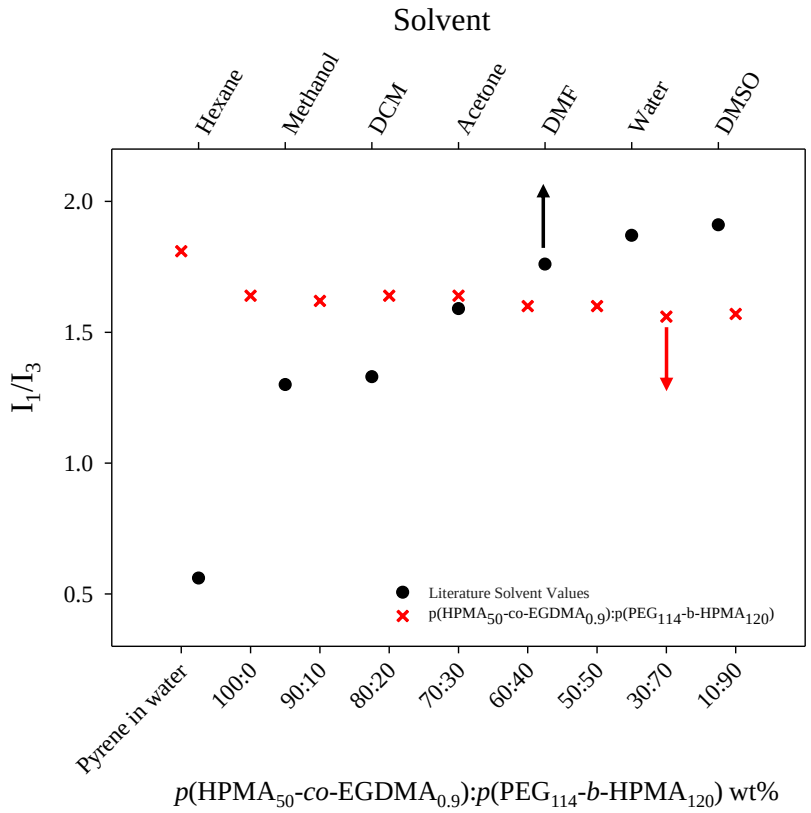

Figure 2.47 Fluorimetry results for the *p*(HPMA$_{50}$-*co*-EGDMA$_{0.9}$):*p*(PEG$_{114}$-*b*-HPMA$_{120}$) series. I_1/I_3 ratio for series of nanoparticles with pyrene encapsulated (red crosses) and common solvents as a reference (black circles).

Table 2.11 I_1/I_3 ratios across the varying ratios of the co-nanoprecipitated particles with encapsulated pyrene.

Sample	Ratio	I_1/I_3
Pyrene in H_2O	-	1.81
p(HPMA$_{50}$-*co*-EGDMA$_{0.9}$)	100:0	1.64
p(HPMA$_{50}$-*co*-EGDMA$_{0.9}$):*p*(PEG$_{114}$-*b*-HPMA$_{120}$)	90:10	1.62
p(HPMA$_{50}$-*co*-EGDMA$_{0.9}$):*p*(PEG$_{114}$-*b*-HPMA$_{120}$)	80:20	1.64
p(HPMA$_{50}$-*co*-EGDMA$_{0.9}$):*p*(PEG$_{114}$-*b*-HPMA$_{120}$)	70:30	1.64
p(HPMA$_{50}$-*co*-EGDMA$_{0.9}$):*p*(PEG$_{114}$-*b*-HPMA$_{120}$)	60:40	1.60
p(HPMA$_{50}$-*co*-EGDMA$_{0.9}$):*p*(PEG$_{114}$-*b*-HPMA$_{120}$)	50:50	1.60
p(HPMA$_{50}$-*co*-EGDMA$_{0.9}$):*p*(PEG$_{114}$-*b*-HPMA$_{120}$)	30:70	1.56
p(HPMA$_{50}$-*co*-EGDMA$_{0.9}$):*p*(PEG$_{114}$-*b*-HPMA$_{120}$)	10:90	1.57

2.11 Conclusion

The synthesis of both linear *p*(HPMA$_{50}$), branched *p*(HPMA$_{50}$-*co*-EGDMA$_{0.9}$) and *p*(PEG$_y$-*b*-HPMA$_x$) linear A-B block copolymers *via* ATRP was successfully achieved. The model nanoprecipitation studies of *p*(HPMA$_{50}$) and *p*(HPMA$_{50}$-*co*-EGDMA$_{0.9}$) were conducted to support the previous views that there is a clear advantage of using branched *p*(HPMA$_{50}$-*co*-EGDMA$_{0.9}$) copolymers rather than linear homopolymers when seeking to achieve narrow, monomodal polymer nanoparticle size distributions. It is evident that branched chains effectively collapse to form relatively large nuclei that assemble to form the larger, colloidally stable nanoparticles. Further to this, multiple nanoprecipitation experiments were conducted without modification of the original nanoparticle size and it is worth emphasising that this procedure provides an option to create samples of increasing concentration *via* a relatively simple strategy after initial removal of good solvent. The co-nanoprecipitation studies of *p*(HPMA$_{50}$-*co*-EGDMA$_{0.9}$) with A−B block copolymers at varying ratios from 100:0-0:100 wt %, leads to nanoparticle behaviour that is different to the individually nanoprecipitated copolymers (branched or A-B block copolymer). The size and PdI values did not show any major trend and generally narrow, monomodal distributions were obtained across each series. As discussed, this method was studied to see if it was possible to improve the properties of charge stabilised nanoparticles of *p*(HPMA$_{50}$-*co*-EGDMA$_{0.9}$) and introduce steric stabilisation *via* an A-B block copolymer. To evaluate the differences in stability, aliquots of NaCl were added to the nanoparticle dispersions and generated different results depending on the chemical composition of the A-B block copolymer and ratio studied. An apparent maximum of salt stability was observed during inclusion of *p*(PEG$_{114}$-*b*-HPMA$_{120}$) A-B block copolymer. This may be indicative of an optimum ratio and A-B block composition necessary for efficient polymer interaction during the co-nanoprecipitation process, and at what point the increased hydrophilic PEG chains provide sufficient stabilisation. A simplified DLVO approach was applied to the co-nanoprecipitated nanoparticles of *p*(HPMA$_{50}$-*co*-EGDMA$_{0.9}$):*p*(PEG$_{45}$-*b*-HPMA$_{120}$) and suggested that the low ζ values present after charge screening in salt solutions should lead to aggregation, and indeed, aggregation is seen if the number of PEG$_{45}$ chains is insufficient to provide a barrier to approaching nanoparticles. Although no evidence was provided by DLS analysis, it is possible that non-uniform decoration of the A−B block copolymer, including the formation of structures predominantly resembling micelles or vesicles, occurs at low concentrations of branched copolymer. The encapsulation of the hydrophobic organic molecule pyrene and

polarity studies has provided further evidence that during addition of increasing levels of A-B block copolymer, the hydrophobicity of the internal core is maintained and only a slight increase is observed when compared with 100 % *p*(HPMA$_{50}$-*co*-EGDMA$_{0.9}$). From these detailed studies, it appears it is most likely that the HPMA from the A-B block copolymer becomes incorporated into the polymer core and the PEG chain resides on the nanoparticle surface. Ongoing studies with the A-B block copolymers and varying branched copolymer core is of interest to establish a more detailed insight into this facile nanoparticle production strategy.

2.12 References

1. R. A. Slater, T. O. McDonald, D. J. Adams, E. R. Draper, J. V. M. Weaver and S. P. Rannard, *Soft Matter*, 2012, **8**, 9816-9827.
2. F. L. Hatton, P. Chambon, T. O. McDonald, A. Owen and S. P. Rannard, *Chemical Science*, 2014, **5**, 1844-1853.
3. F. L. Hatton, L. M. Tatham, L. R. Tidbury, P. Chambon, T. He, A. Owen and S. P. Rannard, *Chemical Science*, 2015, **6**, 326-334.
4. J. Goodwin, *Colloids and Interfaces with Surfactants and Polymers*, John Wiley & Sons, 2nd Edition, UK, 2009.
5. R. Singh and J. W. Lillard Jr, *Experimental and Molecular Pathology*, 2009, **86**, 215-223.
6. L. Zhang, F. X. Gu, J. M. Chan, A. Z. Wang, R. S. Langer and O. C. Farokhzad, *Clinical Pharmacology & Therapeutics*, 2008, **83**, 761-769.
7. K. Matyjaszewski and J. Spanswick, *Materials Today*, 2005, **8**, 26-33.
8. J.-S. Wang and K. Matyjaszewski, *Journal of the American Chemical Society*, 1995, **117**, 5614-5615.
9. M. Kato, M. Kamigaito, M. Sawamoto and T. Higashimura, *Macromolecules*, 1995, **28**, 1721-1723.
10. W. A. Braunecker and K. Matyjaszewski, *Progress in Polymer Science*, 2007, **32**, 93-146.
11. K. Matyjaszewski, *Macromolecules*, 2012, **45**, 4015-4039.
12. K. Matyjaszewski and J. Xia, *Chemical Reviews*, 2001, **101**, 2921-2990.
13. A. P. Narrainen, S. Pascual and D. M. Haddleton, *Journal of Polymer Science Part A: Polymer Chemistry*, 2002, **40**, 439-450.
14. S. Liu and S. P. Armes, *Current Opinion in Colloid & Interface Science*, 2001, **6**, 249-256.
15. A. Ramakrishnan and R. Dhamodharan, *Macromolecules*, 2003, **36**, 1039-1046.
16. V. Coessens, T. Pintauer and K. Matyjaszewski, *Progress in Polymer Science*, 2001, **26**, 337-377.
17. M. L. Adams, A. Lavasanifar and G. S. Kwon, *Journal of Pharmaceutical Sciences*, 2003, **92**, 1343-1355.
18. A. Rösler, G. W. M. Vandermeulen and H.-A. Klok, *Advanced Drug Delivery Reviews*, 2012, **64, Supplement**, 270-279.

19. K. Jankova, X. Chen, J. Kops and W. Batsberg, *Macromolecules*, 1998, **31**, 538-541.
20. K. Robinson, M. Khan, M. de Paz Banez, X. Wang and S. Armes, *Macromolecules*, 2001, **34**, 3155-3158.
21. K. H. Kim, J. Kim and W. H. Jo, *Polymer*, 2005, **46**, 2836-2840.
22. M. Ranger, M.-C. Jones, M.-A. Yessine and J.-C. Leroux, *Journal of Polymer Science Part A: Polymer Chemistry*, 2001, **39**, 3861-3874.
23. R. M. England and S. Rimmer, *Polymer Chemistry*, 2010, **1**, 1533-1544.
24. N. O'Brien, A. McKee, D. C. Sherrington, A. T. Slark and A. Titterton, *Polymer*, 2000, **41**, 6027-6031.
25. F. Isaure, P. A. Cormack, S. Graham, D. C. Sherrington, S. P. Armes and V. Bütün, *Chemical Communications*, 2004, 1138-1139.
26. Z. Wang, J. He, Y. Tao, L. Yang, H. Jiang and Y. Yang, *Macromolecules*, 2003, **36**, 7446-7452.
27. C. Jiang, Y. Shen, S. Zhu and D. Hunkeler, *Journal of Polymer Science Part A: Polymer Chemistry*, 2001, **39**, 3780-3788.
28. I. Bannister, N. C. Billingham, S. P. Armes, S. P. Rannard and P. Findlay, *Macromolecules*, 2006, **39**, 7483-7492.
29. W. Huang, H. Yang, X. Xue, B. Jiang, J. Chen, Y. Yang, H. Pu, Y. Liu, D. Zhang, L. Kong and G. Zhai, *Polymer Chemistry*, 2013, **4**, 3204-3211.
30. S. Graham, S. P. Rannard, P. A. G. Cormack and D. C. Sherrington, *Journal of Materials Chemistry*, 2007, **17**, 545-552.
31. J. Cheng, B. A. Teply, I. Sherifi, J. Sung, G. Luther, F. X. Gu, E. Levy-Nissenbaum, A. F. Radovic-Moreno, R. Langer and O. C. Farokhzad, *Biomaterials*, 2007, **28**, 869-876.
32. E. Lepeltier, C. Bourgaux and P. Couvreur, *Advanced Drug Delivery Reviews*, 2014, **71**, 86-97.
33. J. Xia, S. G. Gaynor and K. Matyjaszewski, *Macromolecules*, 1998, **31**, 5958-5959.
34. P. A. Gurr, M. F. Mills, G. G. Qiao and D. H. Solomon, *Polymer*, 2005, **46**, 2097-2104.
35. H. Deng, J. Liu, X. Zhao, Y. Zhang, J. Liu, S. Xu, L. Deng, A. Dong and J. Zhang, *Biomacromolecules*, 2014, **15**, 4281-4292.
36. R. Ji, J. Cheng, T. Yang, C. C. Song, L. Li, F.-S. Du and Z.-C. Li, *Biomacromolecules*, 2014, **15**, 3531-3539.

37. R. Heeb, S. Lee, N. V. Venkataraman and N. D. Spencer, *ACS Applied Materials & Interfaces*, 2009, **1**, 1105-1112.
38. N. Lebovka, in *Polyelectrolyte Complexes in the Dispersed and Solid State I*, M. Müller, Springer Berlin Heidelberg, 2014, 171, 57-96.
39. C. Schneider, M. Hanisch, B. Wedel, A. Jusufi and M. Ballauff, *Journal of Colloid and Interface Science*, 2011, **358**, 62-67.
40. B. Derjaguin and L. Landau, *Progress in Surface Science*, 1993, **43**, 30-59.
41. E. Verwey and J. T. G. Overbeek, *Journal*, 1948.
42. D. Grasso*, K. Subramaniam, M. Butkus, K. Strevett and J. Bergendahl, *Reviews in Environmental Science and Biotechnology*, 2002, **1**, 17-38.
43. C. Zhang, V. J. Pansare, R. K. Prud'homme and R. D. Priestley, *Soft Matter*, 2012, **8**, 86-93.
44. T. L. Doane, C.-H. Chuang, R. J. Hill and C. Burda, *Accounts of Chemical Research*, 2012, **45**, 317-326.
45. Y. Ishikawa, Y. Katoh and H. Ohshima, *Colloids and Surfaces B: Biointerfaces*, 2005, **42**, 53-58.
46. C. Cruje and D. B. Chithrani, *Reviews in Nanoscience and Nanotechnology*, 2014, **3**, 20-30.
47. T. Tadros, *Advances in Colloid and Interface Science*, 2011, **168**, 263-277.
48. W. Wu, C. F. Majkrzak, S. K. Satija, J. F. Ankner, W. J. Orts, M. Satkowski and S. D. Smith, *Polymer*, 1992, **33**, 5081-5084.
49. M. Li, M. Jiang, Y.-x. Zhang and Q. Fang, *Macromolecules*, 1997, **30**, 470-478.
50. D. C. Dong and M. A. Winnik, *Canadian Journal of Chemistry*, 1984, **62**, 2560-2565.
51. R. Motokawa, K. Morishita, S. Koizumi, T. Nakahira and M. Annaka, *Macromolecules*, 2005, **38**, 5748-5760.

Chapter 3

The Synthesis and Nanoprecipitation Studies of Branched and Block Copolymers with Hydrophobic Block Segments for Co-nanoprecipitated Particle Dispersions and their Pharmacological Studies *in vitro*.

3.1 Introduction

As discussed in Chapter 2, the detailed co-nanoprecipitation studies of branched *p*(HPMA$_{50}$-*co*-EGDMA$_{0.9}$) copolymers with varying *p*(PEG$_x$-*b*-HPMA$_y$) A-B block copolymers resulted in the formation of sterically stabilised nanoparticles. To further investigate the co-nanoprecipitation process, this research chapter will focus upon the synthesis of hydrophobic branched copolymers other than *p*(HPMA$_{50}$-*co*-EGDMA$_{0.9}$) and subsequent aqueous nanoparticle studies in combination with a selection of A-B block copolymers including those previously described. It is of interest to investigate the behaviour of polymers with varying chemical compositions to evaluate the versatility of the co-nanoprecipitation approach.

3.2 Synthesis of hydrophobic branched co/terpolymers *via* ATRP

The research studies presented in Chapter 2 focused on branched *p*(HPMA$_{50}$-*co*-EGDMA$_{0.9}$) copolymers and varying *p*(PEG$_x$-*b*-HPMA$_y$) block copolymers. In order to investigate the versatility of the co-nanoprecipitation process with A-B block copolymers and branched copolymers other than *p*(HPMA$_{50}$-*co*-EGDMA$_{0.9}$), alternative branched copolymers have been synthesised. As discussed, *p*(HPMA$_{50}$-*co*-EGDMA$_{0.9}$) forms stable nanoparticles when nanoprecipitated alone and during co-nanoprecipitation with an A-B block copolymer. Stabilised nanoparticles with varying polymer compositions may offer the potential to tune nanoparticle behaviour. Herein, the hydrophobic monomers *n*-butyl methacrylate (*n*-BMA) and *t*-butyl methacrylate (*t*-BMA) were evaluated for the preparation of branched copolymers.

The ATRP reaction schemes for the various target branched copolymers; *p*(*n*-BMA$_{50}$-*co*-EGDMA$_{0.8}$) (**6**), *p*(*t*-BMA$_{50}$-*co*-EGDMA$_{0.9}$) (**7**), *p*(HPMA$_{25}$-*co*-*n*-BMA$_{25}$-*co*-EGDMA$_{0.9}$) (**8**) and *p*(HPMA$_{25}$-*co*-*t*-BMA$_{25}$-*co*-EGDMA$_{0.9}$) (**9**) are shown in Scheme 3.1. In all cases, to allow behavioural comparison, the targeted DP$_n$ for each primary polymer chain was 50 monomer units; this also allowed comparison to the branched *p*(HPMA$_{50}$-*co*-EGDMA$_{0.9}$) copolymers synthesised in Chapter 2, Section 2.3. The monomer concentration within each polymerisation was of 50 wt % with respect to the solvent unless otherwise stated. All polymers previously synthesised and studied in Chapter 2 were analysed using a DMF triple detection GPC instrument at 60°C with 0.01M LiBr, due to the solubility of the PEG chains within the A-B block copolymers. However, the branched copolymers presented below were analysed using a triple detection GPC

instrument employing a THF eluent containing TEA (2 v/v %), as the branched polymers were initiated with EBiB and were easily solubilised in this solvent.

When using EBiB (**1**) as the initiator, a molar ratio of brancher:initiator of 0.9:1 was employed. These conditions were used previously for *p*(HPMA$_{50}$-*co*-EGDMA$_{0.9}$) in Chapter 2, Section 2.3 in order to obtain a high molecular weight polymer. Generally, this ratio of brancher:initiator was suitable and a high molecular weight, soluble polymer was recovered. However, during the ATRP polymerisation of *p*(*n*-BMA$_{50}$-*co*-EGDMA$_{0.8}$), a 0.9:1 brancher:initiator ratio resulted in the formation of a material which could not be fully solubilised in a good solvent, therefore the EGDMA content was decreased to 0.8 and the resulting polymer was readily soluble.

The selected solvent for the ATRP synthesis of *p*(*n*-BMA$_{50}$-*co*-EGDMA$_{0.8}$) was anhydrous methanol at an elevated temperature of 60°C, which has been previously reported within our research group.[1, 2] Methanol is often used as a precipitant for *p*(*n*-BMA$_x$), yet the Cu-catalysed ATRP in methanol has been shown to yield polymers with desired molecular weights and low dispersities. The reports of *p*(*n*-BMA$_x$) also demonstrated the ability for the temperature of the polymerisation to be lowered to 25°C, but upon sampling, precipitation of the polymer was observed. Therefore, monitoring conversion became increasingly difficult.

The solvent system selected for the preparation of *p*(*t*-BMA$_{50}$-*co*-EGDMA$_{0.9}$) was a mixture of isopropanol (IPA) and H_2O (92.5:7.5) (33.3 wt % based on *t*-BMA), as these ATRP polymerisation conditions were previously reported by Rannard and co-workers as the first room temperature water-borne ATRP of a hydrophobic monomer in homogenous alcoholic media in 2001.[3] A ratio of 92.5:7.5% IPA:H_2O exhibited the ideal ratio in terms of reactivity time without compromising the control of the polymerisation.

For the synthesis of both branched statistical terpolymers (*p*(HPMA$_{25}$-*co*-*t*-BMA$_{25}$-*co*-EGDMA$_{0.9}$) and *p*(HPMA$_{25}$-*co*-*n*-BMA$_{25}$-*co*-EGDMA$_{0.9}$)), the equal ratio of both monomers were completely soluble in anhydrous methanol, therefore the same reaction conditions previously stated for *p*(HPMA$_{50}$-*co*-EGDMA$_{0.9}$) (Chapter 2, Section 2.3) were employed for the ATRP polymerisations.

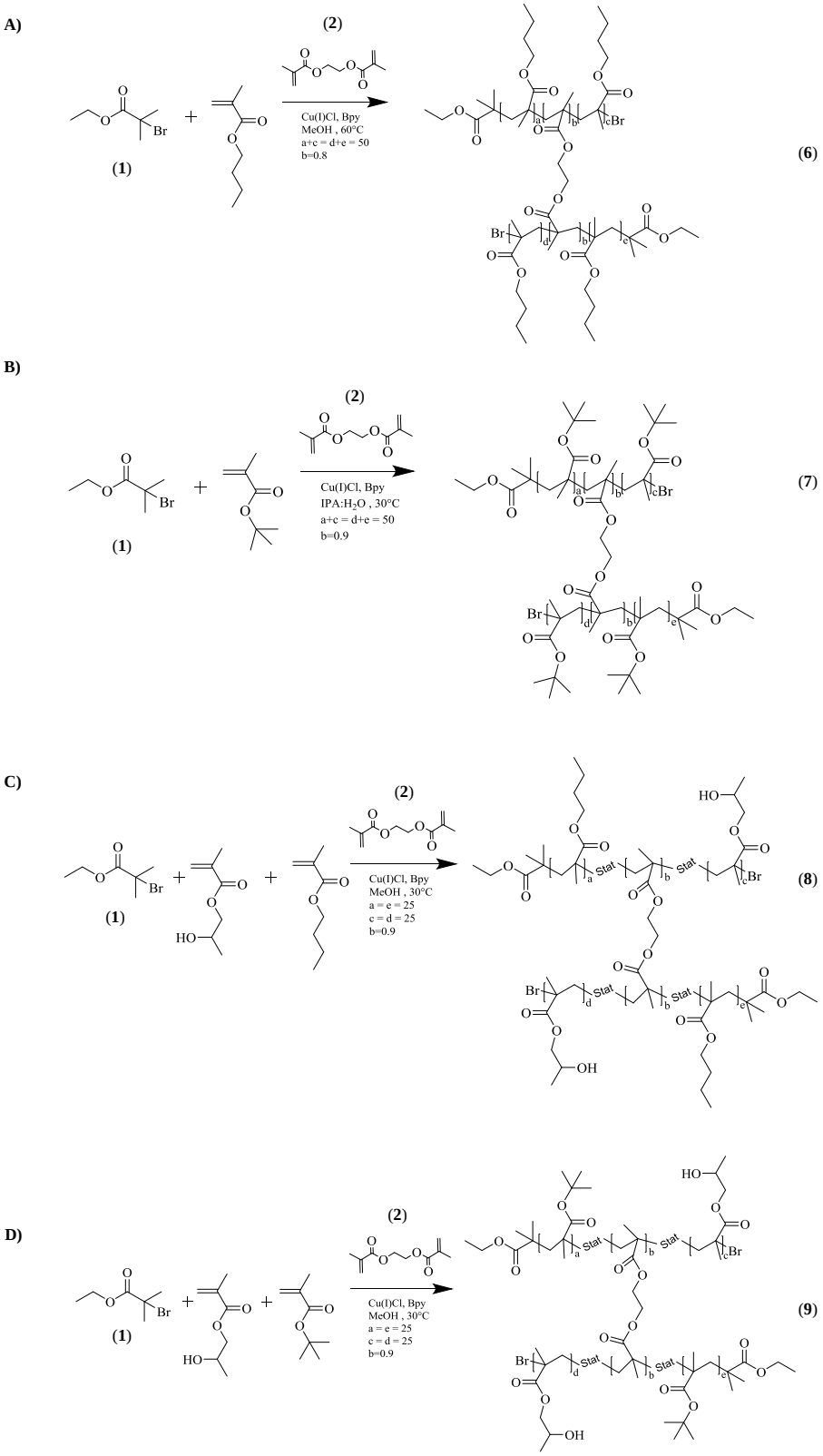

Scheme 3.1 ATRP synthesis of branched hydrophobic polymers. A) *p*(*n*-BMA$_{50}$-*co*-EGDMA$_{0.8}$), B) *p*(*t*-BMA$_{50}$-*co*-EGDMA$_{0.9}$), C) *p*(HPMA$_{25}$-*co*-*n*-BMA$_{25}$-*co*-EGDMA$_{0.9}$), D) *p*(HPMA$_{25}$-*co*-*t*-BMA$_{25}$-*co*-EGDMA$_{0.9}$).

Triple detection GPC was used to determine the molecular weights of the branched copolymers (Table 3.1) and the inclusion of EGDMA yielded high molecular weight polymeric species with broader dispersities than would be obtained for linear polymers (See Appendix, Fig. A20-A22 for GPC example overlays of linear and branched polymers comprised of *n*-BMA, HPMA-*co*-*n*-BMA and HPMA-*co*-*t*-BMA). It is well documented that high M_w branched structures do not form until high conversions are reached, through intermolecular reactions when the linear polymer chains join together *via* a pseudo step-growth mechanism.[4] The high M_w values (Table 3.1) are indicative of the formation of high molecular weight branched copolymers; in all cases the polymerisations reached high conversions > 97%, as monitored by ^{1}H NMR.

Table 3.1 GPC and ^{1}H NMR analysis of branched copolymers synthesised *via* ATRP.

Targeted Polymer Composition	Conversion (%)[a]	M_n (g/mol)	M_w (g/mol)	*Đ*
p(HPMA$_{50}$-*co*-EGDMA$_{0.9}$)	98	39 100	293 100	7.49
p(*n*-BMA$_{50}$-*co*-EGDMA$_{0.8}$)	98	36 000	206 100	5.73
p(*t*BMA$_{50}$-*co*-EGDMA$_{0.9}$)	99	95 100	184 700	1.94
p(HPMA$_{25}$-*co*-*n*-BMA$_{25}$-*co*-EGDMA$_{0.9}$)	97	220 000	3 050 000	13.9
p(HPMA$_{25}$-*co*-*t*BMA$_{25}$-*co*-EGDMA$_{0.9}$)	97	16 000	157 000	9.81

[a] Determined by ^{1}H NMR analysis in DMSO-d$_6$ or MeOD-d$_4$

The conversion was calculated by integration of the vinyl protons to an internal NMR reference (anisole); an example overlay of ^{1}H NMR spectra for branched *p*(HPMA$_{25}$-*co*-*n*-BMA$_{25}$-*co*-EGDMA$_{0.9}$) is shown in the Appendix, Fig. A23. Due to the statistical nature of branching in ATRP, there is a broad distribution of materials present, which range from linear chains to highly branched macromolecules.[5] The RI chromatogram overlay (Figure 3.1A) illustrates the formation of high molecular weight branched copolymers which is evident from elution of polymers at low retention volumes. The analysed ^{1}H NMR spectra of final branched copolymers are presented in the Appendix, Fig. A24-A27.

Although a small RI response is detected at lower retention volumes, a more detailed representation of the large polymeric species is presented by the RALS chromatogram overlay (Figure 3.1B), as this detector is dependent on the size of the polymeric species present. The RI detector indicates the overall concentration of each fraction within the distribution and although the linear primary chains appear as the most common species,

the presence of multiple branched species is also obvious within the analysis. It is worth noting that the height of each peak has been normalised to aid comparison and does not reflect the absolute detector response.

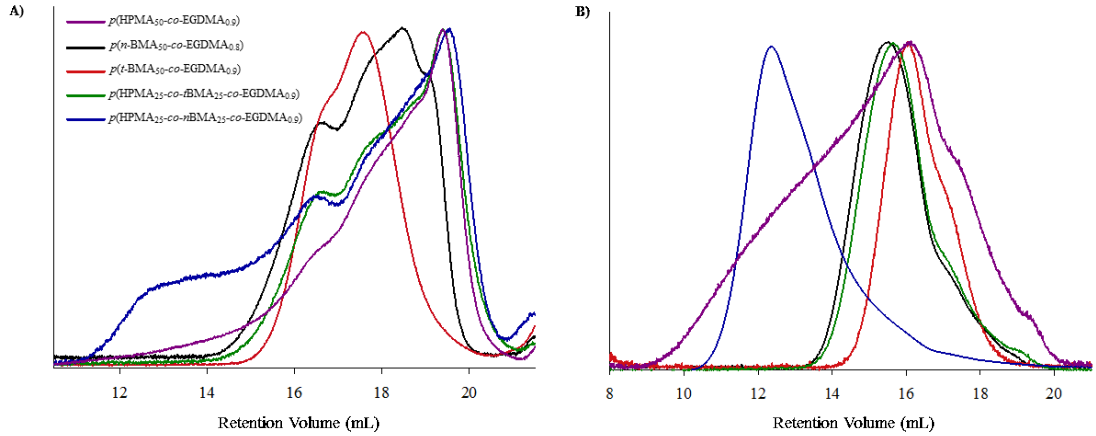

Figure 3.1 GPC analyses for branched copolymers A) RI chromatogram overlays, B) RALS chromatogram overlays.

3.3 Aqueous nanoprecipitation studies

3.3.1 Nanoprecipitation studies of branched co/terpolymers

As previously reported, the formation of aqueous nanoparticles *via* the nanoprecipitation approach is efficient and reproducible.[6, 7] To ensure consistency and aid comparison, the conditions for all branched copolymer nanoprecipitation experiments were as described previously. Therefore, all nanoparticles from this point onwards (unless otherwise stated) will be prepared from 1 mL of a 5 mg/ml polymer solution (acetone) into 5 mL of water. The initial and final concentration of samples prepared by aqueous nanoprecipitation will be described as i_x-f_y, where x represents the initial concentration and y the final concentration in mg/mL, therefore unless otherwise stated, the conditions will be i_5-f_1. Acetone solutions of the branched copolymers and terpolymers; *p*(*n*-BMA$_{50}$-*co*-EGDMA$_{0.8}$), *p*(*t*-BMA$_{50}$-*co*-EGDMA$_{0.9}$), *p*(HPMA$_{25}$-*co*-*n*-BMA$_{25}$-*co*-EGDMA$_{0.9}$) and *p*(HPMA$_{25}$-*co*-*t*-BMA$_{25}$-*co*-EGDMA$_{0.9}$) were nanoprecipitated into water. It was possible that nanoprecipitation of the hydrophobic copolymers *p*(*n*-BMA$_{50}$-*co*-EGDMA$_{0.8}$) and *p*(*t*-BMA$_{50}$-*co*-EGDMA$_{0.9}$) may precipitate upon nanoprecipitation and the statistical terpolymers would be somewhat stabilised due to the presence of HPMA which has some hydrophilic nature although being insoluble in water. Nanoprecipitations were conducted and, as expected, *p*(*n*-BMA$_{50}$-*co*-EGDMA$_{0.8}$) and *p*(*t*-BMA$_{50}$-*co*-EGDMA$_{0.9}$) instantly

precipitated upon addition to water. Although the branched terpolymer *p*(HPMA$_{25}$-*co*-*t*-BMA$_{25}$-*co*-EGDMA$_{0.9}$) was stable upon initially, after 24 hours the polymer precipitated; however, *p*(HPMA$_{25}$-*co*-*n*-BMA$_{25}$-*co*-EGDMA$_{0.9}$) remained stable (Figure 3.3). Although nanoprecipitation of *p*(*n*-BMA$_{50}$-*co*-EGDMA$_{0.8}$) resulted in instant precipitation, the presence of HPMA monomer units in the statistical terpolymer of *p*(HPMA$_{25}$-*co*-*n*-BMA$_{25}$-*co*-EGDMA$_{0.9}$) appeared to provide stabilisation and enabled the formation of nanoparticles. This may be due to the presence of the adsorbed hydroxide ions on the nanoparticle surface of the nanoparticles, facilitated by the HPMA monomer residues, which provide additional stabilisation. This has been reported in the literature for a range of material types including films of polystyrene and poly(2-hydroxyethyl methacrylate).[8-10]

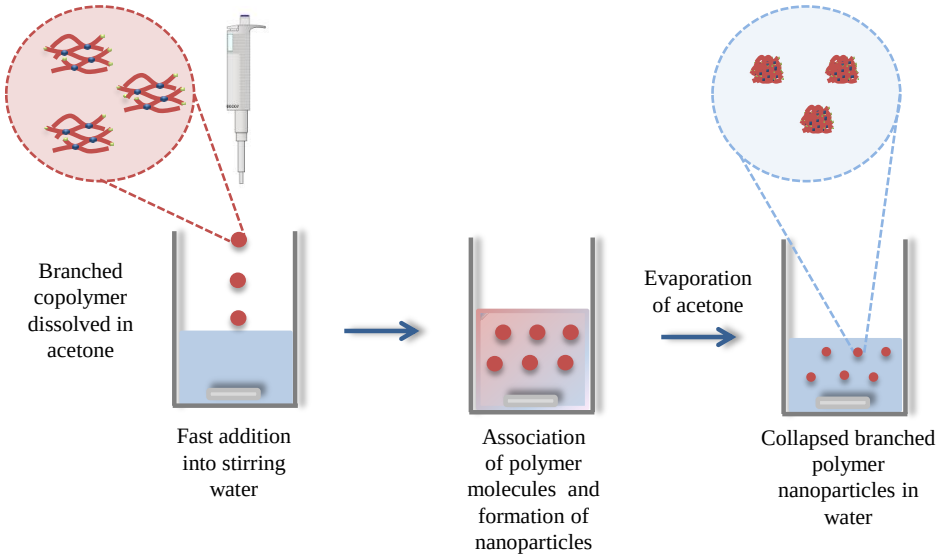

Figure 3.2 Schematic representation of the nanoprecipitation approach of co- and terpolymers.

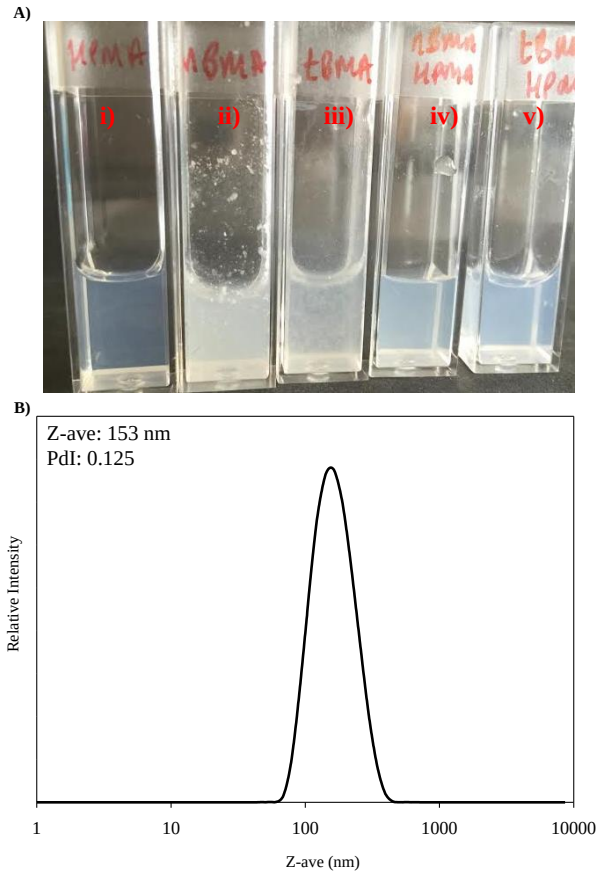

Figure 3.3 Photographs of branched c- and terpolymer nanoprecipitations, final concentration of polymer 1 mg/mL, Ai) *p*(HPMA$_{50}$-*co*-EGDMA$_{0.9}$) ii) *p*(*n*-BMA$_{50}$-*co*-EGDMA$_{0.8}$) iii) *p*(*t*-BMA$_{50}$-*co*-EGDMA$_{0.9}$) iv) *p*(HPMA$_{25}$-*co*-*n*-BMA$_{25}$-*co*-EGDMA$_{0.9}$) v) *p*(HPMA$_{25}$-*co*-*t*-BMA$_{25}$-*co*-EGDMA$_{0.9}$), B) DLS trace for nanoprecipitation of *p*(HPMA$_{25}$-*co*-*n*-BMA$_{25}$-*co*-EGDMA$_{0.9}$).

3.3.2 Co-nanoprecipitation studies of branched copolymers and A-B block copolymers

Following the successful preparation of *p*(*n*-BMA$_{50}$-*co*-EGDMA$_{0.8}$) and *p*(*t*-BMA$_{50}$-*co*-EGDMA$_{0.9}$) branched copolymers, the highly hydrophobic nature prevented the production of stable nanoparticles *via* nanoprecipitation. As witnessed in Chapter 2, the incorporation of an A-B block copolymer within the nanoprecipitation enhanced the stability of nanoparticles, particularly in aqueous salt conditions. It was, therefore, hypothesised that similar benefits could be introduced by application of the co-nanoprecipitation method, in order to produce stable nanoprecipitates from these branched polymers. It may be expected that the synthesised branched co- and terpolymers will interact differently with the A-B block copolymer when co-nanoprecipitated, due to the

varying nature of the monomer chemistry within the different hydrophobic polymer segments.

The A-B block copolymer selected for initial study was *p*(PEG$_{114}$-*b*-HPMA$_{120}$), due to the stability of the co-nanoprecipitates generated when this was incorporated, as previously discussed in Chapter 2. The DLS results for the co-nanoprecipitation experiments at a 50:50 wt % ratio of branched co- and terpolymers to A-B block copolymer are shown in Table 3.2 and Figure 3.4. This ratio of branched co- and terpolymer to A-B block copolymer was selected as previous studies showed successful formation of stabilised nanoparticles without the potential complication of competitive nanoprecipitation (i.e. the concentration of A-B block copolymer was sufficient to stabilise the nanoparticles without also forming nanoprecipitates comprising predominantly of A-B block copolymer).

Table 3.2 DLS results for the co-nanoprecipitation of varying branched copolymers and *p*(PEG$_{114}$-*b*-HPMA$_{120}$).

Sample (50:50 wt %)	Z-ave (d.nm)	PdI	D_n (nm)
p(HPMA$_{50}$-*co*-EGDMA$_{0.9}$):*p*(PEG$_{114}$-*b*-HPMA$_{120}$)	103	0.051	108
p(*n*-BMA$_{50}$-*co*-EGDMA$_{0.8}$):*p*(PEG$_{114}$-*b*-HPMA$_{120}$)	205	0.088	170
p(*t*-BMA$_{50}$-*co*-EGDMA$_{0.9}$):*p*(PEG$_{114}$-*b*-HPMA$_{120}$)	357	0.234	245
p(HPMA$_{25}$-*co*-*n*-BMA$_{25}$-*co*-EGDMA$_{0.9}$):*p*(PEG$_{114}$-*b*-HPMA$_{120}$)	161	0.085	125
p(HPMA$_{25}$-*co*-*t*-BMA$_{25}$-*co*-EGDMA$_{0.9}$):*p*(PEG$_{114}$-*b*-HPMA$_{120}$)	161	0.066	131

When *p*(*n*-BMA$_{50}$-*co*-EGDMA$_{0.8}$) is nanoprecipitated in the absence of the A-B block copolymer, immediate precipitation is observed; however, when the A-B block copolymer is co-nanoprecipitated, stable nanoparticles form with a very narrow polydispersity. So far, it was believed that the formation of co-nanoprecipitates occurred *via* incorporation of the hydrophobic chain (HPMA$_{120}$) from the A-B block copolymer into the branched polymer core resulting in hydrophilic PEG chains on the surface. The resulting D_z for *p*(*n*-BMA$_{50}$-*co*-EGDMA$_{0.8}$):*p*(PEG$_{114}$-*b*-HPMA$_{120}$) was 205 nm, which was ~70 nm higher than diameters obtained for previous nanoparticles from co-nanoprecipitated branched *p*(HPMA$_{50}$-*co*-EGDMA$_{0.9}$). This suggests that co-nanoprecipitated particles including *p*(*n*-BMA$_{50}$-*co*-EGDMA$_{0.8}$) reach colloidal stability at a larger size, although it is not clear

why this would be the case. For *p*(HPMA$_{25}$-*co*-*n*-BMA$_{25}$-*co*-EGDMA$_{0.9}$) and *p*(HPMA$_{25}$-*co*-*t*-BMA$_{25}$-*co*-EGDMA$_{0.9}$), stable nanoparticles were formed in the presence of the A-B block copolymer with virtually identical particle size distributions obtained. However, the inclusion of an A-B block copolymer with *p*(*t*-BMA$_{50}$-*co*-EGDMA$_{0.9}$) demonstrated different behaviour, as the resulting nanoparticles were much larger, with a broader polydispersity, and started to precipitate out of solution after 24 hours; this suggests a poor compatibility between the branched copolymer and A-B block copolymer. The DLS traces (Figure 3.4) illustrate narrow monomodal peaks for all samples with the exception of *p*(*t*-BMA$_{50}$-*co*-EGDMA$_{0.9}$) which has an obviously broader population of nanoparticles and a tail that suggests an appreciable concentration of larger particles (Figure 3.4C).

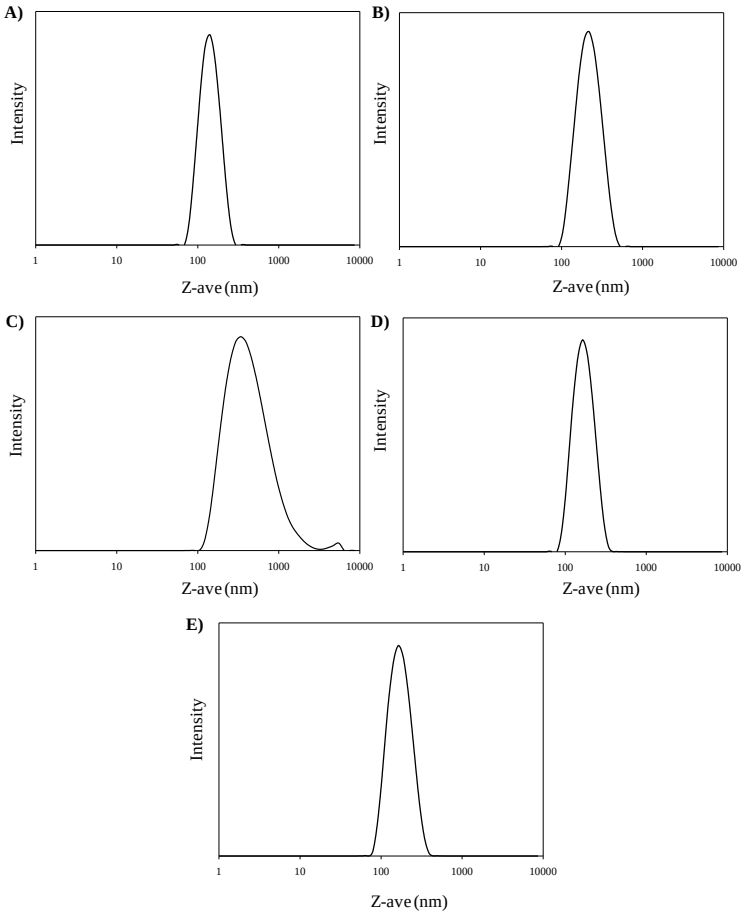

Figure 3.4 DLS analysis of co-nanoprecipitated nanoparticles with varying branched copolymers. A) *p*(HPMA$_{50}$-*co*-EGDMA$_{0.9}$):*p*(PEG$_{114}$-*b*-HPMA$_{120}$), B) *p*(*n*-BMA$_{50}$-*co*-EGDMA$_{0.8}$):*p*(PEG$_{114}$-*b*-HPMA$_{120}$), C) *p*(*t-BMA*$_{50}$-*co*-EGDMA$_{0.9}$):*p*(PEG$_{114}$-*b*-HPMA$_{120}$), D) *p*(HPMA$_{25}$-*co*-*n*-BMA$_{25}$-*co*-EGDMA$_{0.9}$):*p*(PEG$_{114}$-*b*-HPMA$_{120}$), E) *p*(HPMA$_{25}$-*co*-*t-BMA*$_{25}$-*co*-EGDMA$_{0.9}$):*p*(PEG$_{114}$-*b*-HPMA$_{120}$). All 50:50 wt %.

This initial study has highlighted the versatility of the co-nanoprecipitation process. Overall, the co-nanoprecipitation experiments of *p*(PEG$_{114}$-*b*-HPMA$_{120}$) with either *p*(*n*-

BMA$_{50}$-*co*-EGDMA$_{0.8}$), *p*(HPMA$_{25}$-*co*-*n*-BMA$_{25}$-*co*-EGDMA$_{0.9}$) or *p*(HPMA$_{25}$-*co*-*t*-BMA-*co*-EGDMA$_{0.9}$) (50:50 wt %) appears to provide a quick and relatively simple route to stabilising the hydrophobic branched copolymers.

3.4 Synthesis of a *p*(PEG$_{114}$-*n*-BMA$_{120}$) A-B block copolymer and subsequent aqueous nanoparticle studies

It has been established that the chemical composition of the branched co- and terpolymer can be varied and successfully co-nanoprecipitated with *p*(PEG$_{114}$-*b*-HPMA$_{120}$) A-B block copolymer to produce stable nanoparticles; however, the choice of A-B block copolymer stabiliser was purely based on studies in Chapter 2. It was of interest to determine if the co-nanoprecipitation approach was possible with varying A-B block copolymers and whether these materials could also be used to introduce stability into subsequent nanoprecipitates. Utilising the PEG$_{114}$-Br macroinitiator, *p*(PEG$_{114}$-*b*-*n*-BMA$_{120}$) was synthesised and the corresponding GPC data is shown in Table 3.3 and Figure 3.5.

Table 3.3 Table of DMF GPC and ^{1}H NMR molecular weight results.

Targeted Polymer Composition	Target M_n (g/mol)	M_n GPC (g/mol)	M_w GPC (g/mol)	*Đ*	GPC DP_n	Conversion % (^{1}H NMR)	^{1}H NMR DP_n
PEG$_{114}$-Br	~5000	4 300	4 380	1.01	-	-	-
p(PEG$_{114}$-*b*-*n*BMA$_{120}$)	22100	28 000	30 300	1.08	162	97	112

The conditions for the ATRP synthesis of the A-B block copolymer were as previously described for *p*(PEG$_x$-*b*-HPMA$_y$) (Chapter 2, Section 2.5.3); however due to the hydrophobic nature of the monomer, an elevated temperature of 60°C was selected to ensure complete solubilisation in the reaction solvent, MeOH.[2] The GPC chromatogram was monomodal and a narrow dispersity value was obtained. The resulting molecular weights from GPC analysis were slightly higher than expected, which was probably due to the initiator efficiency being less than 100 % for the PEG$_{114}$-Br macroinitiator, as often seen in ATRP reactions.

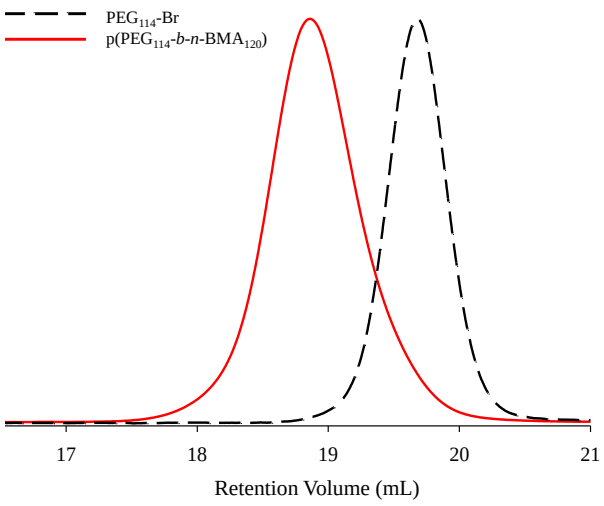

Figure 3.5 GPC refractive index (RI) overlay of PEG_{114}-Br macroinitiator and *p*(PEG_{114}-*b*-*n*-BMA_{120}).

Analysis of *p*(PEG_{114}-*b*-*n*-BMA_{120}) by ^{1}H NMR (See Appendix, Fig. A28) provided a DP_n of 112 monomer units, which was less than obtained from GPC analysis but closer to the value expected. The DP_n calculations by ^{1}H NMR possibly include a small percentage of unreacted initiator as well as those within the copolymer, consequently leading to the calculation of polymer chains that are shorter than the GPC analysis.[11, 12] It is also possible that the reported DP_n for the PEG macroinitiator precursor is not highly accurate and synthesis of the macroinitiator has modified the molecular weight distribution as observed by the lower than expected M_n figure measured for the macroinitiator. The A-B block copolymer was analysed by DMF GPC due to the presence of the high molecular weight PEG segment within the copolymer.

3.4.1 Nanoprecipitation studies during inclusion of *p*(PEG_{114}-*b*-*n*-BMA_{120}) A-B block copolymer

3.4.1.1 Aqueous co-nanoprecipitation studies of *p*(PEG_{114}-*b*-*n*-BMA_{120})

As previously discussed, the co-nanoprecipitation of a branched copolymer and A-B block copolymer which both comprise HPMA monomer residues, generates stable nanoparticles with narrow polydispersity values. Interestingly, when identical nanoprecipitation experiments are conducted with the simple substitution of the HPMA-containing A-B block copolymer for one containing a *p*(*n*-BMA_{120}) block segment, D_z values of ~100nm are still obtained when using the branched copolymer *p*($HPMA_{50}$-co-$EGDMA_{0.9}$), yet a loss of nanoprecipitation control is observed and the polydispersity increases to >0.2, Table 3.4.

As shown previously, the co-nanoprecipitation of *p*(*n*-BMA$_{50}$-*co*-EGDMA$_{0.8}$):*p*(PEG$_{114}$-*b*-HPMA$_{120}$) (50:50 wt %), gave nanoparticles of a larger size (~200 nm) and a narrow polydispersity. However, if both the branched copolymer and A-B block copolymer are composed of *n*-BMA, the size remains ~100 nm and an increase in polydispersity is observed. The DLS traces are shown in Figure 3.6 and although the nanoparticle results for *p*(*n*-BMA$_{50}$-*co*-EGDMA$_{0.8}$):*p*(PEG$_{114}$-*b*-*n*-BMA$_{120}$) (50:50 wt %) show a monodisperse sample, the polymers started to precipitate after 24 hours. In these limited experiments, when the A-B block copolymer comprises a *p*(HPMA) block segment within the co-nanoprecipitation, a narrow dispersity is obtained which increases upon switching to an A-B block copolymer containing *p*(*n*-BMA) block segments. This gave an insight to the possible limitations of the co-nanoprecipitation process, despite variation of the A-B block copolymer allowing nanoprecipitates to be formed. This suggests that an overall increase in hydrophobicity does have an effect on the mechanism of polymer interaction during the co-nanoprecipitation process, but stable nanoparticles are still possible.

Table 3.4 DLS results for the nanoprecipitation or co-nanoprecipitation varying both the branched copolymer and A-B block copolymer.

Sample Name	Ratio (wt%)	Z-ave (d.nm)	PdI
p(HPMA$_{50}$-*co*-EGDMA$_{0.9}$)	100:0	148	0.080
p(*n*-BMA$_{50}$-*co*-EGDMA$_{0.8}$)	100:0	*	*
p(PEG$_{114}$-*b*-*n*-BMA$_{120}$)[a]	100:0	84	0.662
p(HPMA$_{50}$-*co*-EGDMA$_{0.9}$):*p*(PEG$_{114}$-*b*-HPMA$_{120}$)	50:50	108	0.109
p(HPMA$_{50}$-*co*-EGDMA$_{0.9}$):*p*(PEG$_{114}$-*b*-*n*-BMA$_{120}$)	50:50	109	0.232
p(*n*-BMA$_{50}$-*co*-EGDMA$_{0.8}$):*p*(PEG$_{114}$-*b*-HPMA$_{120}$)	50:50	205	0.088
p(*n*-BMA$_{50}$-*co*-EGDMA$_{0.8}$):*p*(PEG$_{114}$-b-*n*-BMA$_{120}$)	50:50	110	0.199

•* Instant precipitation upon addition to water.
•[a] Inadequate scattering data.

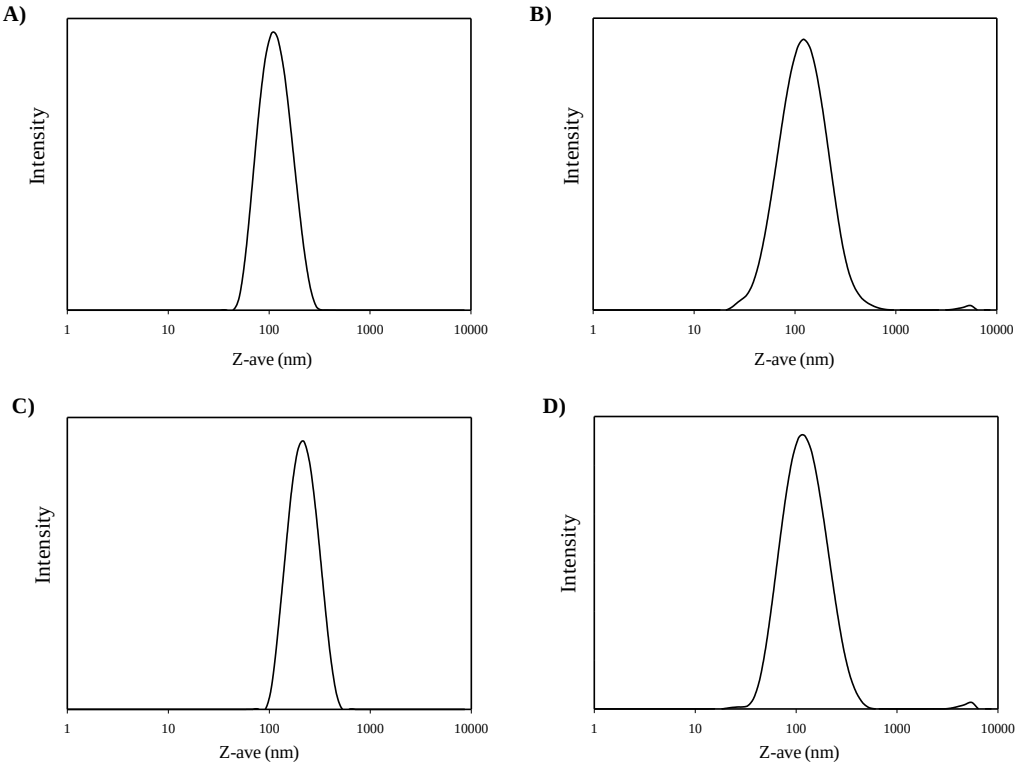

Figure 3.6 DLS results for A) *p*(HPMA$_{50}$-*co*-EGDMA$_{0.9}$):*p*(PEG$_{114}$-*b*-HPMA$_{120}$), B) *p*(HPMA$_{50}$-*co*-EGDMA$_{0.9}$):*p*(PEG$_{114}$-*b*-*n*-BMA$_{120}$), C) *p*(*n*-BMA$_{50}$-*co*-EGDMA$_{0.8}$):*p*(PEG$_{114}$-*b*-HPMA$_{120}$), D) *p*(*n*-BMA$_{50}$-*co*-EGDMA$_{0.8}$):*p*(PEG$_{114}$-*b*-*n*-BMA$_{120}$).

3.5 Probing the internal nanoparticle environment and co-nanoprecipitation mechanism using fluorescent guest molecules

As discussed in Chapter 2, Section 2.10, the guest molecule pyrene can be encapsulated within polymer co-nanoprecipitate particles; this is particularly useful, as its fluorescence emission spectrum is highly sensitive to the polarity of the surrounding environment. Comparison of the fluorescence of pyrene within co-nanoprecipitates of varying composition was hypothesised to provide a more clear indication of the role of the A-B block copolymer stabiliser within this process and the environment within the nanoprecipitates. To compare the I_1/I_3 values of co-nanoprecipitates derived from *p*(HPMA$_{50}$-*co*-EGDMA$_{0.9}$) and *p*(*n*-BMA$_{50}$-*co*-EGDMA$_{0.8}$), pyrene was encapsulated within the *p*(*n*-BMA$_{50}$-*co*-EGDMA$_{0.8}$):*p*(PEG$_{114}$-*b*-*n*-BMA$_{120}$) (50:50 wt %) co-nanoprecipitates. The nanoparticles were prepared as previously described in Chapter 2, Section 2.10 and the DLS traces of the nanoparticles before and after pyrene addition are shown in Figure 3.7.

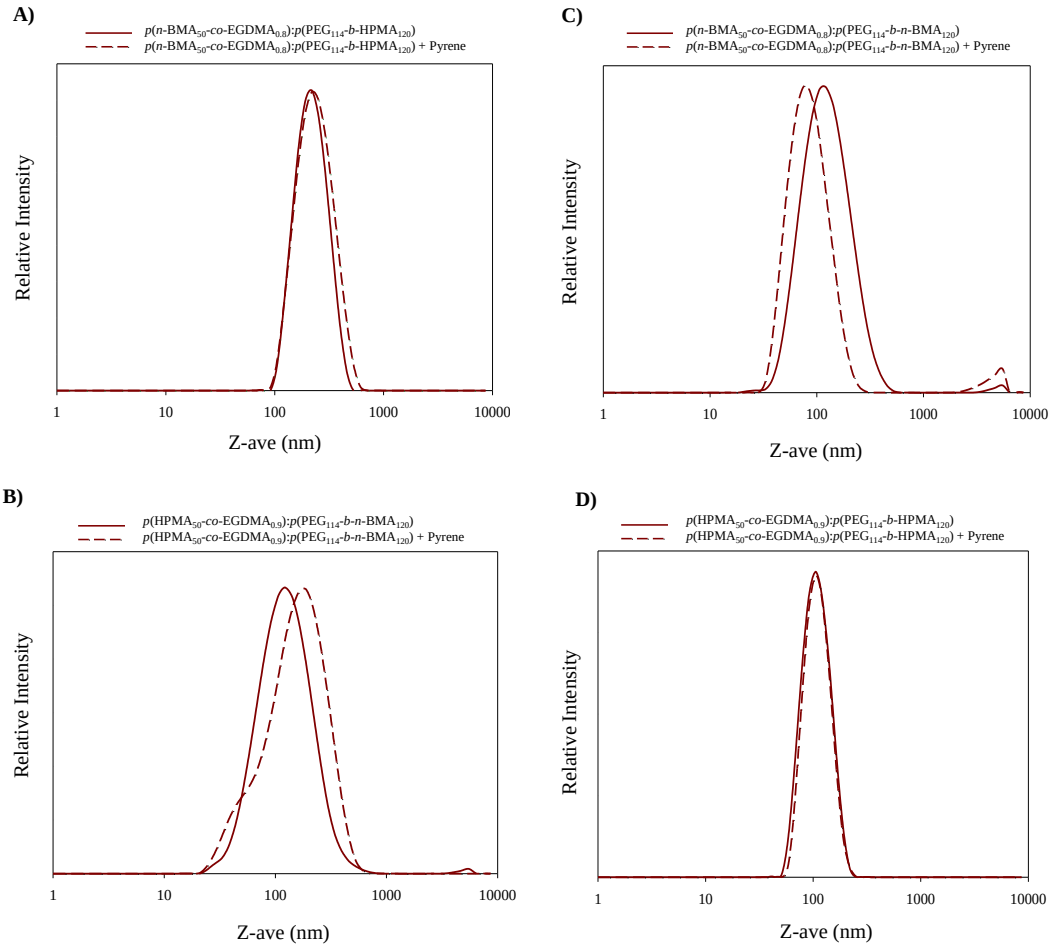

Figure 3.7 DLS size overlays for blank *vs* pyrene encapsulated nanoparticles. A) *p*(*n*-BMA$_{50}$-*co*-EGDMA$_{0.8}$):*p*(PEG$_{114}$-*b*-HPMA$_{120}$), B) *p*(HPMA$_{50}$-*co*-EGDMA$_{0.9}$):*p*(PEG$_{114}$-*b*-*n*-BMA$_{120}$), C) *p*(*n*-BMA$_{50}$-*co*-EGDMA$_{0.8}$):*p*(PEG$_{114}$-*b*-*n*-BMA$_{120}$) and D) *p*(HPMA$_{50}$-*co*-EGDMA$_{0.9}$):*p*(PEG$_{114}$-*b*-*n*-BMA$_{120}$) and *p*(HPMA$_{50}$-*co*-EGDMA$_{0.9}$):*p*(PEG$_{114}$-*b*-HPMA$_{120}$).

Generally, the co-nanoprecipitates which include polymers comprising *n*-BMA, only exhibit small deviations in size for blank *vs* pyrene encapsulated nanoparticles. The nanoparticle sizes are shown in Table 3.5 and the PdI values do tend to increase during the inclusion of pyrene when either the branched copolymer or A-B block copolymer consisting of *n*-BMA is present. After nanoparticle preparation and analysis. The fluorescence emission spectra for polymeric nanoparticles with encapsulation of 0.1 wt % pyrene for *p*(*n*-BMA$_{50}$-*co*-EGDMA$_{0.8}$):*p*(PEG$_{114}$-*b*-HPMA$_{120}$), *p*(*n*-BMA$_{50}$-*co*-EGDMA$_{0.8}$):*p*(PEG$_{114}$-*b*-*n*-BMA$_{120}$) and *p*(HPMA$_{50}$-*co*-EGDMA$_{0.9}$):*p*(PEG$_{114}$-*b*-*n*-BMA$_{120}$) were measured and are shown in the Appendix, Fig. A29.

Table 3.5 DLS results for blank vs pyrene encapsulated nanoparticles and I_1/I_3 values obtained from the fluorimetry experiments.

Sample (50:50 wt %)	Blank		Pyrene Encapsulated		I_1/I_3
	Z-ave (d.nm)	PdI	Z-ave (d.nm)	PdI	
p(*n*-BMA$_{50}$-*co*-EGDMA$_{0.8}$):*p*(PEG$_{114}$-*b*-HPMA$_{120}$)	205	0.088	217	0.132	1.27
p(*n*-BMA$_{50}$-*co*-EGDMA$_{0.8}$):*p*(PEG$_{114}$-*b*-*n*-BMA$_{120}$)	110	0.199	82	0.213	1.28
p(HPMA$_{50}$-*co*-EGDMA$_{0.9}$):*p*(PEG$_{114}$-*b*-*n*-BMA$_{120}$)	109	0.232	124	0.271	1.29
p(HPMA$_{50}$-*co*-EGDMA$_{0.9}$):*p*(PEG$_{114}$-*b*-HPMA$_{120}$)	103	0.068	106	0.051	1.60

In comparison with nanoparticles composed of *p*(HPMA$_{50}$-*co*-EGDMA$_{0.9}$):*p*(PEG$_{114}$-*b*-HPMA$_{120}$) 100:0-50:50 wt %, the co-nanoprecipitations including the branched copolymer *p*(*n*-BMA$_{50}$-*co*-EGDMA$_{0.8}$) and the A-B block copolymers *p*(PEG$_{114}$-*b*-HPMA$_{120}$) and *p*(PEG$_{114}$-*b*-*n*-BMA$_{120}$), resulted in an appreciable decrease in I_1/I_3 values from ~1.6 to 1.28, suggesting a decrease in polarity of the nanoparticle core (Figure 3.8). If the *p*(*n*-BMA) block from the A-B block copolymer was present at the nanoparticle surface it would be expected that for *p*(HPMA$_{50}$-*co*-EGDMA$_{0.9}$):*p*(PEG$_{114}$-*b*-*n*-BMA$_{120}$), the I_1/I_3 value would remain ~1.6, however this is not the case. The decrease in I_1/I_3 values to <1.29 further implied that the *p*(*n*-BMA) segment from the A-B block copolymer was present within the nanoparticle core, as hypothesised previously, Section 3.3.2.

The versatility of the co-nanoprecipitation process has been explored and stable nanoparticles were formed when both the branched polymer and A-B block copolymer stabiliser were modified. The loading capabilities were yet to be further explored so far were considered for pharmacology studies, therefore, a selection of materials were taken forward and their suitability was assessed.

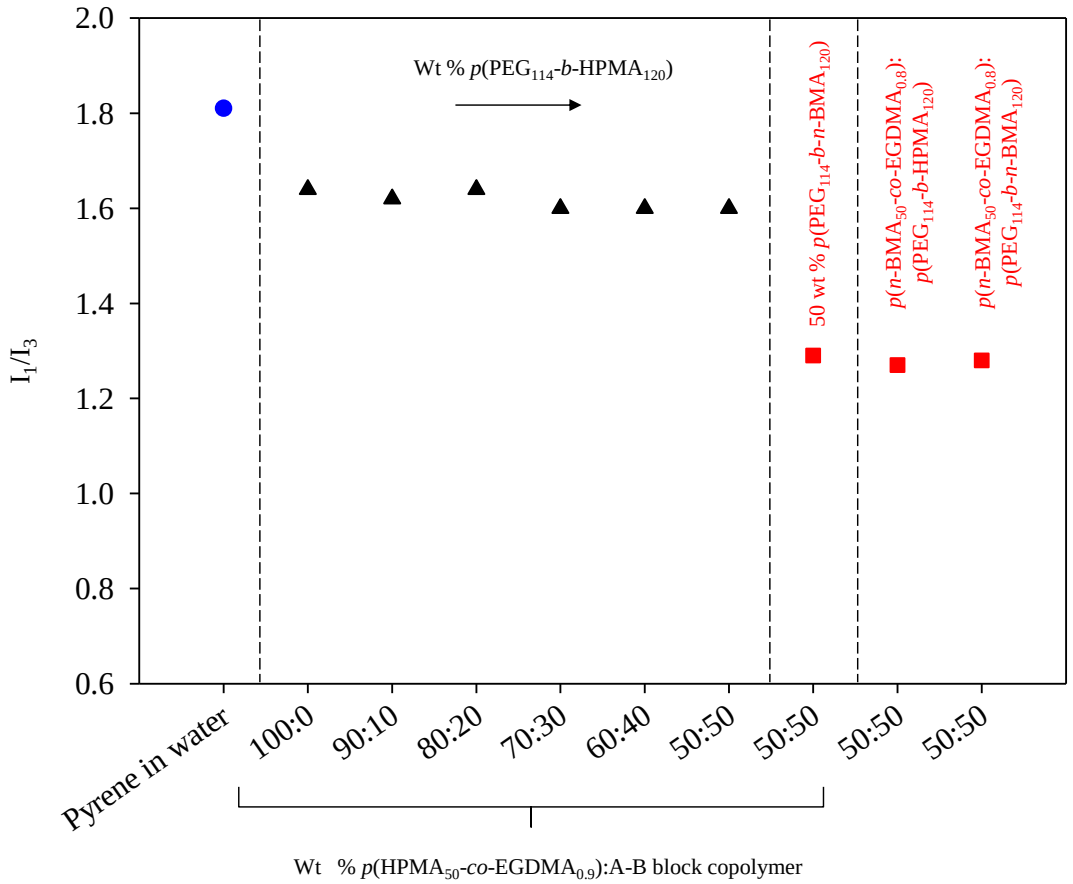

Figure 3.8 Fluorimetry results for co-nanoprecipitation experiments. I_1/I_3 ratios for, blue circle = pyrene in water, black triangle from left to right = *p*(HPMA$_{50}$-*co*-EGDMA$_{0.9}$), *p*(HPMA$_{50}$-*co*-EGDMA$_{0.9}$):*p*(PEG$_{114}$-*b*-HPMA$_{120}$) 90:10 wt %, 80:20 wt %, 70:30 wt %, 60:40 wt %, 50:50 wt %, red square from left to right = *p*(HPMA$_{50}$-*co*-EGDMA$_{0.9}$):*p*(PEG$_{114}$-*b*-*n*-BMA$_{120}$) 50:50 wt %, *p*(*n*-BMA$_{50}$-*co*-EGDMA$_{0.8}$):*p*(PEG$_{114}$-*b*-HPMA$_{120}$) 50:50 wt % and *p*(*n*-BMA$_{50}$-*co*-EGDMA$_{0.8}$):*p*(PEG$_{114}$-*b*-*n*-BMA$_{120}$) 50:50 wt %.

3.6 Pharmacological studies of co-nanoprecipitated nanoparticles

During the design of new polymeric drug carriers, the main route of administration usually targeted is intravenous (IV). For treatment of infectious diseases such as HIV, where patients require a lifetime of treatment it would not be desirable for frequent dosing *via* IV administration and oral dosing is much more appropriate. An injectable antiretroviral formulation has been developed which decreases the dosing from monthly to quarterly administration,[13] however, this is an intramuscular or subcutaneous depot injection and until these formulations can be administered worldwide it is still preferable to administer drugs orally as the administration process is fast, easy and patient adherence is improved. A nanocarrier approach that focuses on HIV, therefore, requires oral delivery of polymeric nanocarriers to generate circulating nanoparticles *via* permeation through the gut

epithelium into the systemic circulation. This has several advantages, including drug accumulation through uptake into macrophages which act as a sanctuary site for HIV, through the poor accumulation of current anti-retroviral drugs in these cells.

To assess whether the co-nanoprecipitated particles could be loaded with a model drug molecule and act as a drug delivery vehicle, a range of pharmacological experiments were performed, mimicking oral dosing. All pharmacological experiments were carried out by researchers in the Molecular and Clinical Pharmacology Department at the University of Liverpool, through collaboration between the Owen and Rannard research groups and will be described in detail in Section 3.6.2.

3.6.1 Preparation of fluoresceinamine encapsulated nanoparticles

Following the success of co-nanoprecipitation studies within this research chapter and those performed in Chapter 2, a selection of the nanoparticles were progressed forward to evaluate their loading capabilities and further suitability for pharmacological studies. The dye molecule fluoresceinamine (FA) (Figure 3.9) was selected as a 'mimic' drug molecule due to its small size and hydrophobic nature which is ideal for encapsulation into various hydrophobic cores.

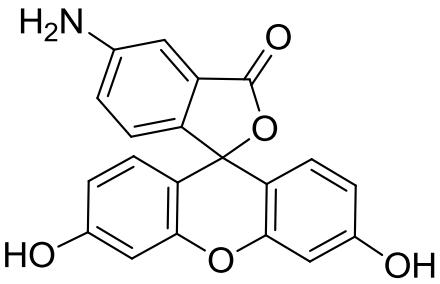

Figure 3.9 Chemical structure for FA (Isomer I).

Nanoprecipitation offers a quick and versatile approach to predict and observe nanoparticle encapsulation interactions before undertaking further more complicated encapsulation studies; loading was achieved by the facile dissolution of polymer and FA (model drug) together in a solvent. A schematic representation of the co-nanoprecipitation process used to encapsulate FA is shown in Figure 3.10 and as highlighted, the FA is dissolved within the good solvent with a branched copolymer and A-B block copolymer, before addition to water. To assess the amount of FA which could be encapsulated into the nanoparticles, a series of loading experiments were carried out at various weight percentages (wt %), with respect to the mass of polymers used. Nanoparticles were

prepared at various weight ratios of branched copolymer:A-B block copolymer and increasing amounts of FA were added (up to 17 wt %, see Appendix, Table A9). Above this amount, the mixtures were observed to instantly precipitate upon addition into water. After a review of previous research and evaluation of future pharmacological experiments, the amount of FA encapsulated within the nanoparticles was 10 wt %. This amount was well above the concentration required for pharmacological assays (10 µM FA) and <17 wt % FA is ideal, in order to avoid any stability issues during future experiments. A comparison of blank (unloaded) *vs.* encapsulated (loaded) nanoparticle diameters are shown in Figure 3.11 and the loaded nanoparticles show only slight deviations in size from the blank nanoparticles.

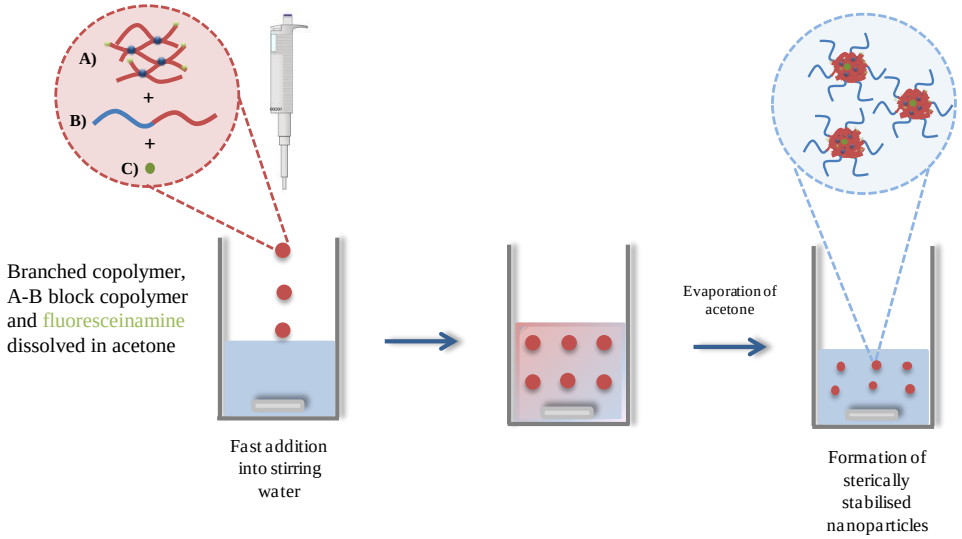

Figure 3.10 Schematic representation of aqueous nanoparticle formation with addition of the hydrophobic dye molecule FA (10 wt %) *via* the co-nanoprecipitation approach, A) branched co/terpolymers, B) amphiphilic A-B block copolymer, C) FA.

Previous nanoprecipitation studies within the Rannard group, which investigated *hyp*-polydendron materials and encapsulation of FA, were limited to 1 wt % loading and precipitation was observed for encapsulation amounts of >1 wt %. However, the co-nanoprecipitation system appears to offer an increased (>10 times) encapsulation capacity when compared with the FA encapsulated *hyp*-polydendron nanoparticles and again, the increased loading further suggests that the PEG moiety is located on the outer surface of the nanoparticles as opposed to becoming entrapped within, potentially generating a more hydrophilic environment.

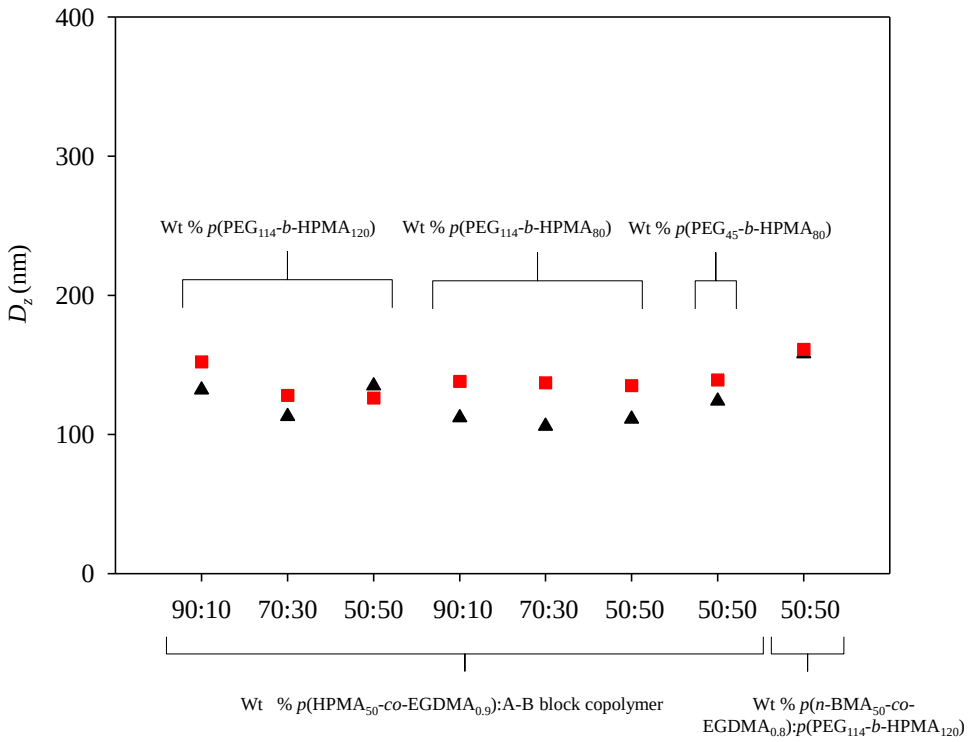

Figure 3.11 Nanoparticle sizes of blank (Black triangles) and after addition of 10 wt % FA (Red squares).

Due to the limited amount of samples which could be assessed in pharmacology, only eight of the branched copolymer:A-B block copolymer nanodispersions were encapsulated with FA for the study. The DLS analysis of FA encapsulated nanoparticles is presented in Table 3.6 and, as noted previously, there are only minor differences between blank and FA encapsulated samples and all PdI values obtained were <0.124. In comparison to the blank (no FA) nanoparticles, the overall ζ values obtained were closer to neutral for the FA encapsulated nanoparticles which may be due to presence of the FA primary amine.

The FA encapsulated nanoparticles were also analysed by SEM, see Figure 3.12 A-H. A similar morphology was observed between the blank and loaded nanoparticle dispersions (See Chapter 2, Figure 2.19 & 2.20). Generally, the FA loaded nanoparticles appear as individual spherical particles, with no crystallised FA observable, indicating that the FA is encapsulated within the polymeric nanoparticles. Although there was clear evidence of nanoparticle formation, SEM imaging of some samples was not simple to achieve and a different morphology was observed, which may be due to PEG film formation or drying out of the particles during sample preparation (Figure 3.12 C&F).

Table 3.6 DLS analysis for blank and FA encapsulated nanoparticles (10 wt %).

Entry	***p*(HPMA$_{50}$-*co*-EGDMA$_{0.9}$) or *p*(nBMA$_{50}$-*co*-EGDMA$_{0.8}$):*p*(PEG*x*-*b*-HPMA*y*)**	**Ratio**	**Blank**				**FA encapsulated nanoparticles (10 wt %)**			
		(wt %)	**Size (d.nm)**	**PdI**	**D_n (nm)**	**ζ (mV)**	**Size (d.nm)**	**PdI**	**D_n (nm)**	**ζ (mV)**
1		90:10	132	0.059	104	-13	152	0.029	129	-18
2	*p*(HPMA$_{50}$-*co*-EGDMA$_{0.9}$):*p*(PEG$_{114}$-*b*-HPMA$_{120}$)	70:30	113	0.069	88	-23	128	0.080	93	-15
3		50:50	135	0.051	108	-15	126	0.079	101	-13
4		90:10	112	0.045	90	-27	138	0.038	117	-13
5	*p*(HPMA$_{50}$-*co*-EGDMA$_{0.9}$):*p*(PEG$_{114}$-*b*-HPMA$_{80}$)	70:30	106	0.124	74	-29	137	0.084	107	-12
6		50:50	111	0.081	84	-21	135	0.039	112	-9
7	*p*(nBMA$_{50}$-*co*-EGDMA$_{0.8}$):*p*(PEG$_{114}$-*b*-HPMA$_{120}$)	50:50	158	0.086	122	-24	161	0.092	122	-13
8	*p*(HPMA$_{50}$-*co*-EGDMA$_{0.9}$):*p*(PEG$_{45}$-*b*-HPMA$_{80}$)	50:50	124	0.055	99	-27	139	0.011	119	-13

Fresh samples of co-nanoprecipitated particles were prepared (formulated from i_5-f_1, see Section 3.3.1) for pharmacological assessment and their stability was determined by addition of both 0.5M NaCl and transport buffer solution (TBS) to mimic physiologically relevant conditions; stability in delivery media is crucial, particularly when future pharmacological studies are carried out. The *in vitro* studies are typically performed in TBS which is, less complex than complete media (Dulbeccos modified eagle medium +15% fetal bovine serum), which means the samples are cleaner when HPLC analysis is carried out, but it still contains all the components that cells need to survive. It is adjusted to physiological pH, and is not meant to model blood, but is more simply a means of delivering the formulations to the cells. The repeat formation of blank nanoparticles showed slight, but not significant, variation of D_z and PdI, see Chapter 2, Section 2.6.3.

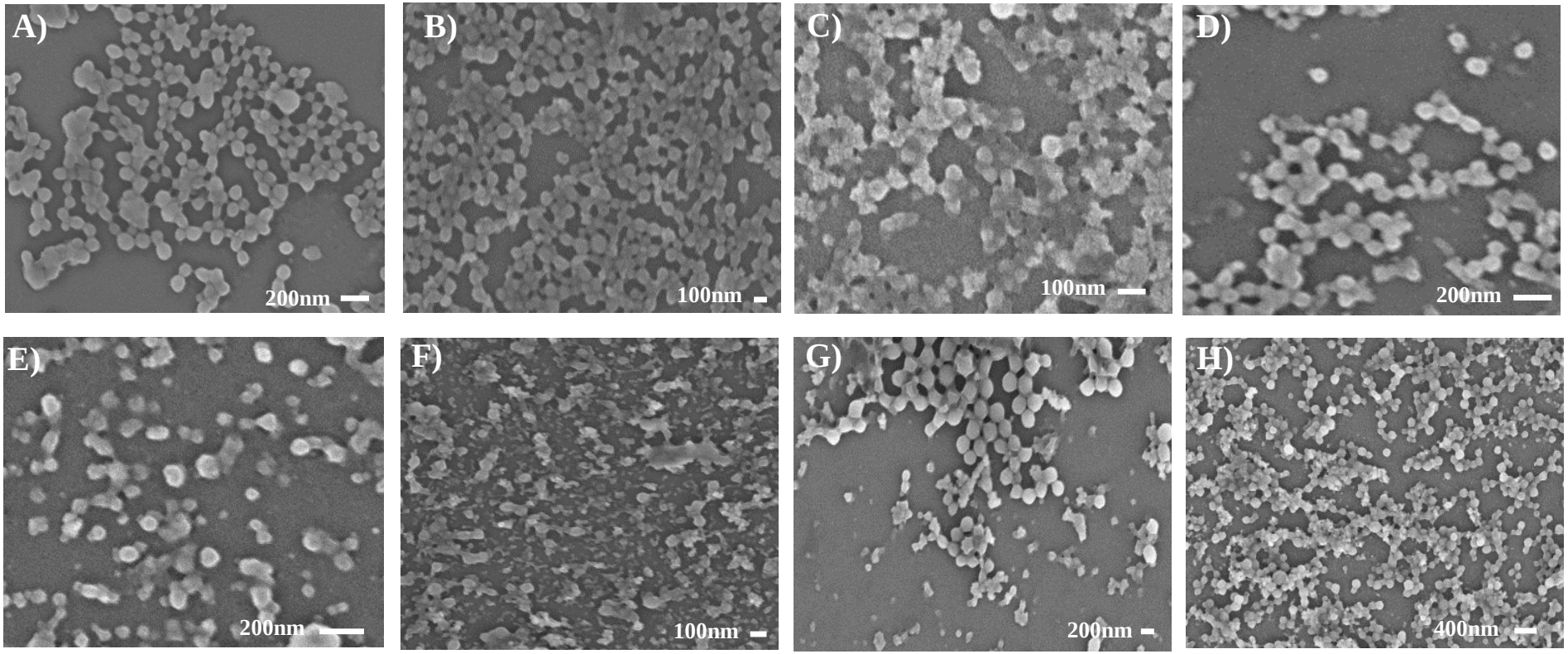

Figure 3.12 SEM imaging of FA encapsulated nanoparticles (10 wt %) *via* co-nanoprecipitation A) *p*(HPMA$_{50}$-*co*-EGDMA$_{0.9}$):*p*(PEG$_{114}$-*b*-HPMA$_{120}$) 90:10 B) 70:30 C) 50:50 D) *p*(HPMA$_{50}$-*co*-EGDMA$_{0.9}$):*p*(PEG$_{114}$-*b*-HPMA$_{80}$) 90:10 E) 70:30 F) 50:50 G) *p*(*n*-BMA$_{50}$-*co*-EGDMA$_{0.8}$):*p*(PEG$_{114}$-*b*-HPMA$_{120}$) 50:50 H) *p*(HPMA$_{50}$-*co*-EGDMA$_{0.9}$):*p*(PEG$_{45}$-*b*-HPMA$_{80}$) 50:50 wt %.

To assess their stability, each FA encapsulated nanodispersion was diluted with both 0.5 M NaCl (final conc 0.01M) (Table 3.7) and TBS (Table 3.8) to mimic physiologically relevant conditions. The NaCl and TBS stability results were promising, as all nanoparticles demonstrated sustained stability over an extended period of 21 days. These stability results highlight how the nanoparticles produced during the co-nanoprecipitation studies are robust to both NaCl and TBS solutions, which is one of the initial steps before *in vitro* studies of nanomaterials. Generally, during the 21 day period, a negligible change in nanoparticle size was observed and PdI values remained <0.1 during NaCl addition. TBS is much more complex than NaCl due to the presence of proteins and buffered saline solution, so this may explain the slight increase in size and PdI. Although stable, the largest increase of 63nm was observed for *p*(HPMA$_{50}$-*co*-EGDMA$_{0.9}$)*:p*(PEG$_{45}$-*b*-HPMA$_{80}$) (50:50 wt %), whilst comparing the blank *vs* 21 day measurement during TBS addition. Interestingly, for *p*(HPMA$_{50}$-*co*-EGDMA$_{0.9}$)*:p*(PEG$_{114}$-*b*-HPMA$_{x}$) and *p*(*n*-BMA$_{50}$-*co*-EGDMA$_{0.8}$)*:p*(PEG$_{114}$-*b*-HPMA$_{x}$) (50:50 wt %), only slight deviations in size were observed in the presence of TBS and the only difference between this dispersion is the length of the PEG$_{114}$ chain present on the A-B block copolymer, which appears to provide additional stabilisation. A photograph to highlight the stability of FA encapsulated nanoparticles is shown in Figure 3.13, and due to the instability of *p*(*n*-BMA$_{50}$-*co*-EGDMA$_{0.8}$) when nanoprecipitated only, *p*(HPMA$_{50}$-*co*-EGDMA$_{0.9}$) was used as the comparison. Charge stabilised nanoparticles that are formed from *p*(HPMA$_{50}$-*co*-EGDMA$_{0.9}$), precipitate immediately upon addition of both TBS and NaCl (Figure 3.13Aii & iii); however, as confirmed by DLS, the addition of the A-B block copolymer *p*(PEG$_{114}$-*b*-HPMA$_{120}$) provides sufficient stabilisation and no precipitation was observed after both addition of TBS and NaCl solution for the *p*(*n*-BMA$_{50}$-*co*-EGDMA$_{0.8}$):*p*(PEG$_{114}$-*b*-HPMA$_{120}$) (50:50 wt %) co-nanoprecipitated nanoparticles (Figure 3.13 i, ii & iii).

Table 3.7 Stability studies of FA loaded nanoparticles (dilution of nanoparticle dispersion to 0.98 mg/mL) in 0.5M NaCl.

Entry	***p*(HPMA$_{50}$-*co*-EGDMA$_{0.9}$) or *p*(*n*-BMA$_{50}$-co-EGDMA$_{0.8}$):*p*(PEG$_x$-*b*-HPMA$_y$)**	**Ratio (wt%)**	**Blank**		**Instant**		**1 day**		**7 day**		**21 day**	
			Size (d. nm)	**PdI**	**Size (d. nm)**	**PdI**	**Size (d. nm)**	**PdI**	**Size (d. nm)**	**PdI**	**Size (d. nm)**	**PdI**
1	*p*(HPMA$_{50}$-*co*-EGDMA$_{0.9}$):*p*(PEG$_{114}$-*b*-HPMA$_{120}$)	90:10	152	0.029	137	0.060	135	0.033	137	0.043	136	0.025
2		70:30	126	0.079	133	0.047	132	0.045	133	0.029	131	0.032
3		50:50	128	0.080	164	0.022	165	0.063	161	0.039	163	0.098
4	*p*(HPMA$_{50}$-*co*-EGDMA$_{0.9}$):*p*(PEG$_{114}$-*b*-HPMA$_{80}$)	90:10	138	0.038	132	0.043	146	0.027	147	0.049	138	0.051
5		70:30	135	0.039	145	0.100	141	0.089	141	0.086	131	0.114
6		50:50	137	0.038	160	0.016	159	0.027	159	0.010	146	0.030
7	*p*(*n*-BMA$_{50}$-*co*-EGDMA$_{0.8}$):*p*(PEG$_{114}$-*b*-HPMA$_{120}$)	50:50	139	0.123	140	0.153	137	0.099	134	0.091	142	0.086
8	*p*(HPMA$_{50}$-*co*-EGDMA$_{0.9}$):*p*(PEG$_{45}$-*b*-HPMA$_{80}$)	50:50	139	0.011	159	0.019	158	0.041	157	0.034	143	0.051

Table 3.8 Stability studies of FA loaded nanoparticles (dilution of nanoparticle dispersions to 0.5 mg/mL) in TBS.

Entry	***p*(HPMA$_{50}$-*co*-EGDMA$_{0.9}$) or *p*(*n*-BMA$_{50}$-co-EGDMA$_{0.8}$):*p*(PEG$_x$-*b*-HPMA$_y$)**	Ratio (wt%)	Blank		Instant		1 day		7 day		21 day	
			Size (d.nm)	PdI	Size (d.nm)	PdI	Size (d.nm)	PdI	Size (d.nm)	PdI	Size (d.nm)	PdI
1	*p*(HPMA$_{50}$-*co*-EGDMA$_{0.9}$):*p*(PEG$_{114}$-*b*-HPMA$_{120}$)	90:10	152	0.029	137	0.060	136	0.052	136	0.027	140	0.095
2		70:30	126	0.079	133	0.047	132	0.066	136	0.063	136	0.103
3		50:50	128	0.080	123	0.045	128	0.131	120	0.090	119	0.103
4	*p*(HPMA$_{50}$-*co*-EGDMA$_{0.9}$):*p*(PEG$_{114}$-*b*-HPMA$_{80}$)	90:10	138	0.038	155	0.075	151	0.043	155	0.070	147	0.053
5		70:30	135	0.039	149	0.116	145	0.109	150	0.166	144	0.181
6		50:50	137	0.038	156	0.060	153	0.030	141	0.099	143	0.132
7	*p*(*n*-BMA$_{50}$-*co*-EGDMA$_{0.8}$):*p*(PEG$_{114}$-*b*-HPMA$_{120}$)	50:50	139	0.123	144	0.131	123	0.057	147	0.154	148	0.130
8	*p*(HPMA$_{50}$-*co*-EGDMA$_{0.9}$):*p*(PEG$_{45}$-*b*-HPMA$_{80}$)	50:50	139	0.011	135	0.035	158	0.060	179	0.106	202	0.156

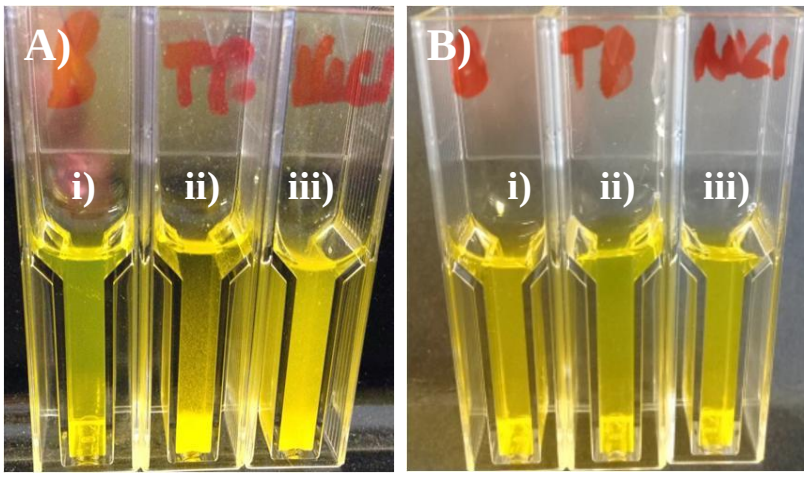

Figure 3.13 A) Photograph of 10 wt % FA nanoparticles *p*(HPMA$_{50}$-*co*-EGDMA$_{0.9}$)* i) blank nanoparticle dispersion, ii) TBS addition, iii) NaCl addition, B) *p*(*n*-BMA$_{50}$-*co*-EGDMA$_{0.8}$):*p*(PEG$_{114}$-*b*-HPMA$_{120}$) 50:50 wt %, i) blank nanoparticle dispersion, ii) TBS addition, iii) NaCl addition. (1 mL to 1 mL of the nanodispersion) and NaCl addition (20 µL 0.5M to 1 mL of the nanodispersion) (**p*(*n*-BMA$_{50}$-*co*-EGDMA$_{0.8}$) does not form stable nanoparticles, therefore, *p*(HPMA$_{50}$-*co*-EGDMA$_{0.9}$)was used here as a comparison).

3.6.2 *In vitro* pharmacological studies

The FA encapsulated nanoparticles (Entries 1-8, Table 3.6) were subject to *in vitro* pharmacological testing following the stability observed in biologically-relevant conditions, as well as the encouraging high loading capabilities. To ensure the nanomaterials were non-toxic to intestinal epithelial cells and could act as drug carrier options, ^{14}C-mannitol permeability and standard cytotoxicity assays were performed. A transwell plate Caco-2 assay was selected to evaluate the permeability of materials across a model intestinal epithelium and mimic permeation into the systemic circulation. Cellular permeability is a characteristic of nanocarriers which is now being considered much earlier in the drug discovery process; hence it is relevant to conduct such Caco-2 transwell assays. It was also important to consider the cellular accumulation of the nanomaterials to ensure drug molecules could accumulate in various types of cells; this will be investigated for both Caco-2 and ATHP-1 cells, which will be discussed in more detail below.

3.6.3 ^{14}C-mannitol permeability and cytotoxicity assays

The transcellular permeability studies of the nanomaterials were carried out using the well characterised, high-throughput Caco-2 cell monolayer assay. The Caco-2 cell line is a continuous line of heterogeneous human epithelial colorectal adenocarcinoma cells. Although derived from the colon, when they are cultured under various conditions they

differentiate to form a confluent epithelial cell monolayer resembling enterocytes, which line the small intestine.[14] These cells express microvilli, tight junctions, enzymes and transporters, which are all characteristic of enterocytes. The tight junctions between cells prevent movement of material along cell boundaries, encouraging drug molecules to passively permeate through the cell or be actively transported. The transport of drug molecules *via* paracellular (between cells) permeation, has been shown for several nanoparticle systems[15] and cellular accumulation studies can be used to distinguish various mechanisms.

To assess which materials could be taken forward to more complex studies, the transcellular permeability was first ascertained. During the preliminary experiment, 10 μM of FA loaded into co-nanoprecipitated materials or 10 μM aqueous FA (spiked with DMSO) were added to the apical or basolateral chamber of the wells, to quantify transport in both Apical>Basolateral (A>B) and Basolateral>Apical (B>A) directions, and the plates were sampled 4 hours after incubation.

The integrity of the Caco-2 monolayer after exposure of the FA loaded nanoparticles is also an important consideration, therefore, 250 μL of TBS containing 2 μL/mL ^{14}C-mannitol was added to the apical compartment and incubated for 1 hour. Scintillation fluid (4 mL) was added to the apical side (100 μL) and ^{14}C-mannitol concentrations were quantified using a scintillation counter. The Caco-2 monolayer was considered compromised if the apparent permeability observed for the ^{14}C-mannitol was >0.953 x 10^{-6} cm s^{-1}.[16] Therefore, *p*(HPMA$_{50}$-*co*-EGDMA$_{0.9}$):*p*(PEG$_{114}$-*b*-HPMA$_{80}$) 90:10, 70:30, 50:50 wt % and *p*(HPMA$_{50}$-*co*-EGDMA$_{0.9}$):*p*(PEG$_{45}$-*b*-HPMA$_{80}$) 50:50 wt % were removed from further pharmacological studies, as they all appeared to compromise the integrity of the Caco-2 cell monolayer (Figure 3.14). The major difference between these materials is the composition of the A-B block copolymer. Interestingly, if either the PEG chain length is below 2000 g/mol or the DP_n of the HPMA chain is <120, the materials appear to compromise the cell monolayer and, until further investigation, it is not clear why. One hypothesis is that a significant, but low, concentration of free A-B block copolymer is present and this is able to disrupt the monolayer. Therefore, the four materials taken forward for cytotoxicity assessment were *p*(HPMA$_{50}$-*co*-EGDMA$_{0.9}$):*p*(PEG$_{114}$-*b*-HPMA$_{120}$) 90:10, 70:30 and 50:50 wt % and *p*(*n*-BMA$_{50}$-*co*-EGDMA$_{0.8}$):*p*(PEG$_{45}$-*b*-HPMA$_{120}$) 50:50 wt %.

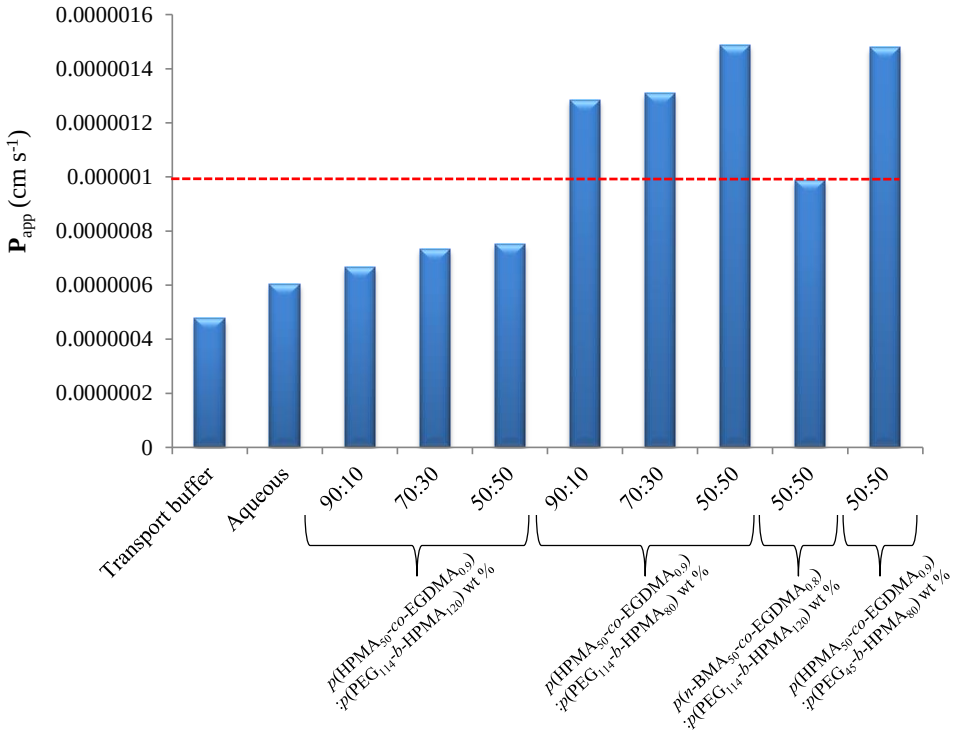

Figure 3.14 The apparent permeability (P_{app}) of ^{14}C-mannitol through a Caco-2 cell monolayer during exposure to FA encapsulated nanoparticles.

3.6.3.1 Cytotoxicity Assays

During the development of new nanomaterials, it is important to determine their cytotoxicity to various cells, particularly Caco-2 cells which are used during the epithelial transwell plate experiment. The two cytotoxicity assays which were conducted for the FA encapsulated materials were the 3-[4,5-dimethylthiazol-2-yl]-2,5 diphenyl tetrazolium bromide (MTT) assay and the adenosine triphosphate (ATP) assay with an incubation period of 5 days across a range of concentrations of FA (0.1 – 15 µM).

3.6.3.2 MTT assay

The MTT assay is a colorimetric assay based on the conversion of MTT (a yellow tetrazole) into formazan (purple crystals) by living cells which determines mitochondrial activity and, therefore, can be used to assess a drug or material's cytotoxic effects.[17] When cells die, they lose the ability to convert MTT to formazan, thus, the colour change is a useful indication of only viable cells. A solubilisation solution, usually DMSO, an acidified ethanol solution, or a solution of the surfactant sodium dodecyl sulfate in diluted hydrochloric acid is added to dissolve the purple formazan crystals and form a

homogeneous coloured solution. The absorbance of this solution is then measured using a plate reader at a wavelength between 500–600 nm.

The co-nanoprecipitated nanoparticles which did not compromise the integrity of the monolayer were taken forward for both cytotoxicity assays. The results of the MTT cytotoxicity assay are shown in Figure 3.15 and, after incubation of Caco-2 cells with each co-nanoprecipitated nanomaterial for 5 days, it was evident that for *p*(HPMA$_{50}$-*co*-EGDMA$_{0.9}$):*p*(PEG$_{114}$-*b*-HPMA$_{120}$) 90:10 wt %, there was a negligible effect on the cell viability when compared with the aqueous control (FA in water, spiked with DMSO). The co-nanoprecipitated particles composed of *p*(HPMA$_{50}$-*co*-EGDMA$_{0.9}$):*p*(PEG$_{114}$-*b*-HPMA$_{120}$) 70:30, 50:50 wt % and *p*(*n*-BMA$_{50}$-*co*-EGDMA$_{0.8}$):*p*(PEG$_{114}$-*b*-HPMA$_{120}$) 50:50 wt %, showed a slight toxicity at 15 µM of FA, however, they were not toxic at the concentration used for the Caco-2 transcellular permeation experiments, which were performed at 10 µM FA.

3.6.3.3 ATP assay

As well as the MTT assay, an ATP based cytotoxicity assay was carried out which utilises the bioluminescent measurement of ATP present in metabolically active cells in order to assess cell viability.[18] The concentration of ATP in cells correlates with cell viability, as only living cells produce ATP. A decrease in cell viability is an indicator of cell death.

The results of the ATP cytotoxicity assay are shown in Figure 3.16 and after incubation of each co-nanoprecipitated FA nanomaterial with Caco-2 cells for 5 days the cell viability remained between 90-100 % for each sample. The low *in vitro* cytotoxicity values obtained during incubation with Caco-2 cells were important if the nanoparticles were to be considered as an oral therapy, as the initial concentration of the drug molecule, in this case FA, will be expected to be within the µM concentration range. Therefore, the following transcellular permeability experiments were conducted at 10µM.

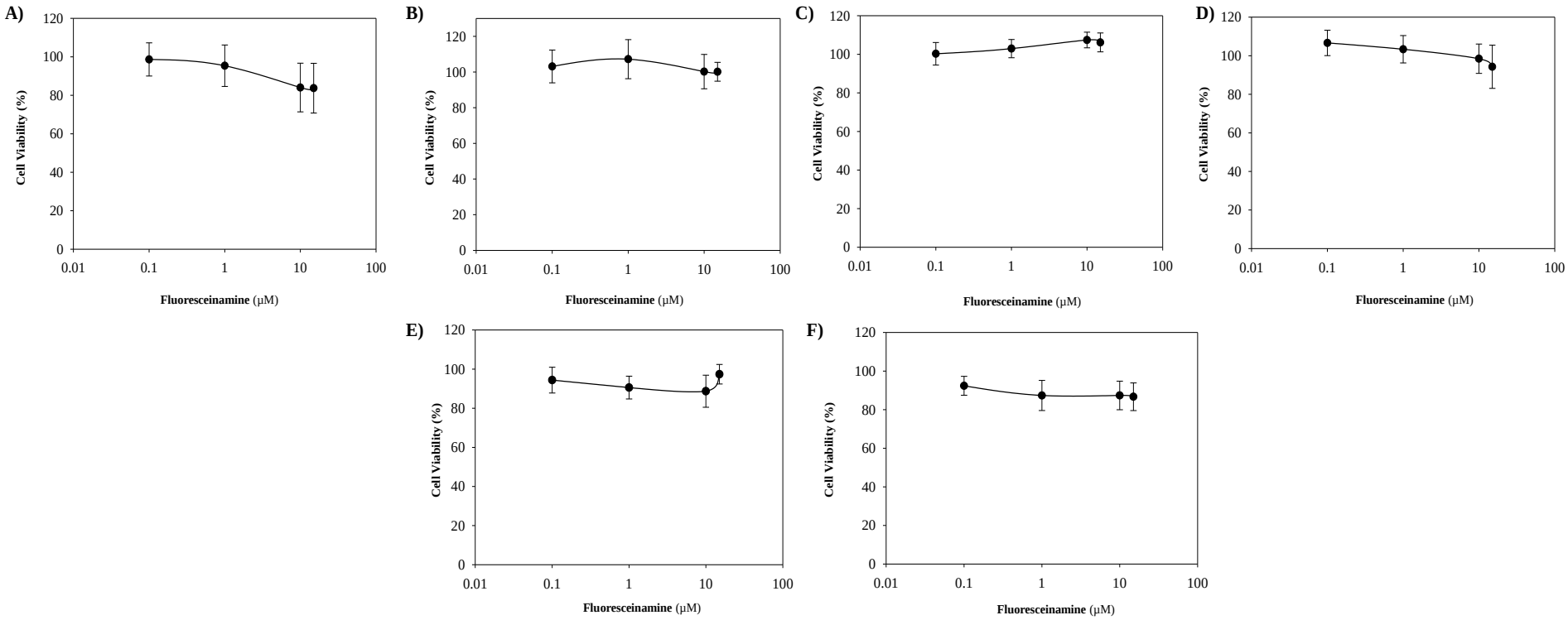

Figure 3.15 *In vitro* cytotoxicity assessment. Caco-2 cell MTT assay, 5 day incubation: A) Aqueous FA solution B) FA in DMSO C) *p*(HPMA$_{50}$-*co*-EGDMA$_{0.9}$):*p*(PEG$_{114}$-*b*-HPMA$_{120}$) 90:10 wt %, D) *p*(HPMA$_{50}$-*co*-EGDMA$_{0.9}$):*p*(PEG$_{114}$-*b*-HPMA$_{120}$) 70:30 wt %, E) *p*(HPMA$_{50}$-*co*-EGDMA$_{0.9}$):*p*(PEG$_{114}$-*b*-HPMA$_{120}$) 50:50 wt %, F) *p*(*n*-BMA$_{50}$-*co*-EGDMA$_{0.8}$):*p*(PEG$_{114}$-*b*-HPMA$_{120}$) 50:50 wt %. Error = Standard deviation.

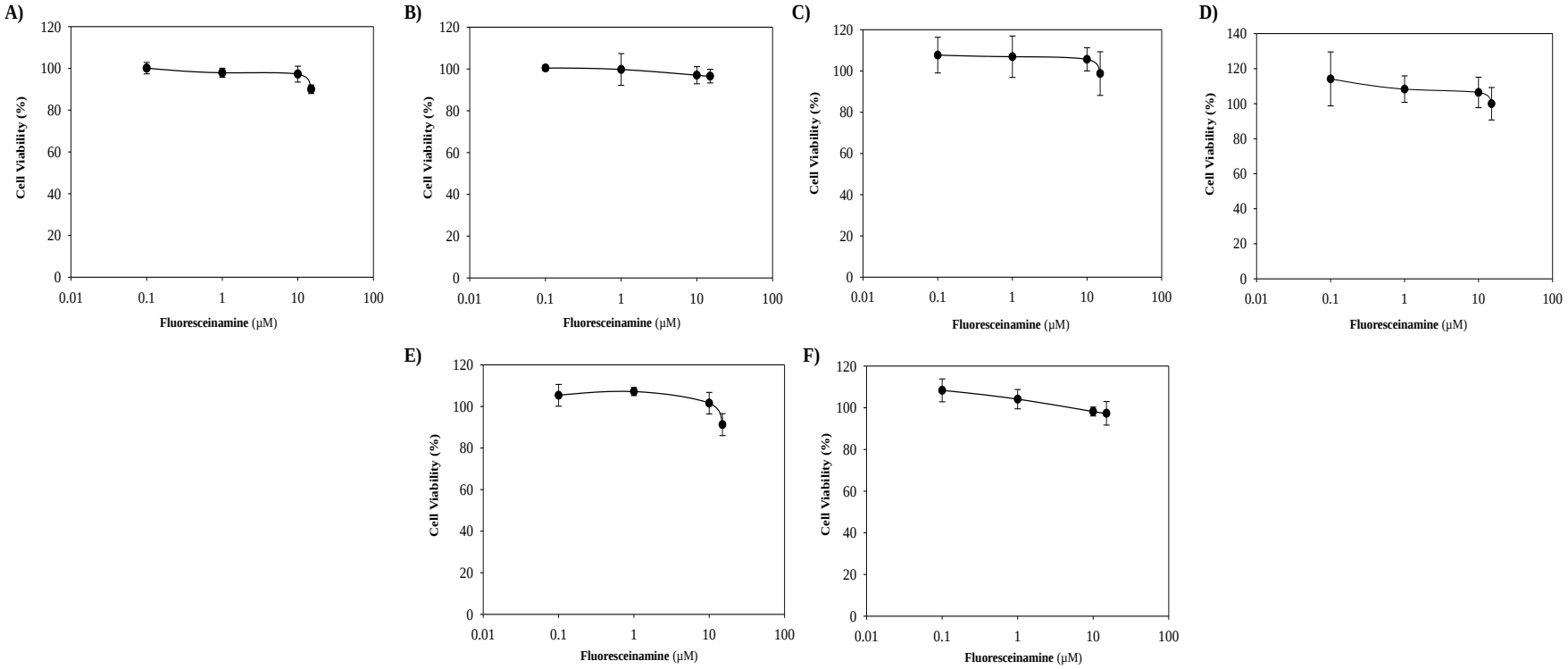

Figure 3.16 *In vitro* cytotoxicity assessment. Caco-2 cell ATP assay, 5 day incubation: A) Aqueous FA solution, B) FA in DMSO C) *p*(HPMA$_{50}$-*co*-EGDMA$_{0.9}$):*p*(PEG$_{114}$-*b*-HPMA$_{120}$) 90:10 wt %, D) *p*(HPMA$_{50}$-*co*-EGDMA$_{0.9}$):*p*(PEG$_{114}$-*b*-HPMA$_{120}$) 70:30 wt %, E) *p*(HPMA$_{50}$-*co*-EGDMA$_{0.9}$):*p*(PEG$_{114}$-*b*-HPMA$_{120}$) 50:50 wt %, F) *p*(*n*-BMA$_{50}$-*co*-EGDMA$_{0.8}$):*p*(PEG$_{114}$-*b*-HPMA$_{120}$) 50:50 wt %. Error = Standard deviation.

3.6.4 Transcellular permeability

A schematic representation of the transwell plate experiment is shown in Figure 3.17 and the apical and basolateral chambers are represented as (A) and (B) respectively. The apical chamber is representative of the gut side of the epithelium whilst the basolateral chamber represents the blood side of the epithelium.

During a typical experiment, the sample is deposited onto the monolayer in the apical compartment and then incubated for four hours, during which the movement of drug molecules from the apical to the basolateral side is measured (A>B) (Figure 3.17 B). The same experiment is conducted to measure the movement across the monolayer from the basolateral compartment to the apical compartment (B>A).

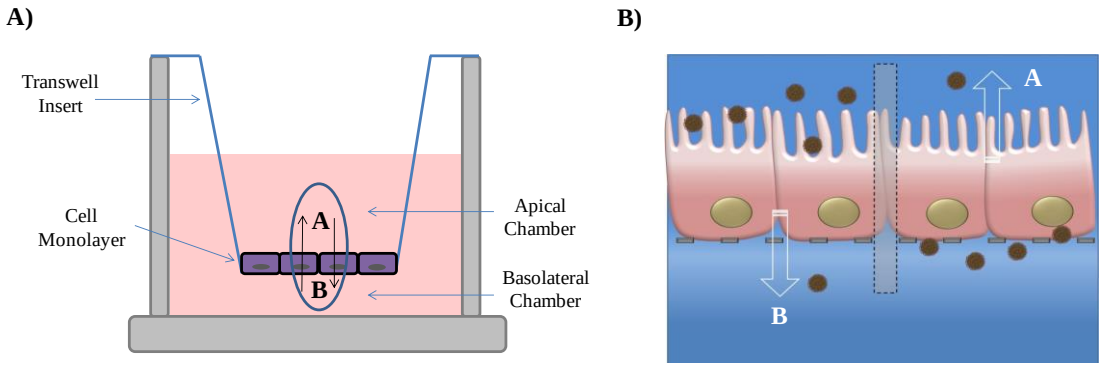

Figure 3.17 A) Caco-2 monolayer transwell experiment setup, B) schematic representation of the Caco-2 monolayer representing the apical (model of the gut side) and basolateral (modelling of the blood side). *From ref*[19]

The transport of molecules across the membrane is usually reported as an apparent permeability (P_{app}). The estimated value of P_{app} is determined using equation (1), where P_{app} is the apparent permeability (x 10^{-6} cm s^{-1}); dQ/dt is the rate of transport (nM min^{-1}); *A* is the surface area of the membrane (cm^2); and C_0 is the initial donor concentration (nM). The resulting P_{app} values obtained from both transport directions (apical to basolateral side and basolateral to apical side) are used for calculation of efflux ratio.

$$P_{app} = \frac{(dQ/dt)}{A \times C_0} \quad (1)$$

Several assumptions need to be made for an accurate estimate of permeability. These include, the amount of drug accumulated within the receiver compartment must be

proportional to time, the system must comply with 'sink' conditions, and, finally cellular accumulation, metabolism and nonspecific binding to plastic-ware are absent.[14] 'Sink' conditions imply that once the material has passed through the monolayer, it does not pass back across; however, this is not always the case for highly permeable materials.

The P_{app} results for the FA encapsulated nanoparticles are shown in Figure 3.18; the movement from the apical to basolateral (A>B) are shown in blue and the basolateral to apical (B>A) are shown in red. The materials which show an increased A>B movement when compared with the aqueous control are *p*(HPMA$_{50}$-*co*-EGDMA$_{0.9}$):*p*(PEG$_{114}$-*b*-HPMA$_{120}$) 70:30 wt % and *p*(*n*-BMA$_{50}$-*co*-EGDMA$_{0.8}$):*p*(PEG$_{114}$-*b*-HPMA$_{120}$) 50:50 wt % and an increased B>A for entries *p*(HPMA$_{50}$-*co*-EGDMA$_{0.9}$):*p*(PEG$_{114}$-*b*-HPMA$_{120}$) 50:50 wt % and *p*(*n*-BMA$_{50}$-*co*-EGDMA$_{0.8}$):*p*(PEG$_{114}$-*b*-HPMA$_{120}$) 50:50 wt % was observed. Overall, *p*(*n*-BMA$_{50}$-*co*-EGDMA$_{0.8}$):*p*(PEG$_{114}$-*b*-HPMA$_{120}$) 50:50 wt % shows a statistically significant increase in both A>B or B>A movement when compared with the aqueous control sample.

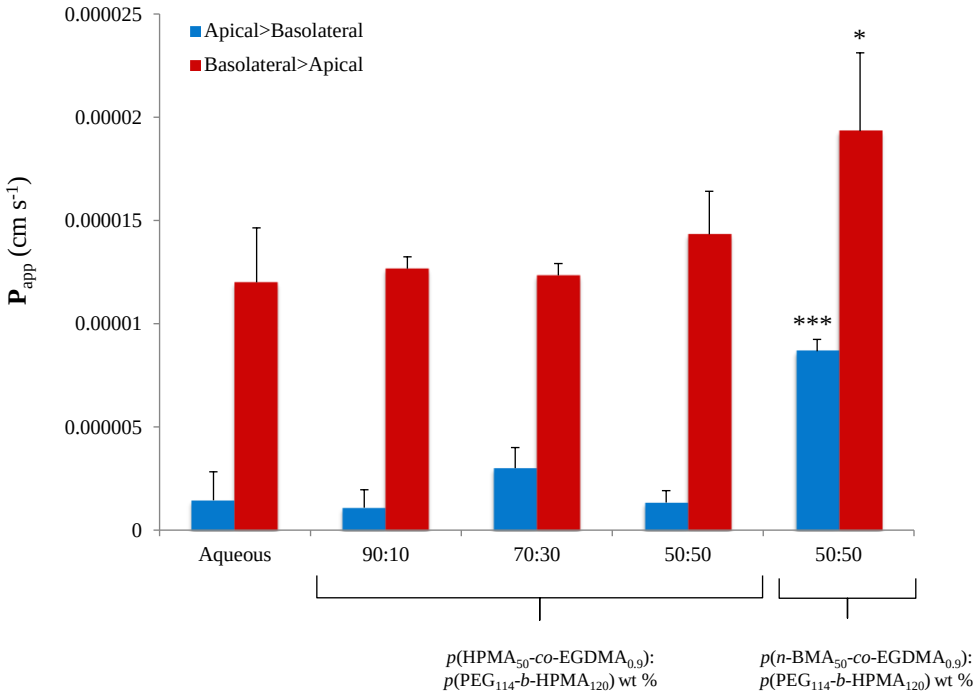

Figure 3.18 Apparent permeability (P_{app}) of FA across the Caco-2 cell monolayer following a 4 hour incubation period with aqueous and FA encapsulated co-nanoprecipitated materials. (*, P <0.05 and ***, P <0.001 (ANOVA) (n=3). Error = Standard deviation.

The P_{app} ratio A>B/B>A gives an indication of the permeability of the materials from the apical to the basolateral side of the monolayer and the results are shown in Figure 3.19.

Both *p*(HPMA$_{50}$-*co*-EGDMA$_{0.9}$):*p*(PEG$_{114}$-*b*-HPMA$_{120}$) 70:30 wt % and *p*(*n*-BMA$_{50}$-*co*-EGDMA$_{0.8}$):*p*(PEG$_{114}$-*b*-HPMA$_{120}$) 50:50 wt % showed an improved A>B/B>A ratio (1.8 and 3.5 fold increases respectively). Although it of interest to determine the efflux of the materials, it is less important here, as this model experiments is conducted under static conditions and does not mimic physiological conditions with blood flow. The lead material taken forward for further testing was composed of the branched copolymer *p*(*n*-BMA$_{50}$-*co*-EGDMA$_{0.8}$) and the A-B block copolymer, *p*(PEG$_{114}$-*b*-HPMA$_{120}$) at a ratio of 50:50 wt %. This was selected due to the statistical significance of the results, highest P_{app} ratio and improved A>B/B>A ratios when compared with the aqueous control. Obviously, this is a proof of concept experiment and further studies including stability in the gastric environment and penetration of the mucus barrier would require further investigation.

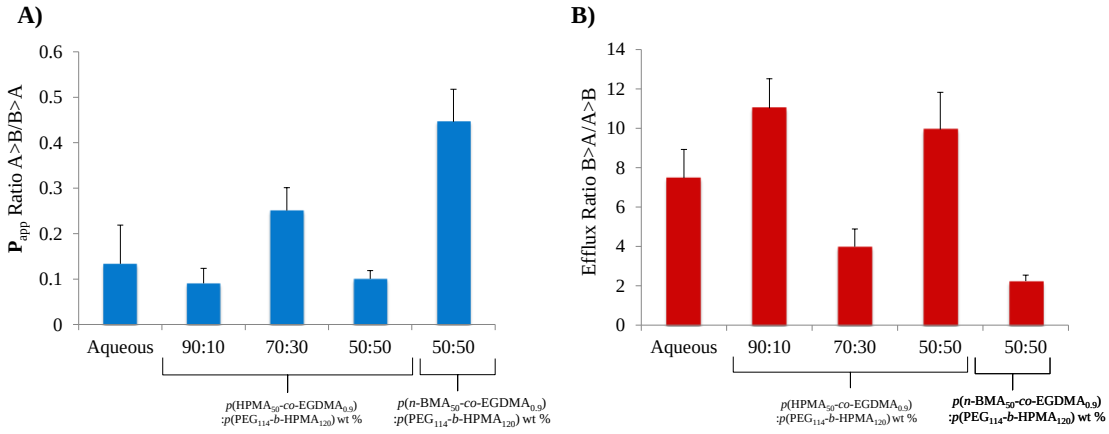

Figure 3.19 A) P_{app} ratio A>B/B>A and B) efflux ratio B>A/A>B for FA encapsulated materials compared to the aqueous preparation of FA. Error = Standard deviation.

Additional toxicity testing was carried out for *p*(*n*-BMA$_{50}$-*co*-EGDMA$_{0.8}$):*p*(PEG$_{114}$-*b*-HPMA$_{120}$) 50:50 wt % using ATHP-1 cells. ATHP-1 cells are monocyte-derived macrophage cells so it was important to ascertain the toxicity of the FA nanomaterials with these cells. The concentrations of FA presented here are much higher than what would be expected to be present in the systemic circulation, therefore, the results within the nM range should be considered. The results obtained for the ATP assay for the FA nanomaterial show a cell viability >80% between 0.1-1 µM (Figure 3.20 Ai,ii). A slight increase in toxicity was observed for the MTT assay and between 0.1-1 µM and the cell viability of the FA nanomaterial remained above ~60%. It is unclear why the FA encapsulated nanoparticles had an increased toxicity when incubated with ATHP-1

derived cells, however, the FA nanomaterial, *p*(*n*-BMA$_{50}$-*co*-EGDMA$_{0.8}$):*p*(PEG$_{114}$-*b*-HPMA$_{120}$) 50:50 wt % was considered suitable for accumulation studies.

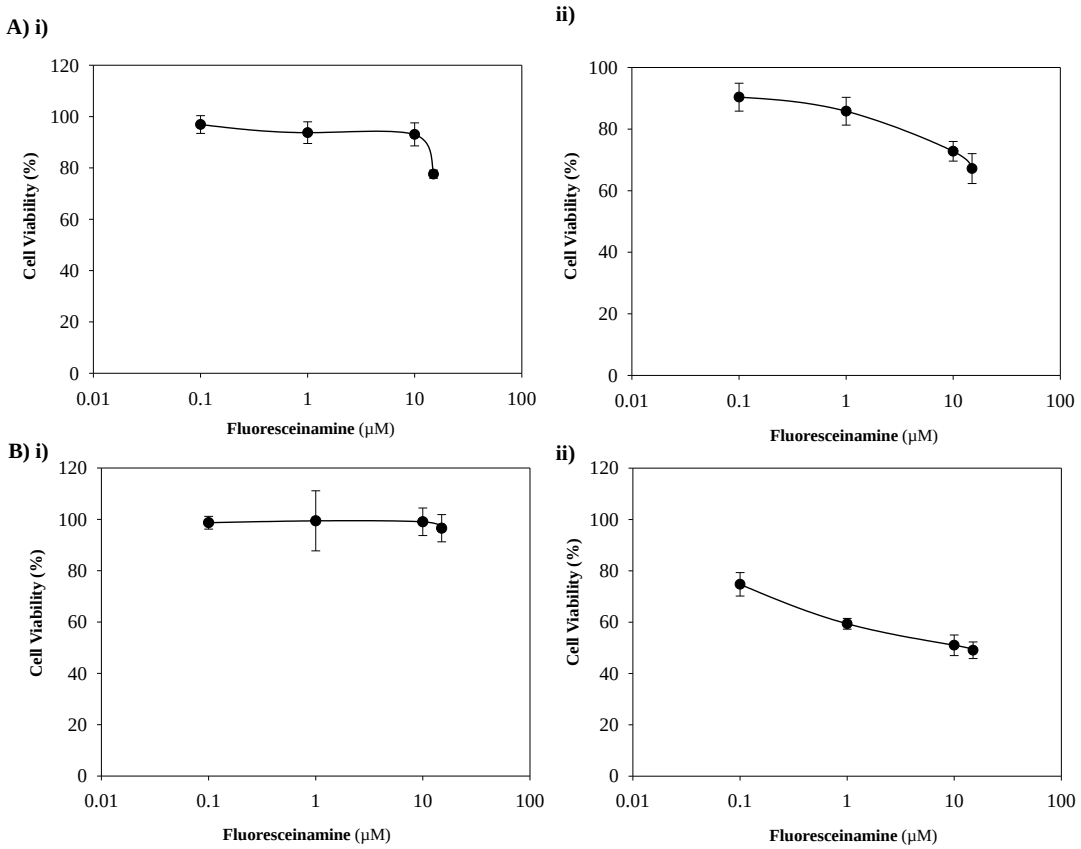

Figure 3.20 *In vitro* cytotoxicity assessment. A) ATHP -1 5 day ATP i) aqueous FA solution ii) *p*(*n*-BMA$_{50}$-*co*-EGDMA$_{0.8}$):*p*(PEG$_{114}$-*b*-HPMA$_{120}$) 50:50 wt %, B) ATHP-1 5 day, MTT i) aqueous FA solution, ii) *p*(*n*-BMA$_{50}$-*co*-EGDMA$_{0.8}$):*p*(PEG$_{114}$-*b*-HPMA$_{120}$) 50:50 wt %. Error = Standard deviation.

3.6.5 Accumulation in Caco-2 and ATHP-1 cells

The lead candidate, consisting of *p*(*n*-BMA$_{50}$-*co*-EGDMA$_{0.8}$):*p*(PEG$_{114}$-*b*-HPMA$_{120}$) 50:50 wt % was further studied and the cellular accumulation ratio (CAR) for both ATHP-1 and Caco-2 cells was ascertained. CAR is a measure of the ratio of intracellular concentration and extracellular concentration and used to determine the uptake of molecules into cells. As discussed, ATHP-1 cells are monocyte derived macrophage cells which are used to determine the accumulation of materials in macrophages and can be indicative of phagocytic uptake mechanisms. Therefore, the measurement of the CAR in macrophages is useful in the study of the treatment of infectious diseases such as HIV as this is one of the cellular viral sanctuary sites. Although not statistically significant, the

FA encapsulated material did show a small increase in CAR in the ATHP-1 cells when compared to the aqueous FA control (Figure 3.20A).

As well as ATHP-1, Caco-2 cells were also selected to determine whether the FA encapsulated nanoparticles were permeating the Caco-2 monolayer *via* a transcellular or paracellular pathway. If the FA loaded materials were present within the Caco-2 cells, this would suggest that permeation occurs through the cell i.e. transcellular. The CAR of *p*(*n*-BMA$_{50}$-*co*-EGDMA$_{0.8}$):*p*(PEG$_{114}$-*b*-HPMA$_{120}$) 50:50 wt %, shown in Figure 3.21B has been plotted against the aqueous control sample. The decreased value for the CAR for this sample, suggests a lower accumulation of FA within Caco-2 cells when compared to the aqueous control for this particular material. This suggests that the movement of the FA from the apical to the basolateral chamber is not transcellular and occurs *via* another mechanism, most likely paracellular, which is the transport between the cells, although it is also possible that the nanoparticles are actively and rapidly transported through the cells and do not leave the endosome to accumulate appreciably within the interior of the Caco-2 cells.

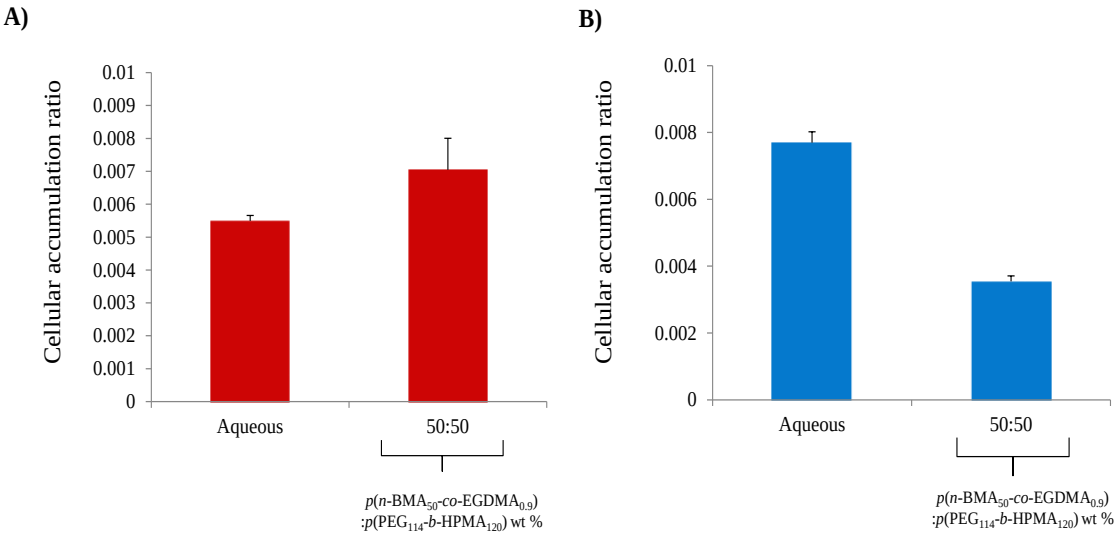

Figure 3.21 Cellular accumulation ratios of aqueous FA and FA encapsulated *p*(*n*-BMA$_{50}$-*co*-EGDMA$_{0.8}$):*p*(PEG$_{114}$-*b*-HPMA$_{120}$) (50:50 wt%) nanoparticles. A) ATHP-1 cells and B) Caco-2 cells. Error = Standard deviation.

3.6.6 Cellular accumulation ratio (CAR) and apparent permeability (P_{app}) of FA and FA encapsulated *p*(*n*-BMA$_{50}$-*co*-EGDMA$_{0.8}$):*p*(PEG$_{114}$-*b*-HPMA$_{120}$) (50:50 wt %) in the presence of inhibitors

To confirm if the uptake of the FA encapsulated nanomaterials was energy dependant, and therefore an active process, the inhibition of active transport (influx and efflux) was conducted by incubating Caco-2 cells with 2-deoxyglucose and rotenone, which are commonly used to inhibit ATP.[20] To determine an appropriate concentration of 2-deoxyglucose and rotenone, a control experiment was conducted, and 2 mg/ml 2-deoxyglucose and 100 nM rotenone were selected over the 3 mg/ml 2-deoxyglucose and 150 nM rotenone, because within error, there was no real overall difference in ATP depletion between the two samples (Figure 3.22A).

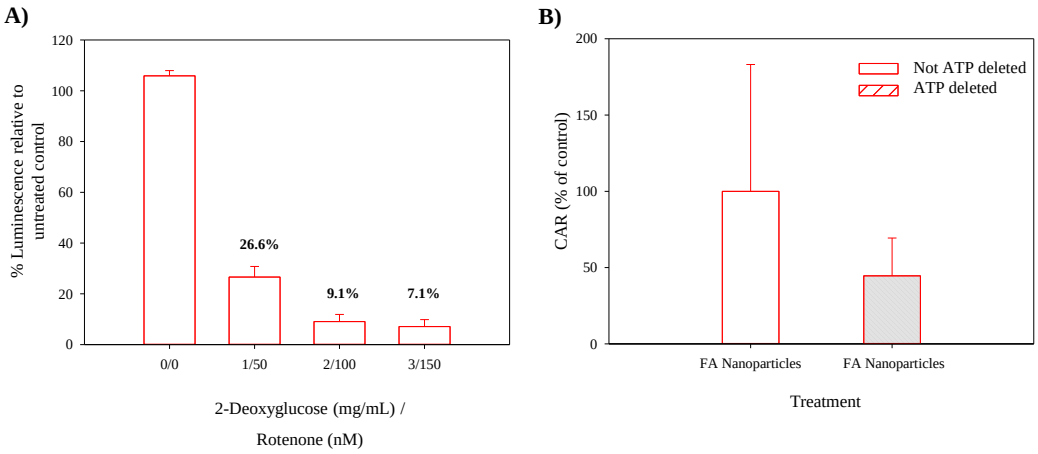

Figure 3.22 A) Control experiment for ATP inhibition, determination of an appropriate concentration of 2-Deoxyglucose and rotenone, B) CAR for FA nanoparticles = *p*(*n*-BMA$_{50}$-*co*-EGDMA$_{0.8}$):*p*(PEG$_{114}$-*b*-HPMA$_{120}$) 50:50 wt %, before and after ATP depletion (the presence of 2-Deoxyglucose (2mg/mL) and rotenone (100 nM). Error = Standard deviation.

Caco-2 cells were pre-incubated with 2 mg/ml 2-deoxyglucose and 100 nM rotenone for 20 min to deplete ATP. Following depletion, cells were washed three times with Hank's Balanced Salt Solution, and replaced with media containing DMSO solubilised (<0.1% v/v) fluoresceinamine or *p*(*n*-BMA$_{50}$-*co*-EGDMA$_{0.8}$):*p*(PEG$_{114}$-*b*-HPMA$_{120}$) (50:50 wt %) (10 µM final fluoresceinamine concentration) and incubated at 37°C under and atmosphere of 5% CO_2 for 24 hours. Extra- and intra-cellular samples were extracted and analysed using HPLC as previously described. The measured CAR during ATP depletion for *p*(*n*-BMA$_{50}$-*co*-EGDMA$_{0.8}$):*p*(PEG$_{114}$-*b*-HPMA$_{120}$) (50:50 wt%), shows a

decrease in accumulation and although not statistically significant, this suggests the process could be energy dependant and proceeds *via* an active mechanism (Figure 3.22B).

The apparent permeability (P_{app}) of the FA encapsulated nanomaterial, *p*(*n*-BMA_{50}-*co*-$EGDMA_{0.8}$):*p*(PEG_{114}-*b*-$HPMA_{120}$) 50:50 wt % through Caco-2 cells has already been investigated in Section 3.6.4, therefore, it was of interest to assess P_{app} in the presence of various endocytic inhibitors. It is worth noting that both the CAR and P_{app} experiments are quite different, as P_{app} is conducted on a monolayer of polarised cells, whereas CAR is carried out on Caco-2 cells that have not been polarised, so the results are not directly comparable. The movement involving the endocytosis pathway is an active process and when the processes were inhibited, a drop in P_{app} for FA was observed (Figure 3.23). This suggests that the movement is not simply passive. This would not be expected due to the low accumulation within Caco-2 cells witnessed earlier (Figure 3.21) and for addition of each inhibitor, a significant decrease in P_{app} is observed. Rather than accumulating into the cells, it can be hypothesised that FA has moved across the monolayer quite rapidly in the transwell experiments, hence a low accumulation.

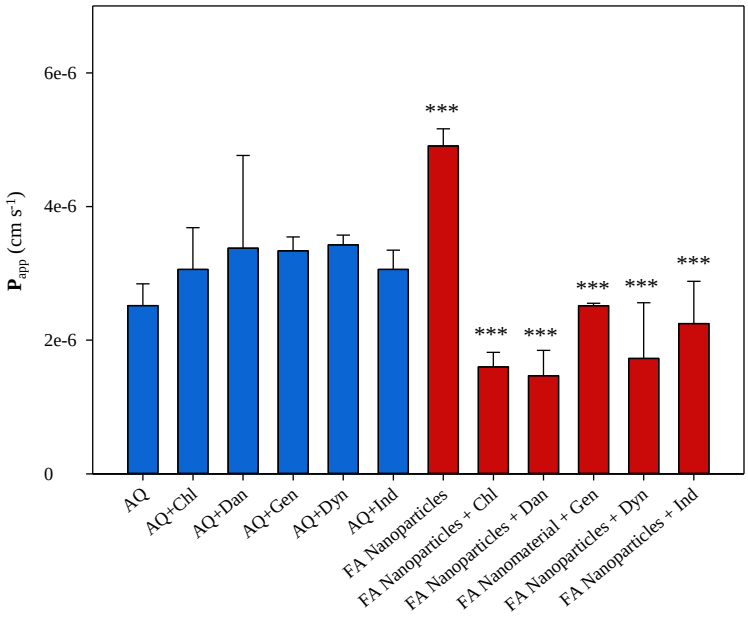

Figure 3.23 Mechanistic evaluation of transcellular permeation through Caco-2 cells, AQ = aqueous FA control, FA nanoparticles = *p*(*n*-BMA_{50}-*co*-$EGDMA_{0.8}$):*p*(PEG_{114}-*b*-$HPMA_{120}$) (50:50 wt%), chl = chlorpromazine (clathrin-mediated endocytosis), dan = dansylcadaverine (receptor-mediated endocytosis), gen = genistein (caveolae-mediated endocytosis), dyn = dynasore (dynamin-dependent endocytosis), ind = indomethacin (caveolae-mediated endocytosis). (***, P <0.001 (ANOVA) (n=3). (FA nanoparticles = *p*(*n*-BMA_{50}-*co*-$EGDMA_{0.8}$):*p*(PEG_{114}-*b*-$HPMA_{120}$) 50:50 wt %). Error = Standard deviation.

To ascertain if the monolayer was compromised after the addition of the inhibitors to the control samples and FA loaded *p*(*n*-BMA$_{50}$-*co*-EGDMA$_{0.8}$):*p*(PEG$_{114}$-*b*-HPMA$_{120}$) 50:50 wt % sample, during the transwell experiment, the Caco-2 monolayer was exposed for 4 hours and incubated with ^{14}C-mannitol as described previously in Section 3.6.3. It is evident that for both the control and FA loaded sample, the monolayer integrity is maintained in the presence of all inhibitors (Figure 3.24 A&B). This control experiment was conducted to ensure the results obtained during inhibition experiments could be interpreted with confidence.

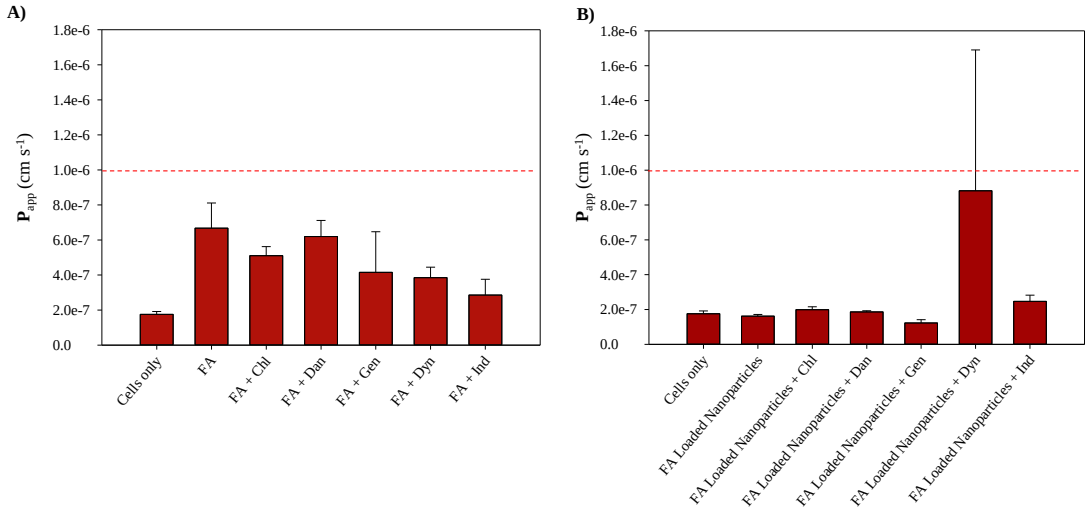

Figure 3.24 Caco-2 monolayer integrity after exposure to endocytic inhibitors; chl = chlorpromazine (clathrin-mediated endocytosis), dan = dansylcadaverine (receptor-mediated endocytosis), gen = genistein (caveolae-mediated endocytosis), dyn = dynasore (dynamin-dependent endocytosis), ind = indomethacin (caveolae-mediated endocytosis). A) FA = fluoresceinamine control (all samples spiked with DMSO), B) FA loaded nanoparticles = *p*(*n*-BMA$_{50}$-*co*-EGDMA$_{0.8}$):*p*(PEG$_{114}$-*b*-HPMA$_{120}$) (50:50 wt%). Error = Standard deviation.

3.7 Conclusion

Throughout this research chapter, the chemical compositions of both the branched co/terpolymers and A-B block copolymer have been varied to include the hydrophobic monomers, *n*-BMA and *t*-BMA. A versatile co-nanoprecipitation system has been presented and the addition of an A-B block copolymer resulted in the formation of stabilised nanoparticles which was not witnessed when the branched co/terpolymers were nanoprecipitated alone. The encapsulation of the hydrophobic guest molecule pyrene and subsequent fluorescence measurements of polymers consisting of *p*(*n*-BMA), provided further information that the A-B block copolymer is becoming entrapped within the

nanoparticle core during the co-nanoprecipitation process. The co-nanoprecipitation of the branched co/terpolymers, A-B block copolymer and addition of 10 wt % FA generated nanoparticles which were stable under physiologically relevant conditions and therefore, progressed forward for pharmacological studies.

A series of pharmacological studies were also conducted; an initial ^{14}C-mannitol permeability assay showed four FA loaded nanomaterials were shown not to compromise Caco-2 monolayers and were the subject of further testing. Subsequent cytotoxicity assays of the FA nanomaterials demonstrated a low toxicity when Caco-2 cells were incubated with the FA loaded nanomaterials, and 90-100% viability was maintained for each material. To determine if the permeation of FA across the Caco-2 monolayer was enhanced when encapsulated within the co-nanoprecipitated materials *vs* non-encapsulated FA, a transcellular permeability assay was carried out. A statistically significant improved A>B/B>A ratio was observed for *p*(*n*-BMA$_{50}$-*co*-EGDMA$_{0.8}$):*p*(PEG$_{114}$-*b*-HPMA$_{120}$) (50:50 wt %), which was taken forward for cellular accumulation studies. The cellular accumulation experiment highlighted that for the FA encapsulated nanomaterial, although not statistically significant, an increased accumulation in the ATHP-1 cells was observed. This would be a desirable property in the oral dosing therapy treatment of infectious diseases such as HIV, where macrophage cells are a sanctuary site for the HIV virus. However, the decreased accumulation in Caco-2 cells suggested that the FA was being transported across the membrane *via* another mechanism, possibly paracellular permeation. The lead FA nanomaterial, *p*(*n*-BMA$_{50}$-*co*-EGDMA$_{0.8}$):*p*(PEG$_{114}$-*b*-HPMA$_{120}$) (50:50 wt %) was further investigated by inhibition of the active transport processes and during ATP depletion, a decrease in cellular accumulation of FA was observed suggesting uptake occurs *via* an active process. The assessment of the Caco-2 transcellular permeability was also carried out in the presence of endocytic inhibitors and a statistically significant decrease in cellular permeability was observed, which suggests the movement of FA is not simply passive and does proceed *via* an active mechanism.

3.8 References

1. A. B. Dwyer, P. Chambon, A. Town, F. L. Hatton, J. Ford and S. P. Rannard, *Polymer Chemistry*, Advance Article, 2015, DOI: 10.1039/C5PY00791G.
2. A. B. Dwyer, P. Chambon, A. Town, T. He, A. Owen and S. P. Rannard, *Polymer Chemistry*, 2014, **5**, 3608-3616.
3. S. McDonald and S. P. Rannard, *Macromolecules*, 2001, **34**, 8600-8602.
4. R. A. Slater, T. O. McDonald, D. J. Adams, E. R. Draper, J. V. M. Weaver and S. P. Rannard, *Soft Matter*, 2012, **8**, 9816-9827.
5. I. Bannister, N. C. Billingham, S. P. Armes, S. P. Rannard and P. Findlay, *Macromolecules*, 2006, **39**, 7483-7492.
6. S. Schubert, J. J. T. Delaney and U. S. Schubert, *Soft Matter*, 2011, **7**, 1581-1588.
7. H. Fessi, F. Puisieux, J. P. Devissaguet, N. Ammoury and S. Benita, *International Journal of Pharmaceutics*, 1989, **55**, R1-R4.
8. S. Inphonlek, N. Pimpha and P. Sunintaboon, *Colloids and Surfaces B: Biointerfaces*, 2010, **77**, 219-226.
9. R. Zangi and J. B. F. N. Engberts, *Journal of the American Chemical Society*, 2005, **127**, 2272-2276.
10. R. A. Van Wagenen, D. L. Coleman, R. N. King, P. Triolo, L. Brostrom, L. M. Smith, D. E. Gregonis and J. D. Andrade, *Journal of Colloid and Interface Science*, 1981, **84**, 155-162.
11. J. Xia, S. G. Gaynor and K. Matyjaszewski, *Macromolecules*, 1998, **31**, 5958-5959.
12. P. A. Gurr, M. F. Mills, G. G. Qiao and D. H. Solomon, *Polymer*, 2005, **46**, 2097-2104.
13. C. D. Andrews, W. R. Spreen, H. Mohri, L. Moss, S. Ford, A. Gettie, K. Russell-Lodrigue, R. P. Bohm, C. Cheng-Mayer, Z. Hong, M. Markowitz and D. D. Ho, *Science*, 2014, **343**, 1151-1154.
14. H. Sun, E. C. Chow, S. Liu, Y. Du and K. S. Pang, *Expert Opinion on Drug Metabolism & Toxicology*, 2008, **4**, 395-411.
15. Y. H. Lin, C. K. Chung, C. T. Chen, H. F. Liang, S. C. Chen and H. W. Sung, *Biomacromolecules*, 2005, **6**, 1104-1112.
16. R. Elsby, D. D. Surry, V. N. Smith and A. J. Gray, *Xenobiotica*, 2008, **38**, 1140-1164.

17. J. van Meerloo, G. L. Kaspers and J. Cloos, in *Cancer Cell Culture*, ed. I. A. Cree, Humana Press, 2011, vol. 731, ch. 20, pp. 237-245.
18. S. P. M. Crouch, R. Kozlowski, K. J. Slater and J. Fletcher, *Journal of Immunological Methods*, 1993, **160**, 81-88.
19. F. L. Hatton, L. M. Tatham, L. R. Tidbury, P. Chambon, T. He, A. Owen and S. P. Rannard, *Chemical Science*, 2015, **6**, 326-334.
20. K. Jones, P. G. Hoggard, S. D. Sales, S. Khoo, R. Davey and D. J. Back, *Aids*, 2001, **15**, 675-681.

Chapter 4

Co-nanoprecipitation:

Encapsulation Studies of HIV Anti-retrovirals

4.1 Introduction

The preparation of sterically stabilised nanoparticles from polymers with varying chemical compositions, was explored in Chapter 3 and highlighted the versatility of the co-nanoprecipitation approach. The ability to tune the chemistry of both polymers (branched copolymer and A-B stabilising block copolymer) is very appealing for the preparation of drug delivery nanoparticles, as both the hydrophobic branched polymer core and A-B block copolymers can be tailored for the encapsulation of a particular hydrophobic drug molecule.

This research chapter aims to assess the encapsulation capabilities of the co-nanoprecipitated materials using clinically relevant antiretroviral drugs used to treat human immunodeficiency virus (HIV). Drug encapsulation studies were conducted for the hydrophobic drug molecules, efavirenz (EFV), lopinavir (LPV) and ritonavir (RTV) (Figure 4.1). Encapsulation into polymeric nanoparticles could potentially increase the concentration and aqueous solubility of these drugs, which is advantageous if they were to be administered as an oral or intravenous solution of drug loaded nanoparticles.

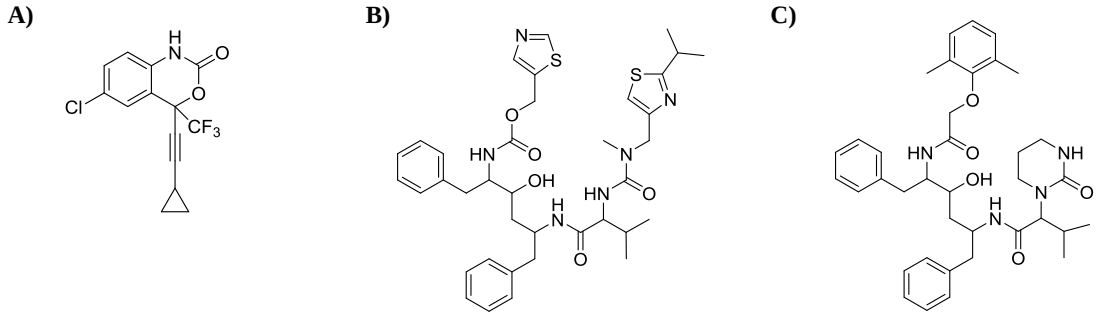

Figure 4.1 Chemical structures of HIV anti-retrovirals A) efavirenz B) ritonavir C) lopinavir.

When a patient is diagnosed with HIV, they are most likely to be treated *via* the administration of multiple drug molecules, known as highly active anti-retroviral therapy (HAART). HAART improves the patient's quality of life by maintaining function of the immune system, and prevents opportunistic infections that are often fatal.[1] EFV is a non-nucleoside reverse transcriptase inhibitor which prevents the replication of HIV type 1,[2] and is the first choice anti-retroviral in an adult and paediatric pharmacotherapy. LPV and RTV are both protease inhibitors[3] and researchers at the University of Liverpool were first to recognise that the co-administration of RTV as a combination therapy with other HIV drugs increases their bioavailability and efficiency, therefore, allowing lower dosages to

be administered.[4] Although RTV is no longer used as a therapeutic drug, it has found considerable use as a 'booster'; enabling longer circulation times of other antiretrovirals by inhibiting their metabolism. RTV and LPV are commonly administered as a dual therapy, with a 400/100 mg dosage ratio (LPV/RTV), known as Kaletra©.[5] These three drugs have made a significant impact on the treatment of HIV patients, however, they all show relatively poor solubility in water.

Examples of biologically relevant polymers, including poly(lactic-*co*-glycolic acid) (PLGA), have been used for the preparation of nanoparticles containing HIV drugs *via* various emulsification methods. For example, Shibata *et al* have reported the individual encapsulation of EFV, RTV and LPV at ~10 wt % *via* emulsion evaporation.[6] To mimic the use of drug combinations, encapsulation of HIV molecules in PLGA nanoparticles has been reported *via* water/oil/water homogenisation and anti-retroviral drug loading averaged at 4.9 wt %, 5.2 wt %, and 1.9 wt % for RTV, LPV, and EFV, respectively.[7] As well as PLGA, poly(caprolactone) (PCL) nanoparticles have also been prepared for encapsulation of LPV (~10 wt %) utilising the oil in water emulsion-solvent evaporation technique.[8] Although drug-loading has been achieved for the examples discussed, their preparation requires homogenisation, ultracentrifugation and lyophilisation steps which can be time consuming and expensive.

HIV drug loaded nanoparticles have also been prepared *via* nanoprecipitation, however, for the examples listed below, nanoparticle dispersion preparation involved combinations of ultracentrifugation, washing with water, lyophilisation and, in some cases, filtration. Das Neves *et al* have described the preparation of daprivine (HIV anti-retroviral) encapsulated PCL nanoparticles with an estimated drug loading of ~12 wt %.[9] Other reports include the encapsulation of the HIV anti-retroviral saquinavir (5 wt %)[10] and EFV (10 wt %)[11] into PCL nanoparticles. It is worth noting that all examples described require additional polymers to be present within the precipitation water (e.g. poly(vinyl alcohol) (PVA) or poly(ethylene glycol) (PEG)), in order to stabilise the nanoparticles. These additional materials and purification steps were not required when preparing encapsulated nanoparticles *via* the co-nanoprecipitation approach, as described in Chapters 2 and 3, providing an efficient, one-step route to stabilised nanoparticles which do not require filtration, centrifugation or surfactants in the water in order to encapsulate a guest molecule effectively (10 wt % fluoresceinamine, Chapter 3, Section 3.6.1).

4.2 Encapsulation of anti-retrovirals utilising the co-nanoprecipitation approach

The selected HIV anti-retrovirals were co-nanoprecipitated with varying branched co/terpolymers and an A-B block copolymer to assess the loading capabilities within the nanoparticles. During a typical co-nanoprecipitation, a HIV drug was dissolved within the good solvent with one of a selection of branched co/terpolymers; *p*(*n*-BMA$_{50}$-*co*-EGDMA$_{0.8}$), *p*(*t*-BMA$_{50}$-*co*-EGDMA$_{0.9}$), *p*(HPMA$_{25}$-*co*-*n*-BMA$_{25}$-EGDMA$_{0.9}$) or *p*(HPMA$_{25}$-*co*-*t*-BMA$_{25}$-*co*-EGDMA$_{0.9}$), and an A-B block copolymer. The nanoparticles were prepared under the same conditions as described previously, i_5-f_1 (from acetone into water). It was hypothesised that the branched co/terpolymers with an increased hydrophobic nature would solubilise an increased amount of hydrophobic drug within the nanoparticle core. Therefore it would be expected that during incorporation of *p*(*n*-BMA$_{50}$-*co*-EGDMA$_{0.8}$) with an A-B block copolymer, an increased loading of hydrophobic drug molecule would be observed.

To assess the drug encapsulation ability within nanoprecipitated particles, a series of loading experiments were carried out at various weight percentages (wt %) of drug, with respect to the mass of the total polymer. The *p*(PEG$_{114}$-*b*-HPMA$_{120}$) A-B block copolymer was selected for this study, due to previously demonstrated stability in physiological environments, and the encouraging *in vitro* pharmacological results discussed in Chapter 3, Section 3.6.2.

4.2.1 Encapsulation of EFV *via* co-nanoprecipitation

Initially, co-nanoprecipitation studies were conducted to investigate the encapsulation ability with EFV. EFV is a relatively small, hydrophobic molecule (Figure 4.1) and has limited aqueous solubility (4 µg/mL);[12] however, when co-nanoprecipitated with a branched co/terpolymer and A-B block copolymer, the drug became encapsulated within the nanoparticles. The DLS analyses for all anti-retroviral co-nanodispersions is shown in Table 4.1. The experiments were carried out using a low starting wt % of EFV with stepwise increases to ascertain the amount (wt %) of EFV which could be tolerated prior to polymer/drug macro-phase separation. The optimum loading of drug molecules into nanoparticles is highlighted in blue in each table from this point onwards.

An example of EFV encapsulation is presented in Figure 4.2i-iv, which shows a comparison of EFV in water *vs* EFV nanoprecipitated with a branched copolymer and A-

B block copolymer. The optimum encapsulation of 9 wt % EFV was achieved when co-nanoprecipitated within *p*(HPMA$_{50}$-*co*-EGDMA$_{0.9}$):*p*(PEG$_{114}$-*b*-HPMA$_{120}$) (50:50 wt %) and the presence of EFV appears to have a negligible effect on resulting nanoparticle sizes when compared with the blank nanoparticle dispersion. The DLS results obtained for nanoparticles with 9 wt % encapsulation is shown in Figure 4.3A, and illustrates a narrow monomodal peak. The presence of spherical nanoparticles after encapsulation of 9 wt % of EFV into *p*(HPMA$_{50}$-*co*-EGDMA$_{0.9}$):*p*(PEG$_{114}$-*b*-HPMA$_{120}$) (50:50 wt %), was further confirmed by scanning electron microscopy (SEM) of the nanoparticles and after 1 month of storage (Figure 4.3 Bi&ii). During addition of 10 wt % EFV, a fine precipitate was observed within the sample after 24 hours giving a broad PdI of 0.435 after DLS analysis.

Table 4.1 DLS analysis of EFV encapsulated nanoparticles prepared *via* co-nanoprecipitation.

Branched co/terpolymer:*p*(PEG$_{114}$-*b*-HPMA$_{120}$) 50:50 wt %	**Efavirenz (wt%)**	**Size (d.nm)**	**PdI**	**D$_n$ (nm)**	**Z-ave (d.nm) / PdI After 3 days**
p(HPMA$_{50}$-*co*-EGDMA$_{0.9}$)	Blank	103	0.051	112	-
	1	101	0.050	79	-
	2	119	0.048	96	-
	5	100	0.073	75	-
	9	107	0.058	82	-
	10	180	0.435	85	-
p(*n*-BMA$_{50}$-*co*-EGDMA$_{0.8}$)	Blank	205	0.088	170	-
	5	240	0.147	189	239 (0.134)
	9	194	0.099	153	193 (0.101)
	15	177	0.175	120	166 (0.092)
	20	139	0.073	105	155 (0.074)
	25	172	0.113	122	187 (0.213)
p(*t*-BMA$_{50}$-*co*-EGDMA$_{0.9}$)	Blank	357	0.234	245	-
	5	389	0.489	182	-
p(HPMA$_{25}$-*co*-*n*-BMA$_{25}$-EGDMA$_{0.9}$)	Blank	161	0.085	125	-
	5	136	0.086	101	135 (0.078)
	9	133	0.075	103	132 (0.098)
	15	117	0.131	76	116 (0.131)
	20	171	0.089	104	143 (0.111)
p(HPMA$_{25}$-*co*-*t*-BMA$_{25}$-*co*-EGDMA$_{0.9}$)	Blank	161	0.066	131	-
	5	150	0.047	125	149 (0.089)
	9	156	0.058	130	154 (0.083)
	15	131	0.037	106	131 (0.096)
	20	113	0.059	89	121 (0.104)
	25	164	0.056	138	169 (0.155)

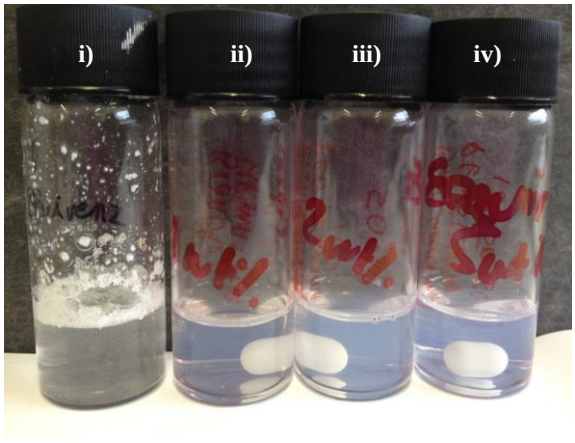

Figure 4.2 Photograph of EFV in water and examples of EFV encapsulated nanoparticles (*p*(HPMA$_{50}$-*co*-EGDMA$_{0.9}$):*p*(PEG$_{114}$-*b*-HPMA$_{120}$) (50:50 wt %)), i) EFV in H_2O, ii) 1 wt %, iii) 2 wt %, iv) 5 wt % EFV.

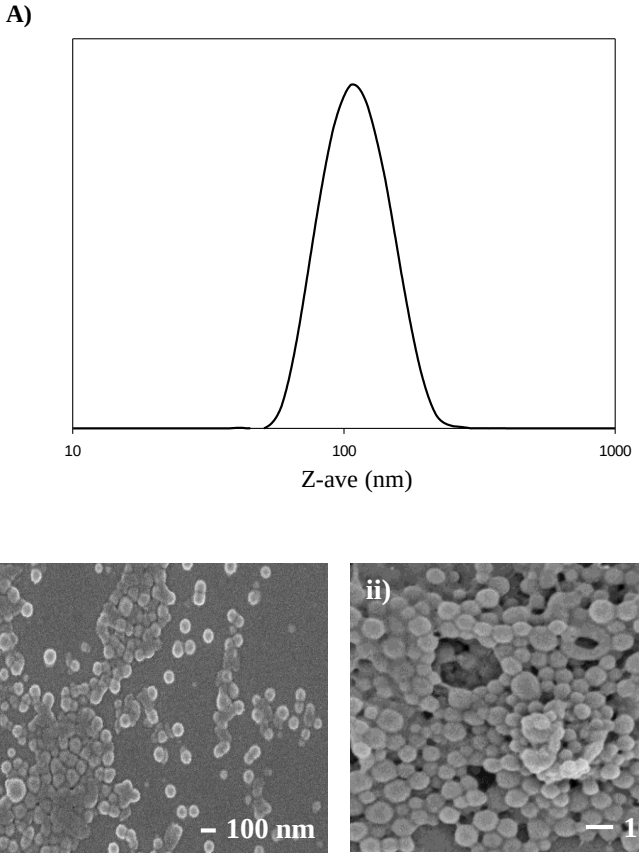

Figure 4.3 A) DLS trace for 9 wt % EFV encapsulated *p*(HPMA$_{50}$-*co*-EGDMA$_{0.9}$):*p*(PEG$_{114}$-*b*-HPMA$_{120}$) 50:50 wt %. B) SEM imagining for 9 wt % encapsulated EFV *p*(HPMA$_{50}$-*co*-EGDMA$_{0.9}$):*p*(PEG$_{114}$-*b*-HPMA$_{120}$) 50:50 wt %, i) nanoparticles after 24 hours, ii) nanoparticles >1 month.

The branched copolymers *p*(*n*-BMA$_{50}$-*co*-EGDMA$_{0.8}$), *p*(*t*-BMA$_{50}$-*co*-EGDMA$_{0.9}$), and terpolymers *p*(HPMA$_{25}$-*co*-*n*-BMA$_{25}$-EGDMA$_{0.9}$), *p*(HPMA$_{25}$-*co*-*t*BMA$_{25}$-*co*-EGDMA$_{0.9}$), were also subject to encapsulation experiments. Interestingly, the co-nanoprecipitation of *p*(*n*-BMA$_{50}$-*co*-EGDMA$_{0.8}$):*p*(PEG$_{114}$-*b*-HPMA$_{120}$) 50:50 wt %, resulted in a 25 wt % loading of EFV, and although there was an increase in the size and PdI values during DLS re-analysis after 3 days, there were no visible signs of polymer/drug macro-phase separation and precipitation.

As previously discussed in Chapter 3, the co-nanoprecipitation studies of *p*(*t*-BMA$_{50}$-*co*-EGDMA$_{0.9}$):*p*(PEG$_{114}$-*b*-HPMA$_{120}$) 50:50 wt %, resulted in polymer nanoparticles with large size and broad PdI values. To determine if the co-nanoprecipitation of branched *p*(*t*-BMA$_{50}$-*co*-EGDMA$_{0.9}$) could yield stable EFV loaded nanoparticles, an encapsulation experiment of 5 wt % was carried out. As shown in Table 4.1 compared to the blank nanodispersion, the size and PdI values increased and after a few hours fine precipitate was observed. Due to these poor encapsulation results, branched *p*(*t*-BMA$_{50}$-*co*-EGDMA$_{0.9}$) was not studied further.

The co-nanoprecipitation studies of blank and EFV encapsulated *p*(HPMA$_{25}$-*co*-*n*-BMA$_{25}$-EGDMA$_{0.9}$):*p*(PEG$_{114}$-*b*-HPMA$_{120}$) (50:50 wt %), yielded nanoparticles with sizes <180 nm and narrow PdI values from each loading experiment. The highest encapsulation of EFV was 20 wt % and a small decrease in size and a narrow PdI was observed after 3 days. Interestingly, *p*(HPMA$_{25}$-*co*-*t*-BMA$_{25}$-*co*-EGDMA$_{0.9}$):*p*(PEG$_{114}$-*b*-HPMA$_{120}$) 50:50 wt % had a loading capability of 25 wt % and were also stable after the 3 day re-analysis.

The DLS analyses of the co-nanoprecipitation studies for the highest loading of EFV are presented in Figure 4.4 and narrow monomodal peaks are observed for all three loaded co-nanodispersions. Overall, the branched co/terpolymers which encapsulated the highest wt % of EFV were *p*(*n*-BMA$_{50}$-*co*-EGDMA$_{0.8}$) and *p*(HPMA$_{25}$-*co*-*t*BMA$_{25}$-*co*-EGDMA$_{0.9}$) with 25 wt % relative to total polymer content.

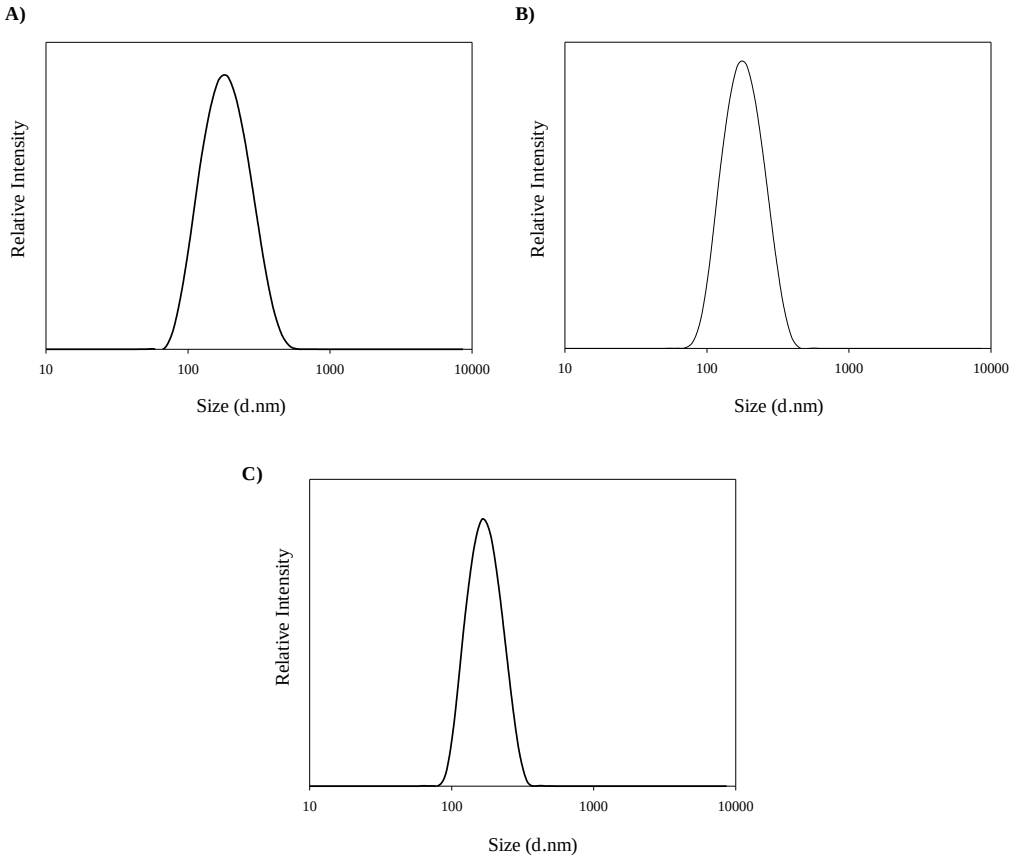

Figure 4.4 DLS analysis of co-nanoprecipitated nanoparticles for highest wt % encapsulation of EFV (25wt %), A) *p*(*n*-BMA$_{50}$-*co*-EGDMA$_{0.8}$):*p*(PEG$_{114}$-*b*-HPMA$_{120}$) 50:50 wt %, B) *p*(HPMA$_{25}$-*co*-*n*-BMA$_{25}$-*co*-EGDMA$_{0.9}$):*p*(PEG$_{114}$-*b*-HPMA$_{120}$) 50:50 wt %, C) *p*(HPMA$_{25}$-*co*-*t*-BMA$_{25}$-*co*-EGDMA$_{0.9}$):*p*(PEG$_{114}$-*b*-HPMA$_{120}$) 50:50 wt %.

4.2.2 Encapsulation of RTV *via* co-nanoprecipitation

The same experiments as described above for EFV, were carried out for the HIV anti-retroviral RTV. Although clinically administered as a dual therapy, it was important to determine if the encapsulation of RTV in the absence of another drug molecule was feasible. The encapsulation studies for varying branched co/terpolymers are shown in Table 4.2 and the optimum wt % loading is highlighted. Interestingly, *p*(HPMA$_{50}$-*co*-EGDMA$_{0.9}$) demonstrated a higher loading capability with RTV when compared to the encapsulation of EFV. The highest loading capability observed was through encapsulation using the branched copolymer, *p*(*n*-BMA$_{50}$-*co*-EGDMA$_{0.8}$). 20 wt % loading was achieved with *p*(HPMA$_{25}$-*co*-*n*-BMA$_{25}$-*co*-EGDMA$_{0.9}$) and *p*(HPMA$_{25}$-*co*-*t*-BMA$_{25}$-*co*-EGDMA$_{0.9}$), without polymer and/or drug precipitation observed after ~24 hours, therefore, an optimum loading for both branched terpolymers was 20 wt % RTV.

Table 4.2 DLS analysis of RTV encapsulated nanoparticles prepared *via* co-nanoprecipitation.

Branched co/terpolymer:*p*(PEG$_{114}$-*b*-HPMA$_{120}$) 50:50 wt %	**Ritonavir (wt%)**	**Z-ave (d.nm)**	**PdI**	**D_n (nm)**	**Z-ave (d.nm) / PdI After 3 days**
p(HPMA$_{50}$-*co*-EGDMA$_{0.9}$)	Blank	111	0.081	112	-
	1	94	0.067	71	-
	4	108	0.057	83	-
	8	123	0.074	95	122 (0.055)
	10	128	0.073	100	128 (0.084)
	15	124	0.085	101	116 (0.051)
	17	121	0.132	90	118 (0.179)
	20	131	0.228	85	X
p(*n*-BMA$_{50}$-*co*-EGDMA$_{0.8}$)	Blank	205	0.088	170	-
	10	242	0.236	158	-
	17	244	0.218	137	-
	20	329	0.250	216	338 (0.333)
	25	143	0.170	100	142 (0.102)
p(HPMA$_{25}$-*co*-*n*-BMA$_{25}$-EGDMA$_{0.9}$)	Blank	161	0.085	125	-
	10	150	0.084	120	148 (0.092)
	17	185	0.083	147	-
	20	141	0.072	109	140 (0.079)
	25	127	0.132	87	133 (0.106)
p(HPMA$_{25}$-*co*-*t*-BMA$_{25}$-EGDMA$_{0.9}$)	Blank	161	0.066	131	-
	10	152	0.077	117	149 (0.079)
	17	130	0.087	97	-
	20	123	0.062	99	123 (0.111)
	25	87	0.047	67	92 (0.116)

Overall, the formulation of co-nanoprecipitated nanoparticles composed of *p*(*n*-BMA$_{50}$-*co*-EGDMA$_{0.8}$) and *p*(PEG$_{114}$-*b*-HPMA$_{120}$) 50:50 wt %, demonstrated the highest loading capability with RTV when compared with nanoparticles formed from the alternative branched co/terpolymers. The DLS results for highest encapsulation (wt %) are presented in Figure 4.5, again highlighting one monomodal population for each nanodispersion.

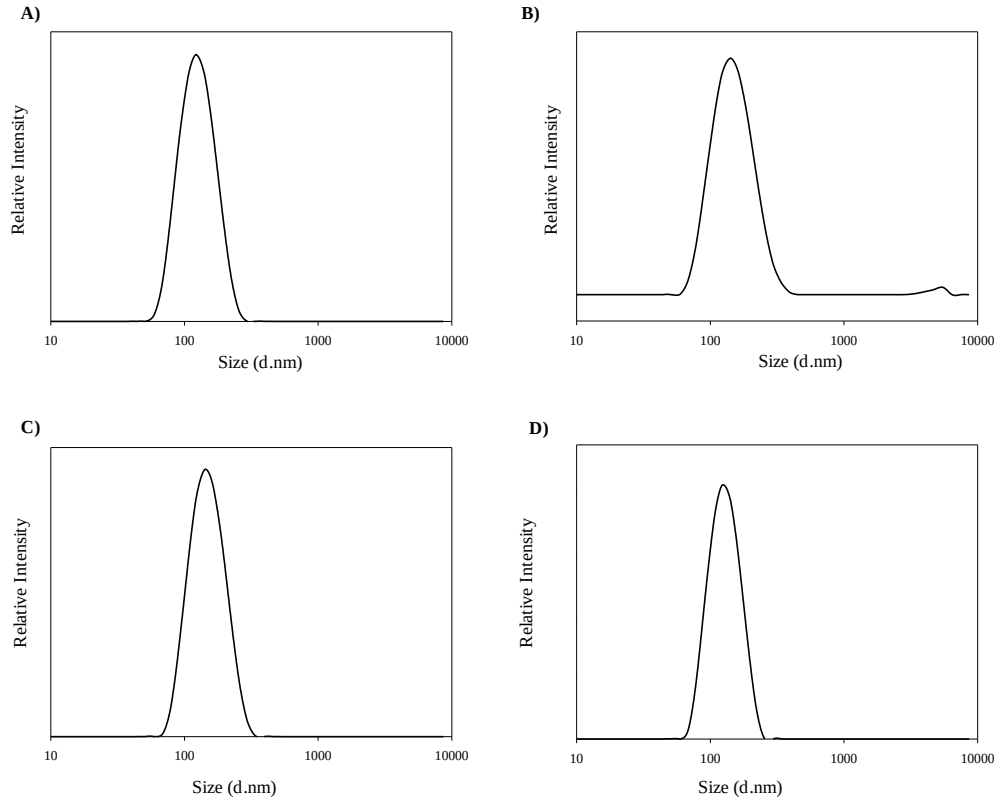

Figure 4.5 DLS analysis of co-nanoprecipitated particles for highest wt % encapsulation of RTV, A) 17wt % RTV + *p*(HPMA$_{50}$-*co*-EGDMA$_{0.9}$):*p*(PEG$_{114}$-*b*-HPMA$_{120}$) 50:50 wt %, B) 25 wt % RTV + *p*(*n*-BMA$_{50}$-*co*-EGDMA$_{0.8}$):*p*(PEG$_{114}$-*b*-HPMA$_{120}$) 50:50 wt %, C) 20 wt % RTV + *p*(HPMA$_{25}$-*co*-*n*-BMA$_{25}$-*co*-EGDMA$_{0.9}$):*p*(PEG$_{114}$-*b*-HPMA$_{120}$) 50:50 wt %, D) 20 wt % RTV + *p*(HPMA$_{25}$-*co*-*t*-BMA$_{25}$-*co*-EGDMA$_{0.9}$):*p*(PEG$_{114}$-*b*-HPMA$_{120}$) 50:50 wt %.

4.2.3 Encapsulation of LPV *via* co-nanoprecipitation

The final HIV anti-retroviral drug molecule encapsulated within varying branched co/terpolymer and A-B block copolymers was LPV. The DLS analysis of the co-nanoprecipitated encapsulated particles is presented in Table 4.3. During the co-nanoprecipitation of LPV and *p*(HPMA$_{50}$-*co*-EGDMA$_{0.9}$):*p*(PEG$_{114}$-*b*-HPMA$_{120}$) 50:50 wt %, an optimum loading of 10 wt % was observed. The behaviour during LPV encapsulation would be expected to be similar to RTV (17 wt % loading), due to the structural similarities between the drug molecules. However, the wt % loading of LPV was similar to that of EFV, which is surprising considering the dissimilarity between the drug molecules. The optimum loading appears to lie between 10-15 wt %, as precipitation of polymer/drug was observed (as also seen for EFV encapsulation). For the branched copolymer, *p*(*n*-BMA$_{50}$-*co*-EGDMA$_{0.8}$), and terpolymers, *p*(HPMA$_{25}$-*co*-*n*-BMA$_{25}$-*co*-EGDMA$_{0.9}$) and *p*(HPMA$_{25}$-*co*-*t*-BMA$_{25}$-*co*-EGDMA$_{0.9}$), 20 wt % encapsulation was

achieved. Although there was a slight increase observed in PdI for both *p*(*n*-BMA$_{50}$-*co*-EGDMA$_{0.8}$) and *p*(HPMA$_{25}$-*co*-*n*-BMA$_{25}$-*co*-EGDMA$_{0.9}$), the polymer and drug molecules did not appear to precipitate. The lowest PdI value was obtained for the co-nanoprecipitation of *p*(HPMA$_{25}$-*co*-*t*-BMA$_{25}$-*co*-EGDMA$_{0.9}$):*p*(PEG$_{114}$-*b*-HPMA$_{120}$) 50:50 wt %, LPV (20 wt %), and a size decrease from 161 to 108 nm was observed when compared with the blank sample, suggesting the presence of LPV resulted in the formation of smaller nanoparticles. The narrow monomodal size distributions for the nanoparticles which achieved the highest encapsulation capabilities are shown in Figure 4.6.

Table 4.3 DLS analysis of LPV encapsulated nanoparticles prepared *via* co-nanoprecipitation.

Branched co/terpolymer:*p*(PEG$_{114}$-*b*-HPMA$_{120}$) 50:50 wt %	**Lopinavir (wt%)**	**Z-ave (d.nm)**	**PdI**	**D_n (nm)**	**Z-ave (d.nm) / PdI After 3 days**
p(HPMA$_{50}$-*co*-EGDMA$_{0.9}$)	Blank	111	0.081	112	-
	1	112	0.075	84	-
	2	104	0.068	78	-
	4	102	0.064	80	-
	8	135	0.139	91	128 (0.108)
	10	130	0.124	96	131 (0.100)
	15	155	0.493	79	155 (0.493)
p(*n*-BMA$_{50}$-*co*-EGDMA$_{0.8}$)	Blank	205	0.088	170	-
	15	227	0.108	179	224 (0.114)
	20	191	0.154	134	200 (0.154)
p(HPMA$_{25}$-*co*-*n*-BMA$_{25}$-EGDMA$_{0.9}$)	Blank	161	0.085	125	-
	15	137	0.063	109	137 (0.088)
	20	125	0.114	84	140 (0.200)
p(HPMA$_{25}$-*co*-*t*-BMA$_{25}$-EGDMA$_{0.9}$)	Blank	161	0.066	131	-
	15	166	0.060	134	165 (0.071)
	20	108	0.062	87	112 (0.062)

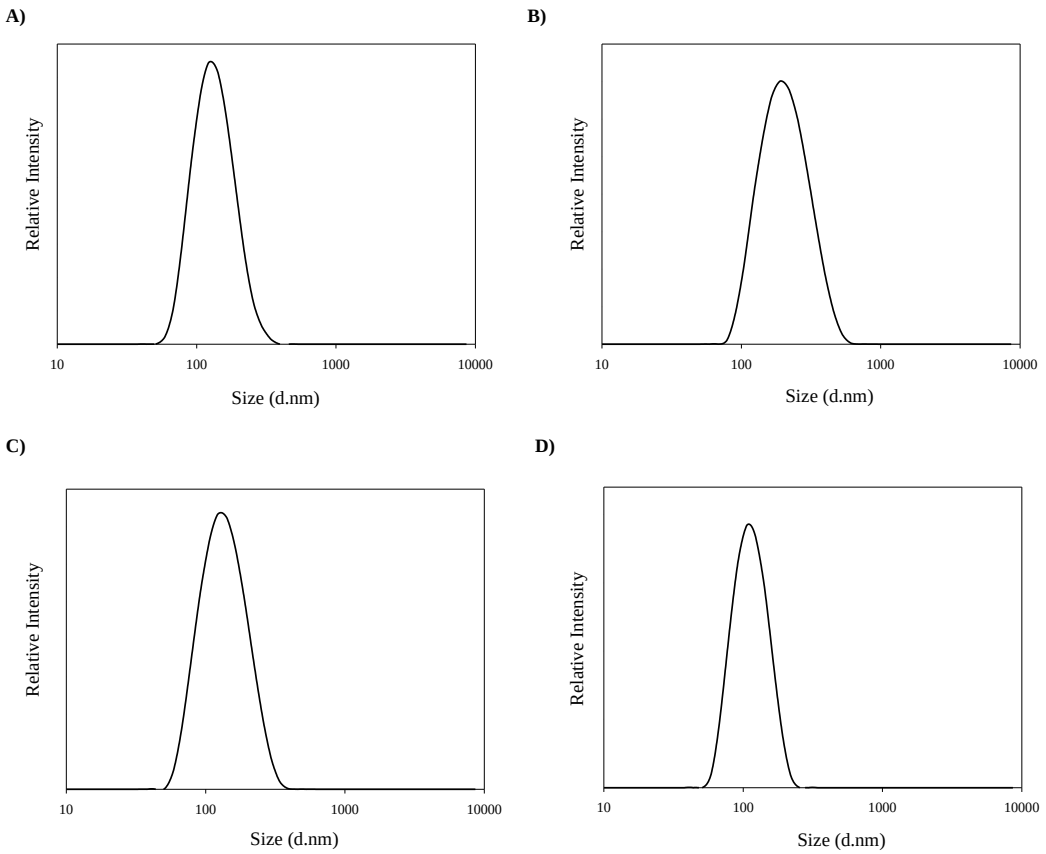

Figure 4.6 DLS analysis for highest loaded LPV nanoparticles, A) 10wt % LPV + *p*(HPMA$_{50}$-*co*-EGDMA$_{0.9}$):*p*(PEG$_{114}$-*b*-HPMA$_{120}$) 50:50 wt %, B) 20 wt % LPV + *p*(*n*-BMA$_{50}$-*co*-EGDMA$_{0.8}$):*p*(PEG$_{114}$-*b*-HPMA$_{120}$) 50:50 wt %, C) 20 wt % LPV + *p*(HPMA$_{25}$-*co*-*n*-BMA$_{25}$-*co*-EGDMA$_{0.9}$):*p*(PEG$_{114}$-*b*-HPMA$_{120}$) 50:50 wt %, D) 20 wt % LPV + *p*(HPMA$_{25}$-*co*-*t*-BMA$_{25}$-*co*-EGDMA$_{0.9}$):*p*(PEG$_{114}$-*b*-HPMA$_{120}$) 50:50 wt %.

Overall, the co-nanoprecipitation method incorporating the branched co/terpolymers *p*(*n*-BMA$_{50}$-*co*-EGDMA$_{0.8}$), *p*(HPMA$_{25}$-*co*-*n*-BMA$_{25}$-*co*-EGDMA$_{0.9}$) and *p*(HPMA$_{25}$-*co*-*t*-BMA$_{25}$-*co*-EGDMA$_{0.9}$) gave a high loading of 20 wt % LPV. A summary of the results for the highest encapsulation (wt %) for the co-nanoprecipitated particles within this chapter are presented in Table 4.4. Interestingly, the branched copolymer *p*(*n*-BMA$_{50}$-*co*-EGDMA$_{0.8}$) demonstrated the highest wt % encapsulation for each hydrophobic drug molecule. As discussed, this may be due to the increased hydrophobicity of this particular polymer, as although the other co/terpolymers are insoluble in water, they contain HPMA monomer units, which have a hydrophilic nature. The blank co-nanoprecipitates containing *p*(*n*-BMA$_{50}$-*co*-EGDMA$_{0.8}$), *p*(HPMA$_{25}$-*co*-*n*-BMA$_{25}$-*co*-EGDMA$_{0.9}$) and *p*(HPMA$_{25}$-*co*-*t*-BMA$_{25}$-*co*-EGDMA$_{0.9}$) and the A-B block copolymer *p*(PEG$_{114}$-*b*-HPMA$_{120}$) 50:50 wt %, were generally larger than those comprising of the branched

copolymer *p*(HPMA$_{50}$-*co*-EGDMA$_{0.9}$), which could suggest there is a relationship between size and encapsulation wt % and further investigation into varying chemical compositions would be required to confirm this.

Table 4.4 Summary of loading capabilities for anti-retroviral encapsulated co-nanoprecipitated particles consisting of a branched co/terpolymer and *p*(PEG$_{114}$-*b*-HPMA$_{120}$) 50:50 wt %.

HIV Antiretroviral	Wt %	Polymer Composition (50:50 wt%)
Efavirenz	25	*p*(*n*-BMA$_{50}$-*co*-EGDMA$_{0.8}$):*p*(PEG$_{114}$-*b*-HPMA$_{120}$) *p*(HPMA$_{25}$-*co*-*t*-BMA$_{25}$-*co*-EGDMA$_{0.9}$):*p*(PEG$_{114}$-*b*-HPMA$_{120}$)
Ritonavir	25	*p*(*n*-BMA$_{50}$-*co*-EGDMA$_{0.8}$):*p*(PEG$_{114}$-*b*-HPMA$_{120}$)
Lopinavir	20	*p*(*n*-BMA$_{50}$-*co*-EGDMA$_{0.8}$):*p*(PEG$_{114}$-*b*-HPMA$_{120}$) *p*(HPMA$_{25}$-*co*-*n*-BMA$_{25}$-*co*-EGDMA$_{0.9}$):*p*(PEG$_{114}$-*b*-HPMA$_{120}$) *p*(HPMA$_{25}$-*co*-*t*-BMA$_{25}$-*co*-EGDMA$_{0.9}$):*p*(PEG$_{114}$-*b*-HPMA$_{120}$)

For encapsulation of drug molecules within polymer nanoparticles, it is useful to consider the hydrophobicity (lipophilicity) of both the drug molecule and polymer. The logP (partition coefficient) is a measure of a drug's hydrophobicity and reflects the relative solubility of a drug in octanol (representing the lipid bilayer of a cell membrane) and water. LogP values may be measured experimentally or, more commonly calculated. The logP values reported within the literature varied between 3.8-4.6 for EFV,[13, 14] 5.98-6.63[15, 16] for RTV and 4.56[17] for LPV. Due to the variation of experimentally determined logP values for drugs investigated, a prediction-based approach was used to obtain the logP values. The Molinspiration property engine[18] was used to calculate the logP values (clogP) for EFV, RTV and LPV and oligomers consisting of 3 monomer repeat units for *p*(HPMA), *p*(*n*-BMA) and *p*(*t*-BMA), see Table 4.5.

Although the clogP values used to assess the environment within the branched polymers are not a true representation of each DP$_{50}$ polymer, they can provide a measure of the differences in hydrophobicity. In terms of the anti-retroviral drugs, the clogP values suggest that RTV has the highest lipophilicity and EFV the least, yet the highest loading of 25 wt % was observed for both RTV and EFV. This suggests that although there are differences between the calculated clogP values for the anti-retroviral drugs, it may be

that the chemical differences between the polymers has a greater effect on the loading capacity. As expected, *p*(*n*-BMA) has a higher clogP than *p*(HPMA), due to the chemical differences between the monomers. This difference is reflected in the loading capacities, as a consistently higher loading is observed when *p*(*n*-BMA_{50}-*co*-$EGDMA_{0.8}$) is included within the co-nanoprecipitation for each anti-retroviral. Although sufficient encapsulation was achieved, addition of *p*($HPMA_{50}$-*co*-$EGDMA_{0.9}$) resulted in a lower wt % of EFV and LPV when compared with the other branched polymers. However, for RTV, a 17 wt % loading was observed, and in terms of differences in clogP values this may not be expected as RTV has the highest clogP (7.51) and HPMA is calculated to have a much lower lipophilicity (clogP = 2.56). For the co-nanoprecipitation experiments which included the terpolymers, high levels of loading were achieved, which may be due to the presence of an increasingly hydrophobic monomer; either *n*-BMA or *t*-BMA. It is worth nothing that the evaluation of the branched co/terpolymers and anti-retrovirals presented here is based on calculated clogP values and structural differences between the polymers to rationalise the wt % capabilities.

Table 4.5 Calculation of logP values for HIV drug molecules and polymers.

	logP*
EFV	4.53
RTV	7.51
LPV	5.69
p($HPMA_3$)	2.56
p(*n*-BMA_3)	7.69
p(*t*-BMA_3)	6.93

*Molinspiration property engine determination of logP.

4.3 Conclusion

To conclude, the formation of anti-retroviral encapsulated nanoparticles *via* the co-nanoprecipitation approach has been successfully achieved and the loading capabilities have been investigated. The variation of the branched co/terpolymers throughout this co-nanoprecipitation study, gave rise to different loading capabilities for each anti-retroviral. Therefore, the hydrophobicity and structural differences of the branched co/terpolymers were taken into consideration and logP values were calculated to rationalise the nanoparticle behaviour in the presence of the anti-retrovirals. During inclusion of the

branched copolymer *p*(*n*-BMA$_{50}$-*co*-EGDMA$_{0.8}$), a consistent high loading was achieved and up to 25 wt % was observed for both EFV and RTV. Generally the higher loading capabilities were achieved when the monomeric unit of the branched co/terpolymers were composed of solely *n*-BMA or partly *n*-BMA and *t*-BMA monomeric units. The co-nanoprecipitation process has provided a fast and efficient route to produce stable anti-retroviral encapsulated nanoparticles, without the need for filtration or the presence of surfactants in the anti-solvent. Further studies are required to investigate stability and drug release from the nanoparticles, as well as pharmacology testing to assess their suitability *in vitro*.

4.4 References

1. A. Mocroft and J. D. Lundgren, *Journal of Antimicrobial Chemotherapy*, 2004, **54**, 10-13.
2. E. De Clercq, *Antiviral Research*, 1998, **38**, 153-179.
3. E. De Clercq, *Journal of Clinical Virology*, 2004, **30**, 115-133.
4. C. Merry, M. G. Barry, F. Mulcahy, M. Ryan, J. Heavey, J. F. Tjia, S. E. Gibbons, A. M. Breckenridge and D. J. Back, *AIDS*, 1997, **11**, F29-F33.
5. R. A. Murphy, V. C. Marconi, R. T. Gandhi, D. R. Kuritzkes and H. Sunpath, *PLoS ONE*, 2012, **7**, e44793.
6. A. Shibata, E. McMullen, A. Pham, M. Belshan, B. Sanford, Y. Zhou, M. Goede, A. A. Date and C. J. Destache, *AIDS Research and Human Retroviruses*, 2013, **29**, 746-754.
7. C. J. Destache, T. Belgum, K. Christensen, A. Shibata, A. Sharma and A. Dash, *BMC Infectious Diseases*, 2009, **9**, 198-206.
8. P. R. Ravi, R. Vats, V. Dalal, N. Gadekar and A. N, *Drug Development and Industrial Pharmacy*, 2013, **41**, 131-140.
9. J. das Neves, F. Araújo, F. Andrade, J. Michiels, K. K. Ariën, G. Vanham, M. Amiji, M. F. Bahia and B. Sarmento, *Molecular Pharmaceutics*, 2013, **10**, 2793-2807.
10. L. K. Shah and M. M. Amiji, *Pharmaceutical Research*, 2006, **23**, 2638-2645.
11. K. P. Seremeta, D. A. Chiappetta and A. Sosnik, *Colloids and Surfaces B: Biointerfaces*, 2013, **102**, 441-449.
12. D. A. Chiappetta, C. Hocht, C. Taira and A. Sosnik, *Nanomedicine*, 2009, **5**, 11-23.
13. T. Chaowanachan, E. Krogstad, C. Ball and K. A. Woodrow, *PLOS ONE*, 2013, **8**, e61416.
14. http://www.drugbank.ca/drugs/db00625 accessed September, 2015,
15. J. A. Baird, B. Van Eerdenbrugh and L. S. Taylor, *Journal of Pharmaceutical Sciences*, 2010, **99**, 3787-3806.
16. S. Sirois, C. Tsoukas, K.-C. Chou, D. Wei, C. Boucher and G. Hatzakis, *Medicinal Chemistry*, 2005, **1**, 173-184.
17. K. Patel, P. Kumar and H. Thakkar, *AAPS PharmSciTech*, 2012, **13**, 1502-1510.
18. http://www.molinspiration.com/docu/mipc/index.html accessed September, 2015,

Chapter 5

Co-nanoprecipitation:

Encapsulation of the Anti-Cancer Drug

SN-38

5.1 Introduction

Cancer is a leading cause of death worldwide and the number of new cases is expected to rise by ~70 % during the next two decades, according to the World Health Organisation.[1] One of the most common treatments for cancer is systemic chemotherapy, however, a high drug concentration in target tissues is required to achieve a therapeutic effect, which frequently results in broad toxicity. During the last few decades, the preparation of drug loaded nanocarriers, including polymeric nanoparticles, liposomes, dendrimers and micelles, have provided promising options to overcome systemic toxicity, stability issues and poor aqueous solubility of anti-cancer drugs.[2] The encapsulation of chemotherapeutic drug molecules into nanocarriers offers many advantages when compared with current delivery methods of chemotherapeutic molecules. Firstly, many anti-cancer drug molecules are hydrophobic and only solubilise when added to solvents such as ethanol or DMSO, which at high concentrations are highly toxic to cells. Therefore, the incorporation of drug molecules into polymeric nanocarriers could potentially enhance the apparent aqueous solubility and would not require additional solvents. Secondly, as described in Chapter 1 Section 1.5.1, nanocarriers are passively targeted to tumours *via* the EPR effect, resulting in a higher concentration at the tumour site and decreased toxicity in healthy tissues.[3] The use of nanocarriers or polymer-drug conjugates for the loading of chemotherapeutic molecules, can also provide an increased bioavailability when compared with administration of free drug molecules which are rapidly eliminated by the liver and/or kidneys.[4, 5]

Camptothecin-11, commonly known as irinotecan (IR), is an anti-cancer chemotherapy drug used for the treatment of metastatic colon or rectal cancer, and was approved by the FDA in 1998. IR inhibits the enzyme topoisomerase I, which is an enzyme involved in DNA replication and RNA transcription. 7-ethyl-10-hydroxyl camptothecin (SN-38) is the active metabolite of IR (Figure 5.1) and is 100-1000 more active than IR. After intravenous administration, unfortunately, only 1–9% of an injected dose of IR is converted to SN-38 in humans.[6] However, the clinical applications of SN-38 have been limited due to its very poor solubility in aqueous solutions and in most pharmaceutically accepted solvents.[7]

The preparation of SN-38 drug delivery nanocarriers is fairly limited due to the hydrophobic nature of SN-38. Recent research which has aimed to increase the aqueous solubility of SN-38 has described the preparation of PEG_x-SN-38 polymer drug

conjugates. Zhang *et al* reported the attachment of a low molecular weight PEG chain (480 g/mol) to SN-38 in a four step synthesis to form an oligoethylene glycol-SN-38 prodrug (OEG-SN-38), and subsequent preparation of polymeric micelles (~29 nm) with a loading of up to 36 wt % of SN-38.[8] A PEG-SN-38 polymer drug conjugate which has progressed to Phase I clinical trial is EZN-2208 which has a reported loading of 3.7% SN-38. The studies of EZN-2208 have been taken forward due to potent *in vitro* cytotoxicity against human cell lines and excellent anti-tumour activity in xenograft models of human breast, colorectal and pancreatic cancers.[9, 10]

Irinotecan **SN-38**

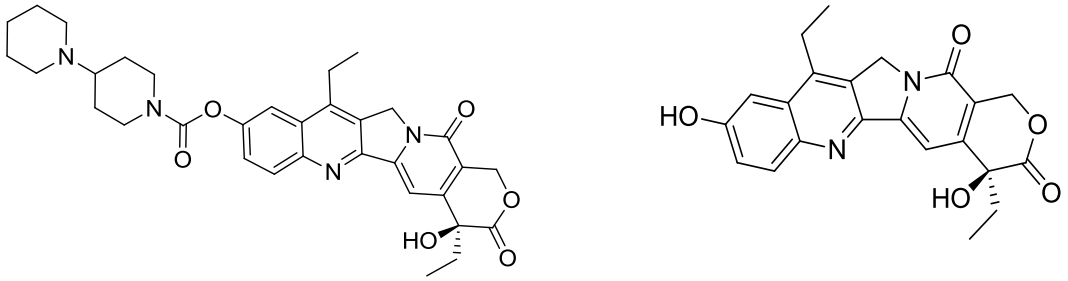

Figure 5.1 Chemical structures of irinotecan and SN-38.

There are also alterative reports to the PEG_x-SN38 pro-drug approach, which describe the loading of free SN-38 into nanocarriers. For example, Gu *et al* described the preparation of micelles, *via* a modified thin film hydration method, which were composed of Pluronic F-108 and PEG_x-*b*-PCL (~125 nm), with an estimated drug loading of 20 wt % of SN-38.[11] Also, recently published reports have described the formation of SN-38 encapsulated polymeric nanoparticles *via* the emulsification solvent evaporation technique. The nanoparticles were prepared from PLGA (using a PVA stabiliser), with an average diameter of ~ 170 nm and a drug loading of ~5 wt % SN-38.[6] Although current research towards SN-38 drug delivery has progressed during recent years, it was of interest to utilise the co-nanoprecipitation approach described throughout this thesis to investigate the encapsulation of SN-38 into nanoparticles consisting of a branched co/terpolymer and an A-B block copolymer.

5.2 Preparation of aqueous nanoparticles and encapsulation of SN-38

As discussed, SN-38 has very limited solubility in water and most biologically acceptable solvents. In order to conduct a nanoprecipitation experiment, both the polymer and drug molecule must completely solubilise in the 'good' solvent. During the initial stages of the research, the solubility of SN-38 was limited to dimethyl sulfoxide (DMSO) (Table 5.1) as this was the only single solvent found to generate useable concentrations. The ^{1}H NMR analysis of SN-38 is presented in the Appendix, Fig. A30, and the integration values obtained for all proton environments were as expected.

Table 5.1 Solubility of SN-38 in commercially available solvents (~1 mg/mL).

Solvent	Solubility
H_2O	X
Dichloromethane	X
Methanol	X
Chloroform	X
Ethanol	X
Ethyl acetate	X
Diethyl ether	X
Acetonitrile	X
Tetrahydrofuran	X
Acetone:Dichloromethane:Methanol 1:1:1	X
Acetone:H_2O 1:1	X
DMSO	✓

5.2.1 Preparation of SN-38 encapsulated particles *via* dialysis

For solvents with high boiling points, such as DMSO (189°C), solvent removal after nanoparticle formation can be difficult if the dropping-evaporation technique is employed. Therefore, co-nanoprecipitation *via* dialysis was considered, as discussed in Chapter 1, Section 1.3.3. The branched copolymer *p*(HPMA$_{50}$-*co*-EGDMA$_{0.9}$), A-B block copolymer *p*(PEG$_{114}$-*b*-HPMA$_{120}$) and SN-38 were all readily soluble in DMSO at the concentrations

required for the nanoprecipitation. During the dialysis experiment, SN-38 (5 wt % to total polymer mass), *p*(HPMA$_{50}$-*co*-EGDMA$_{0.9}$) and *p*(PEG$_{114}$-*b*-HPMA$_{120}$) were dissolved in DMSO at 5 mg/mL for 12-24 hours to ensure complete solubilisation. The stock solution of polymers and SN-38 (1 mL) was added to the dialysis bag with a molecular weight cut off (MWCO) of 2000 g/mol, containing 5 mL of water. After four days and regular water changes, the aqueous solution within the dialysis membrane was isolated and analysed by DLS. The size by intensity trace shows a multimodal size distribution for the SN-38 encapsulated nanoparticles (Figure 5.3Ai). The presence of large particles (though few) in the nanodispersion can distort the size intensity distribution to produce an inaccurate representation of the particle sizes present. It is, therefore, important to take into

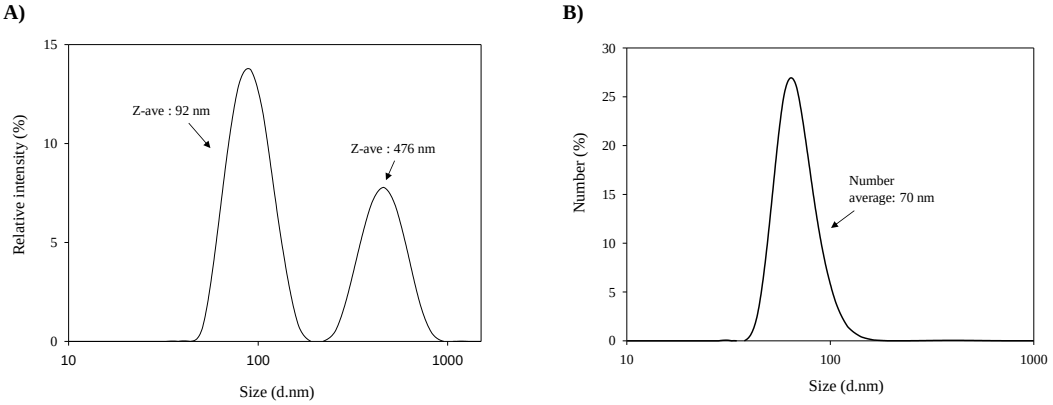

consideration the number distribution and number average diameter D_n (Figure 5.3Bi), which provides a description of relative concentration of particles of each size. Unfortunately, after 24 hours, the sample was no longer colloidally stable and polymer/SN-38 precipitate was visible.

Figure 5.3 DLS traces of polymer nanoparticles prepared *via* the dialysis method, 5 wt % SN-38, *p*(HPMA$_{50}$-*co*-EGDMA$_{0.9}$):*p*(PEG$_{114}$-*b*-HPMA$_{120}$) 50:50 wt %, A) size by intensity, B) size by number.

5.2.2 Preparation of SN-38 encapsulated nanoparticles *via* co-nanoprecipitation

Fortunately, after exploring additional mixed solvent systems, a 1:1 ratio of tetrahydrofuran and acetonitrile (THF:ACN) completely solubilised SN-38 (1 mg/mL), after 4-6 hours. The branched co/terpolymers and A-B block copolymers were also soluble in the mixed solvent (THF:ACN 1:1), and the relatively low boiling points were ideal for fast and easy removal during the co-nanoprecipitation/evaporation experiments. Therefore, the dropping technique was reconsidered, and experiments were conducted as described for the encapsulation of fluoresceinamine in Chapter 3, and HIV anti-retrovirals in Chapter 4.

Nanoparticle dispersions were prepared from a 5 mg/mL polymer solution with SN-38 (0.105 mg/mL, 2 wt %) or (0.265 mg/mL, 5 wt %) and added to 5 mL of water to give a final aqueous concentration of 1 mg/mL polymer and either 0.021 or 0.053 mg/mL of SN-38. For the initial nanoprecipitation experiments, the following SN-38 encapsulated co-nanoprecipitated particles were targeted; *p*(HPMA$_{50}$-*co*-EGDMA$_{0.9}$):*p*(PEG$_{114}$-*b*-HPMA$_{120}$), *p*(*n*-BMA$_{50}$-*co*-EGDMA$_{0.8}$):*p*(PEG$_{114}$-*b*-HPMA$_{120}$), *p*(HPMA$_{25}$-*co*-*t*-BMA$_{25}$-*co*-EGDMA$_{0.9}$):*p*(PEG$_{114}$-*b*-HPMA$_{120}$) (all 50:50 wt %) and 2 wt % SN-38 and *p*(*n*-BMA$_{50}$-*co*-EGDMA$_{0.8}$):*p*(PEG$_{114}$-*b*-HPMA$_{120}$) 50:50 wt % and 5 wt % SN-38 wt %. The polymers and SN-38 were dissolved in THF:ACN 1:1 for 48 hours, before addition to water. After nanoprecipitation and complete evaporation of good solvent, non-homogeneous nanodispersions and a very fine precipitate was observed during inclusion of *p*(HPMA$_{50}$-*co*-EGDMA$_{0.9}$) (2 wt % SN-38) and *p*(*n*-BMA$_{50}$-*co*-EGDMA$_{0.8}$) (5 wt % SN-38). The DLS analysis reflected this and for *p*(HPMA$_{50}$-*co*-EGDMA$_{0.9}$), inadequate scattering data and broad PdI values were obtained (Appendix, Table A10). Although precipitate was visible for two of the samples, the dropping technique was not ruled out for the preparation of SN-38 encapsulated nanoparticles, as further investigation of experimental conditions was required.

To further investigate the nanoprecipitation conditions, stock solutions of branched co/terpolymers polymers *p*(HPMA$_{50}$-*co*-EGDMA$_{0.9}$), *p*(*n*-BMA$_{50}$-*co*-EGDMA$_{0.8}$), *p*(HPMA$_{25}$-*co*-*t*-BMA$_{25}$-*co*-EGDMA$_{0.9}$) with *p*(PEG$_{114}$-*b*-HPMA$_{120}$) (50:50 wt %) and SN-38 (5 wt %) were left to solubilise for 5 weeks (roller) to evaluate if a longer solubilisation time could yield stable nanoparticles. The results for these experiments are shown in Table 5.2 and Figure 5.4.

Table 5.2 DLS results for 5 wt % encapsulated co-nanoprecipitated particles.

Sample (50:50 wt %)	**Size (d.nm)**	**PdI**
p(*n*-BMA$_{50}$-*co*-EGDMA$_{0.8}$):*p*(PEG$_{114}$-*b*-HPMA$_{120}$)	145	0.112
p(HPMA$_{50}$-*co*-EGDMA$_{0.9}$):*p*(PEG$_{114}$-*b*-HPMA$_{120}$)	94	0.076
p(*t*-BMA$_{25}$-*co*-HPMA$_{25}$-*co*-EGDMA$_{0.9}$):*p*(PEG$_{114}$-*b*-HPMA$_{120}$)	118	0.085

Interestingly, the nanoparticles formed were within a reasonable size range with narrow PdI values, and no precipitate was visible within the samples. The longer solubilisation time for the stock solution had clearly affected the co-nanoprecipitation process as stable nanoparticles were produced. It is also worth considering other factors such as temperature, which could have also effected the nanoprecipitation process although this was not studied. The nanoprecipitates showed slight deviations in size when compared with the blank (no SN-38) nanoparticles, see Figure 5.5; the corresponding PdI values are shown in the Appendix, Table A11. The DLS results for the various batches of SN-38 nanoparticles prepared throughout this study are presented in the Appendix, Table A12 and generally for *p*(*n*-BMA$_{50}$-*co*-EGDMA$_{0.8}$):*p*(PEG$_{114}$-*b*-HPMA$_{120}$), the nanoparticles formed are within the size range of ~110-170 nm, *p*(HPMA$_{50}$-*co*-EGDMA$_{0.9}$):*p*(PEG$_{114}$-*b*-HPMA$_{120}$) ~80-110 nm and *p*(tBMA$_{25}$-*co*-HPMA$_{25}$-*co*-EGDMA$_{0.9}$):*p*(PEG$_{114}$-*b*-HPMA$_{120}$) ~100-140 nm. This range of sizes correlates well with literature values, as the optimum size for polymer nanocarriers for drug delivery applications is reported to be within the range of 70-200 nm,[12] to ensure they can easily permeate through targeted biological barriers.

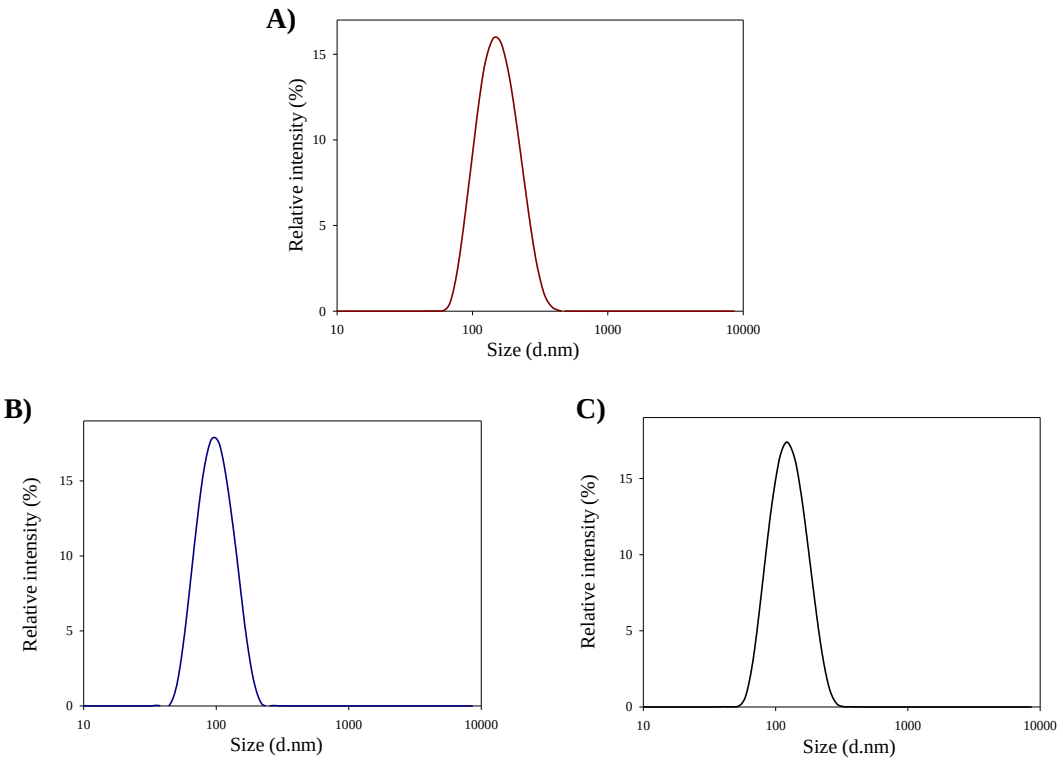

Figure 5.4 DLS results for 5 wt % SN-38 co-nanoprecipitated nanoparticles. A) *p*(*n*-BMA$_{50}$-*co*-EGDMA$_{0.8}$):*p*(PEG$_{114}$-*b*-HPMA$_{120}$), B) *p*(HPMA$_{50}$-*co*-EGDMA$_{0.9}$):*p*(PEG$_{114}$-*b*-HPMA$_{120}$), C) *p*(tBMA$_{25}$-*co*-HPMA$_{25}$-*co*-EGDMA$_{0.9}$):*p*(PEG$_{114}$-*b*-HPMA$_{120}$). All 50:50 wt %.

The same experimental procedure was utilised for the preparation of 10 wt % of SN-38 nanoparticles with the three branched co/terpolymers and *p*(PEG$_{114}$-*b*-HPMA$_{120}$) (50:50 wt %) but, unfortunately, colloidal stability was not achieved and precipitate was visible after complete solvent evaporation. Therefore, all SN-38 nanoparticles prepared *via* co-nanoprecipitation from this point onwards had a targeted loading of 5 wt % SN-38.

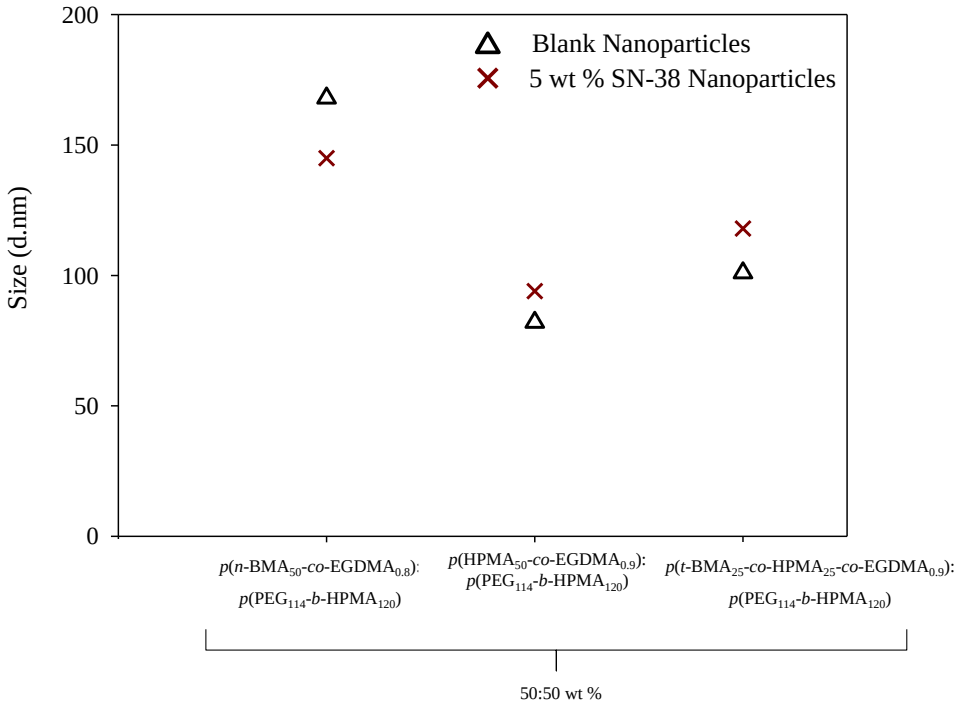

Figure 5.5 DLS results for blank *vs* 5 wt % SN-38 encapsulated co-nanoprecipitated particles.

A range of co-nanoprecipitates were studied using SEM, and images for nanoparticles loaded with 5 wt % SN-38 and comprised of *p*(*n*-BMA$_{50}$-*co*-EGDMA$_{0.8}$):*p*(PEG$_{114}$-*b*-HPMA$_{120}$), *p*(HPMA$_{50}$-*co*-EGDMA$_{0.9}$):*p*(PEG$_{114}$-*b*-HPMA$_{120}$) and *p*(tBMA$_{25}$-*co*-HPMA$_{25}$-*co*-EGDMA$_{0.9}$):*p*(PEG$_{114}$-*b*-HPMA$_{120}$) 50:50 wt % are presented in Figure 5.6, providing evidence for spherical nanoparticle formation.

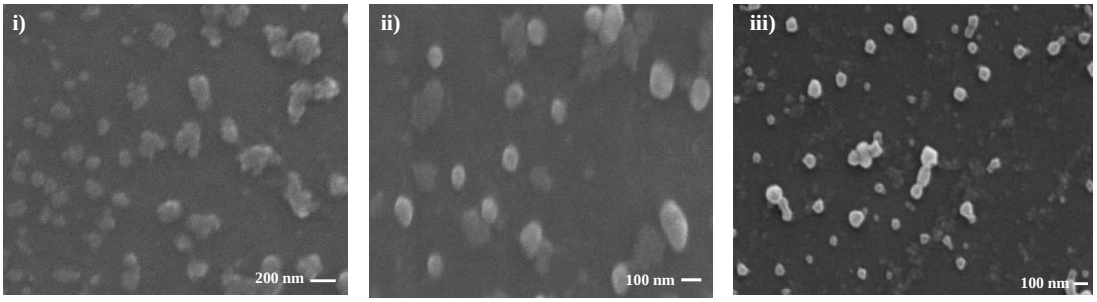

Figure 5.6 SEM images for 5 wt % SN-38 encapsulated nanoparticles, i) *p*(*n*-BMA_{50}-*co*-$EGDMA_{0.8}$):*p*(PEG_{114}-*b*-$HPMA_{120}$), ii) *p*($HPMA_{50}$-*co*-$EGDMA_{0.9}$):*p*(PEG_{114}-*b*-$HPMA_{120}$), iii) *p*(*t*-BMA_{25}-*co*-$HPMA_{25}$-*co*-$EGDMA_{0.9}$):*p*(PEG_{114}-*b*-$HPMA_{120}$) (All 50:50 wt %) (Nanoparticle dispersions were diluted to 0.1 mg/mL for imaging).

5.3 Stability of SN-38 encapsulated nanoparticles

The colloidal stability of the nanoparticles was studied by measuring the D_z, (d.nm) and PdI after both 18 days and 5 months. New nanoparticle samples were prepared throughout this research and the sizes (instant *vs* 18 day) for the various samples are shown in Figure 5.7. It is worth noting that the blank samples were re-measured after 5 months and the size and PdI values were almost identical to the original dispersion (Appendix, Table A13). The results presented for the three different batches of SN-38 encapsulated nanoparticles, confirms the reproducibility in stability across multiple samples. The particles remained colloidally stable and there showed only very minor variations in size for SN-38 encapsulated nanoparticles when comparing instant *vs* 18 day measurements.

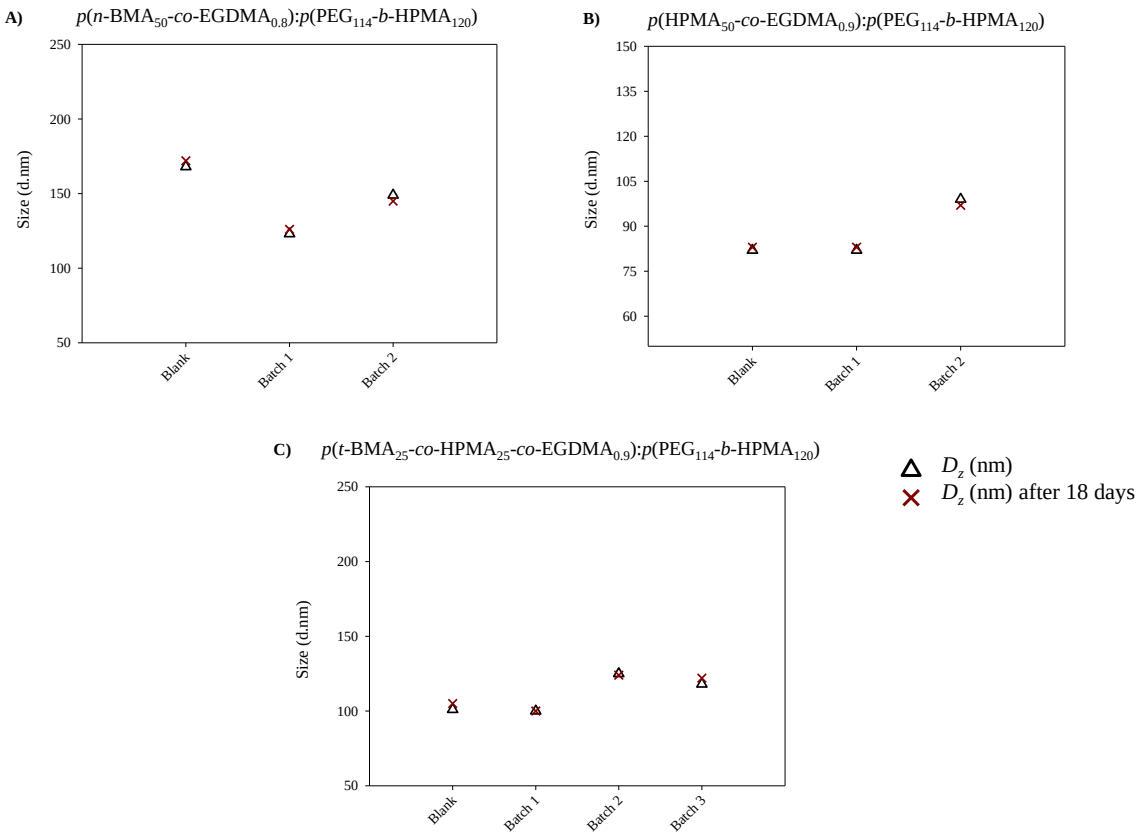

Figure 5.7 DLS analysis of samples during an 18 day time period for 5 wt % encapsulated SN-38 co-nanoprecipitated particles. A) *p*(*n*-BMA$_{50}$-*co*-EGDMA$_{0.8}$):*p*(PEG$_{114}$-*b*-HPMA$_{120}$), B) *p*(HPMA$_{50}$-*co*-EGDMA$_{0.9}$):*p*(PEG$_{114}$-*b*-HPMA$_{120}$), C) *p*(*t*-BMA$_{25}$-*co*-HPMA$_{25}$-*co*-EGDMA$_{0.9}$):*p*(PEG$_{114}$-*b*-HPMA$_{120}$), all 50:50 wt %. The blank samples were re-analysed after 5 months.

After 5 months of storage at ambient temperature and out of direct light, the D_z and PdI values remained similar to those originally measured, see Table 5.3.

Table 5.3 Stability of 5 wt % nanoparticles during a 5 month period.

Sample (50:50 wt%)	Instant Size (d.nm)	PdI	Size after 5 months (d.nm)	PdI
p(*n*-BMA$_{50}$-*co*-EGDMA$_{0.8}$) :*p*(PEG$_{114}$-*b*-HPMA$_{120}$)	167	0.051	155	0.065
p(HPMA$_{50}$-*co*-EGDMA$_{0.9}$):*p*(PEG$_{114}$-*b*-HPMA$_{120}$)	84	0.081	78	0.130
p(*t*-BMA$_{25}$-*co*-HPMA$_{25}$-*co*-EGDMA$_{0.9}$):*p*(PEG$_{114}$-*b*-HPMA$_{120}$)	129	0.054	133	0.097

Evidently, the polymers and SN-38 remained completely dispersed as no precipitate was visible (Figure 5.8 Ai-iii). Therefore, it can be confirmed that these particles remain colloidally stable over extended periods of time, as the variation in size and PdI were not significant (< 12 nm) (Table 5.3 & Figure 5.8 Bi-iii). This level of stability is not often

witnessed in the literature for polymer nanocarriers, and when stability is discussed, changes in size are usually measured during a much shorter time period (< 7 days).[13] The stability under more physiologically-relevant conditions is yet to be investigated.

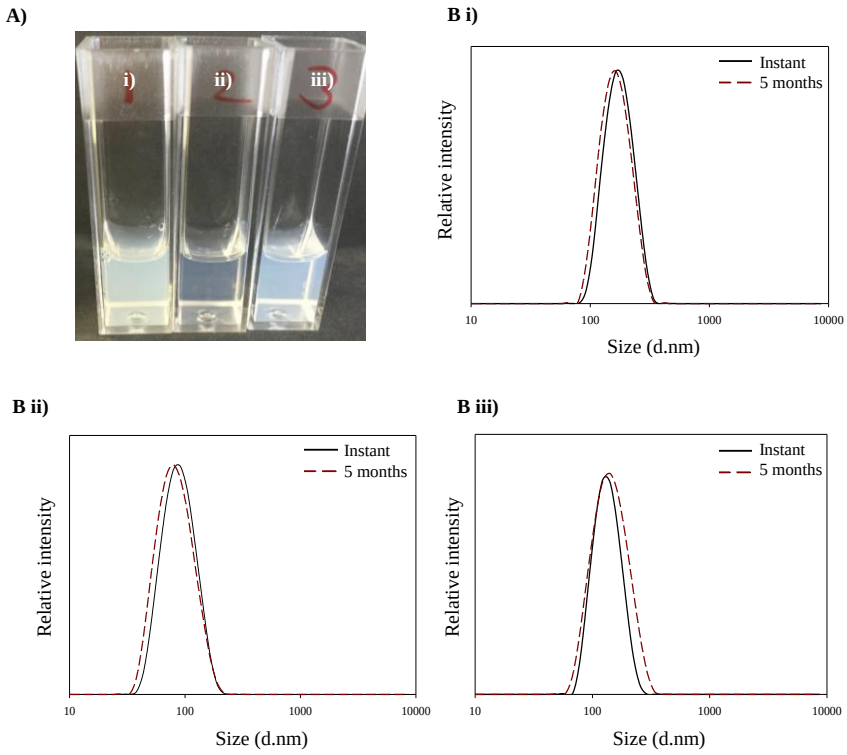

Figure 5.8 Stability of SN-38 encapsulated nanoparticles (5 wt %) during a 5 month period. A) Photograph to show SN-38 nanoparticles after 5 months in storage, i) *p*(*n*-BMA$_{50}$-*co*-EGDMA$_{0.8}$):*p*(PEG$_{114}$-*b*-HPMA$_{120}$), ii) *p*(HPMA$_{50}$-*co*-EGDMA$_{0.9}$):*p*(PEG$_{114}$-*b*-HPMA$_{120}$), iii) *p*(*t*-BMA$_{25}$-*co*-HPMA$_{25}$-*co*-EGDMA$_{0.9}$):*p*(PEG$_{114}$-*b*-HPMA$_{120}$), B) DLS overlays of size distribution by intensity traces for nanoprecipitations, instant *vs* 5 months, i) *p*(*n*-BMA$_{50}$-*co*-EGDMA$_{0.8}$):*p*(PEG$_{114}$-*b*-HPMA$_{120}$) ii) *p*(HPMA$_{50}$-*co*-EGDMA$_{0.9}$):*p*(PEG$_{114}$-*b*-HPMA$_{120}$) iii) *p*(*t*-BMA$_{25}$-*co*-HPMA$_{25}$-*co*-EGDMA$_{0.9}$):*p*(PEG$_{114}$-*b*-HPMA$_{120}$). All 50:50 wt %.

5.4 Pharmacological studies of co-nanoprecipitated nanoparticles

The SN-38 encapsulated nanoparticles with varying chemical compositions were taken forward for *in vitro* testing, due to loading capabilities and enhanced aqueous concentrations of SN-38. The nanoparticles which were selected for study were; *p*(*n*-BMA$_{50}$-*co*-EGDMA$_{0.8}$):*p*(PEG$_{114}$-*b*-HPMA$_{120}$), *p*(HPMA$_{50}$-*co*-EGDMA$_{0.9}$):*p*(PEG$_{114}$-*b*-HPMA$_{120}$) and *p*(*t*-BMA$_{25}$-*co*-HPMA$_{25}$-*co*-EGDMA$_{0.9}$):*p*(PEG$_{114}$-*b*-HPMA$_{120}$) (50:50 wt %). The pharmacological cytotoxicity assays were conducted by researchers in the Molecular and Clinical Pharmacology department, specialising in cancer research at the

University of Liverpool, through collaboration between the Kitteringham and Rannard research groups.

5.4.1 *In vitro* pharmacological studies

As cancer cells are being targeted for this study, it is expected that the SN-38 encapsulated nanoparticles would decrease the cell viability i.e. increase cell death, when compared with blank nanoparticle dispersions (no SN-38). Initial experiments were conducted using the CT26 murine cell line. CT26 is an *N*-nitroso-*N*-methylurethane induced undifferentiated colon carcinoma cell line, which is commonly used for early stages of *in vitro* testing. CT26 were selected as they are readily available and derived from BALB/c mice and can be implanted back into these mice to allow use in an immunocompetent syngeneic murine model. Depending on the results obtained from this study, the materials would be further tested on a human colon carcinoma cell line HCT116. HCT116 cells are known to be tumorigenic in nude nice and therefore suitable for translation into murine work if experiments were to be conducted *in vivo.* When using two different cells lines it is expected that different drug toxicities will be observed, as the cells are derived from different species.

To compare the cytotoxicity of both IR and SN-38 in the absence of any nanomaterials, MTS assays were conducted on both CT26 and HCT116 cell lines (Figure 5.9). The concentration range for SN-38 was between 0–9 µM and 0–300 µM for IR, and cells were incubated for 48 hours prior to MTS addition. Evidently, SN-38 exhibited a high toxicity at much lower concentrations than IR, when tested on both cell lines. During incubation with CT26 cells (Figure 5.9A), SN-38 significantly reduces cell viability, whereas IR did not cause a significant cell toxicity until a much higher concentration (300 µM), where ~10 % cell viability was observed. During incubation of SN-38 and IR with HCT116 cells, as expected, a low cell viability at low concentrations was observed for SN-38 (~40% at 9 µM), whilst for IR there was no change in cell viability between 100-300 µM, and a maximum of ~55% cell viability was obtained at 300 µM (Figure 5.9B).

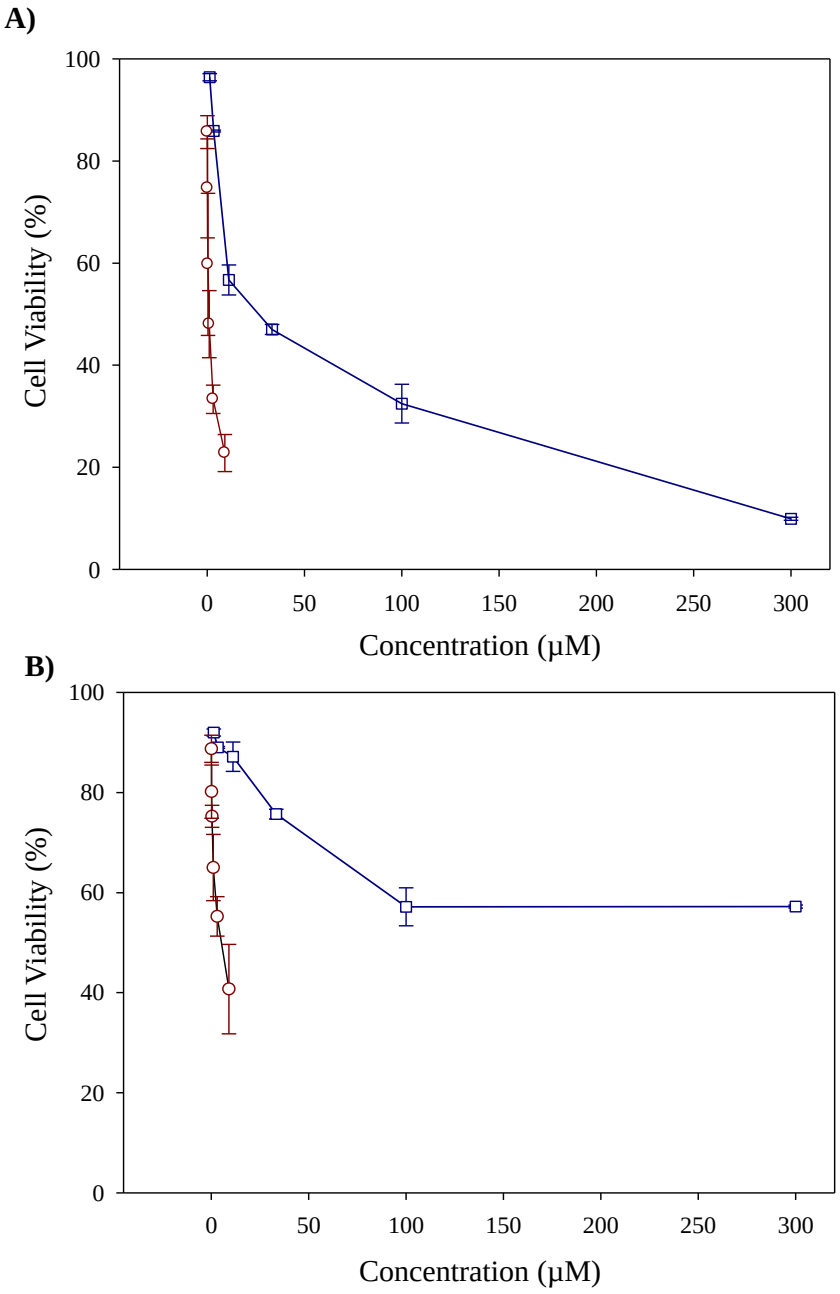

Figure 5.9 *In vitro* cytotoxicity for increasing concentrations of IR (blue open squares) and SN-38 (dark red open circles) A) CT26 cell line, B) HCT116 cell line. Cell viability was calculated as the absorbance ratio of treated to control groups. (IR and SN-38 were both spiked with DMSO).

5.4.2 MTS assays for SN-38 encapsulated nanoparticles – CT26 cell line

An MTS assay was conducted to compare the *in vitro* cytotoxicity of SN-38, 5 wt % SN-38 encapsulated nanoparticles and blank nanoparticles (no SN-38) using CT26 carcinoma cells at concentrations 1, 2 and 4 µM. For all three concentrations, a significant decrease in cell viability was observed for the SN-38 nanodispersions (< 10% for both 4 and 2 µM

and 19% for 1 µM), when compared with the blank nanoparticles (generally > 80% cell viability), see Figure 5.10A-C.

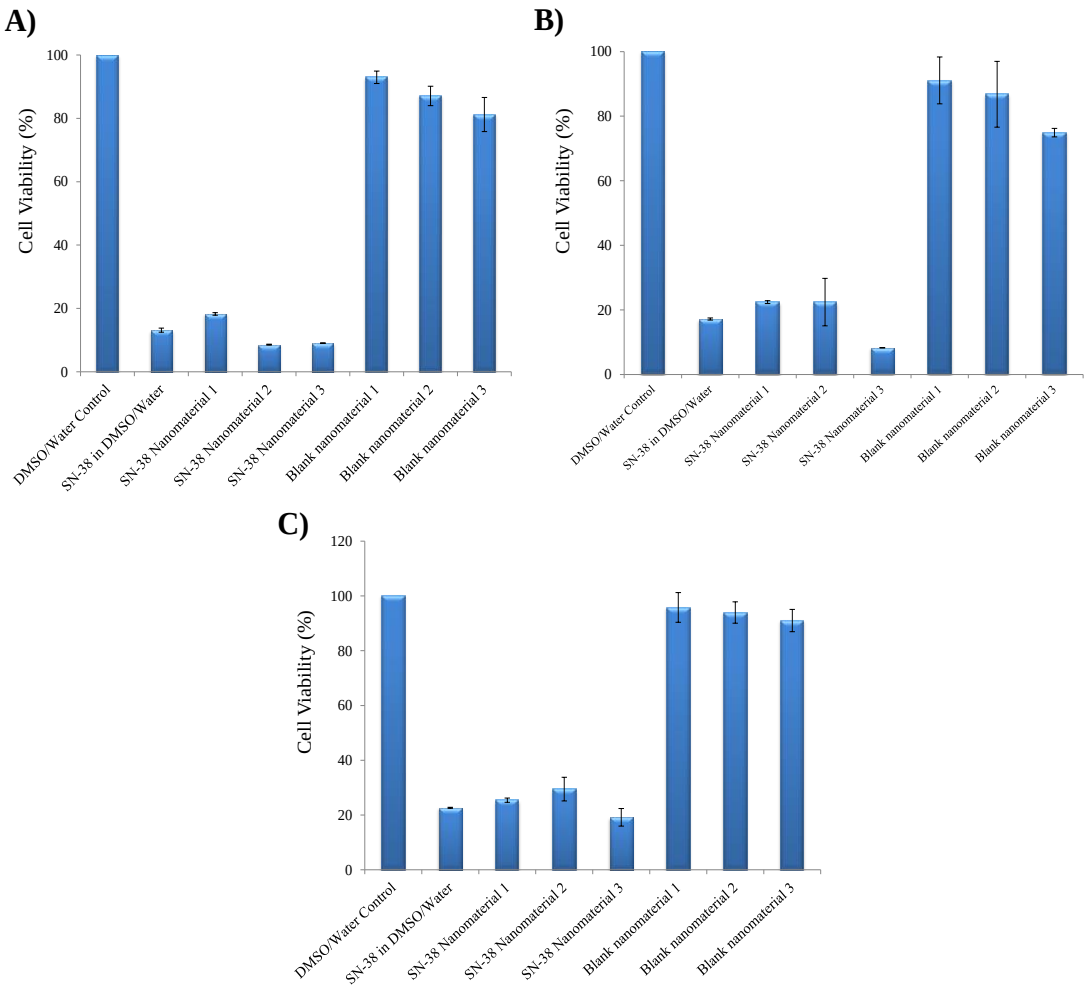

Figure 5.10 *In vitro* viability of CT26 cancer cells treated with free SN-38, SN-38 encapsulated nanoparticles and blank nanoparticles after 48 hour incubation. A) 4 µM, B) 2µM, C) 1 µM. SN-38 nanomaterial 1 = *p*(*n*-BMA$_{50}$-*co*-EGDMA$_{0.8}$) :*p*(PEG$_{114}$-*b*-HPMA$_{120}$) 50:50 wt %, 5 wt % SN-38, SN-38 nanomaterial 2 = *p*(HPMA$_{50}$-*co*-EGDMA$_{0.9}$):*p*(PEG$_{114}$-*b*-HPMA$_{120}$) 50:50 wt %, 5 wt % SN-38, SN-38 nanomaterial 3 = *p*(*t*-BMA$_{25}$-*co*-HPMA$_{25}$-*co*-EGDMA$_{0.9}$):*p*(PEG$_{114}$-*b*-HPMA$_{120}$) 50:50 wt %, 5 wt % SN-38. Same chemical compositions for blanks in the absence of SN-38. (Each experiment was conducted in triplicate).

When compared to free SN-38, an additional decrease in cell viability was observed for nanomaterial 3 (5 wt % SN-38 *p*(*t*-BMA$_{25}$-*co*-HPMA$_{25}$-*co*-EGDMA$_{0.9}$):*p*(PEG$_{114}$-*b*-HPMA$_{120}$) (50:50 wt %), at concentrations 4, 2 and 1 µM, which may suggest the release of SN-38 from nanoparticles into the cells and further studies would be required to confirm this. As an initial toxicity experiment, the low cell viability for SN-38 nanodispersions

were promising, in particularly for *p*(*t*-BMA_{25}-*co*-$HPMA_{25}$-*co*-$EGDMA_{0.9}$):*p*(PEG_{114}-*b*-$HPMA_{120}$) 50:50 wt %, which were comparable with free SN-38.

Due to the increased cytotoxicity observed during incubation with CT26 cancer cells, *p*(*t*-BMA_{25}-*co*-$HPMA_{25}$-*co*-$EGDMA_{0.9}$):*p*(PEG_{114}-*b*-$HPMA_{120}$) 50:50 wt %, this nanomaterial was further assessed within a range of concentrations (0-8 μM) and compared with both free SN-38 and IR. The results are shown in Figure 5.11, and interestingly free SN-38 and 5 wt % SN-38 *p*(*t*-BMA_{25}-*co*-$HPMA_{25}$-*co*-$EGDMA_{0.9}$):*p*(PEG_{114}-*b*-$HPMA_{120}$) 50:50 wt % show an almost identical decrease in cell viability (<40%) when compared with free IR, which remains > 80% at 8 μM. It is worth noting that the SN-38 encapsulated nanomaterials appear to show an enhanced reproducibility, as the standard deviation values across the range of concentrations for free SN-38 are much smaller than those obtained for free SN-38.

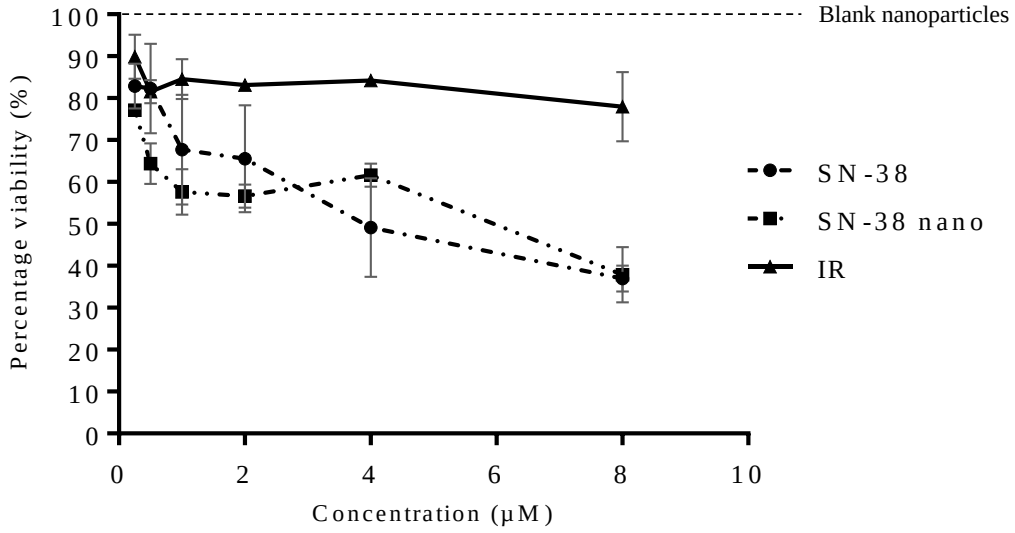

Figure 5.11 *In vitro* viability of CT26 cancer cell line treated with free SN-38, SN-38 encapsulated nanoparticles and irinotecan after 48 hour incubation. Circle = free SN-38, square = 5 wt % SN-38 encapsulated within *p*(*t*-BMA_{25}-*co*-$HPMA_{25}$-*co*-$EGDMA_{0.9}$):*p*(PEG_{114}-*b*-$HPMA_{120}$) 50:50 wt %, triangle = IR. (Both IR and SN-38 were spiked with DMSO and each experiment was conducted in triplicate).

5.4.3 MTS assays for SN-38 encapsulated nanoparticles – HCT116 cell line

Following the results obtained for the SN-38 encapsulated nanoparticles incubated with CT26 cells, MTS assays were performed on HCT116 human carcinoma cells. The determination of cytotoxicity was conducted with the same materials as described for

above for CT26 cells; SN-38 control, 5 wt % SN-38 encapsulated nanoparticles and blank nanoparticles (no SN-38) at concentrations 1, 2 and 4 µM (Figure 5.12A-C).

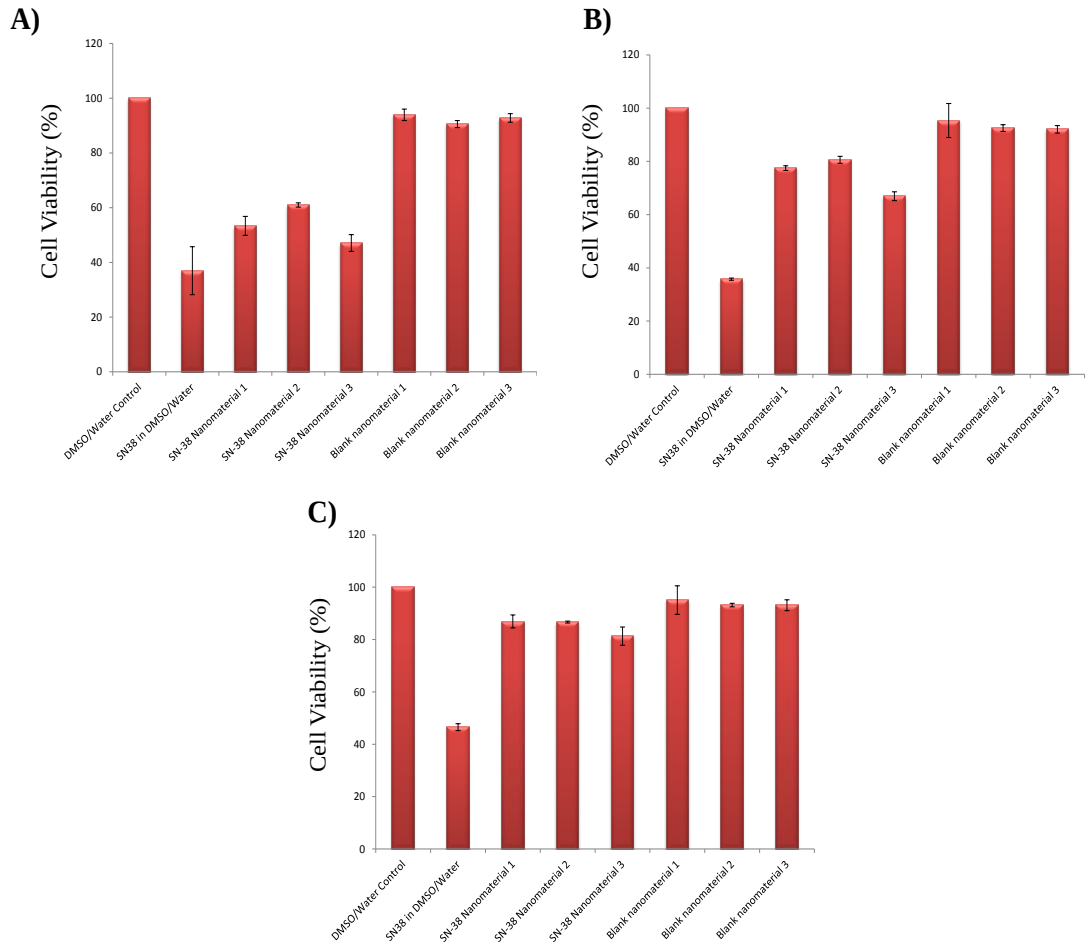

Figure 5.12 *In vitro* viability of HCT116 cancer cells treated with free SN-38, SN-38 encapsulated nanoparticles and blank nanoparticles after 48 hour incubation. A) 4 µM, B) 2µM, C) 1 µM. SN-38 nanomaterial 1 = *p*(*n*-BMA$_{50}$-*co*-EGDMA$_{0.8}$) :*p*(PEG$_{114}$-*b*-HPMA$_{120}$) 50:50 wt %, 5 wt % SN-38, SN-38 nanomaterial 2 = *p*(HPMA$_{50}$-*co*-EGDMA$_{0.9}$):*p*(PEG$_{114}$-*b*-HPMA$_{120}$) 50:50 wt %, 5 wt % SN-38, SN-38 nanomaterial 3 = *p*(*t*-BMA$_{25}$-*co*-HPMA$_{25}$-*co*-EGDMA$_{0.9}$):*p*(PEG$_{114}$-*b*-HPMA$_{120}$) 50:50 wt %, 5 wt % SN-38. Same chemical compositions for blanks in the absence of SN-38. (Each experiment was conducted in triplicate).

The cell viability observed for free SN-38 was ~40% for 4, 2 and 1µM SN-38 and an increase in cytotoxicity with increasing concentration was observed. Therefore, the largest difference in cell viability for the SN-38 encapsulated and blank nanomaterials, was during incubation at 4µM of drug. The material which demonstrated the lowest cell viability (47%) was 5 wt % SN-38 *p*(*t*-BMA$_{25}$-*co*-HPMA$_{25}$-*co*-EGDMA$_{0.9}$):*p*(PEG$_{114}$-*b*-

$HPMA_{120}$) 50:50 wt % and was, therefore, further assessed within a wider range of concentrations (0-8 μM).

The results obtained for the incubation of HCT116 cells with free SN-38, free IR and 5 wt % SN-38 *p*(*t*-BMA_{25}-*co*-$HPMA_{25}$-*co*-$EGDMA_{0.9}$):*p*(PEG_{114}-*b*-$HPMA_{120}$) 50:50 wt % nanomaterial are shown in Figure 5.13. Interestingly, for both free SN-38 and the SN-38 encapsulated nanomaterial, an almost identical decrease in cell viability across the range of concentrations was observed. This was very promising, as this particular nanomaterial has demonstrated a comparable toxicity with free SN-38 as an aqueous nanodispersion during incubation with human cancer cells. As expected, IR did not show a great level of toxicity until reaching higher concentrations (> 4μM drug).

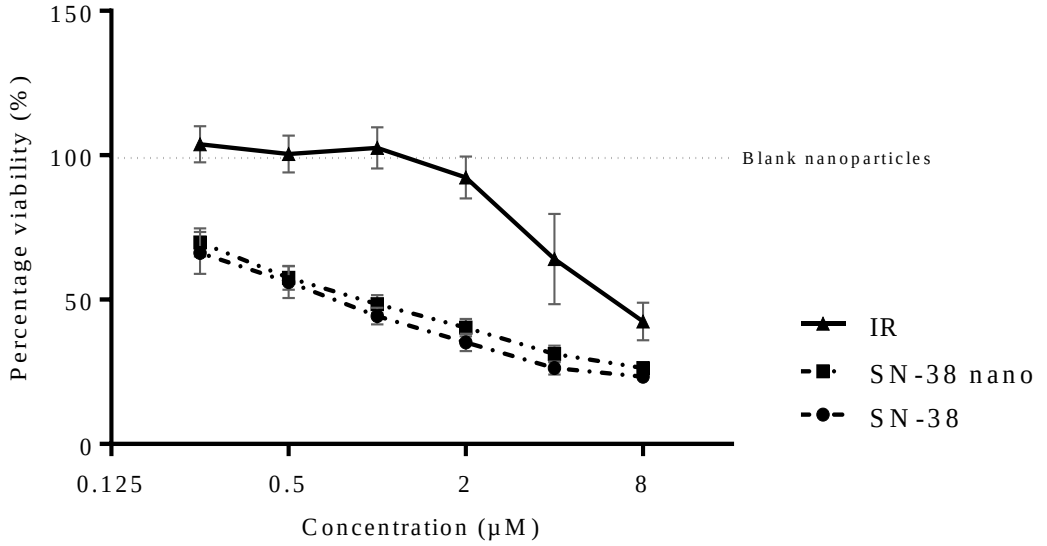

Figure 5.13 *In vitro* viability of HCT116 cancer cell line treated with free SN-38, SN-38 encapsulated nanoparticles and irinotecan after 48 hour incubation. Circle = free SN-38, square = 5 wt % SN-38 encapsulated within *p*(*t*-BMA_{25}-*co*-$HPMA_{25}$-*co*-$EGDMA_{0.9}$):*p*(PEG_{114}-*b*-$HPMA_{120}$) 50:50 wt %, triangle = IR. (Both IR and SN-38 were spiked with DMSO and each experiment was conducted in triplicate).

5.5 Multiple co-nanoprecipitation experiments and encapsulation of SN-38

As discussed in Chapter 2 Section 2.4.2, the formation of colloidally stable *p*($HPMA_{50}$-*co*-$EGDMA_{0.9}$) nanoparticles *via* nanoprecipitation allowed additional subsequent nanoprecipitations into the same anti-solvent mixture. Interestingly, during repeated additions of *p*($HPMA_{50}$-*co*-$EGDMA_{0.9}$) dissolved in good solvent, the existing particles

did not act as nuclei for further growth, and a new nanoparticle distribution of identical size was obtained. This multiple addition technique has not yet been utilised with a branched terpolymer, A-B block copolymer and a hydrophobic drug molecule. The ability to instantly increase the concentration of polymer nanoparticles *via* low volume additions is very appealing for increasing the concentration of a therapeutic drug molecule whilst maintaining a constant volume of water, especially if these materials were to be taken forward *in vivo*.

The *in vitro* cytotoxicity results were most promising for the 5 wt % SN-38 nanomaterial consisting of *p*(*t*-BMA$_{25}$-*co*-HPMA$_{25}$-*co*-EGDMA$_{0.9}$):*p*(PEG$_{114}$-*b*-HPMA$_{120}$) 50:50 wt %, therefore, this material was selected for the multiple nanoprecipitation study. A fresh stock solution of 5 wt % SN-38, *p*(*t*-BMA$_{25}$-*co*-HPMA$_{25}$-*co*-EGDMA$_{0.9}$) and *p*(PEG$_{114}$-*b*-HPMA$_{120}$) dissolved in THF:ACN (1:1) was prepared and left to solubilise for 6 weeks (total polymer concentration 5 mg/mL, SN-38, 0.265 mg/mL). The conditions were kept consistent with previous co-nanoprecipitation experiments, and for the first addition, 1 mL (5 mg/mL polymers, 0.265 mg/mL SN-38) was added quickly into 5 mL of water (i_5-f_1) and analysed by DLS after THF:ACN evaporation. The subsequent additions were carried out into the same nanoparticle mixture and the DLS results are presented in Table 5.4.

Table 5.4 DLS multiple nanoprecipitation results for 5 wt % SN-38 and *p*(*t*-BMA$_{25}$-*co*-HPMA$_{25}$-*co*-EGDMA$_{0.9}$):*p*(PEG$_{114}$-*b*-HPMA$_{120}$) 50:50 wt % for 3 subsequent additions.

Volume of Polymers + SN-38 Added (mL)	Addition no.	D_z (nm)	PdI	D_n (nm)	Derived count rate (kcps)	Concentration of polymers (mg/mL)	Concentration of SN-38 (mg/mL)
1	1	114	0.156	85	309236	1	0.053
1	2	137	0.168	96	346456	2	0.106
1	3	133	0.121	94	390176	3	0.159

As shown in Table 5.4, for repeated additions of the stock solution containing SN-38, branched terpolymer and A-B block copolymer (up to 3 mL), the recorded D_z values of the nanoprecipitated particles were similar, with an observed increase of just 23 nm after the second addition and a minor difference of 4 nm during the third addition. Although there are small changes in PdI, the results suggest that new nanoparticles of identical size are being formed. The DLS traces for each addition (Figure 5.14 A-C) show monomodal size populations, even during the third addition, with an increased final concentration of SN-38 (0.159 mg/mL) and branched terpolymer plus A-B block copolymer (3 mg/mL).

Although the solution became slightly more turbid after removal of solvent during each addition, there was no evidence of polymer precipitation (Figure 5.14 Di-iii). This study has highlighted a fast and efficient method to increasing the concentration of SN-38 within a constant volume of water, and may not be limited to the chemical compositions and drug molecule presented here.

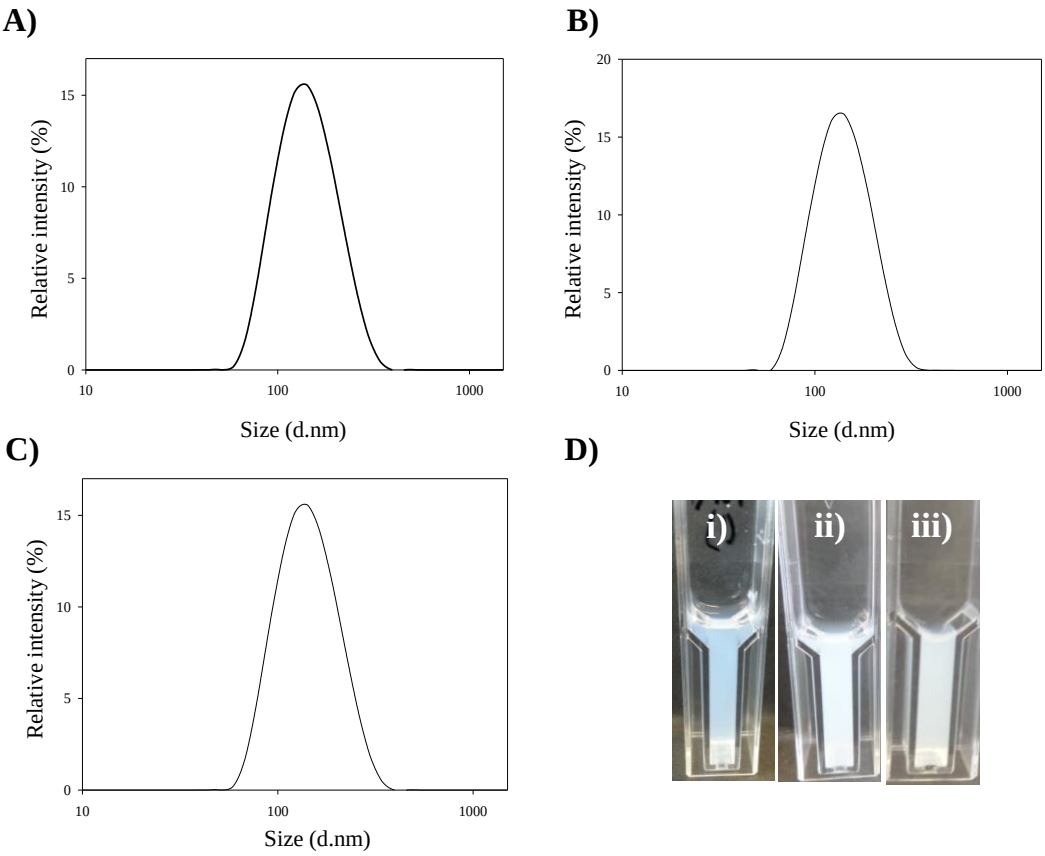

Figure 5.14 Multiple nanoprecipitation study of 5 wt % SN-38 and *p*(*t*-BMA$_{25}$-*co*-HPMA$_{25}$-*co*-EGDMA$_{0.9}$):*p*(PEG$_{114}$-*b*-HPMA$_{120}$) 50:50 wt %, A) DLS trace for first addition of polymer and SN-38 dissolved in good solvent, B) second addition of polymers and SN-38 dissolved in good solvent, C) third addition of polymers and SN-38 into good solvent. The conditions were (i_5-f_1, from THF:ACN into water), D) Photograph to show each subsequent addition of 5 wt % SN-38 and *p*(*t*-BMA$_{25}$-*co*-HPMA$_{25}$-*co*-EGDMA$_{0.9}$):*p*(PEG$_{114}$-*b*-HPMA$_{120}$) 50:50 wt % dissolved in THF:ACN 1:1 into the original 5 mL H_2O, i) 1 mL ii) 2 mL, iii) 3 mL.

5.6 Conclusion

To conclude, the encapsulation of the anti-cancer drug molecule SN-38 has been explored, and after initial solubility issues, nanoparticles were successfully prepared at 5 wt % SN-38 encapsulation *via* the co-nanoprecipitation approach. The SN-38 nanoparticles were

colloidally stable for up to 5 months (longest period tested), demonstrated reproducibility (size and PdI) across a range of samples and were within the size range required for cancer nanotherapies. Three nanomaterials were taken forward for initial *in vitro* cytotoxicity testing and the cell viability was determined for both, CT26 (mouse) and HCT116 (human) cancer cells. The same general trends were observed throughout and generally the SN-38 nanomaterials exhibited a cytotoxicity which was comparable to that of free SN-38. The SN-38 encapsulated nanomaterial which demonstrated an almost identical cell toxicity to free SN-38 was *p*(*t*-BMA_{25}-*co*-$HPMA_{25}$-*co*-$EGDMA_{0.9}$):*p*(PEG_{114}-*b*-$HPMA_{120}$) 50:50 wt %. Due to the promising *in vitro* results, the SN-38 encapsulated nanomaterials were of interest to an external large pharmaceutical company and release studies of SN-38 are currently being conducted prior to a planned more extensive collaboration.

The multiple nanoprecipitation process, first introduced in Chapter 2 Section 2.4.2, was further explored with SN-38 and the two polymers required for a co-nanoprecipitation. Interestingly, the multiple addition was successful and an increased concentration of SN-38 was achieved, whilst maintaining the same volume of anti-solvent.

5.7 References

1. http://www.who.int/mediacentre/factsheets/fs297/en/, accessed June, 2015.
2. D. Peer, J. M. Karp, S. Hong, O. C. Farokhzad, R. Margalit and R. Langer, *Nature Nanotechnolgy*, 2007, **2**, 751-760.
3. Y. Matsumura and H. Maeda, *Cancer research*, 1986, **46**, 6387-6392.
4. R. Singh and J. W. Lillard Jr, *Experimental and Molecular Pathology*, 2009, **86**, 215-223.
5. T. Sun, Y. S. Zhang, B. Pang, D. C. Hyun, M. Yang and Y. Xia, *Angewandte Chemie International Edition*, 2014, **53**, 12320-12364.
6. N. Sepehri, H. Rouhani, F. Tavassolian, H. Montazeri, M. R. Khoshayand, M. H. Ghahremani, S. N. Ostad, F. Atyabi and R. Dinarvand, *International Journal of Pharmaceutics*, 2014, **471**, 485-497.
7. F. Atyabi, A. Farkhondehfai, F. Esmaeili and R. Dinarvand, *Acta Pharmaceutica*, 2009, **59**, 133.
8. H. Zhang, J. Wang, W. Mao, J. Huang, X. Wu, Y. Shen and M. Sui, *Journal of Controlled Release*, 2013, **166**, 147-158.
9. H. Zhao, B. Rubio, P. Sapra, D. Wu, P. Reddy, P. Sai, A. Martinez, Y. Gao, Y. Lozanguiez, C. Longley, L. M. Greenberger and I. D. Horak, *Bioconjugate Chemistry*, 2008, **19**, 849-859.
10. A. Patnaik, K. P. Papadopoulos, A. W. Tolcher, M. Beeram, S. Urien, L. J. Schaaf, S. Tahiri, T. Bekaii-Saab, F. M. Lokiec, K. Rezaï and A. Buchbinder, *Cancer chemotherapy and pharmacology*, 2013, **71**, 1499-1506
11. Q. Gu, J. Z. Xing, M. Huang, C. He and J. Chen, *Nanotechnology*, 2012, **23**, 205101.
12. M. Elsabahy and K. L. Wooley, *Chemical Society Reviews*, 2012, **41**, 2545-2561.
13. H. Liu, H. Lu, L. Liao, X. Zhang, T. Gong and Z. Zhang, *Drug delivery*, 2015, **22**, 701-709.

Chapter 6

Conclusions and Future Work

6.1 Conclusions

The nanoprecipitation conditions for both linear *p*(HPMA$_{50}$) and branched *p*(HPMA$_{50}$-*co*-EGDMA$_{0.9}$) were initially investigated and there was a clear advantage of using branched *p*(HPMA$_{50}$-*co*-EGDMA$_{0.9}$), rather than linear homopolymers when seeking to achieve monomodal polymer nanoparticles. The stability of charge stabilised *p*(HPMA$_{50}$-*co*-EGDMA$_{0.9}$) nanoparticles was improved through the introduction of an A-B block copolymer when simultaneously added to the anti-solvent during nanoprecipitation. A-B block copolymer stabilisers consisting of varying PEG and HPMA (hydrophilic *vs* hydrophobic) blocks were successfully synthesised *via* ATRP and subsequent co-nanoprecipitation experiments were conducted at varying ratios from 100:0 through to 0:100 wt % (branched copolymer:A-B block copolymer respectively) and, generally, the nanoparticles produced were within the range considered ideal for drug delivery applications with exceptionally narrow monomodal distributions obtained. The NaCl stability was determined across the varying ratios and different levels of success were observed, which was useful to determine the region in which stabilised nanoparticles are formed. An apparent optimum of electrolyte stability was observed during inclusion of the *p*(PEG$_{114}$-*b*-HPMA$_{120}$) A-B block copolymer, which was taken forward for further studies. This particular stabiliser was not limited to co-nanoprecipitation experiments with *p*(HPMA$_{50}$-*co*-EGDMA$_{0.9}$), and a variety of branched polymers were also stabilised, including; *p*(*n*-BMA$_{50}$-*co*-EGDMA$_{0.8}$), *p*(*t*-BMA$_{50}$-*co*-EGDMA$_{0.9}$), *p*(HPMA$_{25}$-*co*-*n*-BMA$_{25}$-EGDMA$_{0.9}$) or *p*(HPMA$_{25}$-*co*-*t*-BMA$_{25}$-*co*-EGDMA$_{0.9}$). To further investigate how both the branched polymer and A-B block copolymer associate during a co-nanoprecipitation, the fluorescent dye molecule pyrene was encapsulated within the nanoparticles, to probe the internal environment. The polarity studies provided further evidence that during addition of increasing levels of A-B block copolymer, the hydrophobicity of the internal core was maintained and only slight deviations were observed when compared with 100 % *p*(HPMA$_{50}$-*co*-EGDMA$_{0.9}$). From these detailed studies, it is most likely that the HPMA block from the A-B block copolymer becomes incorporated into the polymer core and the PEG chain resides on the nanoparticle surface. The co-nanoprecipitation approach provided a fast and efficient route to stabilised nanoparticles, without the need for polymeric surfactants as additives within the aqueous anti-solvent solution. The ability to tune both the chemistry of the branched polymer and A-B block co-polymer is very appealing when considering a new drug delivery nanocarrier.

To assess the potential of the nanoparticles as drug delivery vehicles, co-nanoprecipitation experiments were conducted with a guest dye molecule fluoresceinamine (FA) and an encapsulation of up to 17 wt % (relative to total polymer mass) was observed. *In vitro* cytotoxicity and ^{14}C-mannitol permeability assays were performed using the Caco-2 cell line which represents the first barrier to orally dosed materials, the intestinal epithelium. The studies were conducted on a selection of the FA encapsulated nanomaterials, which were stable to both NaCl and transport buffer solution, to ensure the nanoparticles remained dispersed during the pharmacological assays. The materials which appeared to compromise the integrity of the Caco-2 monolayer, and were not further studied, consisted of A-B block copolymers with a PEG chain length of 2000 g/mol and a HPMA block with a $DP_n < 120$ monomer units. The materials taken forward did not cause toxicity to Caco-2 cells across a range of concentrations and 90-100% cell viability was maintained up to relatively high concentrations. The lead material which showed positive potential pharmacological benefits was FA encapsulated *p*(*n*-BMA$_{50}$-*co*-EGDMA$_{0.8}$):*p*(PEG$_{114}$-*b*-HPMA$_{120}$) (50:50 wt %), as an enhanced transcellular permeability was observed when compared with the control (free FA in water/DMSO). The subsequent cellular accumulation experiments highlighted that for the FA nanomaterial, although not statistically significant, an increased accumulation in ATHP-1 cells (macrophages) was observed. This would be a desirable property for an oral dosing therapy of infectious diseases such as HIV, where macrophage cells are a sanctuary site for the HIV virus. However, for Caco-2 cells, a decreased accumulation was observed which suggested that FA was traversing the membrane *via* mechanisms such as paracellular permeation. To gain a greater insight, further experiments were conducted and active transport processes were inhibited. Surprisingly, during ATP depletion, a decrease in cellular accumulation of the FA nanomaterial was observed, suggesting uptake does in fact occur *via* an active process. The assessment of the Caco-2 transcellular permeability was also carried out in the presence of endocytic inhibitors, and a statistically significant decrease in cellular permeability during the presence of each inhibitor was observed, which suggests the movement of the mimic drug molecule was not simply passive and does proceed *via* an active mechanism.

There was huge variability in loading capabilities of the drug molecules studied and interestingly, *p*(*n*-BMA$_{50}$-*co*-EGDMA$_{0.8}$):*p*(PEG$_{114}$-*b*-HPMA$_{120}$) 50:50 wt %, (lead material during early pharmacological studies) also demonstrated an excellent loading potential when co-nanoprecipitated with HIV anti-retrovirals; up to 25 wt % of efavirenz

and ritonavir and 20 wt % lopinavir were encapsulated. To rationalise the behaviour, the calculated logP of the varying branched co/terpolymers was considered and during inclusion of an increasingly hydrophobic polymer, higher loading capabilities were observed.

Further encapsulation studies were conducted for the hydrophobic anti-cancer drug molecule SN-38. After various solubilisation difficulties, co-nanoprecipitation experiments were successfully conducted and stabilised nanoparticles were produced. The nanoparticles were within the preferred size range for drug delivery, remained stable during a minimum of 5 months (study period) and samples were very reproducible. The SN-38 nanoparticles were progressed forward for various *in vitro* cytotoxicity studies and, as cancer cells were being targeted, a decrease in cell viability was expected. Two cancer cell lines were used for the experiments; CT26 (mouse cell line) and HCT116 cells (human cancer cell line). The SN-38 encapsulated nanoparticles showed an almost identical toxicity with free SN-38, yet, the nanoparticles existed as an aqueous nanodispersion, which would be preferred if administered as an intravenous solution. As a comparison, blank nanoparticles (no SN-38) were also subject to toxicity assays and demonstrated a negligible toxicity, therefore, the SN-38 was resulting in toxicity observed for the SN-38 nanoparticles. The nanomaterials which showed an increasing toxicity when compared to other samples was *p*(HPMA$_{25}$-*co*-*t*-BMA$_{25}$-*co*-EGDMA$_{0.9}$), which is currently being studied further. It is worth noting that the encapsulation of SN-38 may not be limited to 5 wt % loading, which is presented here, as the chemistry is yet to be optimised for drug loading.

The multiple nanoprecipitation studies conducted during early stages of the research gave promising results for *p*(HPMA$_{50}$-*co*-EGDMA$_{0.9}$), showing that a single precipitation anti-solvent could be used several times leading to an increase in the concentration of polymer nanoparticles rather than growth of larger particles. This effect was utilised in the co-nanoprecipitation of SN-38 with branched copolymers and linear A-B stabilising block copolymers. Interestingly, the multiple addition experiments were successful and an increased concentration of SN-38-loaded nanoparticles was achieved, whilst maintaining the same volume of anti-solvent. The original nanoparticle size was maintained during each addition suggesting a new nanoparticle dispersion of similar size was generated. It is worth emphasising that this procedure provides an option to create samples of increasing concentration *via* a relatively simple strategy after initial removal of good solvent.

Overall, the properties of the original studied *p*(HPMA$_{50}$-*co*-EGDMA$_{0.9}$) charge stabilised nanoparticles have been greatly improved *via* the addition of an A-B block copolymer stabiliser. Not only is the technique a fast and reproducible route to sterically stabilised nanoparticles, it does not require additional surfactants dissolved in the anti-solvent or subsequent filtration which is regularly reported in the literature. The stability is maintained during encapsulation of hydrophobic drug molecules and generally the size change during encapsulation is negligible. The selection of chemical compositions studied within this research are not limited to those presented and could be further expanded for nanomedicine applications.

6.2 Future Work

The co-nanoprecipitation approach has provided a fast and efficient route to sterically stabilised nanoparticles with high loading (wt %) capabilities. The research presented within this thesis is not limited to the chemical compositions discussed and future research directions will focus a series of avenues listed below:

- Further investigation of the versatility of hydrophobic branched co/terpolymers and A-B block copolymers for increasing loading capabilities of SN-38.
- The use of targeting A-B block copolymers and their inclusion within a branched hydrophobic core e.g. sugars, proteins and the formation of biologically relevant nanoparticles.
- Multiple nanoprecipitation experiments for HIV encapsulated nanoparticles to yield nanoparticles with an increased concentration of anti-retrovirals within the same volume of water.
- Alternative architectures to A-B block copolymers such as A-B-A functional polymers (See 6.3).
- Formation of polymer-drug conjugates and subsequent co-nanoprecipitation experiments (See 6.4).

Additional pharmacological studies:

- Pharmacological studies of efavirenz encapsulated nanoparticles:
  - Cytotoxicity
  - Drug release
- *In vivo* work for 5 wt% SN-38 encapsulated co-nanoprecipitated nanoparticles.

6.3 Preliminary aqueous encapsulation co-nanoprecipitation studies utilising an A-B-A triblock polymer

As well as an A-B block copolymer, it was also of interest to investigate nanoparticle formation during incorporation of an A-B-A triblock polymer, therefore *p*(HPMA$_{120}$-*b*-PEG$_{\sim 105}$-*b*-HPMA$_{120}$) was synthesised from a di-functional PEG macroinitiator (^{1}H NMR, see Appendix A31) and polymerised with HPMA *via* ATRP. The analysis for the di-functional initiator and A-B-A triblock polymer are presented in the Appendix, Fig A32 & A33. To investigate the nanoparticle behaviour, co-nanoprecipitation experiments of both *p*(HPMA$_{120}$-*b*-PEG$_{\sim 105}$-*b*-HPMA$_{120}$) and *p*(HPMA$_{50}$-*co*-EGDMA$_{0.9}$) (50:50 wt%) were conducted. The PEG chain length and particular DP$_n$ of HPMA were selected based upon the success of the co-nanoprecipitation experiments which included the A-B block copolymer *p*(PEG$_{114}$-*b*-HPMA$_{120}$). Due to time constraints, the preliminary experiments were conducted for branched *p*(HPMA$_{50}$-*co*-EGDMA$_{0.9}$) only. When switching from an A-B block copolymer to an A-B-A triblock polymer, it was expected that during the co-nanoprecipitation bridging between the nanoparticles would be observed, and HPMA blocks from the A-B-A triblock could become incorporated into two different branched polymer cores. However, it appears that this did not occur and the nanoparticles formed during addition of the A-B-A to *p*(HPMA$_{50}$-*co*-EGDMA$_{0.9}$) were ~100 nm with a monomodal size distribution (Figure 6.1A).

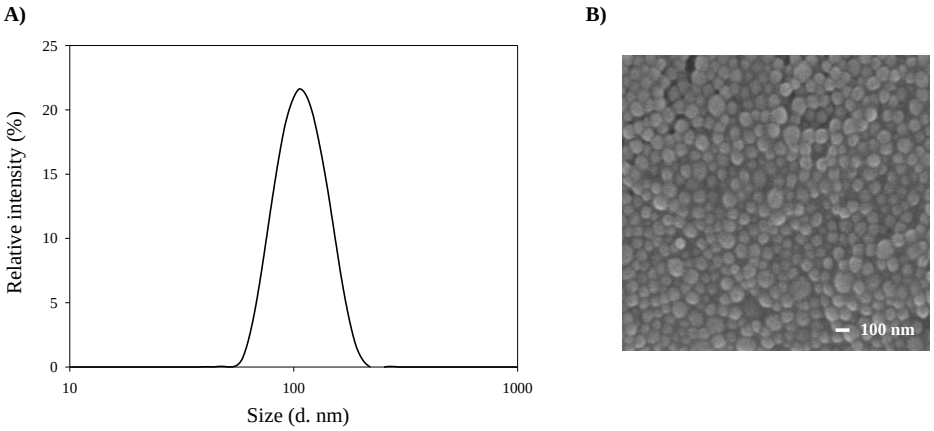

Figure 6.1 A) DLS size by intensity, *p*(HPMA$_{50}$-*co*-EGDMA$_{0.9}$):*p*(HPMA$_{120}$-*b*-PEG$_{\sim 105}$-*b*-HPMA$_{120}$) 50:50 wt %, B) Scanning electron microscopy image of *p*(HPMA$_{50}$-*co*-EGDMA$_{0.9}$):*p*(HPMA$_{120}$-*b*-PEG$_{\sim 105}$-*b*-HPMA$_{120}$) 50:50 wt % (Nanoparticles were diluted to 0.1 mg/mL for imaging).

When compared to the incorporation of the A-B block copolymer *p*(PEG$_{114}$-*b*-HPMA$_{120}$), the sizes obtained were very similar (103 nm), which further suggests bridging between

particles is not occurring. The nanoparticles were also analysed *via* SEM imaging and evidence of spherical nanoparticle formation was observed (Figure 6.1B).

To ascertain if anti-retroviral drug loaded nanoparticles could be prepared *via* co-nanoprecipitation, experiments including the A-B-A triblock polymer, *p*(HPMA$_{120}$-*b*-PEG$_{\sim 105}$-*b*-HPMA$_{120}$) were conducted. The polymers and antiretrovirals were dissolved in a good solvent and completely solubilised before addition to water. The good solvent which has been used for all co-nanoprecipitation experiments previously was acetone, but due to the poor solubility of the A-B-A triblock in this solvent, methanol was preferred. The DLS results for all encapsulation experiments are outlined in Table 6.1 and the corresponding DLS traces are presented in the Appendix, Fig A34. Interestingly, the co-nanoprecipitation of *p*(HPMA$_{50}$-*co*-EGDMA$_{0.9}$), A-B-A triblock polymer and an anti-retroviral gave promising results, as narrow size distributions were obtained for each sample and the nanoparticle sizes were within the range of 86-144nm. To explore the co-encapsulation of both ritonavir and lopinavir, encapsulation experiments at a 1:1 ratio, with a total wt % of 1, 5 and 10 were conducted. The ability to co-encapsulate drug molecules within a nanoparticle is very appealing and for this system 5 wt % of both ritonavir and lopinavir (total 10 wt %) have been co-encapsulated to generate stabilised nanoparticles.

Table 6.1 DLS analysis for *p*(HPMA$_{50}$-*co*-EGDMA$_{0.9}$):*p*(HPMA$_{120}$-*b*-PEG$_{\sim 105}$-*b*-HPMA$_{120}$) 50:50 wt % of encapsulated HIV antiretrovirals.

HIV Antiretroviral	Wt %	Size (d.nm)	PdI
Blank nanoparticles	0	112	0.068
Efavirenz	1	144	0.044
	5	106	0.049
	10	86	0.070
Ritonavir	1	92	0.043
	5	91	0.048
	10	134	0.043
Lopinavir	1	107	0.052
	5	113	0.058
	10	103	0.101
Ritonavir + Lopinavir (1:1)	1	103	0.050
	5	93	0.046
	10	95	0.058

The resulting nanoparticles formed after encapsulation and co-encapsulation are presented in Figure 6.2, and highlight the insolubility of the anti-retrovirals *vs* the dispersions obtained when co-nanoprecipitated with *p*(HPMA$_{50}$-*co*-EGDMA$_{0.9}$):*p*(HPMA$_{120}$-*b*-PEG$_{\sim 105}$-*b*-HPMA$_{120}$) 50:50 wt %. Although ritonavir and lopinavir are administered as a 4:1 ratio, this initial experiment has highlighted the possibility of encapsulating two drug molecules within a co-nanoprecipitated particle. The spherical shape of the nanoparticles was confirmed by SEM imaging (Figure 6.3). The maximum wt % of the antiretrovirals which could be encapsulated within co-nanoprecipitated particles which contain an A-B-A triblock polymer is yet to be investigated. The initial results from this study suggest that the co-nanoprecipitation process is not limited to incorporation of A-B block copolymers, and A-B-A triblock polymers also form stabilised nanoparticles with drug loading capabilities.

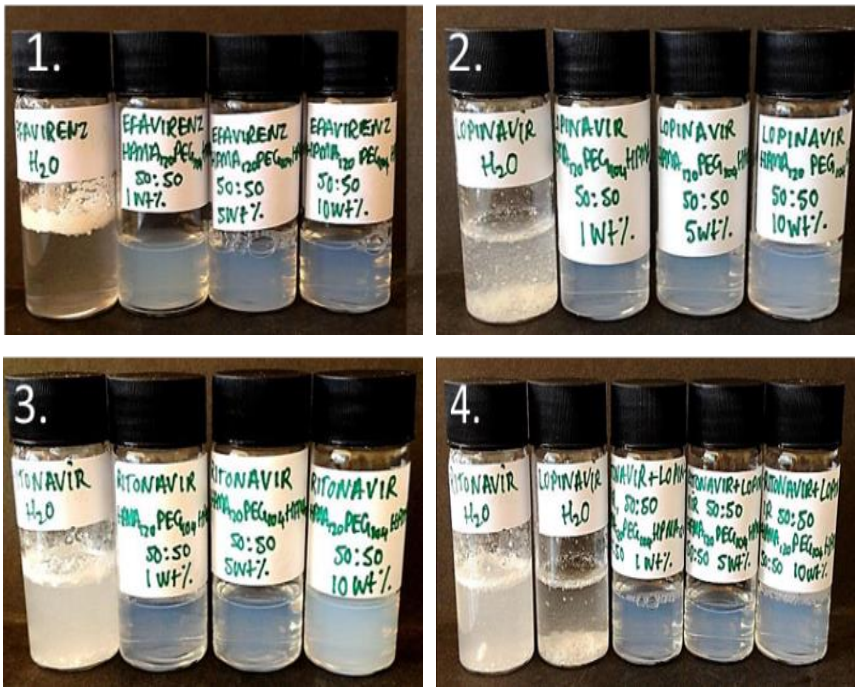

Figure 6.2 Photographs to show the solubility of 1) efavirenz, 2), lopinavir 3), ritonavir and 4) ritonavir and lopinavir (1:1) in water and the corresponding encapsulated co-nanoprecipitated particles of *p*(HPMA$_{50}$-*co*-EGDMA$_{0.9}$):*p*(HPMA$_{120}$-*b*-PEG$_{\sim 105}$-*b*-HPMA$_{120}$) (50:50 wt%) and each anti-retroviral, from left to right – 1 wt %, 5 wt % and 10 wt %.

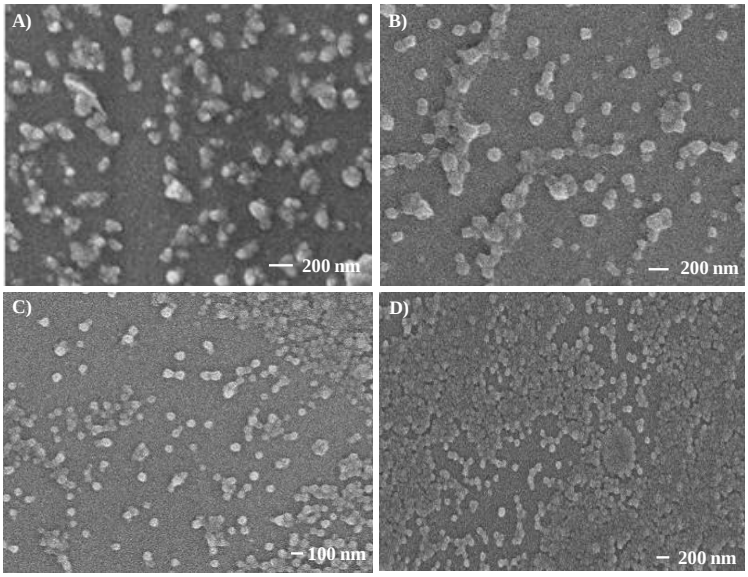

Figure 6.3 Scanning electron microscopy images of HIV encapsulated particles prepared from *p*(HPMA$_{50}$-*co*-EGDMA$_{0.9}$):*p*(HPMA$_{120}$-*b*-PEG$_{\sim 105}$-*b*-HPMA$_{120}$) 50:50 wt %, A) efavirenz 10 wt %, B) ritonavir 10 wt %, C) lopinavir 10 wt %, D) ritonavir and lopinavir (1:1) 10 wt %.

6.4 The preparation of ibuprofen polymer-drug conjugates and their incorporation into aqueous nanoparticles

6.4.1 Synthesis of ibuprofen modified polymers *via* ATRP

Polymer-drug conjugation is a widely exploited technique which is often utilised to improve the therapeutic properties of small therapeutic molecules, as discussed in Chapter 1, Section 1.2.4. Drug molecules which contain reactive functional groups such as carboxyl or hydroxyl moieties can be converted to a wide variety of polymerisable derivatives. The monomeric unit 2-hydroxypropyl methacrylate (HPMA) (**1**), has a pendant alcohol group, which can be further reacted with a small hydrophobic drug molecule. The drug molecule selected for the preliminary experiments was Ibuprofen (IBU) (**2**), due to the presence of a reactive carboxylic acid functional group. **1** and **2** were reacted *via* an activated Steglich esterification and IbuPMA (**3**) was successfully synthesised[1] (Scheme 6.1). For analysis of IbuPMA, see Appendix, Figure A35 & A36.

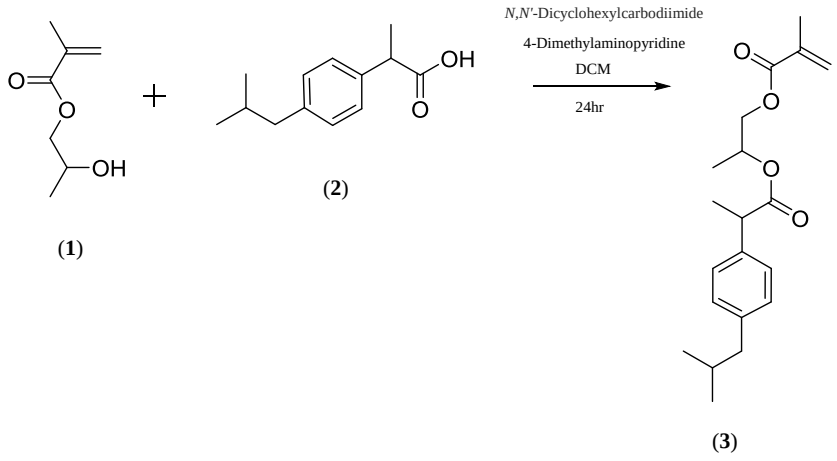

Scheme 6.1 Synthesis of IbuPMA.

Following the successful synthesis of IbuPMA, the preparation of the statistical copolymer, *p*(PEG$_{114}$-*co*-IbuPMA$_{20}$-*co*-HPMA$_{60}$) was conducted *via* ATRP (Scheme 6.2). For detailed GPC and ^{1}H NMR analysis, see Appendix, Table A14 & Fig. A37. The number of IbuPMA units determined by ^{1}H NMR was ~15 units per chain, and a higher M_n and M_w were achieved (M_n = 25600 & M_w = 31400 g/mol) when compared with *p*(PEG$_{114}$-*b*-HPMA$_{80}$) A-B block copolymer (M_n = 20600 & M_w = 25000 g/mol), which would be expected due to the increasing molecular weight of the IbuPMA monomeric unit.

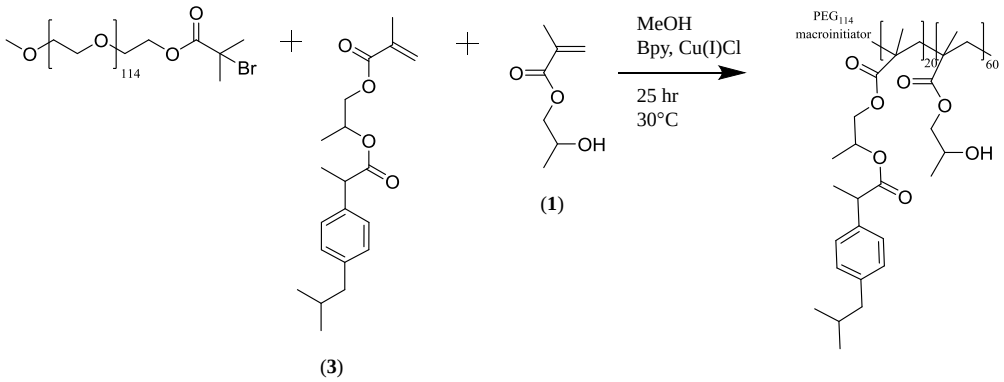

Scheme 6.2 Synthesis of *p*(PEG$_{114}$-*co*-IbuPMA$_{20}$-*co*-HPMA$_{60}$) *via* ATRP.

As well as incorporation of the monomeric unit IbuPMA, the post modification of *p*(PEG$_{114}$-*b*-HPMA$_{120}$) was also considered and IBU was directly reacted with the A-B block copolymer *via* an esterification reaction. The targeted polymer was *p*(PEG$_{114}$-*co*-HPMA$_{80}$-*co*-IbuPMA$_{40}$), as 40 HPMA monomer units were targeted with IBU. For detailed GPC and ^{1}H NMR analysis see Appendix, Table A15 & Fig. A38. The predicted number of IbuPMA units present by ^{1}H NMR was ~17 per chain, and an increase in

molecular weight was observed during GPC analysis (M_n = 37400, M_w = 47800 g/mol) when compared with the initial A-B block copolymer (M_n = 29500, M_w 37500 g/mol).

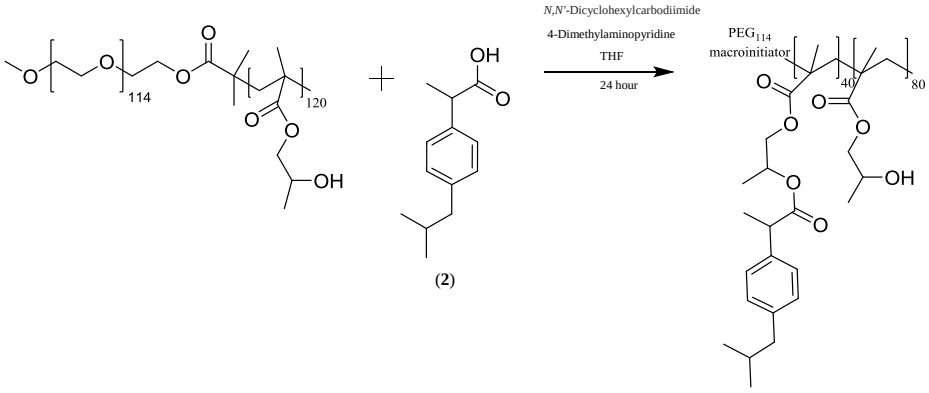

Scheme 6.3 Post modification of *p*(PEG_{114}-*b*-$HPMA_{120}$).

IbuPMA was successfully incorporated into two A-B polymers *via* two different methods, a statistical copolymerisation and post modification of an A-B block copolymer, therefore, the next step was to prepare an IBU modified branched polymer. IbuPMA, HPMA and EGDMA were polymerised *via* ATRP and the branched polymer targeted was *p*($HPMA_{60}$-*co*-$IbuPMA_{20}$-*co*-$EGDMA_{0.85}$) (Scheme 6.4). A high monomer conversion was achieved (98%) and the GPC results (M_n = 60000 and M_w = 986000 g/mol) suggested the formation of a high molecular weight branched architecture. For GPC analysis, see Appendix, A39.

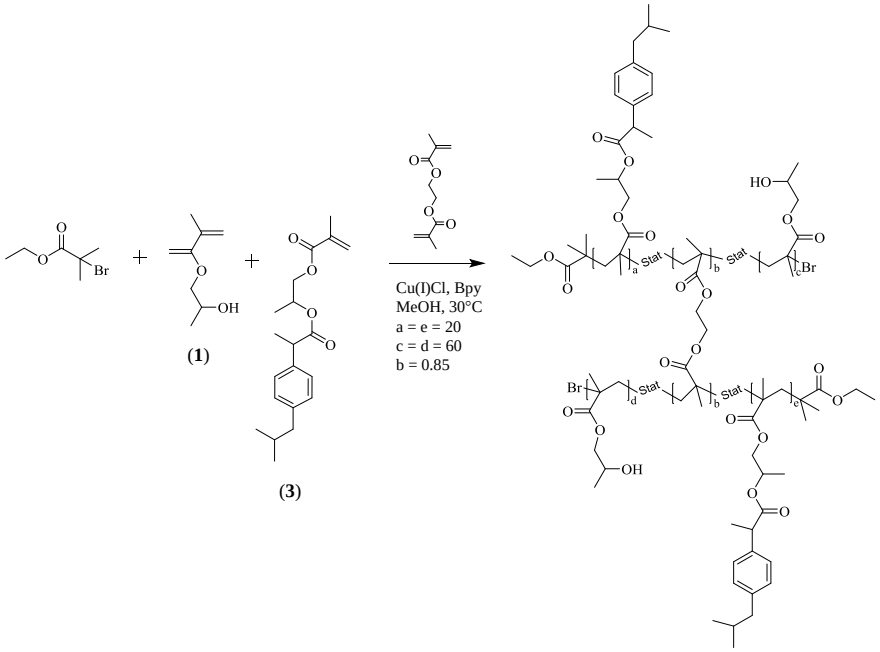

Scheme 6.4 Synthesis of *p*($HPMA_{60}$-*co*-$IbuPMA_{20}$-*co*-$EGDMA_{0.85}$).

6.4.2 Aqueous nanoprecipitation studies of an IBU polymer-drug conjugate

After successful synthesis of the IBU incorporated materials, co-nanoprecipitation experiments were conducted to determine if it was A) possible to co-nanoprecipitate an IBU modified A-B block copolymer and *p*(HPMA$_{50}$-*co*-EGDMA$_{0.9}$), B) co-nanoprecipitate IBU modified *p*(HPMA$_{60}$-*co*-IbuPMA$_{20}$-*co*-EGDMA$_{0.85}$) with an A-B block copolymer, C) co-nanoprecipitate IBU modified *p*(HPMA$_{60}$-*co*-IbuPMA$_{20}$-*co*-EGDMA$_{0.85}$) and an IBU modified A-B block copolymer and finally, D) co-nanoprecipitate IBU modified branched *p*(HPMA$_{50}$-*co*-EGDMA$_{0.9}$), IBU modified A-B block with free IBU (Figure 6.4).

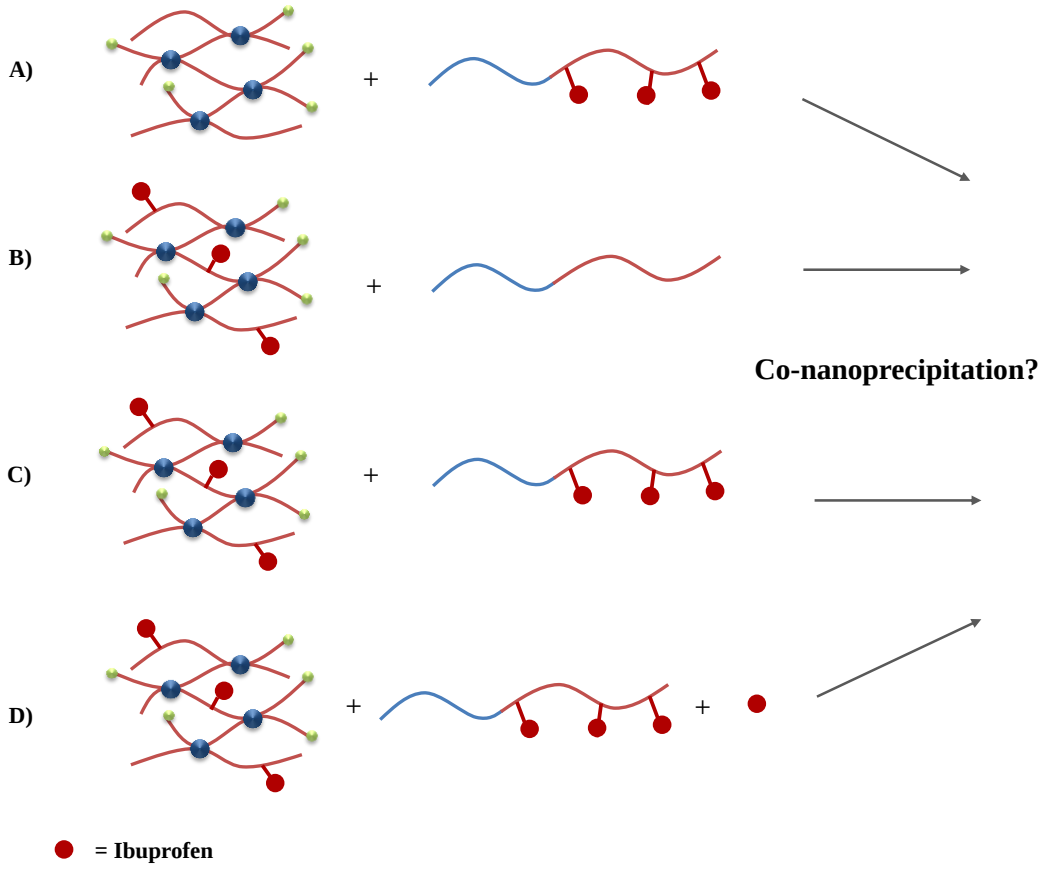

Figure 6.4 Schematic representation of the co-nanoprecipitation of the IBU incorporated materials.

During a typical co-nanoprecipitation experiment, 25 mg of an A-B polymer and 25 mg of a branched polymer were added to 10 mL of MeOH and solubilised for 6-8 hours. 1 mL of the 5 mg/mL solution of polymers was quickly added to 5 mL of stirring water and left for 24 hours for complete solvent evaporation.

During the co-nanoprecipitation of *p*(HPMA$_{50}$-*co*-EGDMA$_{0.9}$):*p*(PEG$_{114}$-*co*-HPMA$_{60}$-IbuPMA$_{20}$) (50:50 wt %), the nanoparticles formed had a broad PdI of 0.230 when compared with the co-nanoprecipitation conducted in the absence of IBU (Table 6.2). This suggests that the presence of the IbuPMA on the A-B polymer does affect the co-nanoprecipitation process, as a broader distribution of nanoparticles are formed. Interestingly, for the co-nanoprecipitation experiment including post modified *p*(PEG$_{114}$-*co*-HPMA$_{80}$-*co*-IbuPMA$_{40}$) and *p*(HPMA$_{50}$-*co*-EGDMA$_{0.9}$), stable nanoparticles with a size of 99 nm, PdI 0.156 were produced and were not too dissimilar from the comparison, *p*(HPMA$_{50}$-*co*-EGDMA$_{0.9}$):*p*(PEG$_{114}$-*b*-HPMA$_{120}$) (50:50 wt %). During inclusion of the IBU modified polymeric core, *p*(HPMA$_{80}$-*co*-IbuPMA$_{20}$-*co*-EGDMA$_{0.85}$) and the A-B block copolymer *p*(PEG$_{114}$-*b*-HPMA$_{80}$), there were minor differences in the absence of IBU suggesting the nanoprecipitation including *p*(HPMA$_{80}$-*co*-IbuPMA$_{20}$-*co*-EGDMA$_{0.85}$) generates stable nanoparticles with a narrow size distribution.

Table 6.2 DLS results for IBU co-nanoprecipitation experiments.

Figure 6.4 Ref.	Sample 50:50 wt %		Size (d.nm)	PdI
A)	No IBU	*p*(HPMA$_{50}$-*co*-EGDMA$_{0.9}$):*p*(PEG$_{114}$-*b*-HPMA$_{80}$)	111	0.081
	Incorporation of IbuPMA	*p*(HPMA$_{50}$-*co*-EGDMA$_{0.9}$):*p*(PEG$_{114}$-*co*-HPMA$_{60}$-*co*-IbuPMA$_{20}$)	108	0.230
A)	No IBU	*p*(HPMA$_{50}$-*co*-EGDMA$_{0.9}$):*p*(PEG$_{114}$-*b*-HPMA$_{120}$)	135	0.051
	Post modification of HPMA	*p*(HPMA$_{50}$-*co*-EGDMA$_{0.9}$):*p*(PEG$_{114}$-*co*-HPMA$_{80}$-*co*-IbuPMA$_{40}$)	99	0.156
B)	No IBU	*p*(HPMA$_{50}$-*co*-EGDMA$_{0.9}$):*p*(PEG$_{114}$-*b*-HPMA$_{80}$)	111	0.081
	Incorporation of IbuPMA to the branched core	*p*(HPMA$_{80}$-*co*-IbuPMA$_{20}$-*co*-EGDMA$_{0.85}$):*p*(PEG$_{114}$-*b*-HPMA$_{80}$)	114	0.116
C)	Combined IBU modified core and IBU A-B block (Statistical)	*p*(HPMA$_{80}$-*co*-IbuPMA$_{20}$-*co*-EGDMA$_{0.85}$):*p*(PEG$_{114}$-*co*-HPMA$_{60}$-*co*-IbuPMA$_{20}$)	72	0.266
C)	Combined IBU modified core and IBU A-B block (Post modified)	*p*(HPMA$_{80}$-*co*-IbuPMA$_{20}$-*co*-EGDMA$_{0.85}$):*p*(PEG$_{114}$-*co*-HPMA$_{80}$-*co*-IbuPMA$_{40}$)	63	0.122
D)	Combined Ibu core and Ibu A-B block + Free ibuprofen	*p*(HPMA$_{80}$-*co*-IbuPMA$_{20}$-*co*-EGDMA$_{0.85}$):*p*(PEG$_{114}$-*co*-HPMA$_{80}$-*co*-IbuPMA$_{40}$) + Free Ibuprofen (3 wt %)	92	0.217

To determine if stable nanoparticles could be prepared when both polymers included IBU, both *p*(HPMA$_{80}$-*co*-IbuPMA$_{20}$-*co*-EGDMA$_{0.85}$) and *p*(PEG$_{114}$-*co*-HPMA$_{60}$-*co*-IbuPMA$_{20}$) were co-nanoprecipitated. Although a broad PdI value was obtained, the nanoparticles appeared to be stabilised and macrophase separation was not observed. Interestingly, during the co-nanoprecipitation of *p*(HPMA$_{80}$-*co*-IbuPMA$_{20}$-*co*-EGDMA$_{0.85}$) and the post modified A-B polymer *p*(PEG$_{114}$-*co*-HPMA$_{80}$-*co*-IbuPMA$_{40}$), reasonably narrow nanoparticles were formed with a size of 63 nm. As a final experiment, all three components were co-nanoprecipitated, including *p*(HPMA$_{80}$-*co*-IbuPMA$_{20}$-*co*-

EGDMA$_{0.85}$)*:p*(PEG$_{114}$-*co*-HPMA$_{80}$-*co*-IbuPMA$_{40}$) 50:50 wt % + free Ibuprofen (3 wt %) and although a broad PdI was observed the formation of stable nanoparticles was achieved.

The ability to attach a hydrophobic drug molecule to both an A-B block copolymer and a branched copolymer has been successfully achieved and early co-nanoprecipitation experiments have shown that the formation of stabilised nanoparticles is possible. It is worth noting that the polymer-drug conjugate experiments were purely proof of concept in order to explore the versatility of the co-nanoprecipitation method. Further work would include cleavage of the hydrolysable ester bonds present and determination of the amount of IBU which is released, as the main purpose of polymeric prodrugs is the achievement of controlled drug release.

6.5 References

1. M. Babazadeh, M. Sheidaei, S. Abbaspour and L. Edjlali, *Scientia Pharmaceutica*, 2013, **81**, 281.

Chapter 7

Experimental

7.1 Experimental techniques

Both gel permeation chromatography (GPC) and dynamic light scattering (DLS) were used frequently throughout this PhD research and will be discussed in more detail below.

7.1.1 Gel permeation chromatography

Gel permeation chromatography (GPC) is a type of size exclusion chromatography (SEC) that separates molecules on the basis of size in an appropriate eluent. The separation of the different chain lengths within a polymer molecular weight distribution is performed by utilising columns containing porous beads with various pore sizes. The smaller polymeric materials can enter the pores more easily and therefore have a longer path length, increasing their retention time. Conversely, larger molecules spend little if any time in the pores and are eluted quickly. All columns have a range of molecular weights that can be separated.

Triple detection systems use refractive index (RI), differential viscometry and light scattering detectors to calculate the absolute molecular weight of the polymer. Each detector can be used to calculate different parameters which collectively determine the molecular weights of the different fractions within the polymer sample. The calculations conducted with the data collected by each detector are shown in equations (1) - (3) below, where, K_{RI}, K_V and K_{LS} are instrument calibration constants, *conc* is the concentration, and *dn/dc* is the change in RI (the RI increment) with the change in concentration. The RI detector is a concentration sensitive detector that simply measures the difference in refractive index between the eluent in the reference side, and the sample plus eluent in the sample side. The *dn/dc* is an important parameter and is calculated from the concentration entered when injecting the sample, whilst the viscometer also calculates the intrinsic viscosity of the sample based on this entered concentration. The differential refractometer calculates the *dn/dc* from the concentration entered when injecting the sample, whilst the viscometer also calculates the intrinsic viscosity of the sample based on the entered concentration. The absolute molecular weight calculated by light scattering is also dependant on the concentration and the square of the *dn/dc*. Therefore, it is crucial when using a triple detection GPC system, to calculate the concentration of the sample accurately as any errors can result in inaccurate calculation of molecular weights. Alternatively, if the *dn/dc* for the polymer is known, then it is possible to calculate the concentration of the sample and therefore the molecular weights and dispersity.

$$Refractometer = K_{RI}\, x\, \frac{dn}{dc}\, x\, conc \quad (1)$$

$$Viscometer = K_v\, x\, intrinsic\ viscosity\, x\, conc \quad (2)$$

$$Light\ scattering = K_{LS}\, x\, molecular\ weight\, x\, \left(\frac{dn}{dc}\right)^2\, x\, conc \quad (3)$$

7.1.2 Dynamic light scattering

Dynamic Light Scattering (DLS) works by measuring the intensity of light scattered by the molecules in the sample as a function of time. DLS is a well-established technique which relies on the calculation of particle size using Brownian motion. Brownian motion is the random movement of particles due to the bombardment by solvent molecules surrounding them. The smaller the particle is, the more rapid the Brownian motion and the larger the particle is, the slower the Brownian motion becomes. The velocity of the Brownian motion is defined by a property known as the translational diffusion coefficient (usually given the symbol, D). The size of the particle is calculated from the translational diffusion coefficient using the Stokes-Einstein equation;

$$d(H) = \frac{kT}{3\pi\eta D}$$

Where:-

d(H) = hydrodynamic diameter

k = Boltzmann's constant

T = absolute temperature

η = viscosity

D = translational diffusion coefficient

As well as D_z, the number average and volume average may also be calculated and can provide information about the particle population present in a sample. For the size distribution by intensity calculations, the intensity in light scattered is proportional to the diameter to the power of 6, therefore larger particles have a greater effect on the population. Therefore if an equal mixture of 10 and 100 nm particles was measured, the number average would be equal for both populations as they are present in a ratio of 1:1. The size distribution by volume would be 10^3 higher for the 100 nm compared to the 10 nm particle (the volume of a sphere is described as $4/3\pi(d/2)^3$). Whilst the size distribution by intensity will be even more weighted towards the 100 nm population as the 100 nm particles will scatter 10^6 as much light as the 10 nm particle. If a multimodal distribution

is observed, the number of particles present should be taken into consideration as although the larger nanoparticle population may appear, it is possible that the smaller particles present dominate.

7.2 Materials

Poly(ethylene glycol) monomethyl ether (M_n ~2,000 g/mol), poly(ethylene glycol) monomethyl ether (M_n ~5,000 g/mol), poly(ethylene) glycol (M_n ~4600 g/mol), triethylamine (TEA, 99%), 4-dimethylaminopyridine (DMAP, 99%), *N*,*N*′-dicyclohexylcarbodiimide, α-bromoisobutyryl bromide (BIBB, 98%), 2-hydroxypropyl methacrylate (HPMA, 97% mixture of isomers, contains 180-220 ppm monomethyl ether hydroquinone as inhibitor), ethyl α-bromoisobutyrate (EBiB, 98%), Cu(I)Cl (99%), 2,2'-bipyridyl (bpy, 99%), ethylene glycol dimethacrylate (EGDMA, 98%), tert-butyl methacrylate (*t*-BMA, 98%, contains 200 ppm monomethyl ether hydroquinone as inhibitor), *n*-butyl methacrylate (*n*-BMA, 99%, contains 10 ppm monomethyl ether hydroquinone as inhibitor), anisole (99%), fluoresceinamine, isomer I, pyrene (98 %), basic aluminium oxide and Dowex marathon exchange beads were purchased from Sigma Aldrich and used without any further purification. 2-(4-Isobutylphenyl)propionic Acid (98%) was purchased from TCI Europe. Efavirenz, lopinavir and ritonavir were purchased from LGM pharma. Biotech CE dialysis tubing, pre-wetted and hydrophilic (MWCO – 2000 g/mol, 100 kg/mol) was purchased from spectrum labs and used as received. All solvents were analytical grade and purchased from Fisher scientific and used as received.

7.3 Instrumentation

^{1}H and ^{13}C nuclear magnetic resonance (NMR) spectra were recorded in chloroform-d, methanol-d_4, acetone-d_6, DMSO-d_6 or D_2O using a 400 MHz Bruker Avance spectrometer. Chemical shifts are reported in parts per million (ppm) with respect to an internal reference of tetramethylsilane (0 ppm).

Average molecular weights (M_n & M_w g/mol) and dispersities (*Đ*) were estimated using; i) A triple detection gel permeation chromatography instrument (GPC; Malvern/Viscotek) equipped with a GPC max VE2001 auto-sampler, two Viscotek D6000 columns (and a guard column) and a triple detector array TDA305 (refractive index, light scattering and viscometer) with a mobile phase of DMF containing 0.01 M lithium bromide at 60°C and a flow-rate of 1 mL/min or ii) Malvern Viscotek instrument equipped with a GPCmax VE2001 auto-sampler, two Viscotek T6000

columns (and a guard column), a refractive index (RI) detector VE3580 and a 270 Dual Detector (light scattering and viscometer) with a mobile phase of THF (2 v/v % TEA) and a flow rate of 1.0 mL/min.

Dynamic light scattering (DLS) measurements were performed using a Malvern Zetasizer Nano ZS (4 mW He–Ne 633 nm laser) on nanoparticle dispersions at 1 mg/mL (unless otherwise stated) at 25 °C. Size measurements were obtained as an average of 3 individual measurements. Nanoparticle dispersions were measured directly without additional filtration or centrifugation. Zeta potentials were determined using the same apparatus described above. The measurements were obtained for aqueous dispersions at 1 mg/mL (unless otherwise stated) and 25°C using disposable capillary zeta cells.

Scanning electron microscopy (SEM) images were obtained using a Hitachi S-4800 FE-SEM. Aqueous nanoparticle samples (0.1 mg/mL in water) were dropped onto a silicon wafer mounted on an aluminum stub with a carbon tab, dried overnight at ambient temperature and then gold sputter-coated (EMITECH K550X) at 20 mA for 30 seconds.

Fluorescence spectra were obtained using a Shimadzu RF-5301PC spectrofluorophotometer. Emission spectra for pyrene were recorded between 300 and 500 nm. An excitation wavelength of λ_{ex} = 335 nm was used for all studies, as well as an excitational slit width of 1.5 nm and an emission slit width of 1.5 nm with a scan rate of 100 nm/min.

7.4 Chapter 2

7.4.1 Synthesis

7.4.1.1 Synthesis of linear *p*(HPMA$_{50}$) *via* ATRP

In a typical ATRP synthesis, EBiB (0.14 g, 0.69 mmol, 1 eq.), HPMA (DP_n = 50 monomer units, 5 g, 34.68 mmol, 50 eq.) and anisole (0.2 mL) were added to a round-bottomed flask equipped with a nitrogen inlet/outlet and a stirrer bar. Anhydrous methanol was added (50 wt %, based on HPMA) and the solution was degassed *via* nitrogen sparge for 10-15 minutes. The copper salt Cu(I)Cl (0.069 g, 0.69 mmol, 1 eq.) and bpy ligand (0.22 g, 1.39 mmol, 2 eq.) were added to the flask and

the reaction medium was further degassed for 5 mins. The reaction was carried out at 30°C and the monomer conversion was monitored by ^{1}H NMR spectroscopy. The polymerisation was terminated by exposure to air and addition of THF when the HPMA monomer had reached > 98 % conversion, judged by ^{1}H NMR. The polymer was purified using Dowex Marathon exchange beads (~10 g) in order to remove excess copper catalyst followed by passing the sample through a basic alumina column. Excess THF was removed under vacuum to concentrate the sample before precipitation into cold hexane. The resulting polymer was characterised by ^{1}H NMR in DMSO-d_6 and triple detection GPC with a mobile phase of DMF. ^{1}H NMR (400 MHz, DMSO-d_6) δ ppm = 4.85-4.5 (br, OH), 4.12-3.150 (br, 3H, CH_2 and CH from pendant group), 2.11-1.52 (br, 2H, CH_2 from polymer backbone), 1.32-0.50 (br, 6H, CH_3 from polymer backbone and CH_3 from pendant group).

7.4.1.2 Synthesis of *p*(HPMA$_{50}$-*co*-EGDMA$_{0.9}$) branched copolymer *via* ATRP

The branched copolymer, *p*(HPMA$_{50}$-*co*-EGDMA$_{0.9}$) was synthesised and purified using the procedure described above for linear *p*(HPMA$_{50}$) with the addition of the branching agent/co-monomer EGDMA (0.12 g, 0.62 mmol, 0.9 eq. to EBiB initiator). The resulting branched material was characterised by ^{1}H NMR in DMSO-d_6 and triple detection GPC with a mobile phase of DMF. ^{1}H NMR (400 MHz, DMSO-d_6) δ ppm = 4.85-4.50 (br, OH), 4.12-3.15 (br, 3H, CH_2 and CH from pendant group), 2.11-1.52 (br, 2H, CH_2 from polymer backbone), 1.32-0.50 (br, 6H, CH_3 from the polymer backbone and CH_3 from pendant group).

7.4.1.3 Synthesis of poly(ethylene glycol) mono-functional ATRP macro-initiator (PEG$_{45}$-Br)

For a typical synthesis, PEG$_{45}$-OH (30 g, 15 mmol, 1 eq.) was dissolved in toluene (100 mL) in the presence of triethylamine (2.275 g, 22.5 mmol, 1.5 eq.) and 4-dimethyl-aminopyridine (0.092 g, 0.75mmol 0.05 eq.) in a two necked round-bottomed flask fitted with an addition funnel, a nitrogen inlet/outlet and a stirrer bar. α-bromoisobutyryl bromide (5.175 g, 22.5 mmol, 1.5 eq.), diluted with toluene (15 mL), was placed into an addition funnel. The reactor was put under stirring at ambient temperature and the α-bromoisobutyryl bromide solution was added slowly over a period of 20-30 min and the reaction was left to stir for 24 hours. The rapid formation of a white precipitate (triethylamine salt $Et_3NH^+Br^-$) indicated the progress

of the reaction. The reaction medium was filtered and concentrated on the rotary evaporator. The resulting product was diluted in acetone and purified by precipitation into cold petroleum ether (40-60). This last step was repeated and the product was finally dried under vacuum at 40 °C for 24 hours. The resulting macro-initiator was confirmed by ^{1}H NMR in D_2O, triple detection GPC with a mobile phase of DMF and MALDI-TOF mass spectrometry. Yield = 75 %. ^{1}H NMR (400 MHz, D_2O) δ ppm = 4.31 (m, 2H), 3.76 (m, 2H), 3.56-3.4 (m, 181H), 3.55 (m, 2H), 3.31 (s, 3H) and 1.89 (s, 6H). MALDI-TOF: MNa^+ = distribution ~ 2054 Da.

7.4.1.4 Synthesis of poly(ethylene glycol) mono-functional ATRP macro-initiator (PEG_{114}-Br)

During a typical synthesis, MeO-PEG_{114}-OH (20 g, 4 mmol, 1 eq.) was dissolved in toluene (160 mL) in the presence of triethylamine (0.61 g, 6 mmol, 1.5 eq.) and 4-dimethyl-aminopyridine (0.024 g, 0.2 mmol, 0.05 eq.) in a two necked round-bottomed flask fitted with an addition funnel, a nitrogen inlet/outlet and a stirrer bar. α-bromoisobutyryl bromide (1.38 g, 6 mmol, 1.5 eq.), diluted with toluene (15 mL), was placed into an addition funnel. The reactor was put under stirring at ambient temperature and the α-bromoisobutyryl bromide solution was added slowly over a period of 20-30 minutes and the reaction was left to stir for 24 hours. The rapid formation of a white precipitate (triethylamine salt $Et_3NH^+Br^-$) indicated the progress of the reaction. The reaction medium was filtered and concentrated on the rotary evaporator. The resulting product was diluted in acetone and purified by precipitation into cold petroleum ether (40-60). This last step was repeated and the product was finally dried under vacuum at 40 °C for 24 hours. Yield = 71 %. ^{1}H NMR (400 MHz, D_2O) δ ppm = 4.31 (m, 2H), 3.76 (m, 2H), 3.56-3.4 (m, 456H), 3.55 (m, 2H), 3.31 (s, 3H) and 1.89 (s, 6H).

7.4.1.5 Synthesis of linear *p*(PEG_{45}-*b*-$HPMA_x$) *via* ATRP

In a typical reaction, targeting a number average degree of polymerisation (DP_n) of 120 monomer units, PEG_{45}-Br macroinitiator (0.62 g, 0.29 mmol, 1 eq.) and HPMA (5 g, 34.68 mmol, 120 eq.) and anisole (0.2 mL) were added to a round-bottomed flask equipped with a nitrogen inlet/outlet and a stirrer bar. Anhydrous methanol was added (50 wt %, based on HPMA) and the solution was degassed *via* nitrogen sparge for 10-15 minutes. The copper salt Cu(I)Cl (0.029 g, 0.29 mmol, 1 eq.) and bpy ligand (0.09 g, 0.58 mmol, 2 eq.) were added to the flask and the reaction medium was further degassed for 5 mins. The

reaction was carried out at 30°C and the monomer conversion was monitored by ^{1}H NMR spectroscopy. The polymerisation was terminated by exposure to air and addition of THF when the HPMA monomer had reached >97% conversion. The copper catalytic system was removed by passing the polymer solution through an alumina column. The solution was concentrated by rotary evaporation and the sample was purified by precipitation into 40-60 petroleum ether. The resulting polymer was characterised by ^{1}H NMR in DMSO-d_6 and triple detection GPC with a mobile phase of DMF. ^{1}H NMR (400 MHz DMSO-d_6) δ ppm = 4.94-4.50 (br, OH), 3.94-3.56 (br, 3H, CH_2 and CH from pendant group), 3.56-3.40 (br, 184H), 3.24 (s, 3H), 2.10-1.50 (br, 2H, CH_2 from polymer backbone), 1.30-0.50 (br, 6H, CH_3 from polymer backbone and CH_3 from pendant group). The resulting polymer was characterised by ^{1}H NMR in DMSO-d_6 and triple detection GPC with a mobile phase of DMF. The procedure described above was used for all other degree of polymerisations for HPMA 40 and 80.

7.4.1.6 Typical ATRP synthesis of a linear *p*(PEG$_{114}$-*b*-HPMA$_x$)

The same experimental applies as above for the synthesis of *p*(PEG$_{114}$-*b*-HPMA$_x$) with MeO-PEG$_{114}$-Br as opposed to the MeO-PEG$_{45}$-Br macroinitiator. The DP_n of HPMA targeted was 40, 80 and 120. The ATRP of *p*(PEG$_{114}$-*b*-*n*-BMA$_{120}$) was also carried out utilising the MeO-PEG$_{114}$-Br macroinitiator in MeOH at an increased temperature of 60°C and 50 wt % MeOH (relative to the HPMA monomer).

7.4.2 Aqueous nanoparticle formation

7.4.2.1 Typical nanoprecipitation

During a typical nanoprecipitation experiment, 50 mg of polymeric material was dissolved in 10 mL of analytical grade acetone for 12-24 hours for complete solubilisation. 1 mL of the resulting 5 mg/mL solution of polymers was added rapidly to 5 mL of deionised water (under vigorous stirring). The mixture was left for 24 hours at ambient temperature to ensure complete acetone evaporation leading to a final polymer concentration in water of 1 mg/mL.

7.4.2.2 Typical co-nanoprecipitation

During a typical co-nanoprecipitation, targeting a weight fraction of 50 wt % A-B block copolymer and 50 wt % branched copolymer, a total mass of 50 mg of material was weighed out (25 mg of *p*(HPMA$_{50}$-*co*-EGDMA$_{0.9}$) and 25 mg of *p*(PEG$_{45}$-*b*-HPMA$_{120}$)) into a vial. The polymers were dissolved in 10 mL of analytical grade acetone over a

period of 12-24 hours to ensure complete solubilisation. 1 mL of the resulting 5 mg/mL solution of polymers was added rapidly to 5 mL of deionised water (under vigorous stirring). The mixture was left for 24 hours at ambient temperature to ensure complete acetone evaporation leading to a final polymer concentration in water of 1 mg/mL.

7.4.2.3 Co-nanoprecipitation of *p*(HPMA$_{50}$-*co*-EGDMA$_{0.9}$) into aqueous solution of A-B block copolymer

A stock solution of *p*(HPMA$_{50}$-*co*-EGDMA$_{0.9}$) (2.5 mg/mL) was prepared in acetone and 1 mL of this solution was added to an A-B block copolymers solubilised in H_2O (0.1 mg/mL in 5 mL H_2O). The mixture was left for 24 hours at ambient temperature to ensure complete acetone evaporation leading to a final polymer concentration in water of 1 mg/mL.

7.4.2.4 Encapsulation of the hydrophobic guest molecule pyrene

Pyrene was dissolved in acetone to give a stock solution (0.1 mg/mL). The stock solution (300 μL, 0.1 mg/mL) was added to an empty vial and the acetone was allowed to evaporate to leave 30 μg of dye. For a typical 50:50 wt % co-nanoprecipitation, *p*(HPMA$_{50}$-*co*-EGDMA$_{0.9}$) (15 mg), *p*(PEG$_{45}$-*b*-HPMA$_{120}$) (15 mg) and 6 mL of acetone were added to the vial to give a final concentration of polymer 5 mg/mL and pyrene 5 μg/mL. The solution was left to stir for period of 12-24 hours for complete solubilisation. The nanoparticles were prepared by rapid addition of 1 mL of the solution into vigorously stirring deionised water (5 mL). The mixture was left for 24 hours at ambient temperature to ensure complete acetone evaporation leading to a final polymer concentration in water of 1 mg/mL and 1 μg/mL pyrene in water.

7.4.2.5 Solubility evaluation of *p*(PEG$_{45}$-*b*-HPMA$_{120}$)

The solubility of *p*(PEG$_{45}$-*b*-HPMA$_{120}$) in H_2O was determined by rolling a 0.5 mg/mL solution of *p*(PEG$_{45}$-*b*-HPMA$_{120}$) in deionised H_2O for 24 hour. The sample was then allowed to settle and 3 mL of the supernatant was added to a pre-weighed dish. After water evaporation (vacuum oven) the weight was recorded and the amount of *p*(PEG$_{45}$-*b*-HPMA$_{120}$) was calculated. This procedure was repeated 3 times to generate an average value.

7.4.2.6 NaCl stability studies

Prior to study, 1 mL of the 1 mg/mL nanodispersion was added to a vial and 20 µL of an aqueous NaCl (0.5M) solution was added. For the instant addition measurement, the solution was agitated before addition to a disposable sizing cuvette for DLS analysis (average of 3 measurements). The sample was returned to the vial for the 1, 7 and 21 day measurements and studies were carried out as described above.

7.2.4.7 Repeated aqueous NaCl addition

Prior to study, 1 mL of the 1 mg/mL nanodispersion was added to a disposable sizing cuvette and multiple additions of aqueous NaCl (0.5M, 2 µL- 2000 µL) were added, agitated quickly and instantly measured using DLS (average of 2 measurements).

7.2.4.8 Dialysis experiments

During a typical dialysis experiment, *p*(HPMA$_{50}$-*co*-EGDMA$_{0.9}$) (10 mg) and *p*(PEG$_{45}$-*b*-HPMA$_{120}$) (10 mg) were dissolved in acetone (5 mg/mL) and nanoprecipitated into H_2O (4 mL of polymer solution into 20 mL H_2O). After complete acetone evaporation, the nanoparticle dispersion was transferred into a 100 kg/mol MWCO dialysis membrane and placed into 1L of H_2O and left to stir for ~5 days (The solution within the dialysis membrane was sampled and measured by DLS at various time points), after which both solutions outside and within the dialysis membrane were concentrated *in vacuo* and further analysed by GPC.

7.5 Chapter 3

7.5.1 Synthesis of branched copolymers *via* ATRP

7.5.1.1 Synthesis of *p*(*n*-BMA$_{50}$-*co*-EGDMA$_{0.8}$) branched copolymer (Synthesised by Pierre Chambon – Rannard research group)

For the synthesis of *p*(*n*-BMA$_{50}$-*co*-EGDMA$_{0.8}$)**,** targeting a number average degree of polymerisation (DP_n) = 50 monomer units, EBiB initiator (137.2 mg, 0.70 mmol, 1 eq.), *n*-BMA (5 g, 35.16 mmol, 50 eq.), EGDMA (111.5 mg, 0.56 mmol, 0.8 eq.) and anisole (0.2 mL) were added to a round-bottomed flask equipped with a nitrogen inlet/outlet and a stirrer bar. To this, anhydrous MeOH (50 wt % based on *n*-BMA) was added and the solution was stirred and deoxygenated using a nitrogen (N_2) purge for 15 minutes. Cu(I)Cl (69.61 mg, 0.70 mmol, 1 eq.) and bpy (219.65 mg, 1.4 mmol, 2 eq.) were added to the

flask and left to purge for a further 5 minutes under a positive flow of N_2. The polymerisation mixture was left to polymerise at 60^0C and samples were taken periodically from the reaction mixture for ^{1}H NMR analysis. Reactions were terminated when > 98 % conversion was reached, as judged by ^{1}H NMR, by exposure to oxygen and addition of THF. The catalyst residues were removed by passing the mixture through a basic alumina column. THF was removed under vacuum to concentrate the sample before precipitation into cold methanol and drying in the vacuum oven overnight.

7.5.1.2 Synthesis of *p*(*t*-BMA$_{50}$-*co*-EGDMA$_{0.9}$) branched copolymer (Synthesised by Hannah Rogers – Rannard research group)

For the synthesis of *p*(*t*-BMA$_{50}$-*co*-EGDMA$_{0.9}$)**,** targeting a number average degree of polymerisation (DP_n) = 50 monomer units, EBiB initiator (109.7 mg, 0.56 mmol, 1 eq.), *t*-BMA (4 g, 28.13 mmol, 50 eq.) and EGDMA (100.36 mg, 0.50 mmol) and anisole (0.2 mL) were added to a round-bottomed flask equipped with a nitrogen inlet/outlet and a stirrer bar. To this, degassed aqueous isopropanol (IPA/H_2O) (92.5/7.5 %) (38.4 % v/v based on *t*-BMA) was added and the solution was stirred and deoxygenated using a nitrogen (N_2) purge for 15 minutes. Cu(I)Cl (55.7 mg, 0.56 mmol, 1 eq.) and bpy (175.7 mg, 1.125 mmol, 2 eq.) were added to the flask and left to purge for a further 5 minutes under a positive flow of N_2. The polymerisation mixture was left to polymerise at 30°C and samples were taken periodically from the reaction mixture for ^{1}H NMR analysis. Reactions were terminated when > 98 % conversion was reached, as judged by ^{1}H NMR, by exposure to oxygen and addition of THF. The catalyst residues were removed by passing the mixture through a basic alumina column. THF was removed under vacuum to concentrate the sample before precipitation into hexane and drying in the vacuum oven overnight.

7.5.1.3 Synthesis of *p*(HPMA$_{25}$-*co*-*n*-BMA$_{25}$-*co*-EGDMA$_{0.9}$) branched statistical copolymer

For the synthesis of *p*(HPMA$_{25}$-*co*-*n*-BMA$_{25}$-*co*-EGDMA$_{0.9}$), targeting a total number average degree of polymerisation (DP_n) = 50 monomer units, EBiB initiator (150 mg, 0.769 mmol, 1 eq.), HPMA (2.772g, 19.23 mmol, 25 eq.) *n*-BMA (2.735g, 19.23 mmol, 25 eq.), EGDMA (137.2 mg, 0.69 mmol, 0.9 eq.) and anisole (0.2 mL) were added to a round-bottomed flask equipped with a nitrogen inlet/outlet and a stirrer bar. To this, anhydrous MeOH (50 wt % based on *n*-BMA and HPMA) was added and the solution was stirred and deoxygenated using a nitrogen (N_2) purge for 15 minutes. Cu(I)Cl (76.1

mg, 0.769 mmol, 1 eq.) and bpy (240.2 mg, 1.54 mmol, 2 eq.) were added to the flask and left to purge for a further 5 minutes under a positive flow of N_2. The polymerisation mixture was left to polymerise at 30°C and samples were taken periodically from the reaction mixture for ^{1}H NMR analysis. Reactions were terminated when > 98 % conversion was reached, as judged by ^{1}H NMR, by exposure to oxygen and addition of THF. The catalyst residues were removed by passing the mixture through a basic alumina column. THF was removed under vacuum to concentrate the sample before precipitation into cold hexane and drying in the vacuum oven overnight.

7.5.1.4 Synthesis of *p*(HPMA$_{25}$-*co*-*t*-BMA$_{25}$-*co*-EGDMA$_{0.9}$) branched statistical copolymer

For the synthesis of *p*(HPMA$_{25}$-*co*-*t*-BMA$_{25}$-*co*-EGDMA$_{0.9}$), targeting a total number average degree of polymerisation (DP_n) = 50 monomer units, EBiB initiator (150 mg, 0.769 mmol, 1 eq.), HPMA (2.772g, 19.23 mmol, 25 eq.) *n*-BMA (2.735g, 19.23 mmol, 25 eq.), EGDMA (137.2 mg, 0.693 mmol, 0.9 eq.) and anisole (0.2 mL) were added to a round-bottomed flask equipped with a nitrogen inlet/outlet and a stirrer bar. To this, anhydrous MeOH (50 wt % based on *t*-BMA and HPMA) was added and the solution was stirred and deoxygenated using a nitrogen (N_2) purge for 15 minutes. Cu(I)Cl (76.1 mg, 0.769 mmol, 1 eq.) and bpy (240.2 mg, 1.538 mmol, 2 eq.) were added to the flask and left to purge for a further 5 minutes under a positive flow of N_2. The polymerisation mixture was left to polymerise at 30^{0}C and samples were taken periodically from the reaction mixture for ^{1}H NMR analysis. Reactions were terminated when >98 % conversion was reached, as judged by ^{1}H NMR, by exposure to oxygen and addition of THF. The catalyst residues were removed by passing the mixture through a basic alumina column. THF was removed under vacuum to concentrate the sample before precipitation into cold hexane and drying in the vacuum oven overnight.

7.1.1.5 ATRP synthesis of a linear *p*(PEG$_{114}$-*b*-*n*-BMA$_{120}$)

Same synthesis as described for *p*(PEG$_{114}$-*b*-HPMA$_x$) at an elevated temperature of 60°C (Section 7.4.1.6).

7.5.1.6 Encapsulation of fluoresceinamine (FA)

During a typical nanoparticle preparation, targeting 10 wt % FA, 5.56 mL of a 1 mg/mL acetone solution of FA was added to a vial and left to evaporate overnight. To this vial, 25 mg of the branched co/terpolymer and 25 mg of the A-B block copolymer were added

and dissolved in 10 mL of acetone during 6-8 hours to ensure complete solubilisation. 1 mL of the 5 mg/mL solution of polymers and FA was added to 5 mL of vigorously stirring deionised water and left for 24 hours for complete acetone evaporation (final concentration of polymer 1 mg/mL, FA 0.11 mg/mL).

7.5.1.7 Stability of FA encapsulated co-nanoprecipitated particles

For NaCl addition, as described in Section 7.4.2.6

For transport buffer solution (TBS) addition - prior to study, 1 mL of the 1 mg/mL nanodispersion was added to a vial and 1 mL of TBS solution was added. For the instant addition measurement, the solution was agitated before addition to a disposable sizing cuvette for DLS analysis (average of 3 measurements). The sample was returned to the vial for the 1, 7 and 21 day measurements and studies were carried out as described above.

7.6 Pharmacological Studies (Chapter 3)

As discussed throughout, pharmacology assessment of various co-nanoprecipitated materials was conducted. The fluoresceinamine encapsulated materials were studied to assess their cytotoxicity to Caco-2 cells, permeation through Caco-2 cell monolayers, cellular accumulation and permeation and accumulation in the presence of inhibitors.

7.6.1 Materials

Dulbecco's Modified Eagles Medium (DMEM), Hanks buffered saline solution (HBSS), Trypsin-EDTA, bovine serum albumin (BSA), FA, 3-(4,5-Dimethylthiazol-2-yl)-2,5-diphenyltetrazolium bromide (MTT reagent), acetonitrile (ACN) and all general laboratory reagents were purchased from Sigma (Poole, UK). Foetal bovine serum (FBS) was purchased from Gibco (Paisley, UK). The CellTiter-Glo® Luminescent Cell Viability Assay kit was from Promega (UK). The 24-well HTS transwell plates were obtained from Corning (New York, USA). The 96-well black walled, flat bottomed plates were from Sterilin (Newport, UK). Rotenone, 2-deoxyglucose, chlorpromazine hydrochloride, dansylcadaverine, indomethacin, genistein, dynasore hydrate were all purchased from Sigma Aldrich.

7.6.2 Characterisation

Cell count and viability was determined using a Countess automated cell counter (Invitrogen). Absorbance was read using a Tecan Genosis plate reader at 560 nm (Tecan Magellan, Austria).

Luminescence was then measured using a Tecan Genios plate reader (Tecan Magellan, Austria).

Fluoresceinamine encapsulated samples were run on a Dionex HPLC using a Fortis C18 column (100 mm x 4.6 mm i.d., 3 μm). The mobile phase consisted of: (A) 95% H_2O; 5% ACN; 5 mM NH_4FA (B) 95% ACN; 5% H_2O; 5 mM NH_4FA. Elution peaks were monitored with a fluorescence detector at; 490 (λ_{ex}), 530 (λ_{em}) (Thermo Spectrasystem FL3000) and subsequently analysed using Chromeleon v.6.8. software.

7.6.3 Routine cell culture/cell maintenance

Caco-2 cells were purchased from American Type Culture Collection (ATCC, USA) and maintained in Dulbecco's Modified Eagles Medium (DMEM) supplemented with 15 % filtered sterile foetal bovine serum. Cells were incubated at 37°C and 5 % CO_2 and were routinely sub-cultured every 4 days when 90 % confluent. Cell count and viability was determined using a Countess automated cell counter (Invitrogen).

7.6.4 Cytotoxicity studies (FA)

Caco-2 cells were seeded at a density of 1.0 x 10^4 cells / 100 μL in DMEM supplemented with 15 % FBS into each well of a 96 well plate (Nunclon, Denmark) and incubated at 37 °C and 5 % CO_2. Cells from 4 separate flasks of biological replicates of each cell type were used (N1-4) to improve statistical power. Media was then aspirated from column 1 and replaced with media containing each co-nanoprecipitated material or aqueous FA solution at an equivalent 1 μM FA concentration then diluted 1:1 in media across the plate up to column 11. For the aqueous preparation of fluoresceinamine the total DMSO added is <0.1% of the total volume of media. Column 12 served as a negative control and consisted of media and untreated cells. Following co-nanoprecipitated material addition, the plates were incubated for 24 hours or 5 days at 37 °C, 5 % CO_2 prior to assessment of cytotoxicity.

7.6.4.1 MTT cytotoxicity assay

Following incubation of treated plates for 24 hours or 120 h, 20 µL of 5 mg/mL MTT reagent was added to each well and incubated for 2 hours. Subsequently, 100 µL MTT lysis buffer (50 % *N*-*N*-Dimethylformamide in water containing 20 % SDS, 2.5 % glacial acetic acid and 2.5 % hydrochloric acid, pH 4.7) was added to each well to lyse overnight at 37 °C, 5 % CO_2. Following incubation the absorbance of each well was read using a Tecan Genosis plate reader at 560 nm (Tecan Magellan, Austria).

7.6.4.2 ATP cytotoxicity assay

Following incubation of treated plates for 24 hours or 5 days, cells were equilibrated to room temperature for approximately 30 minutes. All but 20 µL of media was removed from each well and 20 µL CellTiter-Glo® (Promega, UK) reagent was added. All reagents were made fresh and in accordance with the manufacturer's instructions. Plates were put on an orbital shaker for 10 minutes to mix contents and allow for stabilisation of luminescence signal. Luminescence was then measured using a Tecan Genios plate reader (Tecan Magellan, Austria).

7.6.5 Caco-2 permeation studies (FA)

Transwells were set up and propagated to a monolayer over a 21 day period as previously described. Only wells with TEER values >800 Ω were used. 10 µM of fluoresceinamine co-nanoprecipitated material or 10 µM aqueous fluoresceinamine (transport buffer spiked with DMSO dissolved fluoresceinamine, DMSO final volume <1 % of total volume), was added to the apical or basolateral compartment of the wells to quantify transport in both Apical>Basolateral (A>B) and Basolateral>Apical (B>A) directions (n=3). Plates were sampled following 4 hours incubation at 37°C, 5 % CO_2, apical and basolateral contents were stored at -30°C prior to analysis. To assess monolayer integrity following incubation, 250 µL of transport buffer containing 2 µL/mL ^{14}C mannitol was added to the apical compartment and incubated for 1 hour. 4 mL of scintillation fluid was added to 100 µL of the sampled contents and quantified on the scintillation counter (Packard 3100 TR).

7.6.6 Aqueous fluoresceinamine solution for cellular studies

An aqueous FA solution was prepared in DMSO at 1 mg/mL final concentration and used to spike either complete growth media or transport buffer. The resulting 1 µM final concentration FA solution was subsequently used in cytotoxicity assays or for transcellular permeability assessment respectively. Transport buffer consisted of; Hanks

buffered Saline Solution (HBSS), 25 mM 4-(2-hydroxyethyl)-1-piperazineethanesulfonic acid (HEPES), and 1 mg/mL Bovine Serum Albumin (BSA), adjusted to pH 7.4.

7.6.7 Extraction and quantification of fluoresceinamine

150 µL of sample and prepared calibration for each co-nanoprecipitated material, were extracted using 9 volumes of acetone, sonicated for 6 min and centrifuged for 3 min prior to drying at 30°C on a vacuum centrifuge. Each sample was reconstituted using 150 µL of 25 % DMSO. Samples were run on a Dionex HPLC using a Fortis C18 column (100 mm x 4.6 mm i.d., 3 µm). The mobile phase consisted of: (A) 95% H_2O; 5% ACN; 5 mM NH4FA (B) 95% ACN; 5% H_2O; 5 mM NH4FA. Elution peaks were monitored with a fluorescence detector at; 490 (λ_{ex}), 530 (λ_{em}) (Thermo Spectrasystem FL3000) and subsequently analysed using Chromeleon v.6.8. software.

7.6.8 Cellular accumulation of fluoresceinamine in Caco-2 and ATHP-1 cells

Caco-2 cells were seeded into 6 well plates (NunclonTM) at a density of 4 x 10^6 per well and incubated at 37°C 5 % CO_2 for 24 hours. THP-1 cells were seeded at a density of 4 x 10^6 cells per well in a 6 well plate and allowed to differentiate to ATHP-1 cells for 7 days in 10 nM PMA supplemented RPMI-1640 10% FBS prior to use. Following incubation, the media was aspirated and cells washed twice with HBSS (37°C) and subsequently replaced with pre-warmed (37°C) transport buffer solution containing either 10 µM (final concentration) aqueous fluoresceinamine or 10 µM (final concentration) co-nanoprecipitated fluoresceinamine material. Following 24 hours incubation at 37°C, 5 % CO_2, 150 µL of the extracellular media was sampled. The remaining media was aspirated and cells were washed twice with ice cold 290 HBSS. The ice cold HBSS was aspirated and replaced with 500 µL of a 50% acetone 50% water solution and incubated for 24 hours at -20°C, 150 µL of the lysate was subsequently sampled. Finally, 9 volumes of acetone was added to each intracellular and extracellular sample to extract fluoresceinamine for quantification on the HPLC as previously described, see Section 7.6.7. Average cell volumes were previously determined using a Scepter 2.0 Automated Cell Counter (Millipore) and used to calculate Cellular Accumulation Ratios (CAR); (Intracellular concentration/Volume)/(Extracellular concentration/Volume).

7.6.9 ATP depletion of Caco-2 cells using varying concentrations of 2-deoxyglucose and rotenone

Caco-2 cells were incubated with varying concentrations of 2-deoxyglucose and rotenone as outlined for 20 min at 37ºC 5% CO_2. Following incubation, ATP assays were carried out using CellTiter-GLO® kit to determine relative depletion of ATP compared to an untreated control.

7.6.10 Cellular accumulation ratio (CAR) of fluoresceinamine

Caco-2 cells were pre-incubated with 2 mg/ml 2-deoxyglucose and 100 nM rotenone for 20 min to deplete ATP. Following depletion, cells were washed three times using pre-warmed HBSS and replaced with media containing DMSO (<0.1% v/v) solubilised fluoresceinamine or co-nanoprecipitated fluoresceinamine material (10 µM final fluoresceinamine concentration) and incubated at 37ºC 5% CO_2 for 24 hours. Extra- and intracellular samples were extracted and analysed using HPLC as previously described. *, $P < 0.05$ (ANOVA) (n=4).

7.6.11 Apparent permeability (P_{app}) for fluoresceinamine encapsulated materials

Caco-2 cell monolayers were pre-incubated for 30 min in transport buffer containing either: 30 µM chlorpromazine (Chl); 200 µM dansylcadaverine (Dan); 10 µM genistein (Gen); 150 µM dynasore (Dyn); or 150 µM Indomethacin (Ind) prior to washing three times with pre-warmed (37ºC) HBSS. Following washing, the Caco-2 monolayers were co-incubated with the various endocytosis inhibitors as outlined, and either aqueous (DMSO spiked ; <0.1% v/v) or nanocarrier formulated fluoresceinamine for 4 h at 37˚C 5% CO_2. ***, $P < 0.001$ (ANOVA) (n=4).

7.6.12 Caco-2 permeation studies (FA) after presence of inhibitors and polymer nanocarrier materials

As described in section 7.6.5.

7.7 Chapter 4

7.7.1 Preparation of aqueous HIV anti-retroviral encapsulated nanoparticles (typical 10 wt % loading)

During a typical nanoparticle preparation, targeting 10 wt % anti-retroviral, 5.56 mL of a 1 mg/mL acetone solution of anti-retroviral was added to a vial and left to evaporate

overnight. To this vial, 25 mg of the branched co/terpolymer and 25 mg of the A-B block copolymer were added and dissolved in 10 mL of acetone during 6-8 hours to ensure complete solubilisation. 1 mL of the 5 mg/mL solution of polymers and anti-retroviral was added to 5 mL of quickly stirring deionised water and left for 24 hours for complete acetone evaporation (final concentration of polymer 1 mg/mL, anti-retroviral 0.11 mg/mL).

7.8 Chapter 5

7.8.1 Preparation of aqueous SN-38 encapsulated nanoparticles (typical 5 wt % loading)

Before conducting the co-nanoprecipitation experiments, a stock solution of SN-38 was prepared in THF:Acetonitrile 1:1 (1 mg/mL). During a typical co-nanoprecipitation, 2.635 mL of the SN-38 stock solution was added to a vial and to this, 25 mg of a branched copolymer and 25 mg of A-B block copolymer were added and dissolved in 7.365 mL of THF:Acetonitrile (1:1). The solution was tightly sealed and left rolling for 5 weeks to ensure complete solubilisation. 1 mL of the resulting 5 mg/mL solution of polymers and SN-38 was added rapidly to 5 mL of deionised water (under vigorous stirring). The mixture was left for 24 hours at ambient temperature to ensure complete THF and acetonitrile evaporation leading to a final polymer concentration in water of 1 mg/mL, 0.053 mg/mL SN-38).

7.8.2 Preparation of SN-38 nanoparticles *via* dialysis

During a typical dialysis experiment, 2.65 mL of SN-38 dissolved in DMSO solution (1 mg/mL), 25 mg of the branched copolymer and 25 mg of the A-B block copolymer were dissolved in 7.35 mL of DMSO during 6-8 hours to ensure complete solubilisation. 1 mL of the 5 mg/mL solution of polymers was added to a dialysis membrane with a molecular weight cut off (MWCO) of 2000 g/mol and left to dialyse in deionised water during 4 days (regular water changes).

7.9 Pharmacology Studies (Chapter 5)

7.9.1 Materials

Irinotecan and SN-38 were purchased from J&HChem chemical company. [3-(4,5-dimethylthiazol-2-yl)-5-(3-carboxymethoxyphenyl)-2-(4-sulfophenyl)-2H-tetrazolium, inner salt;MTS] CellTiter 96® AQ_{ueous} One Solution Cell Proliferation Assay (MTS) from promega. All general laboratory reagents were purchased from Sigma Aldrich. CT26 cells

were purchased from American Type Culture Collection (ATCC) and HCT116 from European Collection of Cell Cultures (ECACC). Dulbecco's Modified Eagles Medium (DMEM) and Roswell Park Memorial Institute (RPMI) 1640 medium were purchased from Sigma Aldrich. Trypsin-EDTA and fetal bovine serum (FBS) were purchased from life technologies. Greiner CELLSTAR® 96 well plates and Varioskan™ Flash Multimode reader at 490 nm was used for all assays.

7.9.2 Determination of cell viability - MTS assay

During a typical experiment, CT26 or HCT116 cells were seeded at a density of 0.5 x 10^4 cells / 100 µL in DMEM supplemented with 10 % FBS into each well of a 96 well plate and left overnight to adhere. Media was then aspirated from each well and replaced with media containing each co-nanoprecipitated material or control solution at the desired concentrations. Following co-nanoprecipitated material addition, the plates were incubated for 48 hours at 37 °C, 5 % CO_2 prior to assessment of cytotoxicity. MTS/ phenazine methosulfate was added (20µL per well) and the plates were incubated for 2.5 hours, after which the absorbance was recorded at 490 nm.

7.9.3 *In vitro* cytotoxic effect of different concentrations of irinotecan and SN-38 (free drug molecules)

7.9.3.1 Irinotecan

During a typical experiment, CT26 or HCT116 cells were seeded at 96 well plate with 5000-10000 cells / well (0.5-1 x 10^6 per ml) in DMEM supplemented with 10 % FBS into each well and incubated at 37 °C and 5 % CO_2. The cells were left overnight to adhere. After 24 hours, the media was aspirated and 100uL each concentration after vortexing were dosed with irinotecan at 300, 100, 33.3, 11.1, 3.7, 1.23 and 0 µM and the control of DMSO in media. Wells were 0.375% DMSO by volume**.** The plates were incubated for 48 hours at 37 °C, 5 % CO_2 prior to assessment of cytotoxicity. MTS/ phenazine methosulfate was added (20µL per well) and the plates were incubated for 2.5 hours, after which the absorbance was recorded at 490 nm using the plate reader.

7.9.3.2 SN-38

Same as for irinotecan above (Section, 7.9.3.1) but within the concentration range, 9, 3, 1, 0.33, 0.11 and 0.037 µM.

7.9.3.3 *In vitro* cycotxicity for co-nanoprecipitated materials, irinotecan and SN-38 for both CT26 and HCT116 cells

96 well plate with 10000 cells / well (10 x 10^5 per ml) 100µL. 5mg/ml MTT dissolved in Hanks – as before MTS. Plate out cells at 5000 per well per plate which were left overnight to adhere. **For SN-38 co-nanoprecipitated materials -** 100µL consisting of either SN-38 co-nanoprecipitated materials, blank co-nanodispersions, media and water final concentrations 4µM 2µM and 1µM. **For 100% SN-38 in DMSO -** 4µM, 2µM and 1µM. **For controls -** 1.6µL DMSO was added to 968.4µL media followed by 30µL sterile water. Add 30uL sterile water to 970µL media. **For blank co-nanoprecipitated materials -** Concentrations 4µM, 2µM and 1µM. Media was aspirated on a 96 well plate and dosed with 100µL of each solution in triplicate. This was left for 48 followed by MTS addition. 20µL MTS was added per well and left for 2.5 hours and the absorbance was measured at 490 nm using the plate reader.

7.9.4 *In vitro* cycotxicity dose response for irinotecan SN-38 and co-nanoprecipitated nanomaterials for both CT26 and HCT116

7.9.4.1 Irinotecan

The MTS assay was conducted as discussed above. A 40mM irinotecan stock solution (2.346mg in 100µL DMSO). 5µl of this stock solution was added to 2147.2µL of water + 77.8µL DMSO (ensuring complete solubilisation) giving a 89.77µM stock solution (Irinotecan in DMSO/water – 0.32% DMSO. A serial dilution of this stock was then carried out to give the following concentrations: 8µM, 4µM, 2µM, 1µM, 0.5µM and 0.25µM. 100µL added of each.

7.9.4.2 SN-38

This MTS assay was conducted as discussed above. A 2.5mM stock SN-38 solution (2mg in 2000uL DMSO) (SN-38 in DMSO/water – 0.32% DMSO). 10µL of this solution was added to 269µL of water (ensure all dissolved) giving a 89.77µM stock solution. A serial dilution of this stock was then carried out to give the following concentrations: 8µM, 4µM, 2µM, 1µM, 0.5µM and 0.25µM. The two control experiments were media and water and media, water and DMSO.

7.9.4.3 Blank co-nanoprecipitated materials

The MTS assay was conducted as discussed above. A serial dilution of this stock was then carried out to give the following concentrations of co-nanoprecipitated materials: 8µM, 4µM, 2µM, 1µM, 0.5µM and 0.25µM. 100µL added of each.

7.9.4.4 SN38 co-nanoprecipitated materials

The MTS assay was conducted as discussed above. A serial dilution of this stock was then carried out to give the following concentrations of co-nanoprecipitated materials: 8µM, 4µM, 2µM, 1µM, 0.5µM and 0.25µM. 100µL added of each.

7.10 Chapter 6

7.10.1 Preparation of an A-B-A triblock and subsequent nanoparticles studies

7.10.1.1 Synthesis of Br-PEG~$_{105}$-Br bifunctional macro-initiator

During a typical synthesis, OH-PEG~$_{105}$-OH (M_n ~4600g, 20 g, 4.35 mmol, 1 eq.), TEA (13.05 mmol, 1.819 mL, 3 eq.) and DMAP (0.053 g, 0.435 mmol, 0.1 eq.) were added to toluene (80 mL) in a two necked round bottom flask fitted with a nitrogen inlet/outlet and stirrer bar. α-bromo isobutyryl bromide (13.05 mmol, 1.613 mL, 3 eq.) diluted in toluene (20mL) was added drop-wise over 15 minutes through an additional funnel and left to stir at ambient temperature for 24 hours. Excess amine was removed using DOWEX marathon exchange beads. This was then filtered and the solvent removed by rotary evaporation. The product was dissolved in acetone, concentrated and purified by precipitation into cold petroleum ether 40-60°C and dried under vacuum. The difunctional macro-initiator was analysed by ^{1}H NMR and GPC. Yield = 72%. ^{1}H NMR (400 MHz, D_2O) δ ppm= 1.8 (s, CH_3), 3.7-3.4 (m, CH_2 polymer backbone), 4.6 (m, polymer backbone signals).

7.10.1.2 Synthesis of *p*(HPMA$_{120}$-*b*-PEG~$_{105}$-*b*-HPMA$_{120}$) *via* ATRP

In a typical reaction, targeting a number average degree of polymerisation (DP_n) of a total of 240 monomer units, Br-PEG$_{\sim 105}$-Br macroinitiator (1.063 g, 0.23 mmol, 1 eq.) and HPMA (8.0 g, 55.4 mmol, 240 eq.) and anisole (0.2 mL) and anhydrous methanol (50 wt %, based on HPMA) was added to a round bottomed flask fitted with an nitrogen inlet/outlet and stirrer bar. The solution was degassed *via* nitrogen sparge for 10-15 minutes. The copper salt Cu(I)Cl (0.023 g, 0.23 mmol, 1 eq.) and bpy ligand (0.072 g, 0.46 mmol, 2 eq.) were added to the flask and the reaction medium was further degassed for 5 mins. The reaction was carried out at 30°C and the monomer conversion was

monitored by ^{1}H NMR spectroscopy. The polymerisation was terminated by exposure to air and addition of methanol when the HPMA monomer had reached > 99% conversion. The copper catalytic system was removed by passing the polymer solution through an alumina column. The solution was concentrated by rotary evaporation and the sample was purified by precipitation into cold hexane. The resulting block copolymer was analysed by ^{1}H NMR and GPC.

7.10.1.3 Preparation of aqueous polymer nanoparticles including an A-B-A triblock polymer and anti-retroviral encapsulation

Methanol was used as the good solvent and the procedure was as previously described in Section 7.7.1.

7.10.2 Ibuprofen modified polymers

7.10.2.1 Synthesis of the ibuprofen modified HPMA (IbuPMA)

During a typical synthesis, HPMA (1.5 g, 10.40 mmol 1 eq.), Ibuprofen (2.79 g, 13.52 mmol 1.3 eq), DMAP (0.64 g, 5.2 mmol, 0.5 eq) and DCC (2.79g, 13.53 mmol, 1.3 eq) were dissolved in 30 mL of THF in a round bottom flask and stirred at ambient temperature for 24 hours. The DCU salt was filtered and the product was washed with THF followed by rotary evaporation. DCM (100 mL) was added and the product washed with 1M sodium bisulfate solution to remove excess DCU, then dried over $NaSO_4$ and concentrated *in vacuo*. Residual DCU was removed by storage of the monomer at -20°C and a minimal amount of ethyl acetate followed by filtration. The final product was stored at -20°C. Yield = 68%. ^{1}H NMR (400 MHz, $CDCl_3$) δ ppm, 7.10 (m, 4H, CH), 6.02 (m, 1H, CH), 5.52 (m, 1H, CH), 5.2 (m, 1H CH), 4.15 (m, 2H CH_2), 3.69 (m, 1H, CH), 2.43 (d, 2H, CH_2), 2-1.75 (m, 4H), 1.47 (d, 3H, CH_3), 1.19 (d, 3H, CH_3), 0.88 (d, 6H, CH_3).

7.10.2.2 Synthesis of *p*(PEG$_{114}$-*b*-HPMA$_{60}$-*co*-IbuPMA$_{20}$) *via* ATRP

The targeted degree of polymerisation (DP_n) was HPMA$_{60}$-IbuPMA$_{20}$. MeO-PEG$_{114}$-Br macroinitiator (0.59 g, 0.116 mmol, 1 eq.) and HPMA (1 g, 6.96 mmol, 60 eq.) and IbuPMA (0.77 g 2.32 mmol, 20 eq.) were added to a round-bottomed flask equipped with a nitrogen inlet/outlet and a stirrer bar. Methanol was added (43 wt %, based on HPMA + IbuPMA) and the solution was stirred vigorously under nitrogen for 10-15 minutes. The copper catalyst Cu(I)Cl (11.48 mg, 0.116 mmol, 1 eq.), bpy (0.036 g, 0.232 mmol, 2 eq.) and anisole (0.2 mL) were added to the flask and the temperature was fixed at 30°C. The reaction was monitored by ^{1}H NMR spectroscopy and terminated with methanol when

both monomers had reached >98% conversion. The polymer was purified using a neutral alumina column flushed with THF to remove excess copper catalyst. Excess THF was removed under vacuum to concentrate the sample before precipitation into cold 40-60 petroleum ether. The resulting polymer was confirmed by ^{1}H NMR in methanol-d_4, triple detection GPC with a mobile phase of THF.

7.10.2.3 Post modification of *p*(PEG$_{114}$-*b*-HPMA$_{120}$)

MeO-PEG$_{114}$-HPMA$_{120}$ (1 g, 0.033 mmol, 1 eq.), Ibuprofen (0.27 g, 1.33 mmol, 40 eq.), DCC (0.274 g, 1.33 mmol, 40 eq.) and DMAP ($1x10^{-3}$ g) were dissolved in THF (12 mL) and left to react for 24 hours. The DCU salt was filtered off and the product was washed with THF and concentrated *in vacuo*. The polymer was dissolved in a minimal amount of THF and precipitated into cold hexane. Excess DMAP and DCU were removed by dissolving the product in DCM, washing with 1M sodium bisulfate, dried with $MgSO_4$ and dried under vacuum. The resulting polymer was confirmed by ^{1}H NMR in DMSO-d_6, triple detection GPC with a mobile phase of THF.

7.10.2.4 Synthesis of *p*(HPMA$_{60}$-*co*-IbuPMA$_{20}$-*co*-EGDMA$_{0.85}$) *via* ATRP

The targeted degree of polymerisation (DP_n) monomeric units of HPMA. During a typical ATRP synthesis, EBiB initiator (0.012 g, 0.060 mmol 1 eq.) and HPMA (0.52 g, 0.217 mmol 60 eq.) and IbuPMA (0.4 g, 0.012 mmol, 20 eq.) were added to a round-bottomed flask equipped with a nitrogen inlet/outlet and a stirrer bar. Methanol was added (50 wt%, based on HPMA + IbuPMA) and the solution was stirred vigorously under nitrogen for 10-15 minutes. The branching agent EGDMA (0.1015 g, 0.051 mmol 0.85 eq. to EBiB initiator), copper catalyst Cu(I)Cl (0.0059, 0.06 mmol, 1 eq.) and bpy (0.0188 g, 0.121 mmol 2 eq.) and anisole (0.2 mL) were added to the flask and the temperature was fixed at 30°C. The reaction was monitored by ^{1}H NMR spectroscopy and terminated with methanol when the monomers had reached >98% conversion. The polymer was purified using a neutral alumina column flushed with THF. Excess THF was removed under vacuum to concentrate the sample before precipitation. The polymer was precipitated from MeOH into cold petroleum ether 40-60. The resulting polymer was confirmed by ^{1}H NMR in methanol-d_4, triple detection GPC with a mobile phase of THF.

7.10.3 Aqueous nanoparticle preparation including ibuprofen modified polymers

During a typical nanoparticle preparation, targeting 50 wt % of each polymer, 25 mg of block copolymer and 25 mg of branched polymer were added to 10 mL of MeOH during

6-8 hours to ensure complete solubilisation over 6-8 hours. 1 mL of the 5 mg/mL solution of polymers was added to 5 mL of vigorously stirring deionised water and left for 24 hours for complete methanol evaporation.

The same procedure was repeated for other variations of the nanoparticles using the same experimental as described above. Free ibuprofen was also added at the desired wt % based on the total mass of both polymers into the good solvent methanol.

Appendix

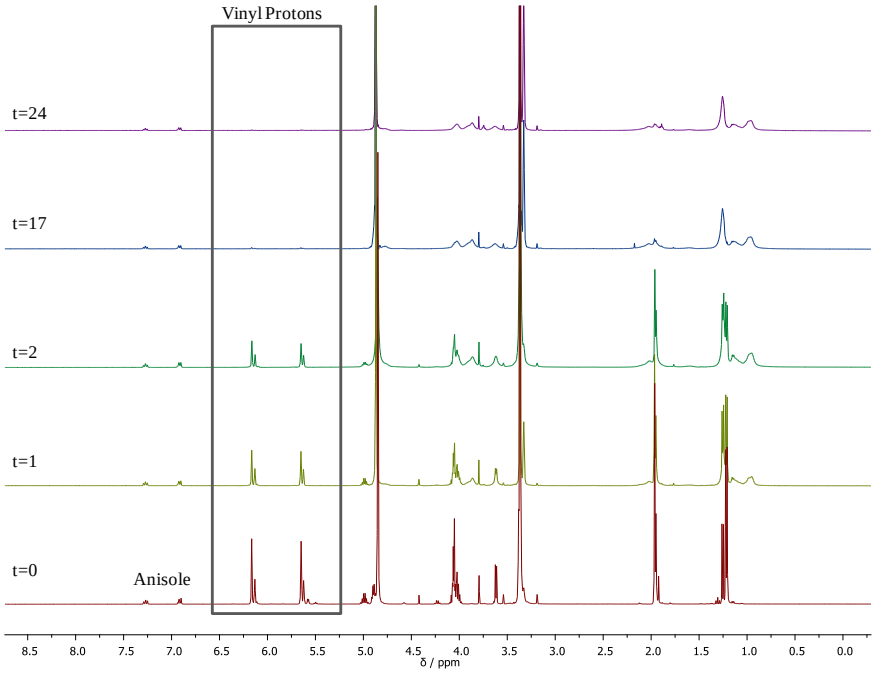

Figure A1 Overlay of branched *p*(HPMA$_{50}$-*co*-EGDMA$_{0.9}$) ^{1}H NMR conversion during polymerisation.(MeOD-d$_4$, 400 MHz).

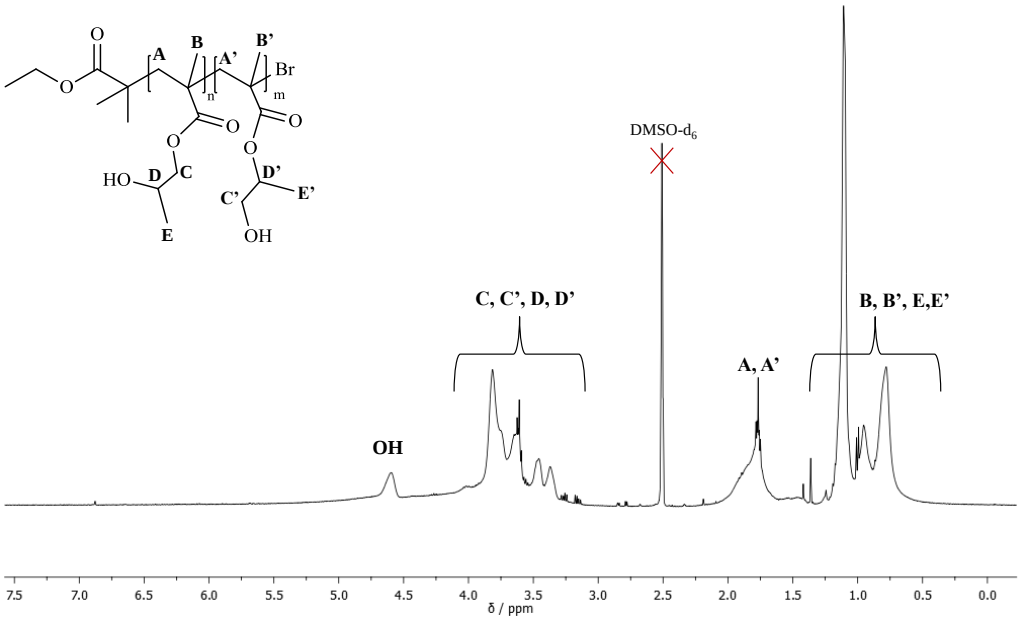

Figure A2 ^{1}H NMR analysis of *p*(HPMA$_{50}$) (DMSO-d$_6$, 400 MHz).

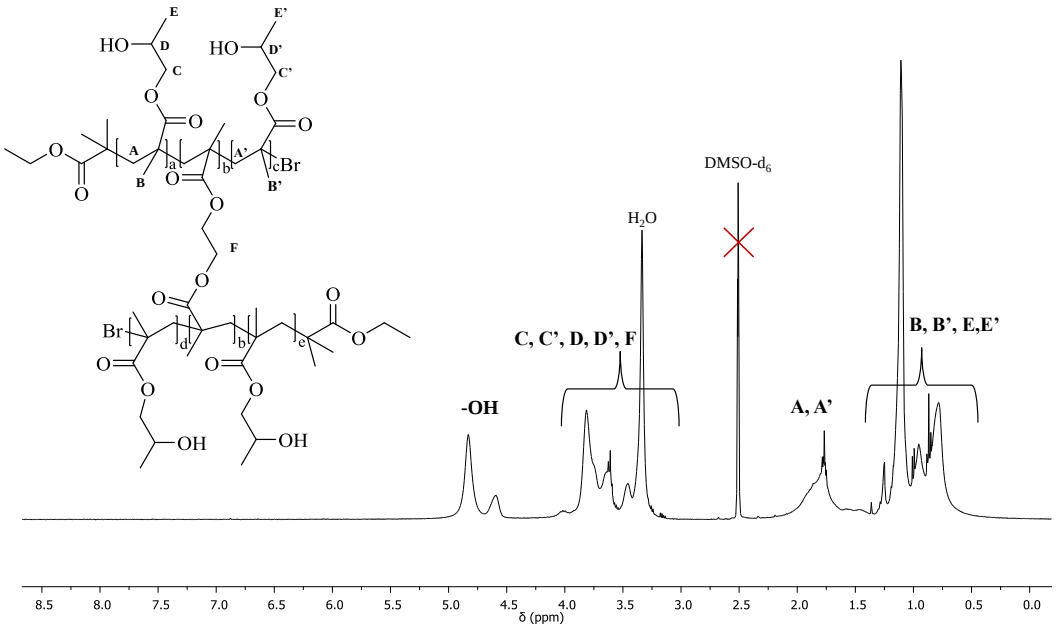

Figure A3 ^{1}H NMR analysis of *p*(HPMA$_{50}$-*co*-EGDMA$_{0.9}$) (DMSO-d$_6$, 400 MHz).

Table A1 DLS analysis for nanoprecipitation studies of *p*(HPMA$_{50}$-*co*-EGDMA$_{0.9}$) before and after solvent addition.

Good Solvent Volume (mL)	Before Evaporation			After Evaporation		
	Dz (nm)	PdI	Derived Count Rate (kcps)	Dz (nm)	PdI	Derived Count Rate (kcps)
Acetone						
0.5	140	0.117	1394010	120	0.067	1696472
1	135	0.064	591488	111	0.081	1359462
2	156	0.048	341167	132	0.097	1570382
3	226	0.099	90623	170	0.053	571615
4	47	0.233	694	1098	0.352	30864
5	35	0.288	554	989	0.345	67004
8	51	0.339	614	2154	0.195	9665
THF						
0.5	177	0.109	1485997	144	0.105	1731661
1	177	0.073	641263	123	0.062	1680069
2	381	0.011	646167	221	0.166	1556198
3	475	0.085	163221	307	0.355	315311
4	604	0.218	11148	368	0.189	239010
5	31	0.628	1034	372	0.447	12652
8	23	0.768	769	1554	0.757	29254

Table A2 DLS analysis for increasing multiple nanoprecipitation experiments

Volume of Polymer in Solution Added (mL)	Addition no.	D_z (nm)	PdI	Derived count rate (kcps)
Acetone				
3	1	162	0.054	1443879
	2	293	0.156	1369079
4	1	452	0.132	531722
	2	831	0.541	49720
THF				
3	1	143	0.047	1471637
	2	*	*	*
4	1	538	0.145	527875
	2	*	*	*

* Polymer precipitated visible, sample not suitable for DLS analysis

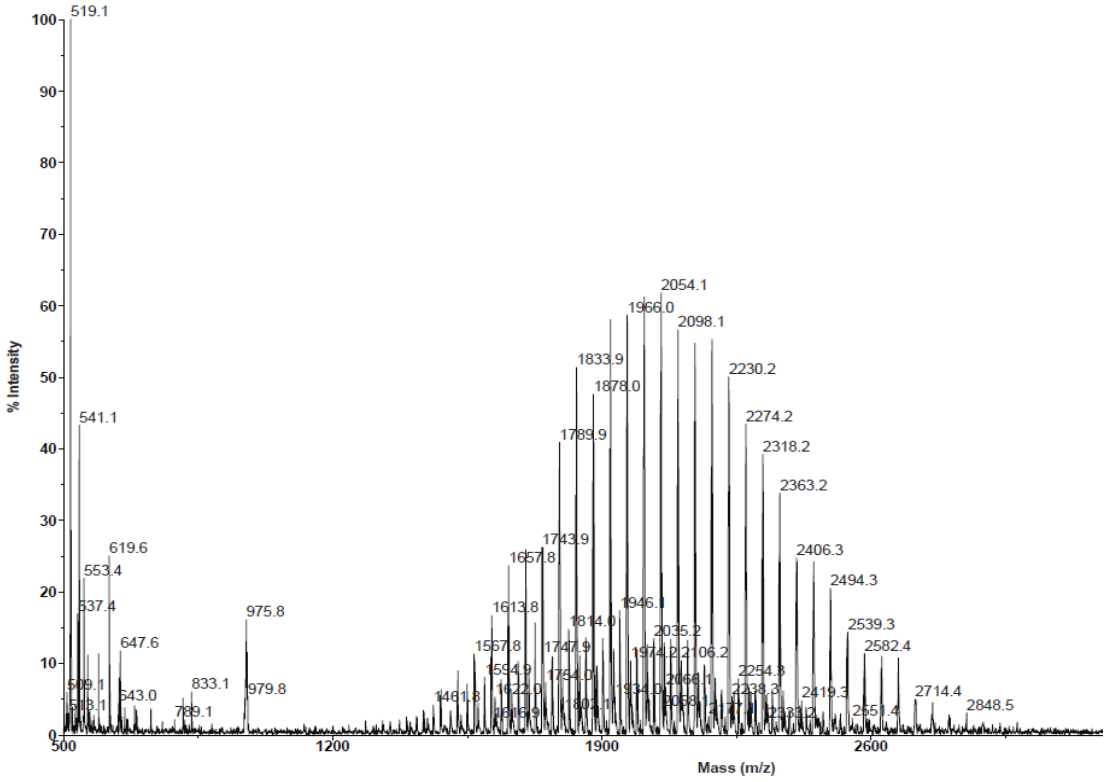

Figure A4 MALDI-TOF mass spectrum of the mono-functional ATRP macro-initiator, PEG_{45}-Br.

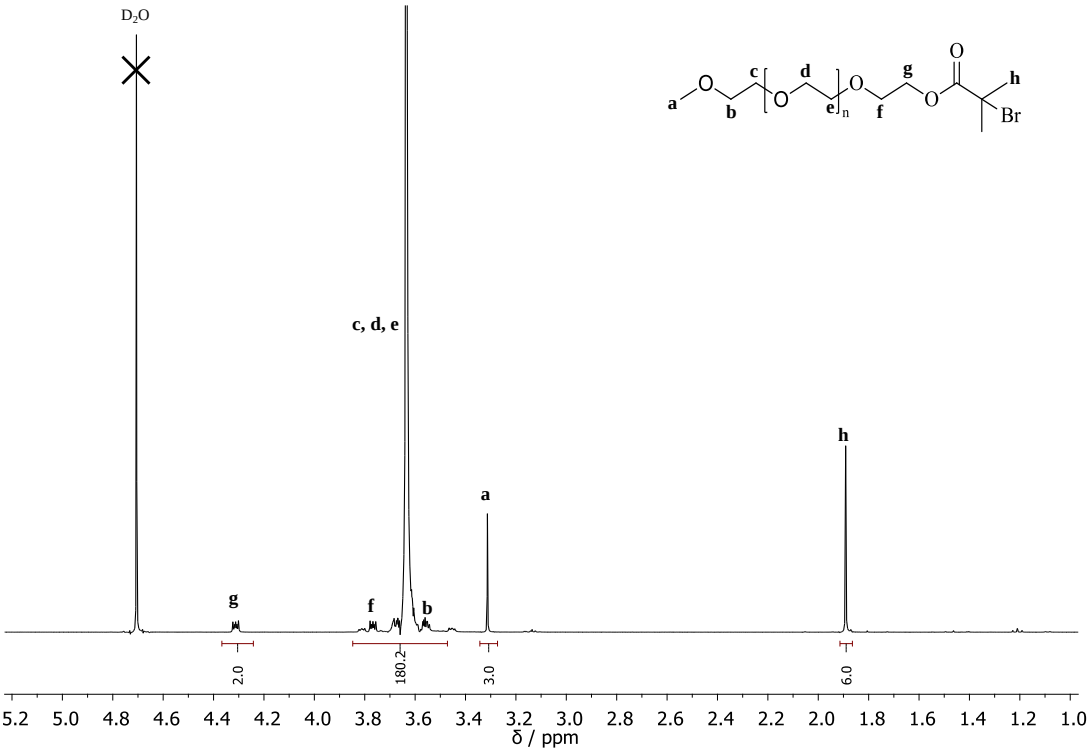

Figure A5 ^{1}H NMR PEG_{114}-Br (D_2O, 400 MHz) of the mono-functional ATRP macro-initiator, PEG_{114}-Br.

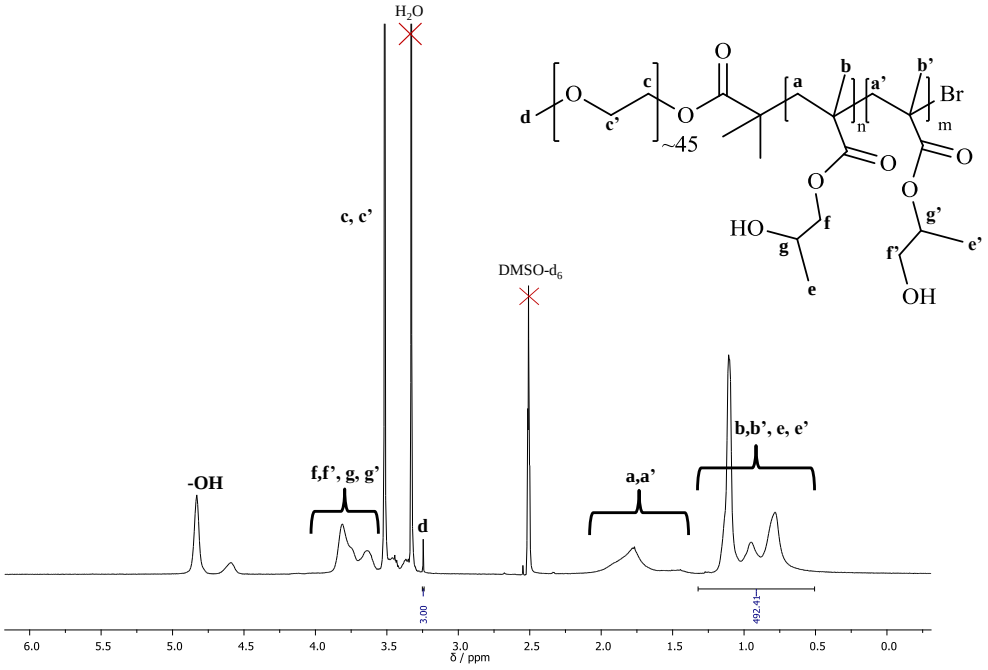

Figure A6 ^{1}H NMR *p*(PEG_{45}-*b*-$HPMA_{80}$) (DMSO-d_6, 400 MHz).

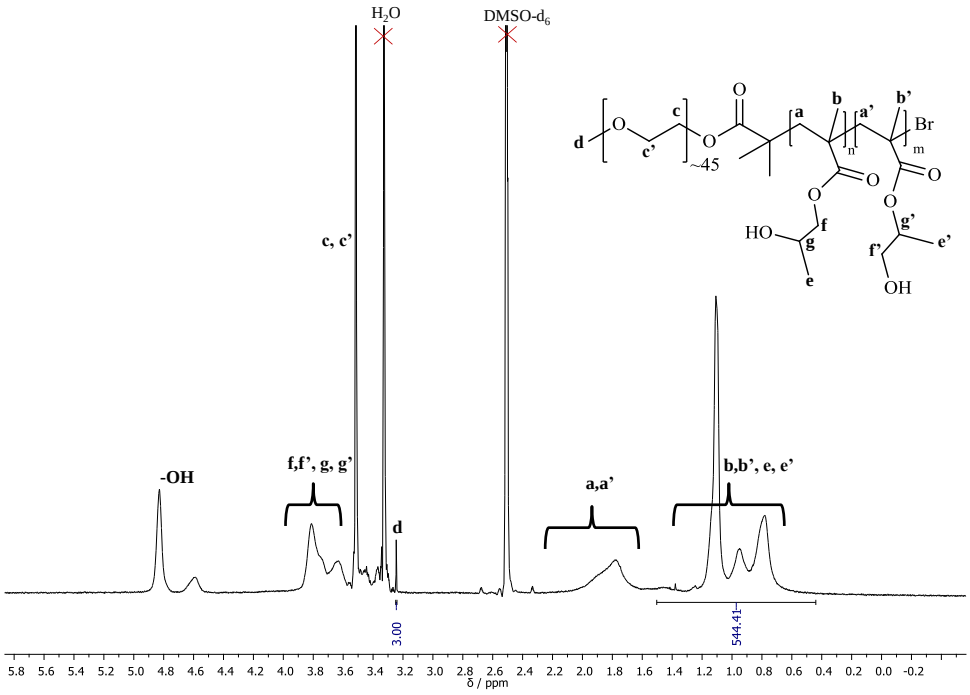

Figure A7 ^{1}H NMR *p*(PEG$_{45}$-*b*-HPMA$_{120}$) (DMSO-d$_6$, 400 MHz).

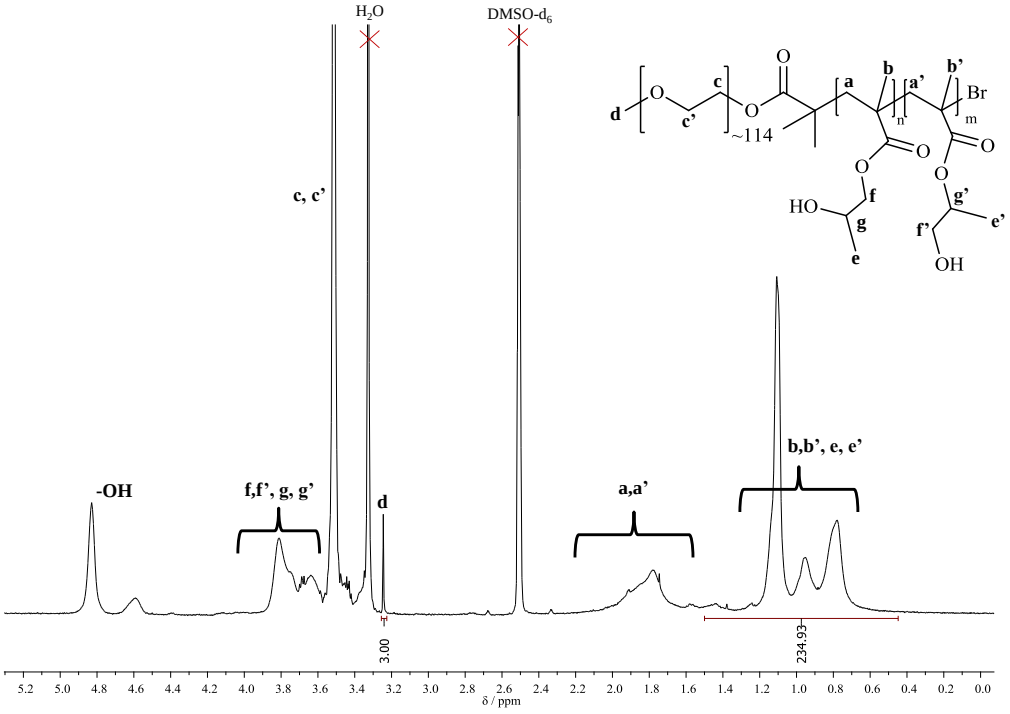

Figure A8 ^{1}H NMR *p*(PEG$_{114}$-*b*-HPMA$_{40}$) (DMSO-d$_6$, 400 MHz).

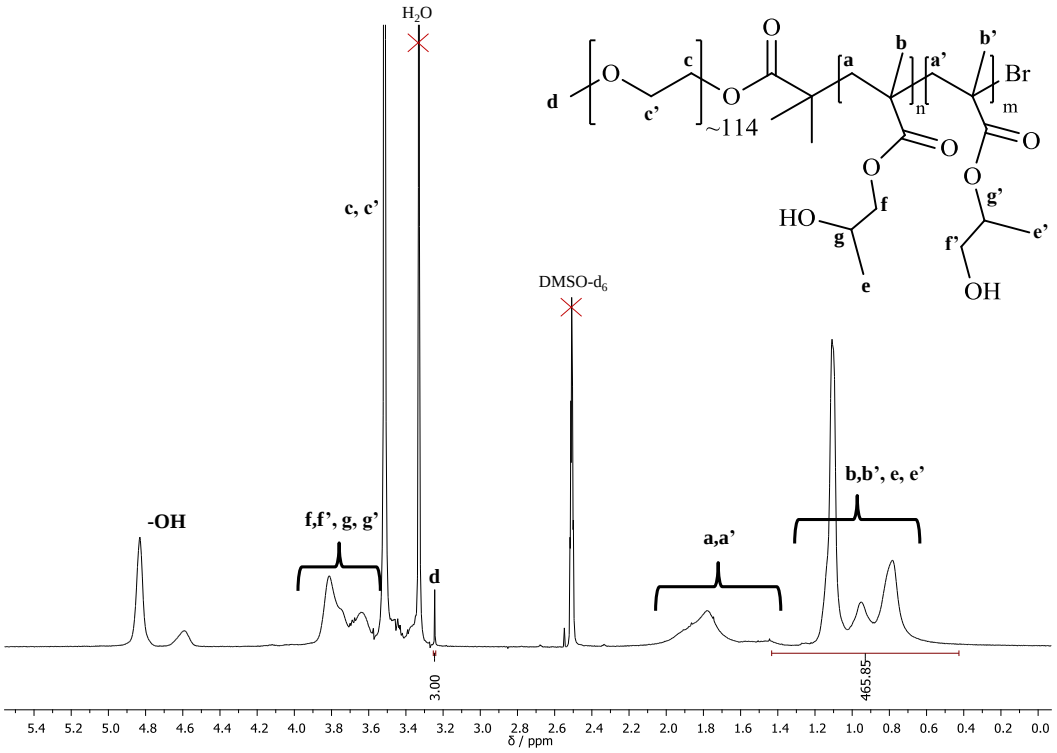

Figure A9 ^{1}H NMR *p*(PEG$_{114}$-*b*-HPMA$_{80}$) (DMSO-d$_6$, 400 MHz).

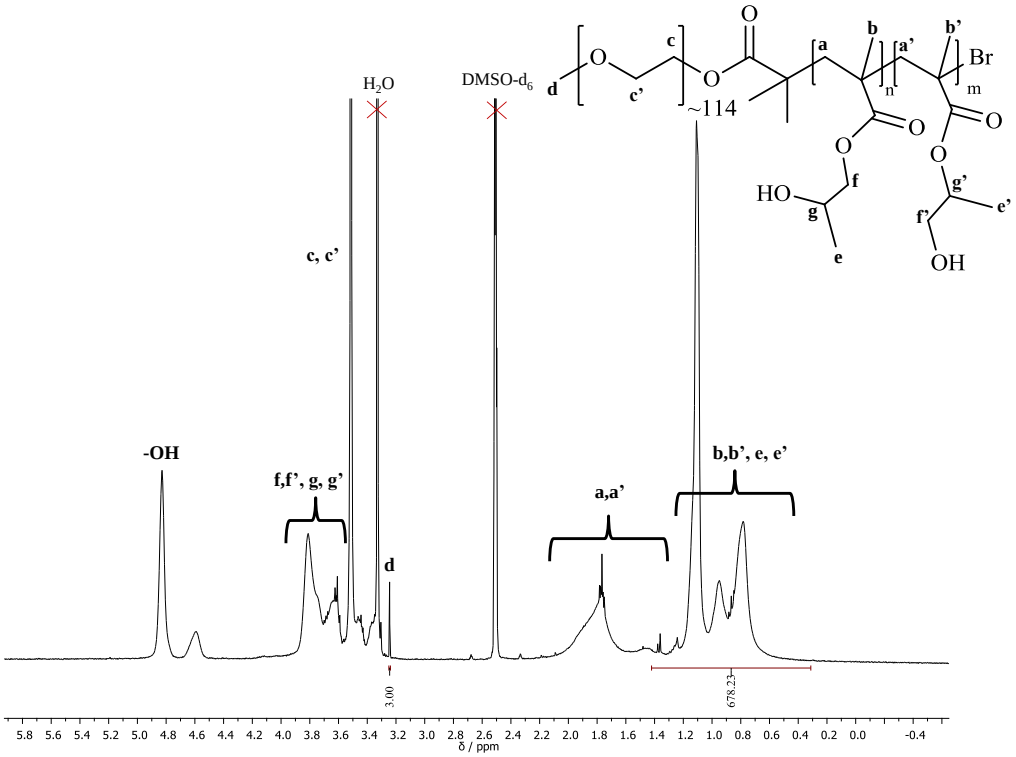

Figure A10 ^{1}H NMR *p*(PEG$_{114}$-*b*-HPMA$_{120}$) (DMSO-d$_6$, 400 MHz).

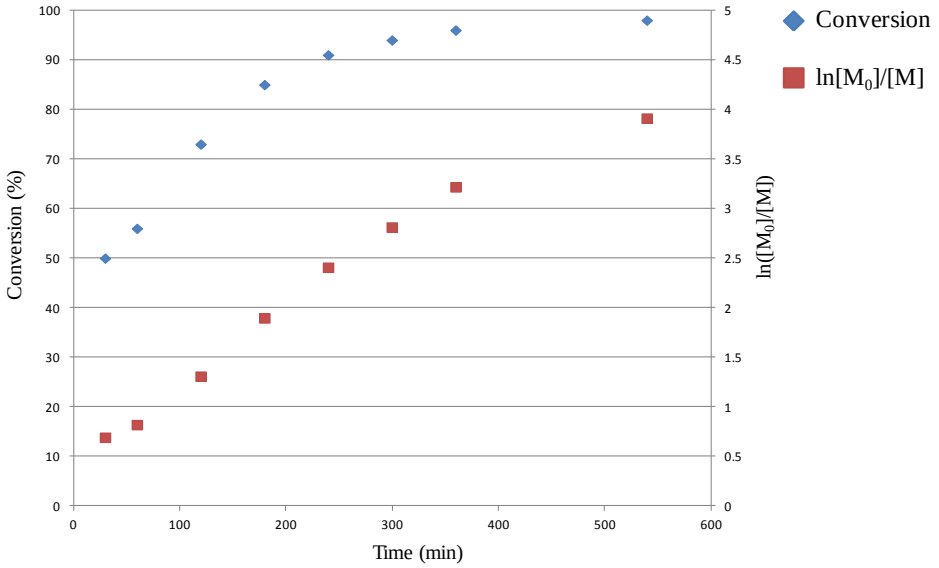

Figure A11 ^{1}H NMR kinetics for *p*(PEG$_{45}$-*b*-HPMA$_{40}$) (methanol-d$_4$, 400 MHz).

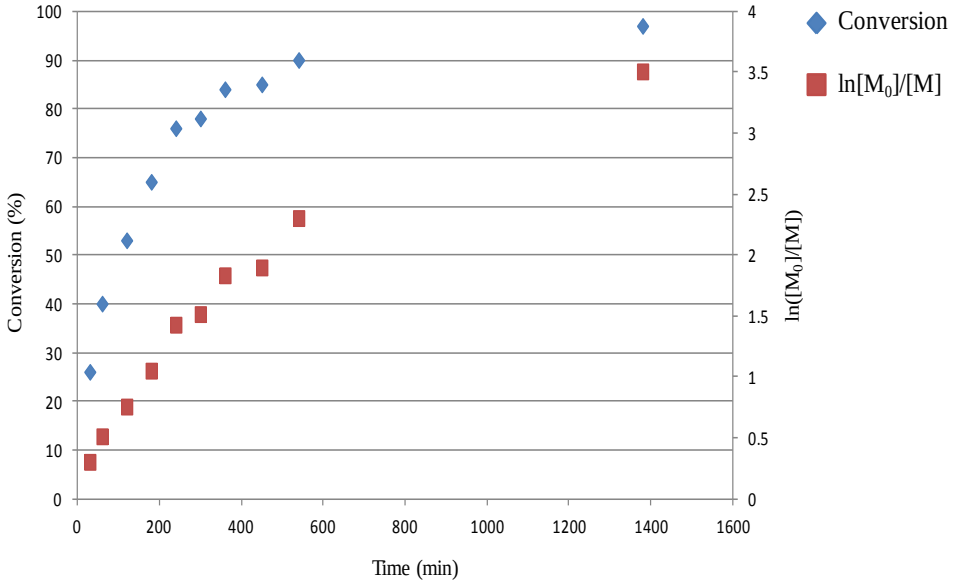

Figure A12 ^{1}H NMR kinetics for *p*(PEG$_{114}$-*b*-HPMA$_{40}$) (methanol-d$_4$, 400 MHz).

Table A3 Various batches of branched *p*(HPMA$_{50}$-*co*-EGDMA$_{0.9}$) nanoparticles.

Various Batches of *p*(HPMA$_{50}$-*co*-EGDMA$_{0.9}$) Nanoparticles	**Z-ave (d.nm)**	**PdI**	**D_n (nm)**
1	148	0.080	112
2	115	0.089	84
3	186	0.030	161
4	116	0.051	89

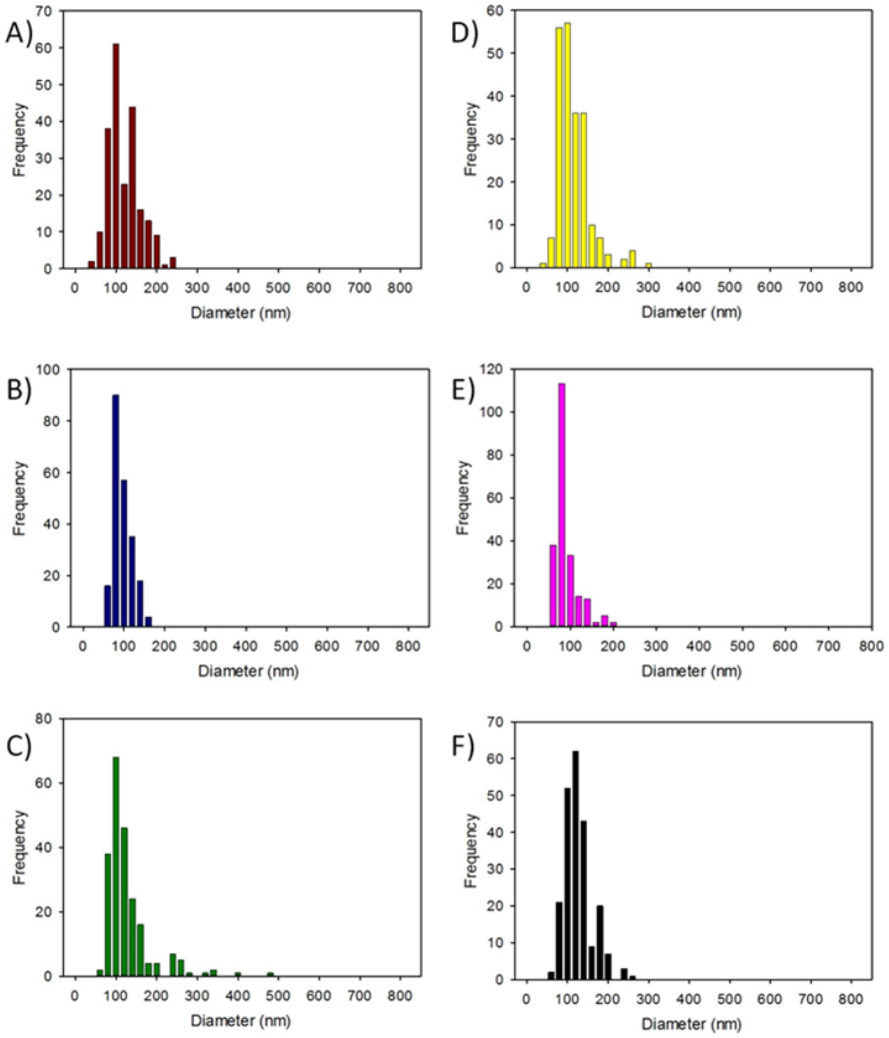

Figure A13 Histograms showing size distributions (diameters; nm) of nanoprecipitates and co-nanoprecipitates comprising various *p*(HPMA$_{50}$-*co*-EGDMA$_{0.9}$):*p*(PEG$_{45}$-*b*-HPMA$_{120}$) ratios: A) 50:50 (dark red), B) 60:40 (dark blue), C) 70:30 (dark green), D) 80:20 (yellow), E) 90:10 (pink), and F) 100:00 (black).

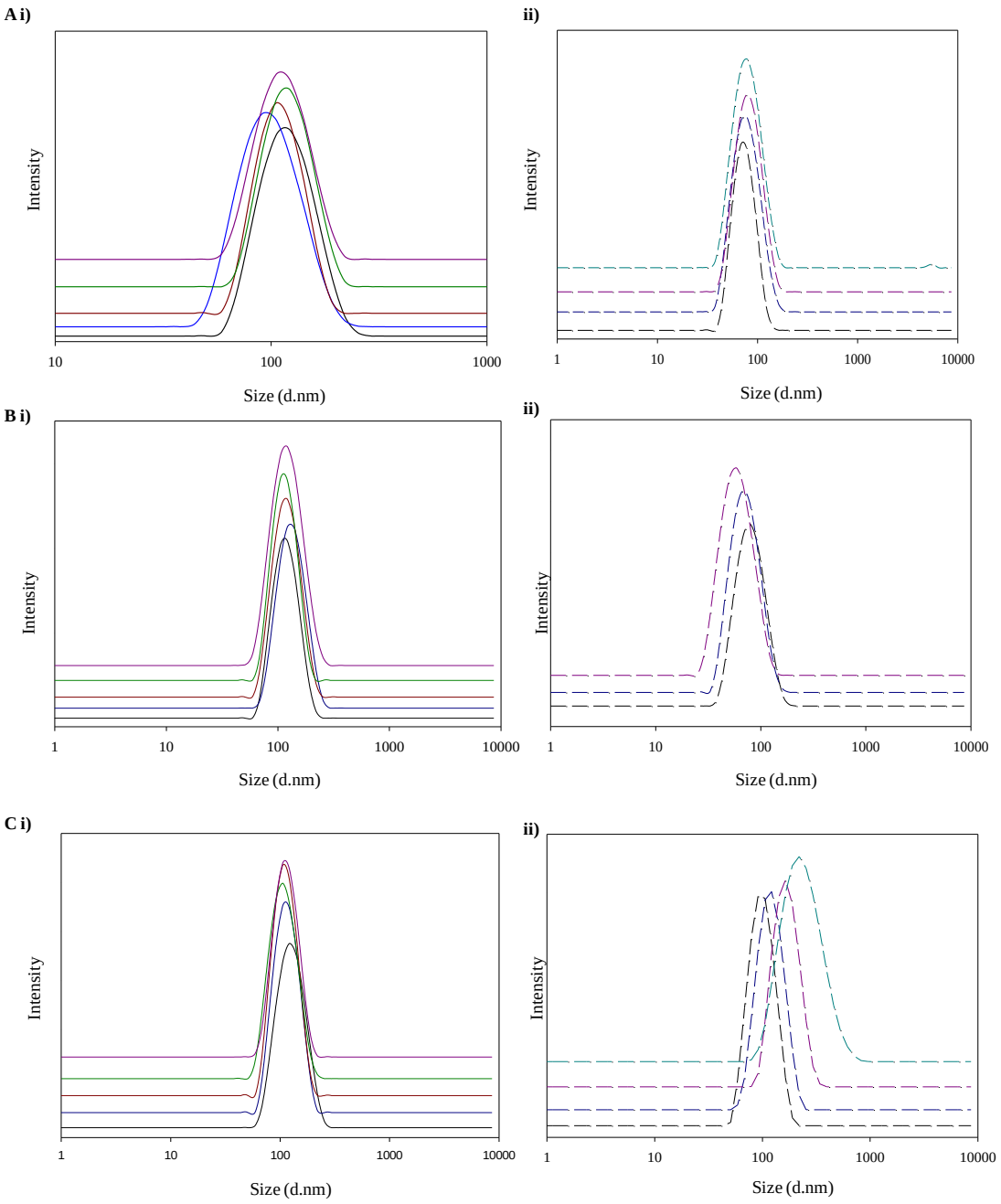

Figure A14 DLS analyses of co-nanoprecipitates: A) overlay of *p*(HPMA$_{50}$-*co*-EGDMA$_{0.9}$):*p*(PEG$_{45}$-*b*-HPMA$_{40}$) ratios i) 90:10 (black), 80:20 (dark blue), 70:30 (dark red), 60:40 (green) and 50:50 (dark pink), ii) 40:60 (dashed black), 30:70 (dashed blue), 20:80 (dashed dark pink), 10:90 (dashed cyan), B) overlay of *p*(HPMA$_{50}$-*co*-EGDMA$_{0.9}$):*p*(PEG$_{45}$-*b*-HPMA$_{80}$) ratios C) overlay of *p*(HPMA$_{50}$-*co*-EGDMA$_{0.9}$):*p*(PEG$_{45}$-*b*-HPMA$_{120}$) ratios, all same colours apply to ratios as for A).

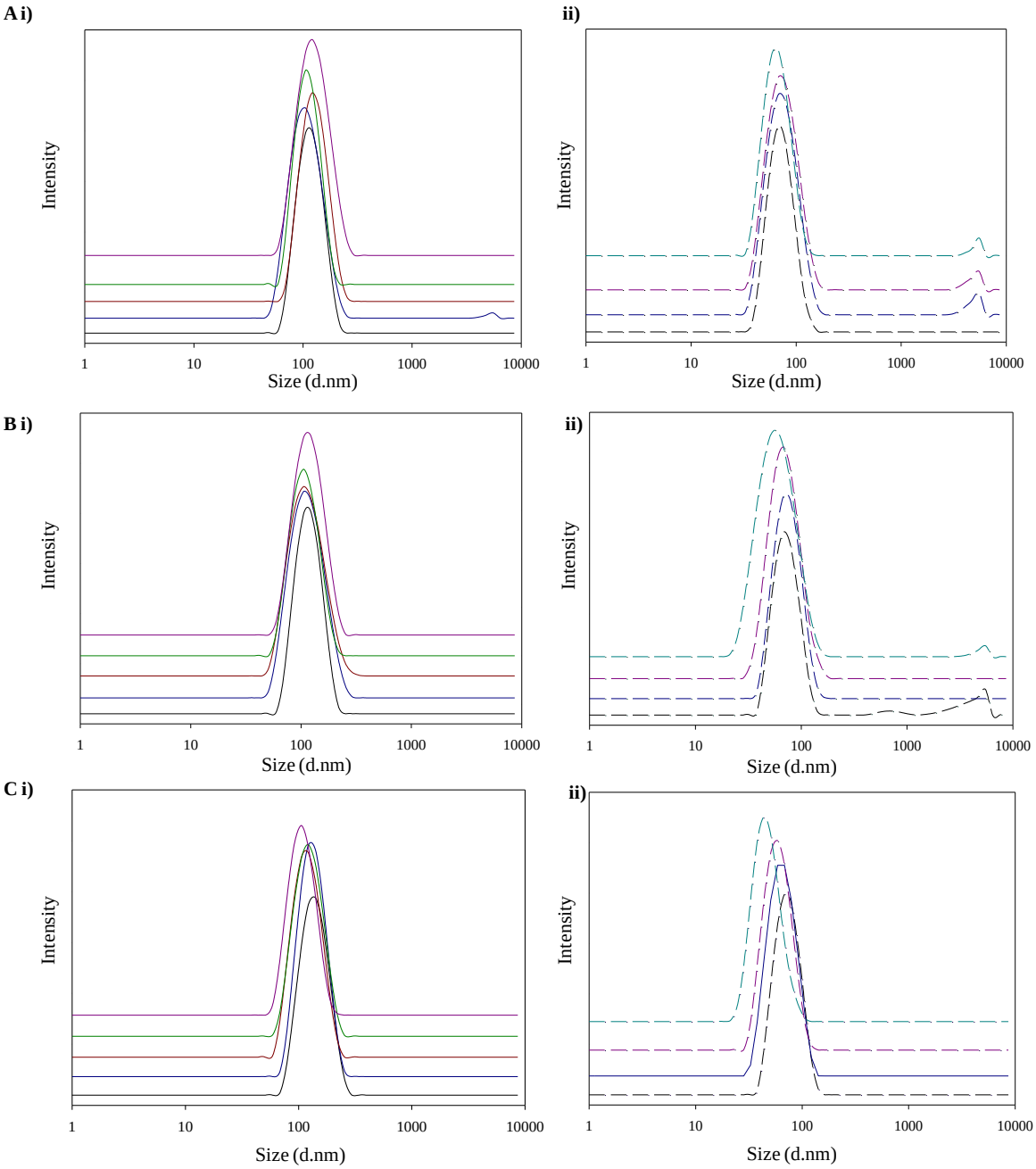

Figure A15 DLS analyses of co-nanoprecipitates: A) overlay of *p*(HPMA$_{50}$-*co*-EGDMA$_{0.9}$):*p*(PEG$_{114}$-*b*-HPMA$_{40}$) ratios i) 90:10 (black), 80:20 (dark blue), 70:30 (dark red), 60:40 (green) and 50:50 (dark pink), ii) 40:60 (dashed black), 30:70 (dashed blue), 20:80 (dashed dark pink), 10:90 (dashed cyan), B) overlay of *p*(HPMA$_{50}$-*co*-EGDMA$_{0.9}$):*p*(PEG$_{114}$-*b*-HPMA$_{80}$) ratios C) overlay of *p*(HPMA$_{50}$-*co*-EGDMA$_{0.9}$):*p*(PEG$_{114}$-*b*-HPMA$_{120}$) ratios, all same colours apply to ratios as for A).

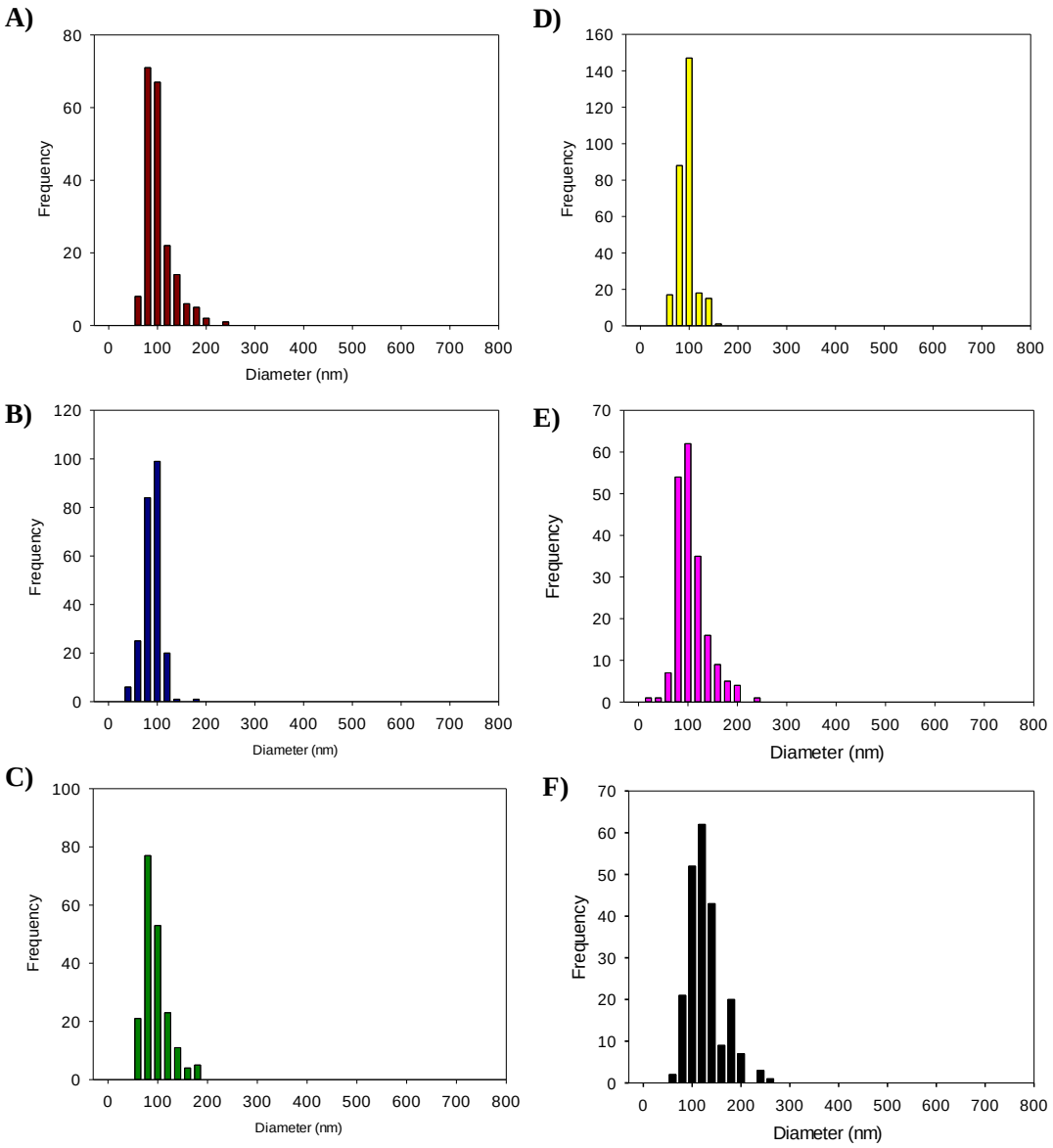

Figure A16 Histograms showing size distributions (diameters; nm) of nanoprecipitates and co-nanoprecipitates comprising various *p*(HPMA$_{50}$-*co*-EGDMA$_{0.9}$):*p*(PEG$_{114}$-*b*-HPMA$_{120}$) ratios: A) 50:50 (dark red), B) 60:40 (dark blue), C) 70:30 (dark green), D) 80:20 (yellow), E) 90:10 (pink), and F) 100:00 (black).

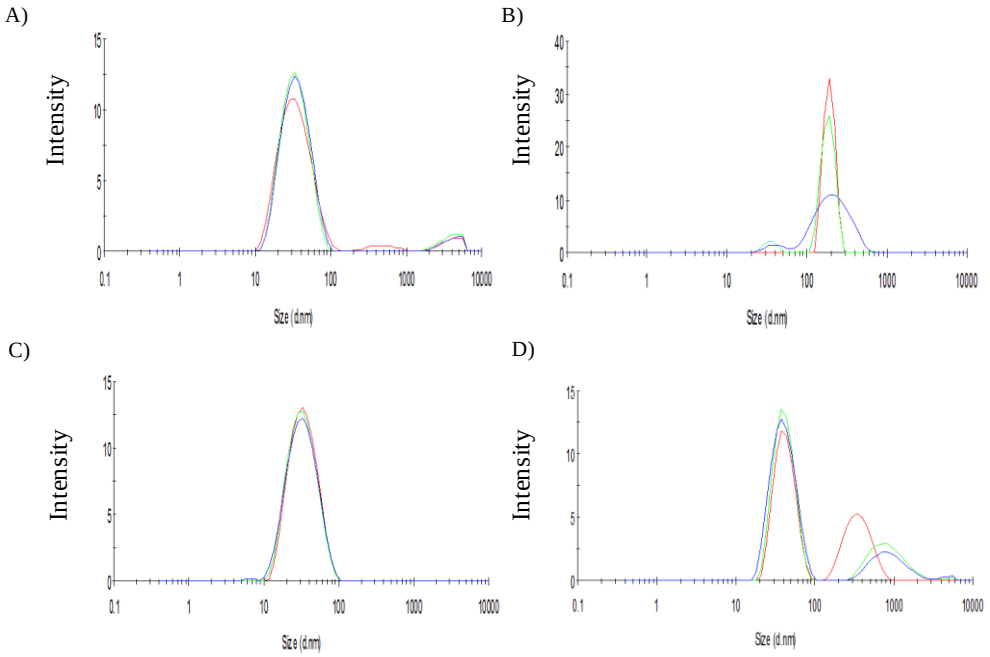

Figure A17 DLS results during solubilisation of A-B block copolymers in water at 1 mg/mL. A) *p*(PEG$_{45}$-*b*-HPMA$_{40}$), B) *p*(PEG$_{114}$-*b*-HPMA$_{40}$), C) *p*(PEG$_{114}$-*b*-HPMA$_{80}$), D) *p*(PEG$_{114}$-*b*-HPMA$_{120}$).

Table A4 DLS results during solubilisation of A-B block copolymers in water at 1 mg/mL.

Polymer	D_z (nm)	**PdI**	**Derived count rate** (kcps)
p(PEG$_{45}$-*b*-HPMA$_{40}$)	31 (37nm 95%, 4045nm 5%)	0.316	520
p(PEG$_{114}$-*b*-HPMA$_{40}$)*	355	0.462	880
p(PEG$_{114}$-*b*-HPMA$_{80}$)	29	0.157	1310
p(PEG$_{114}$-*b*-HPMA$_{120}$)	53 (43nm 64%, 367nm 36%)	0.396	6910

* Inadequate scattering data

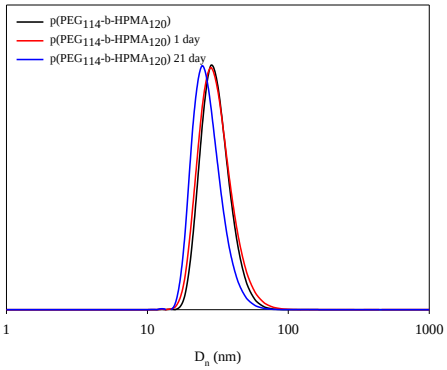

Figure A18 Number average (nm) for *p*(PEG$_{114}$-*b*-HPMA$_{120}$), In absence of NaCl (black line), NaCl addition 1 day (red line) and NaCl addition 21 day (blue line)

Table A5 Summary of DLS results for NaCl addition to varying ratios of *p*(HPMA$_{50}$-*co*-EGDMA$_{0.9}$):*p*(PEG$_{45}$-*b*-HPMA$_x$), (20 µL addition to 1 mL of nanodispersion). (X = polymer precipitation , * inadequate scattering data

	***p*(HPMA$_{50}$-*b*-EGDMA$_{0.9}$):*p*(PEG$_{45}$-*b*-HPMA$_{40}$)**					***p*(HPMA$_{50}$-EGDMA$_{0.9}$):*p*(PEG$_{45}$-*b*-HPMA$_{80}$)**					***p*(HPMA$_{50}$-EGDMA$_{0.9}$):*p*(PEG$_{45}$-*b*-HPMA$_{120}$)**				
Wt%	Blank	Instant	24hour	7 day	21 day	Blank	Instant	24hour	7 day	21 day	Blank	Instant	24hour	7 day	21 day
90:10															
D_z (nm)	113	1846*	X	X	X	114	320	255	252	260	120	2660	X	X	X
PdI	0.067	0.48				0.045	0.278	0.221	0.192	0.185	0.066	0.57			
80:20															
D_z (nm)	94	771*	X	X	X	127	129	129	128	126	111	193	225	213	221
PdI	0.123	0.581				0.061	0.06	0.056	0.032	0.053	0.033	0.117	0.202	0.083	0.111
70:30															
D_z (nm)	106	195	234	322	X	115	117	128	141	149	108	123	150	173	X
PdI	0.029	0.077	0.03	0.047		0.053	0.033	0.018	0.024	0.021	0.037	0.045	0.056	0.032	
60:40															
D_z (nm)	115	139	203	240	265	111	114	119	128	142	103	107	125	149	174
PdI	0.047	0.024	0.019	0.032	0.083	0.037	0.031	0.027	0.024	0.079	0.069	0.065	0.044	0.027	0.023
50:50															
D_z (nm)	109	172	173	212	251	115	117	191	198	220	109	109	167	211	X
PdI	0.0480	0.038	0.020	0.020	0.112	0.071	0.093	0.132	0.052	0.119	0.032	0.069	0.125	0.118	
40:60															
D_z (nm)	75	75	166	108	107	76	81	268*	X	X	95	112	260*	X	X
PdI	0.152	0.066	0.223	0.015	0.067	0.113	0.112	0.035			0.051	0.109	0.082		
30:70															
D_z (nm)	75	93	140*	106	107	69	90	286*	X	X	114	122	225	X	X
PdI	0.166	0.222	0.2	0.039	0.04	0.122	0.136	0.08			0.061	0.066	0.124		
20:80															
D_z (nm)	78	78	153	96	99	56	112	239	159	159	159	156	246	X	X
PdI	0.111	0.109	0.456	0.034	0.038	0.126	0.149	0.102	0.119	0.108	0.068	0.034	0.538		
10:90															
D_z (nm)	77	76	185*	X	X	76	81	195	144	143	215	265	209	253	349*
PdI	0.163	0.123	0.555			0.113	0.112	0.174	0.092	0.08	0.167	0.25	0.048	0.086	0.544
0:100															
D_z (nm)	268	152	121	164	230	131	134	124	275	266	372	404	256	363	466
PdI	0.338	0.314	0.688	0.595	0.361	0.227	0.171	0.209	0.203	0.287	0.145	0.179	0.066	0.229	0.212

Table A6 Summary of DLS results for NaCl addition to varying ratios of *p*(HPMA$_{50}$-*co*-EGDMA$_{0.9}$):*p*(PEG$_{114}$-*b*-HPMA$_x$), (20 µL addition to 1 mL of nanodispersion). (X = polymer precipitation , * inadequate scattering data).

	***p*(HPMA$_{50}$-EGDMA$_{0.9}$):*p*(PEG$_{114}$-*b*-HPMA$_{40}$)**					***p*(HPMA$_{50}$-EGDMA$_{0.9}$):*p*(PEG$_{114}$-*b*-HPMA$_{80}$)**					***p*(HPMA$_{50}$-EGDMA$_{0.9}$):*p*(PEG$_{114}$-*b*-HPMA$_{120}$)**				
Wt%	Blank	Instant	24hour	7 day	21 day	Blank	Instant	24hour	7 day	21 day	Blank	Instant	24hour	7 day	21 day
90:10															
D_z (nm)	111	2173*	x	x	x	112	122	142	151	161	132	130	130	131	132
PdI	0.055	0.311				0.045	0.03	0.014	0.039	0.015	0.059	0.060	0.044	0.033	0.036
80:20															
D_z (nm)	103	415	291	343	522	106	139	109	114	118	127	126	127	125	126
PdI	0.152	0.432	0.205	0.171	0.33	0.118	0.272	0.055	0.025	0.032	0.043	0.057	0.060	0.046	0.048
70:30															
D_z (nm)	121	143	194	236	275	106	121	107	106	110	113	113	112	110	113
PdI	0.061	0.037	0.007	0.027	0.037	0.124	0.22	0.086	0.061	0.195	0.069	0.060	0.068	0.044	0.049
60:40															
D_z (nm)	107	116	165	206	235	103	105	105	110	103	117	117	117	114	115
PdI	0.028	0.023	0.014	0.013	0.021	0.065	0.045	0.057	0.148	0.057	0.059	0.060	0.036	0.051	0.045
50:50															
D_z (nm)	117	113	120	150	134	111	109	107	112	116	103	101	103	104	104
PdI	0.048	0.079	0.029	0.031	0.018	0.081	0.089	0.062	0.083	0.191	0.045	0.05	0.06	0.043	0.091
40:60															
D_z (nm)	76	72	104	91	321*	84	73	96	74	956*	70	71	69	75	276*
PdI	0.178	0.118	0.218	0.04	0.404	0.332	0.165	0.279	0.203	0.857	0.085	0.136	0.056	0.193	0.441
30:70															
D_z (nm)	75	71	78	83	104	71	71	70	69	271*	62	61	60	62	154*
PdI	0.224	0.112	0.093	0.115	0.082	0.096	0.076	0.065	0.125	0.497	0.085	0.058	0.013	0.135	0.509
20:80															
D_z (nm)	75	68	72	101	318*	67	70	67	117	442*	56	55	55	80	64
PdI	0.212	0.112	0.073	0.246	0.498	0.14	0.182	0.073	0.271	0.58	0.075	0.067	0.065	0.253	0.249
10:90															
D_z (nm)	73	81	69	77	1010*	56	60	75	64	1254*	46	47	47	59	186*
PdI	0.254	0.214	0.214	0.192	0.913	0.184	0.175	0.278	0.245	0.89	0.152	0.088	0.106	0.32	0.276
0:100															
D_z (nm)	317	289	276	272	268	89	86	86	93	66	49	50	59	44	39
PdI	0.373	0.392	0.301	0.358	0.369	0.738	0.322	0.396	0.249	0.466	0.265	0.292	0.322	0.131	0.121

Table A7 DLS results for encapsulation of pyrene for varying ratios of *p*(HPMA$_{50}$-*co*-EGDMA$_{0.9}$):*p*(PEG$_{45}$-*b*-HPMA$_{120}$)**.**

Ratio *p*(HPMA$_{50}$-*co*-EGDMA$_{0.9}$): *p*(PEG$_{45}$-*b*-HPMA$_{120}$)	Blank size (d.nm)	PdI	Pyrene encapsulated size (d.nm)	PdI
100:0	99	0.058	93	0.047
90:10	120	0.066	151	0.058
80:20	121	0.036	123	0.067
70:30	108	0.038	110	0.061
60:40	121	0.028	110	0.034
50:50	124	0.069	107	0.024

Table A8 DLS results for encapsulation of pyrene for varying ratios of *p*(HPMA$_{50}$-*co*-EGDMA$_{0.9}$):*p*(PEG$_{114}$-*b*-HPMA$_{120}$)**.**

Ratio *p*(HPMA$_{50}$-*co*-EGDMA$_{0.9}$): *p*(PEG$_{114}$-*b*-HPMA$_{120}$)	Size (d.nm)	PdI	Pyrene encapsulated Size (d.nm)	PdI
100:0	99	0.058	93	0.047
90:10	97	0.045	91	0.033
80:20	99	0.054	94	0.046
70:30	107	0.080	96	0.038
60:40	105	0.062	95	0.048
50:50	103	0.068	106	0.051
30:70	92	0.110	92	0.075
10:90	63	0.156	72	0.230

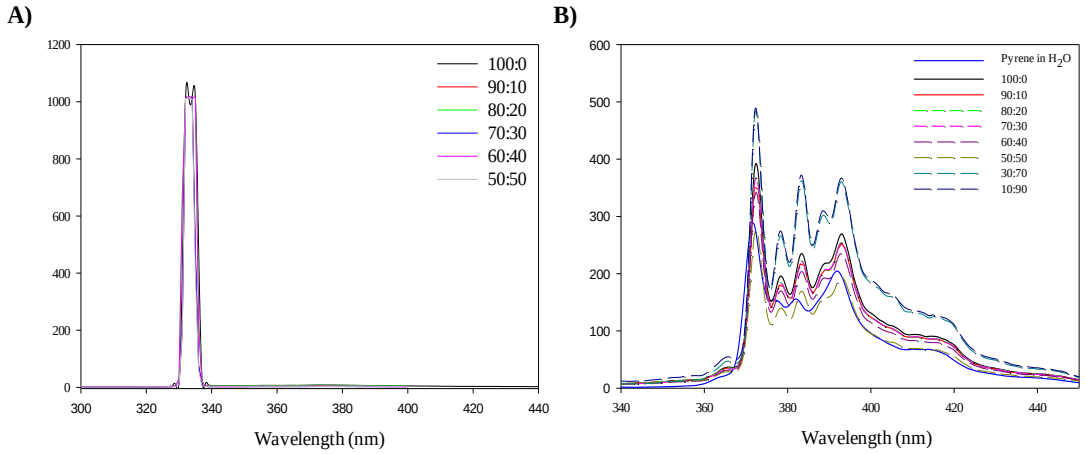

Figure A19 Fluorescence data for *p*(HPMA$_{50}$-*co*-EGDMA$_{0.9}$):*p*(PEG$_{114}$-*b*-HPMA$_{120}$)**,** A) Control fluorescence emission spectrum for blank polymeric nanoparticles B) Fluorescence emission spectrum for pyrene in H_2O and polymeric nanoparticles with encapsulation of 0.1 w/w% pyrene.

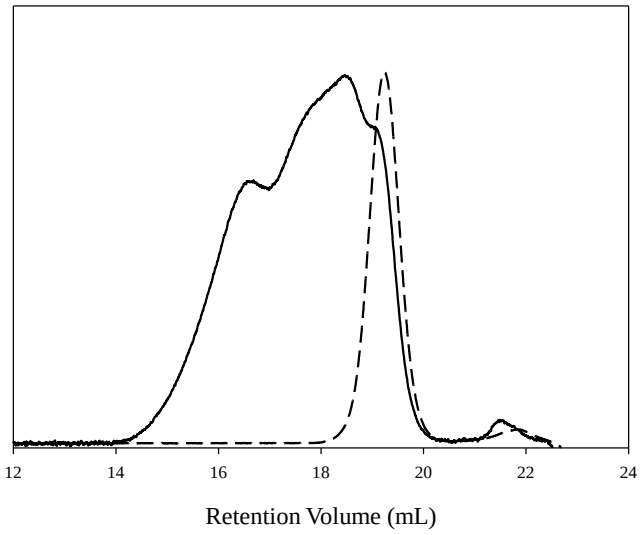

Figure A20 GPC refractive index (RI) chromatogram overlay, black line = branched *p*(*n*-BMA_{50}-*co*-$EGDMA_{0.9}$), black dashed line = linear *p*(*n*-BMA_{50}). (Synthesised by Dr. Pierre Chambon – Rannard research group).

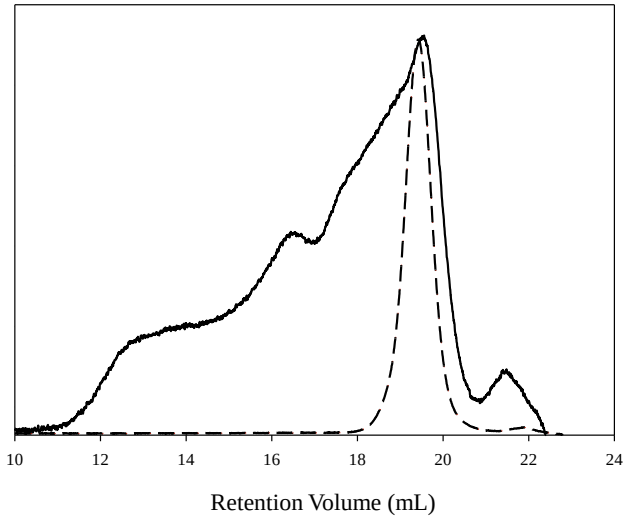

Figure A21 GPC refractive index (RI) chromatogram overlay, black line = branched *p*($HPMA_{25}$-*co*-*n*-BMA_{25}-*co*-$EGDMA_{0.9}$), black dashed line = linear *p*($HPMA_{25}$-*co*-*n*-BMA_{25}).

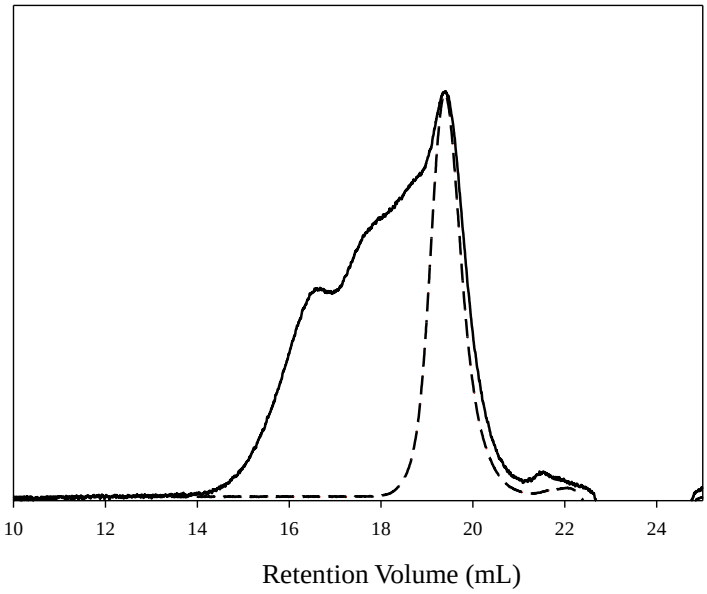

Figure A22 GPC refractive index (RI) chromatogram overlay, black line = branched *p*(HPMA$_{25}$-*co*-*t*-BMA$_{25}$-*co*-EGDMA$_{0.9}$), black dashed line = linear *p*(HPMA$_{25}$-*co*-*t*-BMA$_{25}$).

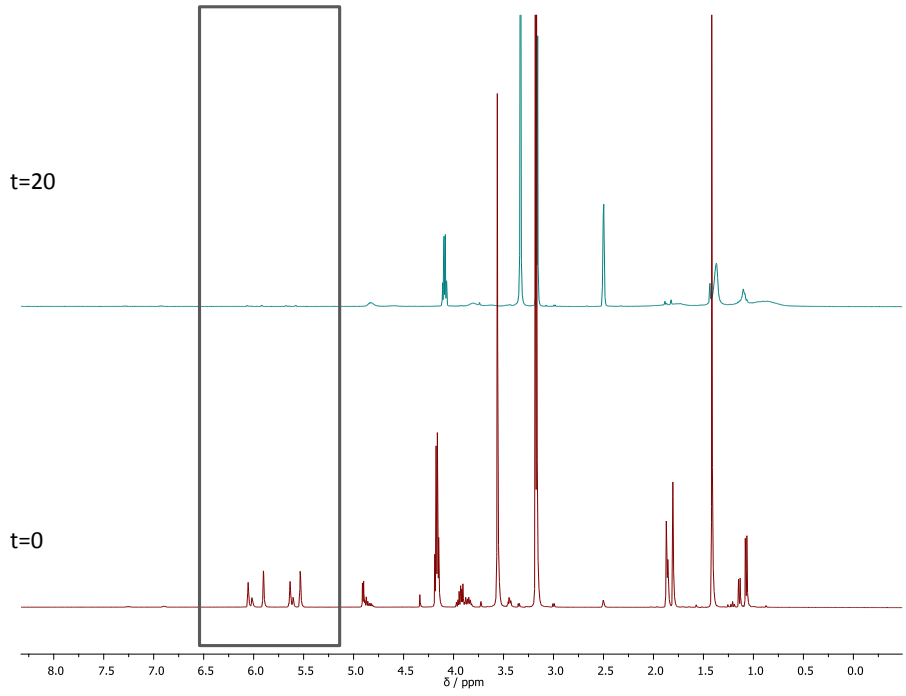

Figure A23 Overlay of branched *p*(HPMA$_{25}$-*co*-*n*-BMA$_{25}$-*co*-EGDMA$_{0.9}$) NMR conversion during polymerisation (MeOD-d$_4$, 400 MHz).

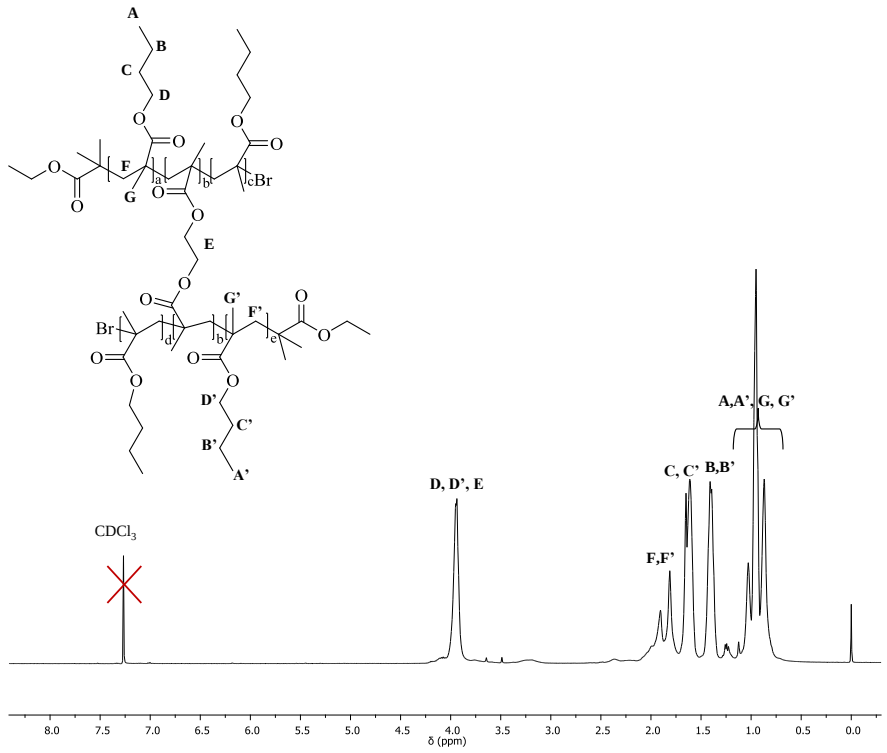

Figure A24 ^{1}H NMR analysis of *p*(*n*-BMA$_{50}$-*co*-EGDMA$_{0.8}$) ($CDCl_3$, 400 MHz). (Synthesised by Pierre Chambon with the Rannard research group).

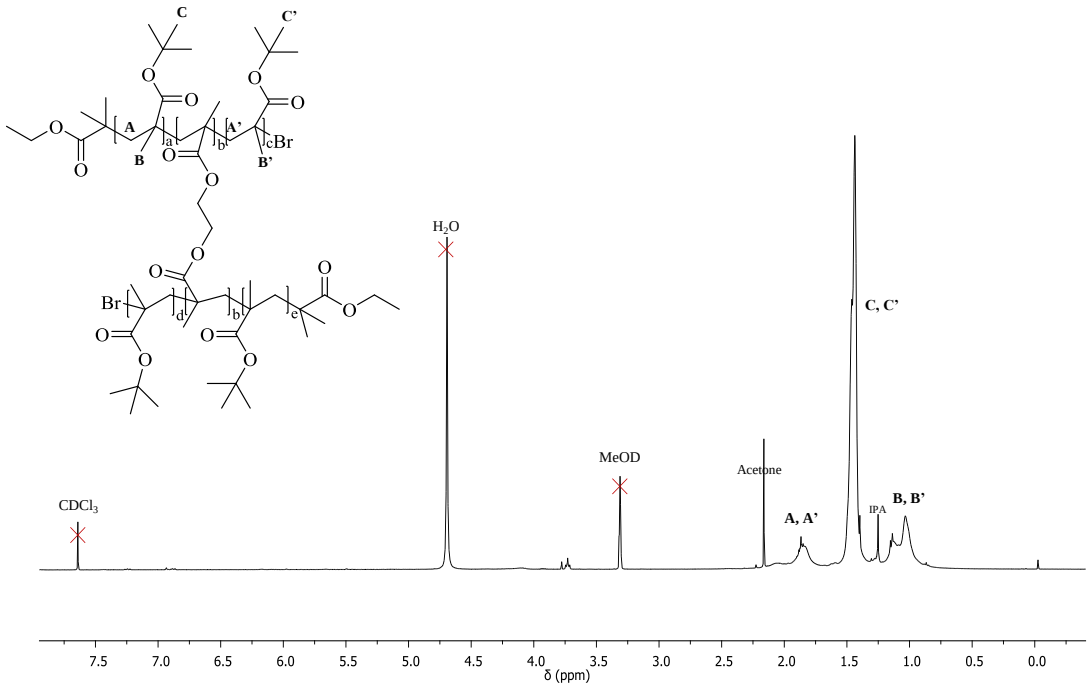

Figure A25 ^{1}H NMR analysis of *p*(*t*-BMA$_{50}$-*co*-EGDMA$_{0.9}$) ($CDCl_3$, + MeOD 400 MHz). (Synthesised by Hannah Rogers with the Rannard research group).

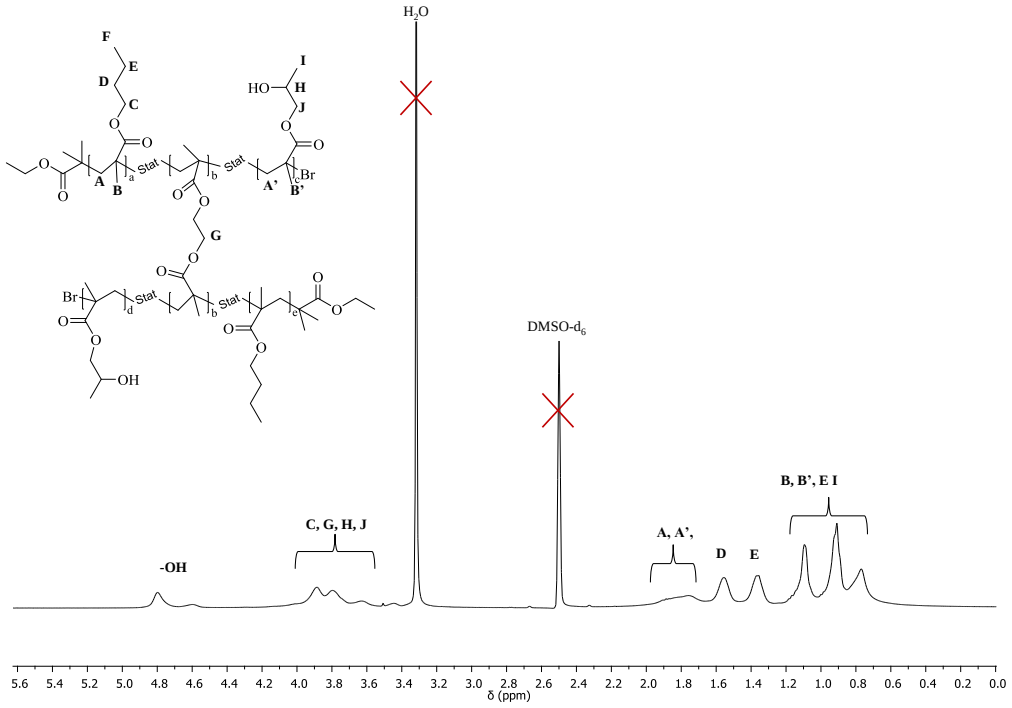

Figure A26 ^{1}H NMR analysis of *p*(HPMA$_{25}$-*co*-*n*-BMA$_{25}$--*co*-EGDMA$_{0.9}$) (DMSO-d$_6$, 400 MHz).

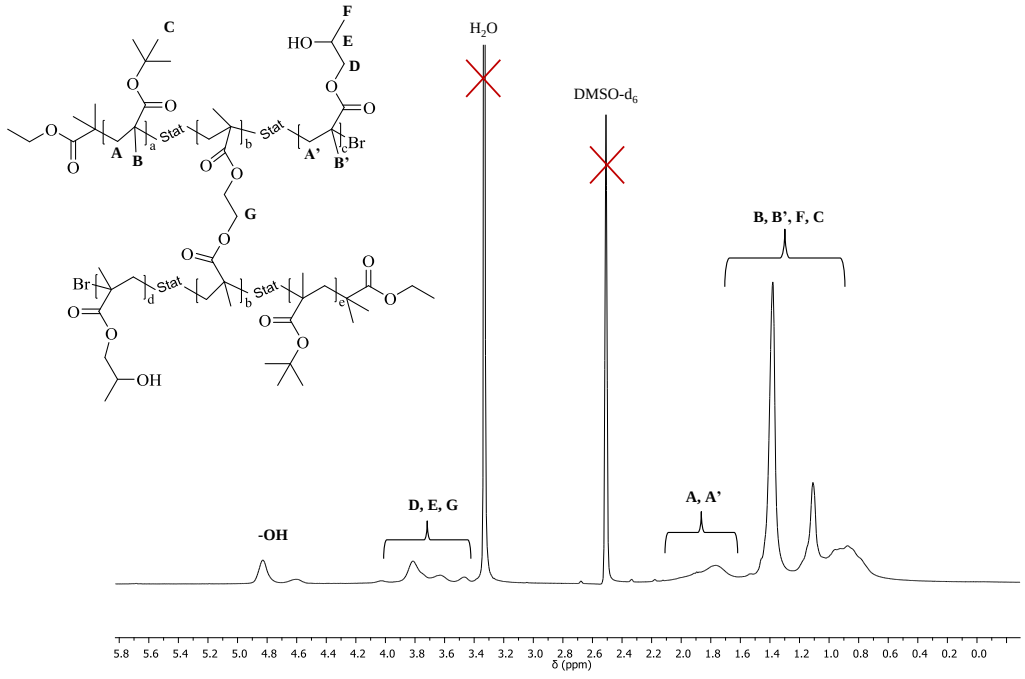

Figure A27 ^{1}H NMR analysis of *p*(HPMA$_{25}$-*co*-*t*-BMA$_{25}$-*co*-EGDMA$_{0.9}$) (DMSO-d$_6$, 400 MHz).

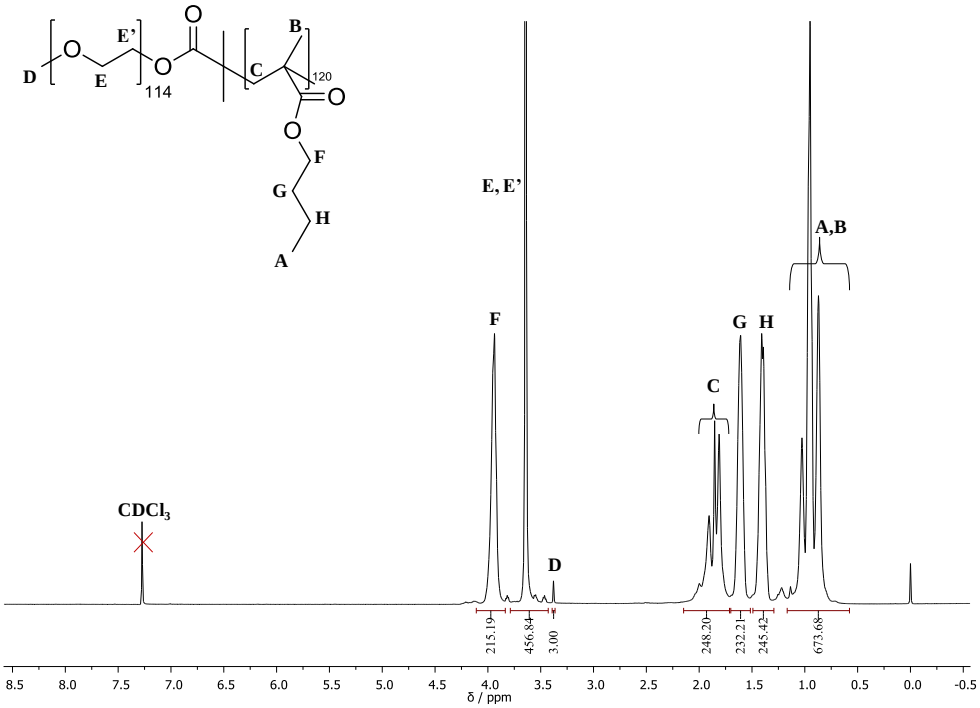

Figure A28 ^{1}H NMR analysis of *p*(PEG$_{114}$-*b*-*n*-BMA$_{120}$) ($CDCl_3$, 400 MHz).

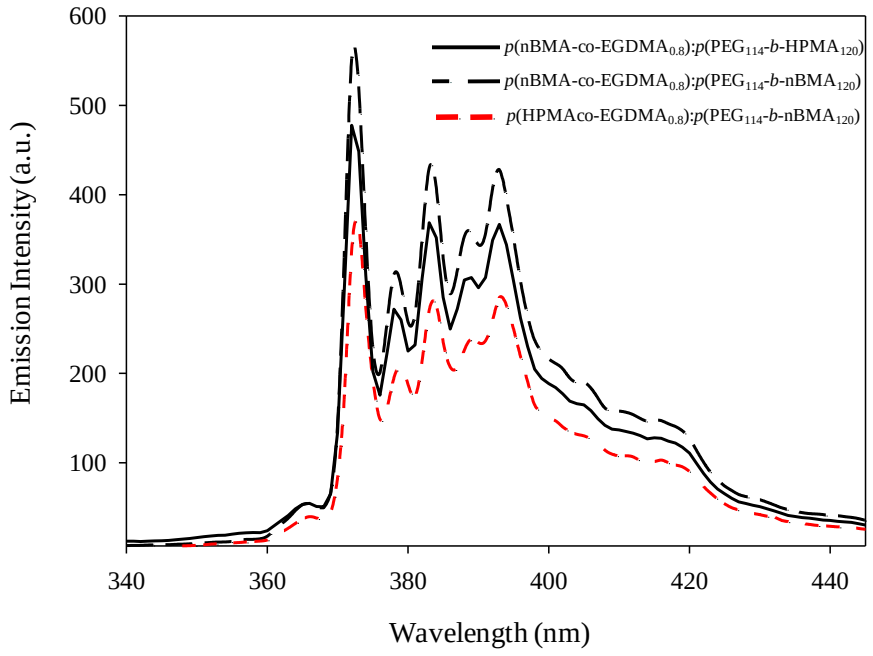

Figure A29 Fluorescence emission spectrum for polymeric nanoparticles encapsulated with pyrene.

Table A9 DLS analysis for 17 wt% fluoresceinamine encapsulated co-nanoprecipitated particles

Sample (50:50 wt %)	Fluoresceinamine (wt %)	Z-ave (d.nm)	PdI
p(HPMA$_{50}$-*co*-EGDMA$_{0.9}$):*p*(PEG$_{45}$-*b*-HPMA$_{40}$)	17	218	0.108
p(HPMA$_{50}$-*co*-EGDMA$_{0.9}$):*p*(PEG$_{114}$-*b*-HPMA$_{80}$)	17	160	0.026
p(HPMA$_{50}$-*co*-EGDMA$_{0.9}$):*p*(PEG$_{114}$-*b*-HPMA$_{120}$)	17	125	0.081

Chapter 5 - Co-nanoprecipitation: Encapsulation of the Anti-Cancer Drug SN-38

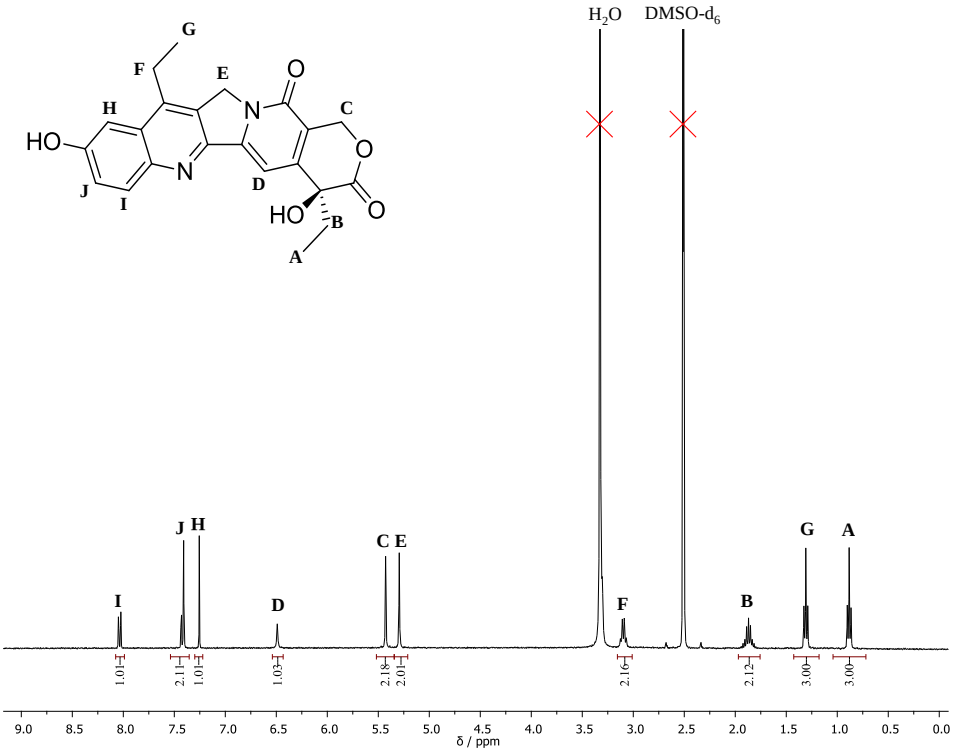

Figure A30 ^{1}H NMR (DMSO-d$_6$, 400 MHz) of SN-38.

Table A10 DLS results for nanoparticles prepared *via* the dropping technique after 48 hour solubilisation. 2 wt % and 5 wt % SN-38.

Sample (50:50 wt %)	SN-38 (wt %)	Size (d.nm)	PdI
p(HPMA$_{50}$-*co*-EGDMA$_{0.9}$):*p*(PEG$_{114}$-*b*-HPMA$_{120}$)	2	105*	0.278
p(*n*-BMA$_{50}$-*co*-EGDMA$_{0.8}$):*p*(PEG$_{114}$-*b*-HPMA$_{120}$)	2	146	0.205
p(*t*-BMA$_{25}$-*co*-HPMA$_{25}$-*co*-EGDMA$_{0.9}$):*p*(PEG$_{114}$-*b*-HPMA$_{120}$)	2	103	0.275
p(*n*-BMA$_{50}$-*co*-EGDMA$_{0.8}$):*p*(PEG$_{114}$-*b*-HPMA$_{120}$)	5	280	0.368

* Result does not meet DLS quality criteria

Table A11 Blank *vs* encapsulated PdI values SN-38 encapsulated nanoparticles

Sample (50:50 wt%)	Blank PdI	Encapsulated PdI
p(*n*-BMA$_{50}$-*co*-EGDMA$_{0.8}$):*p*(PEG$_{114}$-*b*-HPMA$_{120}$)	0.168	0.112
p(HPMA$_{50}$-*co*-EGDMA$_{0.9}$):*p*(PEG$_{114}$-*b*-HPMA$_{120}$)	0.188	0.076
p(tBMA$_{25}$-*co*-HPMA$_{25}$-*co*-EGDMA$_{0.9}$):*p*(PEG$_{114}$-*b*-HPMA$_{120}$)	0.166	0.085

Table A12 DLS results for various batches of SN-38 (5 wt%) co-nanoprecipitated particles

Sample 50:50 wt % + 5 wt % SN-38	Batch	Size (d.nm)	PdI
p(*n*-BMA$_{50}$-*co*-EGDMA$_{0.8}$):*p*(PEG$_{114}$-*b*-HPMA$_{120}$)	1	145	0.112
	2	123	0.079
	3	149	0.156
p(HPMA$_{50}$-*co*-EGDMA$_{0.9}$):*p*(PEG$_{114}$-*b*-HPMA$_{120}$)	1	94	0.076
	2	82	0.085
	3	99	0.079
p(*t*-BMA$_{25}$-*co*-HPMA$_{25}$-*co*-EGDMA$_{0.9}$):*p*(PEG$_{114}$-*b*-HPMA$_{120}$)	1	118	0.085
	2	100	0.120
	3	125	0.064

Table A13 DLS results for blank co-nanoprecipitated nanoparticles - 5 month stability

Sample 50:50 wt %	Instant size (d.nm)	PdI	Size after 5 months (d.nm)	PdI
p(*n*-BMA$_{50}$-*co*-EGDMA$_{0.8}$):*p*(PEG$_{114}$-*b*-HPMA$_{120}$)	168	0.168	172	0.073
p(HPMA$_{50}$-*co*-EGDMA$_{0.9}$):*p*(PEG$_{114}$-*b*-HPMA$_{120}$)	82	0.188	83	0.101
p(*t*-BMA$_{25}$-*co*-HPMA$_{25}$-*co*-EGDMA$_{0.9}$):*p*(PEG$_{114}$-*b*-HPMA$_{120}$)	101	0.166	105	0.170

Chapter 6 – Conclusions and Future Work

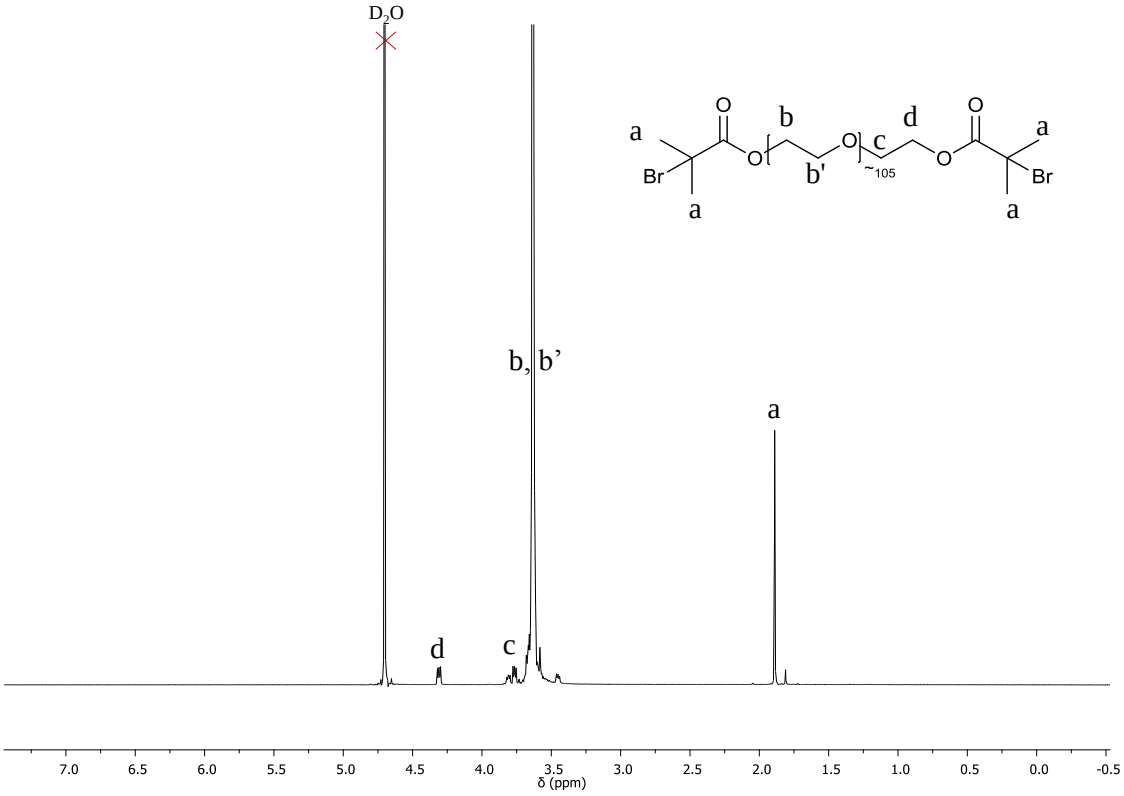

Figure A31 ^{1}H NMR *p*(Br-PEG$_{\sim 105}$-Br) (D_2O, 400 MHz).

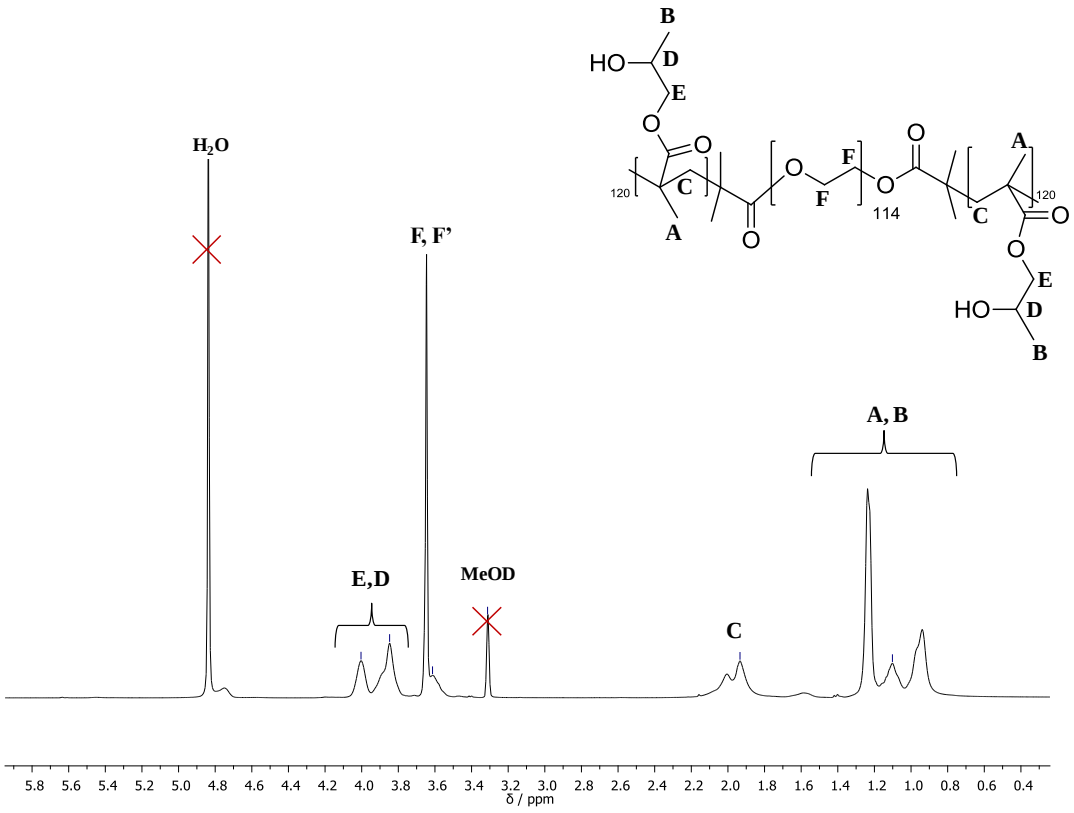

Figure A32 ^{1}H NMR *p*($_{120}$HPMA-*b*-PEG$_{\sim 105}$-*b*-HPMA$_{120}$) (Methanol-d$_4$, 400 MHz).

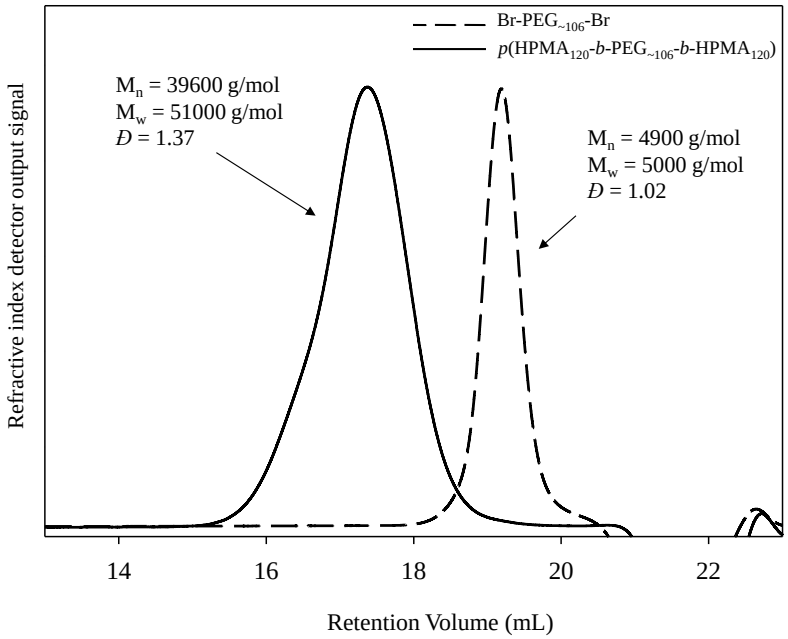

Figure A33 GPC RI overlay for (Br-PEG$_{\sim 105}$-Br) bifunctional macroinitiator and *p*($_{120}$HPMA-*b*-PEG$_{\sim 105}$-*b*-HPMA$_{120}$) polymer.

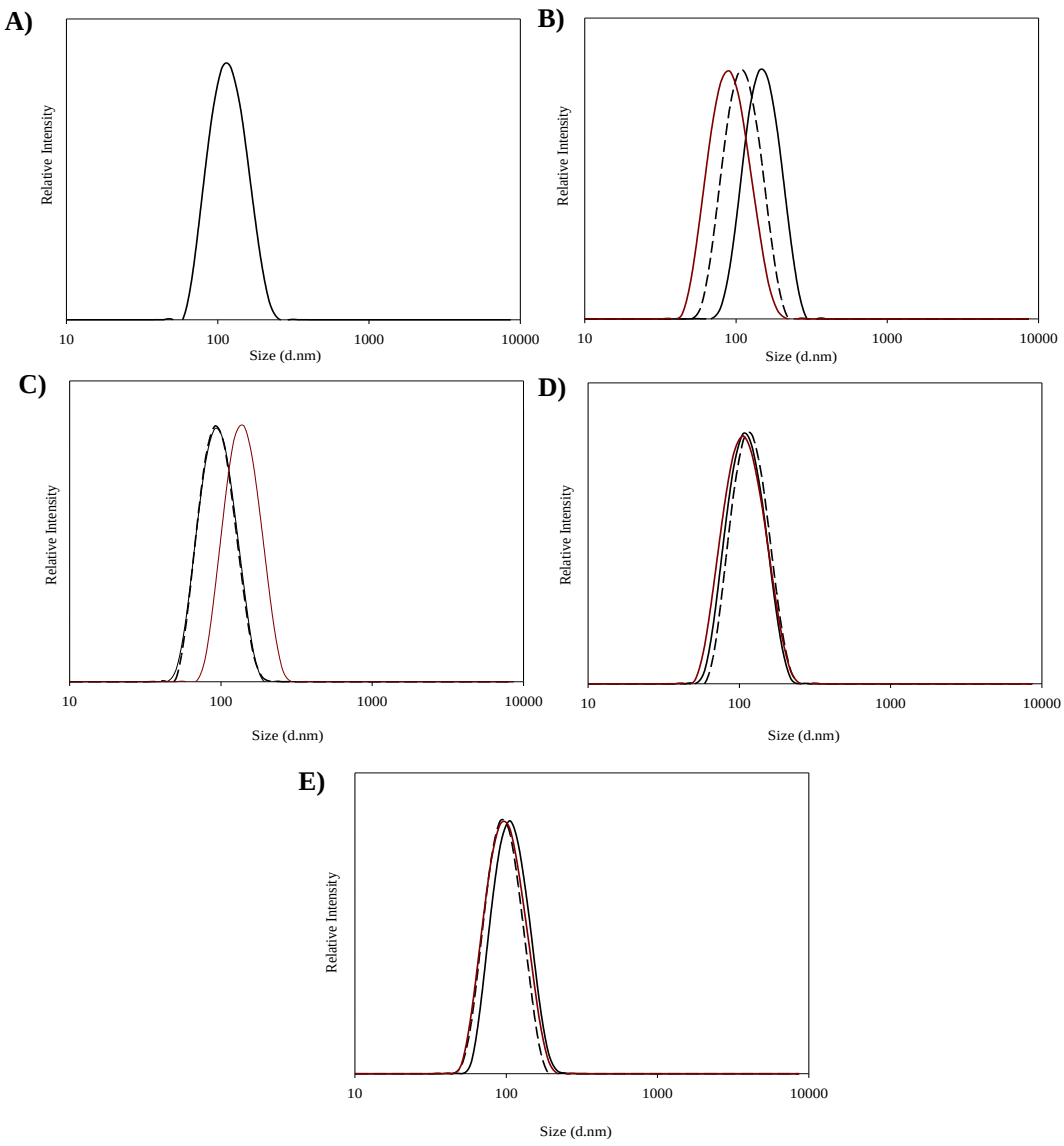

Figure A34 A) *p*(HPMA$_{50}$-*co*-EGDMA$_{0.9}$):*p*(HPMA$_{120}$-*b*-PEG$_{\sim 105}$-*b*-HPMA$_{120}$) 50:50 wt%, B) Efavirenz encapsulated co-nanoprecipitated nanoparticles, C) ritonavir encapsulated nanoparticles, D) lopinavir encapsulated nanoparticles, E) Ritonavir + lopinavir encapsulated nanoparticles (1:1). Black = 1 wt%, black dashed = 5 wt%, dark red = 10 wt %.

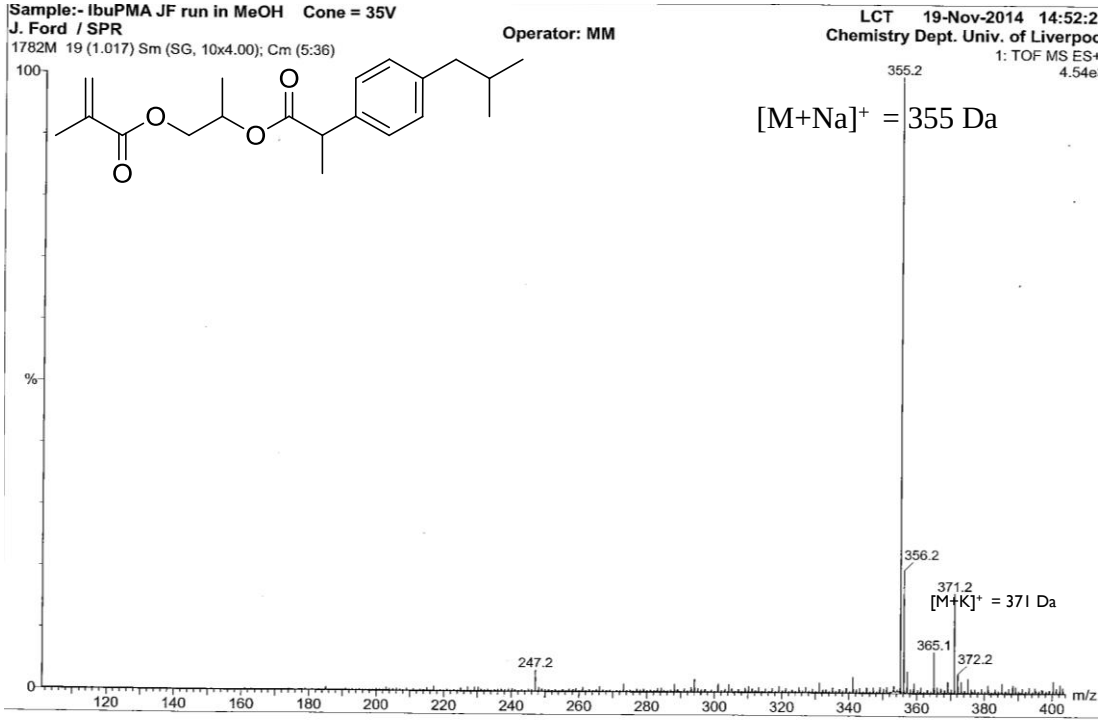

A35 Mass spectrum (ES-MS) of IbuPMA.

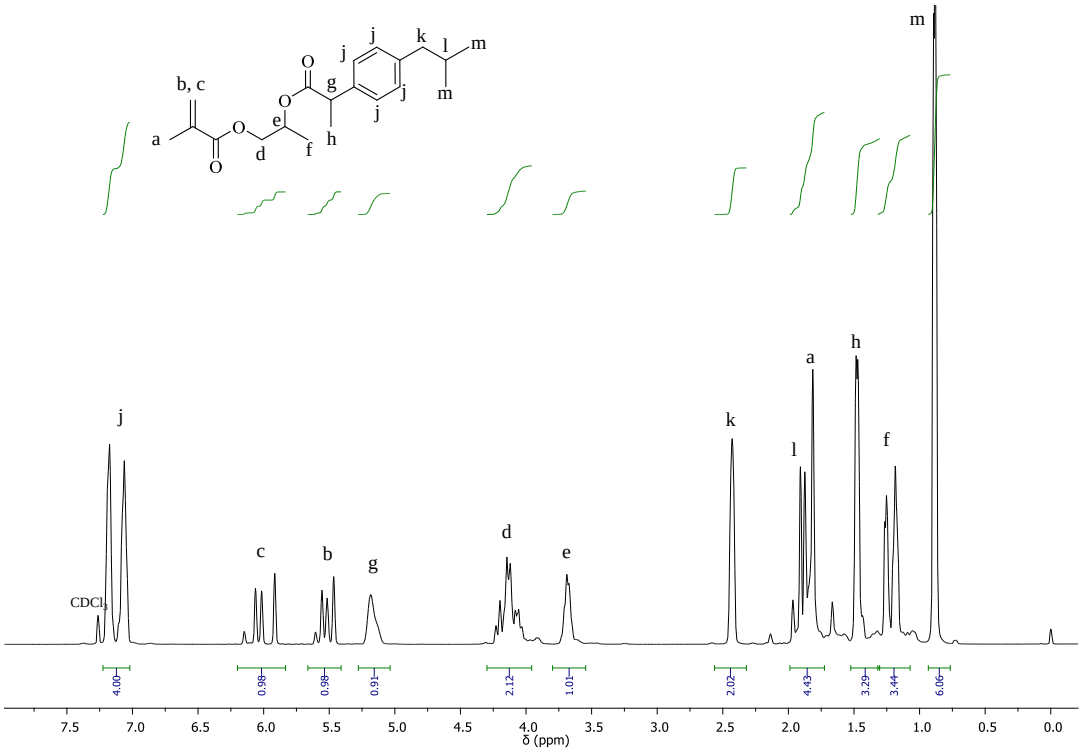

A36 ^{1}H NMR analysis of IbuPMA ($CDCl_3$, 400 MHz).

Table A14 GPC results for incorporation of IbuPMA. (DMF GPC system)

Sample	Targeted M_n (g/mol)	M_n (g/mol)	M_w (g/mol)	Đ	DP ^{1}H NMR	^{1}H NMR Conversion
PEG_{114}-Br	~5000	5500	5550	1.01	113	-
p(PEG_{114}-*b*-$HPMA_{80}$)	16500	20600	25000	1.21	65 HPMA	99
p(PEG_{114}-*co*-$HPMA_{60}$-*co*-$IbuPMA_{20}$) (Assuming 1:1 monomer conversion)	20300	25600	31400	1.23	~15 IBU units per chain	97

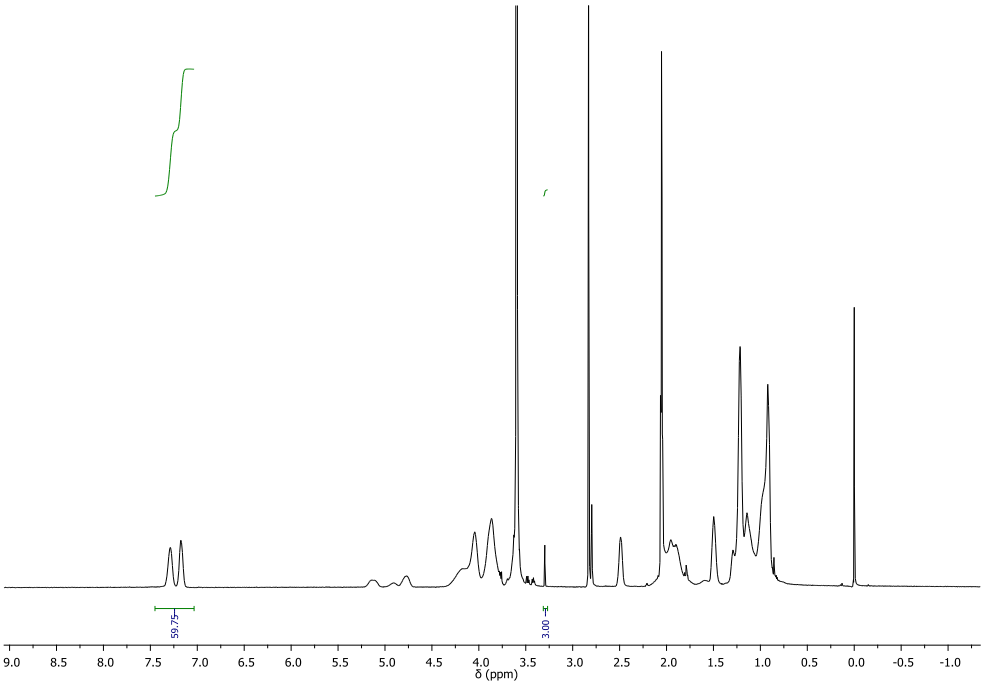

Figure A37 ^{1}H NMR *p*(PEG_{114}-*co*-$HPMA_{60}$-*co*-$IbuPMA_{20}$) (DMSO-d_6, 400 MHz).

Table A15 GPC results for post modification of *p*(PEG_{114}-*b*-$HPMA_{120}$). (DMF GPC system)

Sample	Targeted M_n (g/mol)	M_n (g/mol)	M_w (g/mol)	Đ	DP ^{1}H NMR	^{1}H NMR Conversion
PEG_{114}-Br	~5000	5500	5550	1.01	113	-
p(PEG_{114}-*b*-$HPMA_{120}$)	22300	29500	37500	1.27	115 HPMA	99
Post modified p(PEG_{114}-*co*-$HPMA_{80}$-*co*-$IbuPMA_{40}$)	29800	37400	47800	1.28	~17 IBU units per chain	-

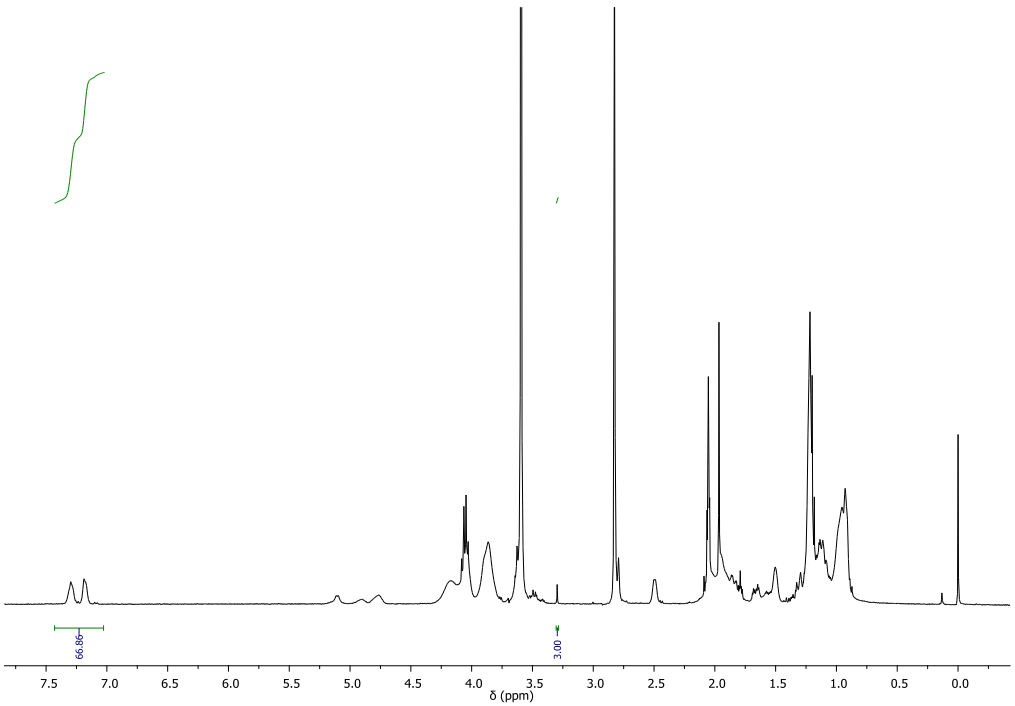

Figure A38 ^{1}H NMR *p*(PEG$_{114}$-*co*-HPMA$_{80}$-*co*-IbuPMA$_{40}$) (DMSO-d$_6$, 400 MHz).

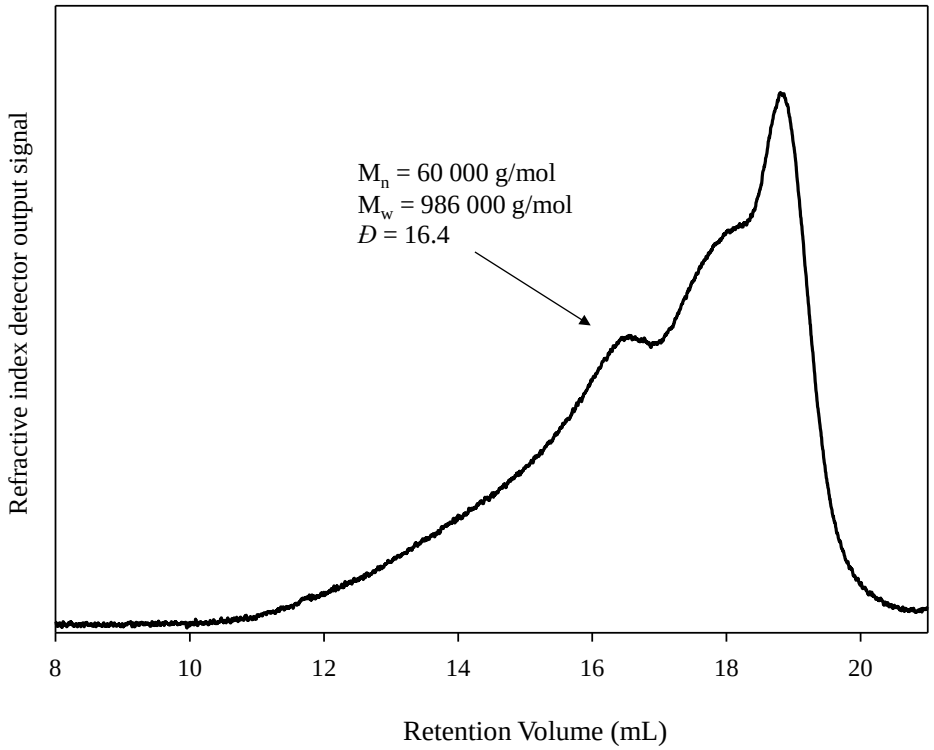

Figure A39 GPC analysis for *p*(HPMA$_{60}$-*co*-IbuPMA$_{20}$-*co*-EGDMA$_{0.85}$).